TE4193-76-75

COO-2690-1
Distribution Category UC-96

FINAL REPORT

FEASIBILITY TEST ON COMPOUNDING THE INTERNAL COMBUSTION ENGINE FOR AUTOMOTIVE VEHICLES

TASK II

CONTRACT NO. E(11-1)-2690

Prepared for

Energy Research and Development Administration
Division of Transportation Energy Conservation
Office of Highway Vehicle Systems
Washington, D. C.

Prepared by

Thermo Electron Corporation
101 First Avenue
Waltham, Massachusetts 02154

DISCLAIMER

TABLE OF CONTENTS

LIST OF ILLUSTRATIONS

LIST OF TABLES

1. INTRODUCTION

Increasing emphasis on improving both fuel economy and emissions provides a strong incentive for development of systems that convert currently wasted energy in automotive vehicles to useful power.

The major portion of the waste energy in an internal combustion engine is associated with the exhaust gases. This exhaust energy is available at temperatures in the range from 700°F to 1500°F at full load, depending upon the type of internal combustion engine. However, at the off-design power levels encountered in typical duty cycles the exhaust gas temperature drops significantly. Thus, the maximum temperatures available for use in the waste heat recovery process are limited. For automotive application, the sink temperature would correspond to the ambient temperature at which the system is expected to operate. Therefore, any practical waste heat utilization system would have to perform efficiently in a relatively low temperature range.

The organic Rankine-cycle system (ORCS) offers the best potential for utilizing the exhaust energy of an internal combustion engine because of relatively high cycle efficiency at moderate, peak-cycle temperatures of 550°F to 650°F. For efficient waste heat recovery, the temperature difference between the exhaust gas and the organic fluid must be held to a minimum during the heat addition process; thus the thermodynamic irreversibilities are reduced while the maximum possible heat is still extracted from the exhaust. The thermodynamic properties of the organic fluid, Fluorinol-50, make it possible to maintain this minimum temperature difference even at the relatively high fluid pressure required for good cycle efficiency.

The organic Rankine bottoming cycle can be considered for various automobile and truck applications. The most attractive use, however, is in large, heavy-duty diesel trucks for long distance hauling. Here, the engine load and speed requirements are nearly constant over a large portion of the operating hours, and high mileages are accumulated. Thus, the potential fuel savings are sufficient to justify the added cost of a bottoming cycle system.

A conceptual design study of compounding the diesel truck engine with an ORCS was made and the results of the study are presented in the Task I Interim Report. This report has been included as an Appendix. Based on the results of the conceptual design study which showed a 15 percent fuel economy improvement potential over the duty cycle, an early feasibility demonstration test of the system was initiated. The demonstration system uses a Mack ENDT 676 diesel engine with existing but nonoptimum ORCS hardware made available from an earlier automotive Rankine-cycle program. This report presents the results of these feasibility demonstration tests, both steady-state and transient, over the operating range of the diesel engine.

2. SYSTEM DESCRIPTION

The design of the compound engine for installation in a truck was previously presented in the Task I Interim Report, attached as an Appendix. This compound engine makes use of an ORCS to recover energy from the exhaust of the diesel engine. A flow schematic showing all the major components of the system is presented in Figure 2. 1. The conditions shown on the figure are for a prototype system with the diesel engine operating at full power and at 2100 rpm using Fluorinol-50 for the ORCS working fluid.

There are three interfaces in the truck between the ORCS and the diesel engine. The first interface is between the exhaust gas of the diesel engine and the organic fluid in the vapor generator of the ORCS; the second is the mechanical coupling of the ORCS power to the diesel engine; and the third is the cooling interface between the ORCS condenser and the diesel radiator.

During the feasibility tests, conditions at the interface in the vapor generator were the same as those in a truck, whereas the conditions at the other two interfaces were simulated. A vapor generator, designed to meet operating conditions in a truck, was fabricated specifically for these tests. Since the existing turbine-gearbox unit had to be run at twice diesel speed to obtain high efficiency, the diesel engine and ORCS were not coupled directly but were run on two separate dynamometers at a fixed ratio of turbine speed to diesel engine speed. With two separate dynamometers, no attempt was made to match conditions at the cooling interface; but instead, conditions were simulated by setting the ORCS condenser pressure at the optimum

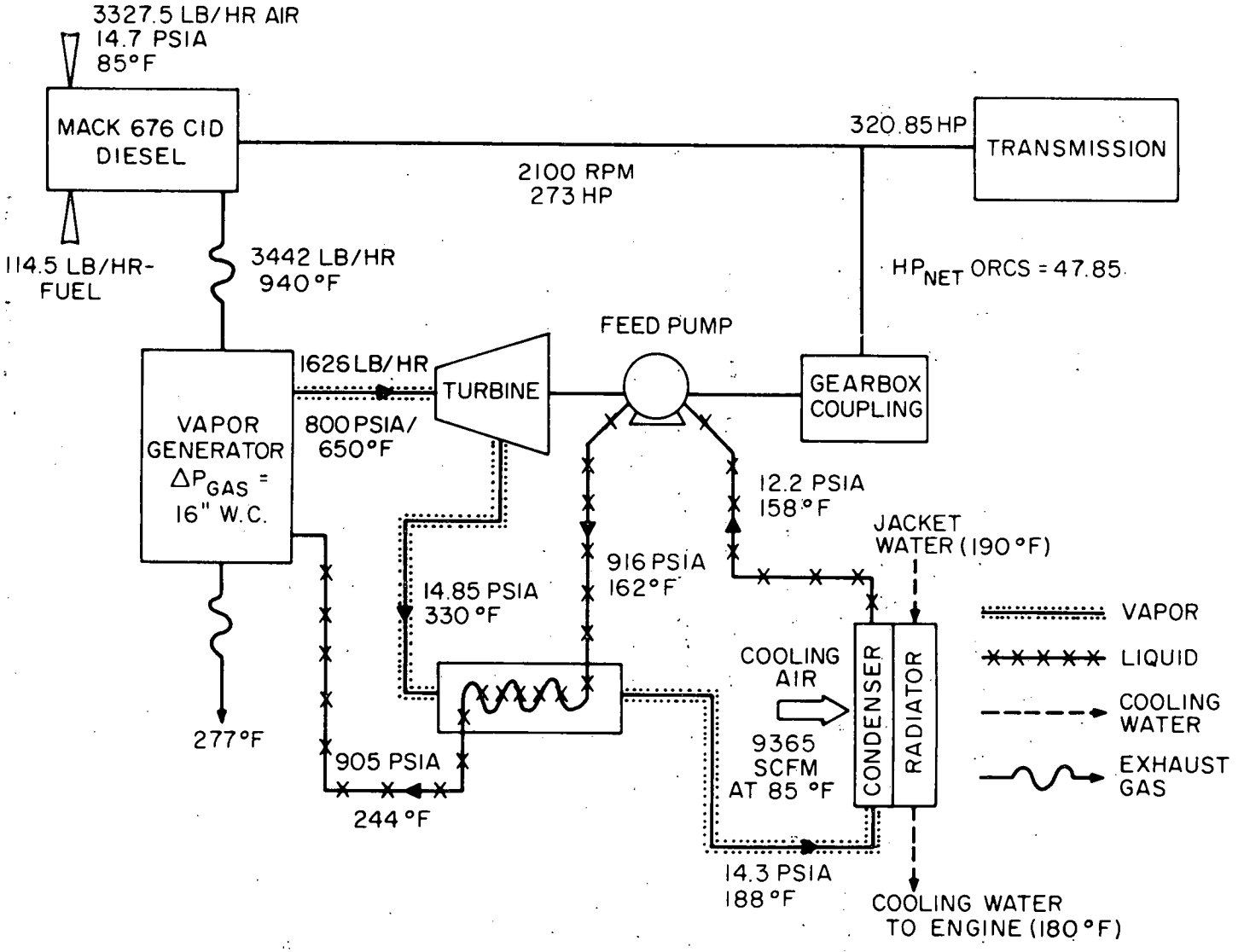

Figure 2.1 Diesel-Organic, Rankine-Cycle, Compound Engine - Flow Schematic

value determined during the design study for each of the diesel engine running conditions. Figure 2.2 is a schematic which shows the predicted, state-point conditions for the feasibility demonstration of the diesel-ORCS compound engine at full power and 2100 rpm.

Most of the ORCS components used in the demonstration tests were the same as those fabricated previously for the automotive Rankine-cycle powerplant. These components include a condenser, regenerator, feedpump, and boost pump. The diesel truck engine is a Mack Model ENDT 676 supplied to TECO as part of the subcontract with Mack Trucks, Inc. The description of the reference truck diesel engine and the performance measurements for the production engine made at Mack Trucks, Inc. are presented in the Task I Interim Report.

A 150 hp, turbine-gearbox unit (TGU) originally designed for the automotive application was available for the feasibility demonstration tests. However, it had to be modified to match the conditions for this application. Also required was a vapor generator to recover the heat from the diesel exhaust. The designs of the vapor generator and turbine gearbox used in these tests are described below.

2.1 VAPOR GENERATOR

The vapor generator used in these demonstration tests was designed with a staggered tube arrangement with solid fins brazed to the tube. The design-point characteristics of the vapor generator are shown in Table 2.1.

The unit consists of three sections which were individually fabricated and subsequently assembled together. It has three parallel

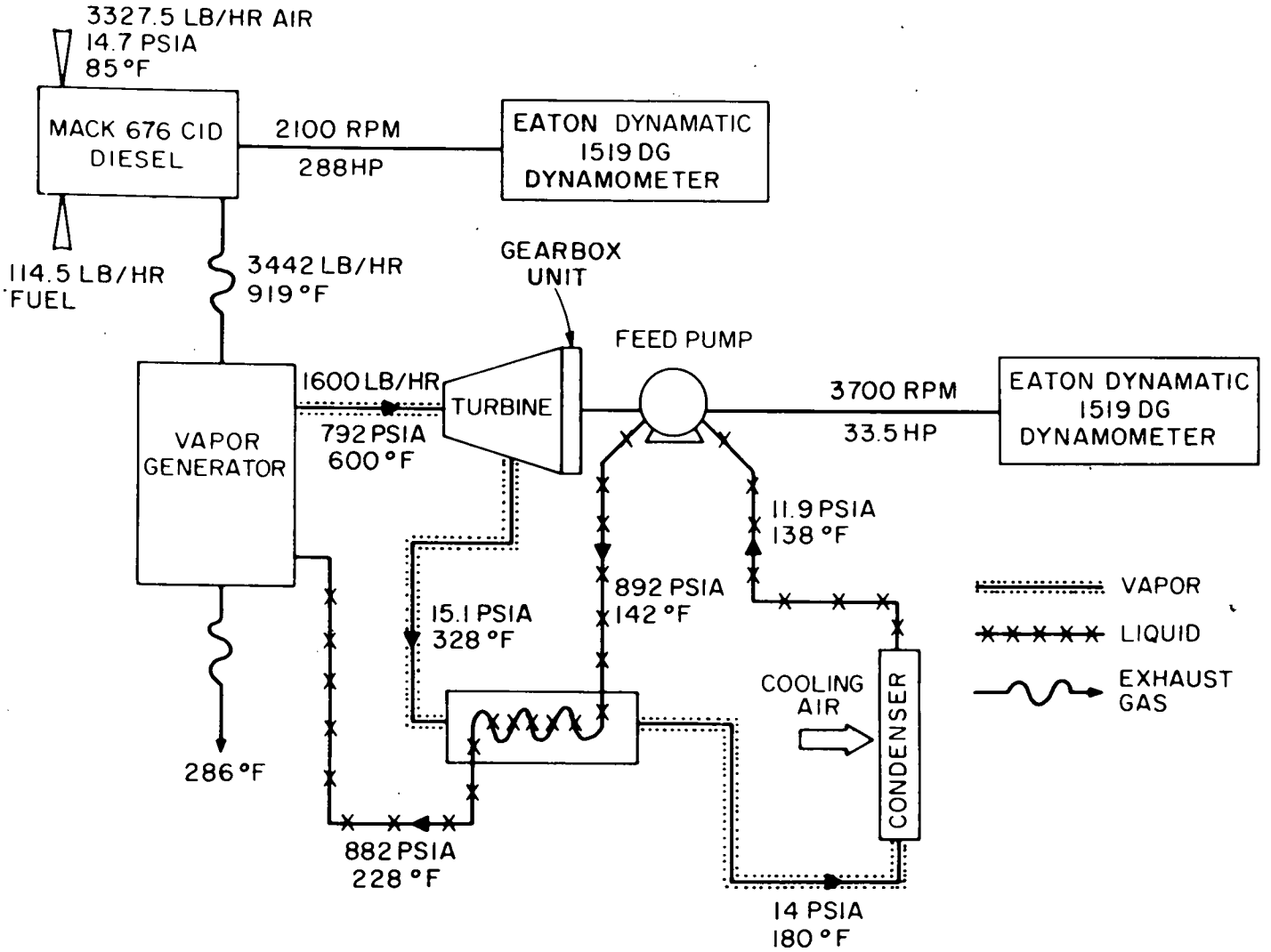

Figure 2.2 Diesel-ORCS, Compound Engine Demonstration Hardware - Flow Schematic

TABLE 2.1

DESIGN POINT CHARACTERISTICS OF VAPOR GENERATOR FOR DEMONSTRATION TEST

1. Performance Characteristics	
Heat Transfer Rate	581,300 Btu/hr
Working Fluid - Fluorinol 50	
Flow Rate	1,600 lbm/hr
Inlet Temperature	226°F
Inlet Pressure	881 psia
Outlet Temperature	607°F
Outlet Pressure	810 psia
Diesel Exhaust Gas	
Flow Rate	3,442 lbm/hr
Inlet Temperature	919°F
Outlet Temperature	286°F
Pressure Drop	16-inch WC
2. Salient Features	
Type of Flow	Cross-counterflow
Type of Construction	Banks of finned tubing staggered arrangement
Number of Parallel Circuits	3
Number of Passes	52
3. Dimensions	
Tube	
Outside Diameter/Inside Diameter	0.375 inch/0.305 inch
Total Finned Length	312 ft
Fin	
Type	Wound, brazed, solid fins
Thickness	0.021 inch
Height	5/16 inch
Pitch	10 fpi
Transfer Area/ft of Tubing	1.256 ft^2/ft
Tube Spacing	1-1/8 inch equilateral triangular spacing
4. Heat Transfer Characteristics	
Effectiveness	
Preheat region	0.83
Boiling region	0.64
Superheat region	0.31
UA	
Preheat region	3,240 Btu/°F
Boiling region	929 Btu/°F
Superheat region	413 Btu/°F

circuits with each circuit traversing twice in the same pass. The U-bends and tubes were furnace-brazed together.

2.2 TURBINE-GEARBOX UNIT

The TGU has a 5.5 inch diameter, single-stage, partial admission, axial impulse turbine and a single-stage gearbox with a speed reduction ratio of 9.436. A new nozzle block, with five nozzles of 7.51 expansion ratio, was designed for the turbine to meet the new pressure ratio and flow requirements. To improve performance, a partial exhaust with a built-in diffuser was designed to eliminate some of the pumping losses of the rotor. The turbine rotor shrouding also was modified to reduce the windage losses. A double mechanical face seal, with a pressurized buffer space between the sealing faces, was installed to isolate the turbine from the gearbox.

A high TGU speed is required to achieve good efficiency, but the maximum TGU output speed is limited to 3700 rpm for stress reasons. The duty cycle study indicated that the TGU peak efficiency should occur at a diesel engine speed of 1850 rpm. Thus, the TGU speed was maintained at twice the diesel speed until it reached 3700 rpm, and then it was maintained constant.

3. TEST FACILITY

The feasibility demonstration tests of the diesel-ORCS compound engine were performed at the Thermo Electron engine development facility. As shown in Figure 3. 1, the diesel truck engine and vapor generator were installed in one test cell, and the remaining ORCS components were installed in an adjacent cell. Diesel engine power and ORCS power were measured independently with this arrangement. Figure 3. 2 is a photograph showing the diesel engine coupled to the dynamometer in the expander test facility. A photograph of the encased vapor generator with the connecting diesel exhaust line is shown in Figure 3. 3. The turbine-gearbox unit with other ORCS components such as the feedpump, regenerator, and condenser are shown mounted in the system test cell in Figure 3. 4.

A schematic of the facility with the compound diesel-ORCS engine is shown in Figure 3. 5. The facility permits both steady-state and transient testing of the ORCS over the normal operating range of the diesel truck engine. Instrumentation installed in the test facility measures all the parameters such as pressure, temperature, flow rate, torque, and speed required to evaluate the performance of the entire system, as well as individual components. Also, safety devices such as pressure, temperature, and flow switches were installed in the test facility as indicated in Figure 3. 5.

Automatic data recording instrumentation was incorporated into the system. A Datel digital data acquisition system automatically prints out the test parameters required for performance evaluation of the diesel-ORCS. The Datel system consists of solid-state,

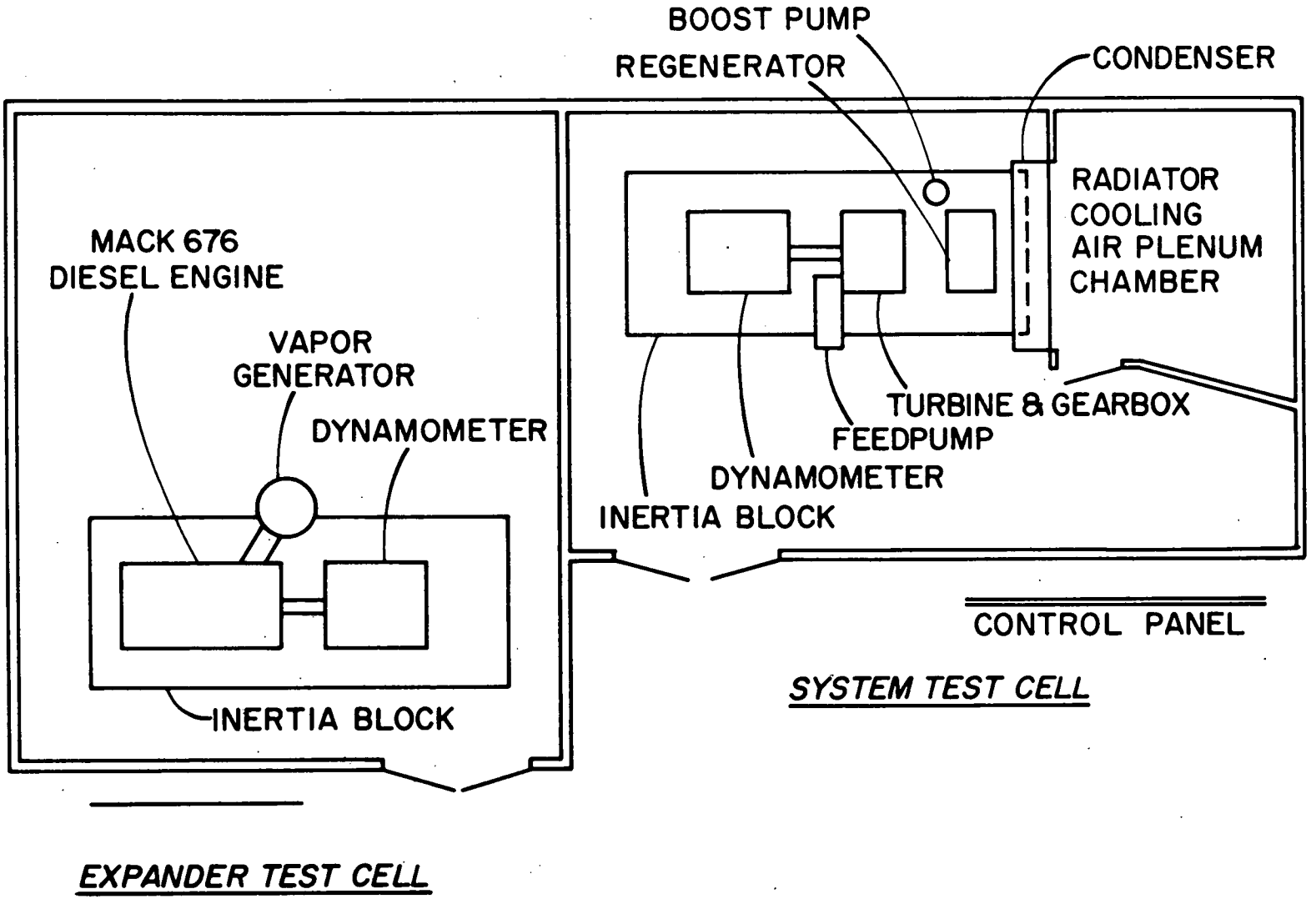

Figure 3.1 Plan View of TECO Test Facilities

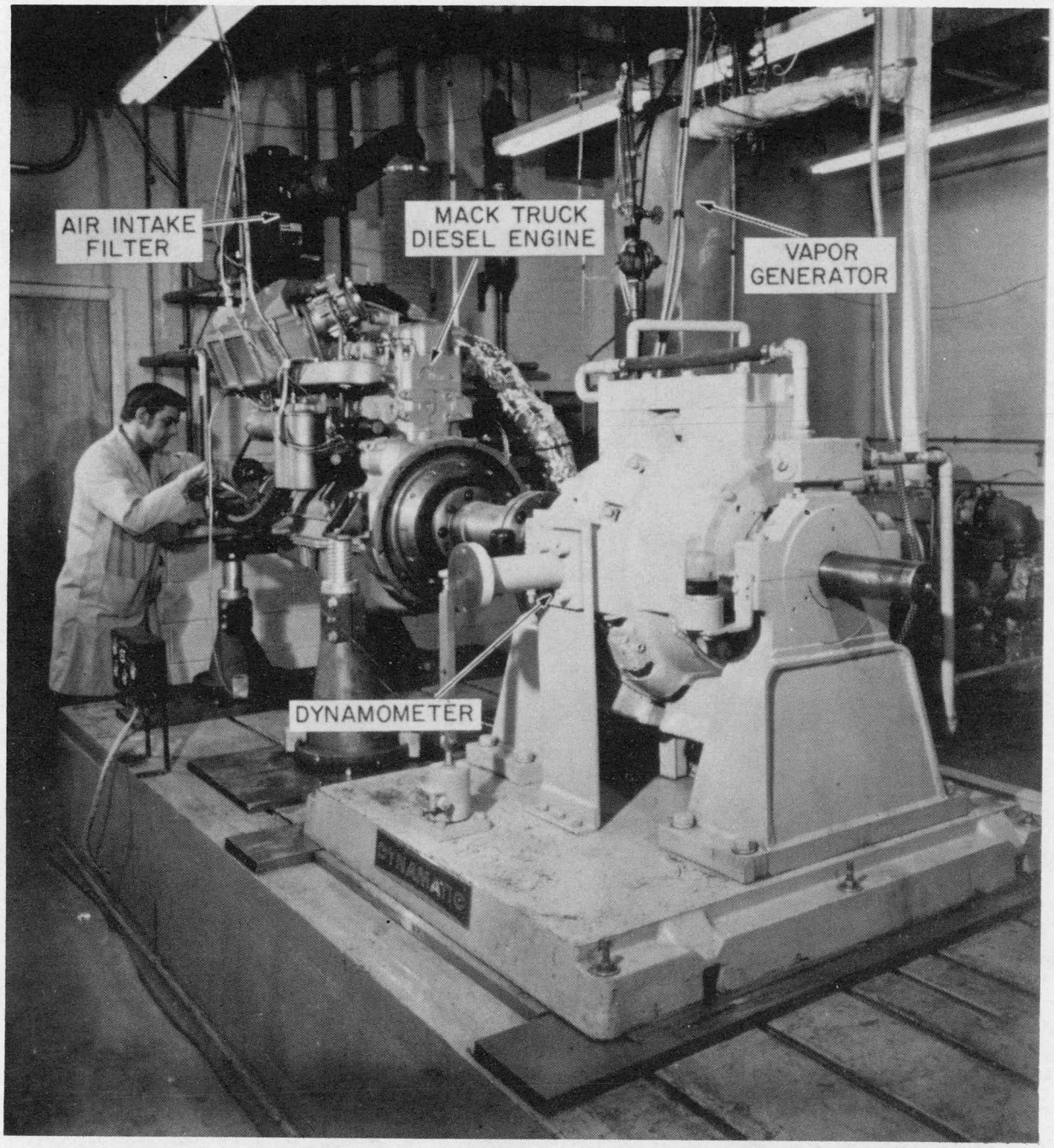

Figure 3.2 Diesel Engine Installed in TECO Test Facility

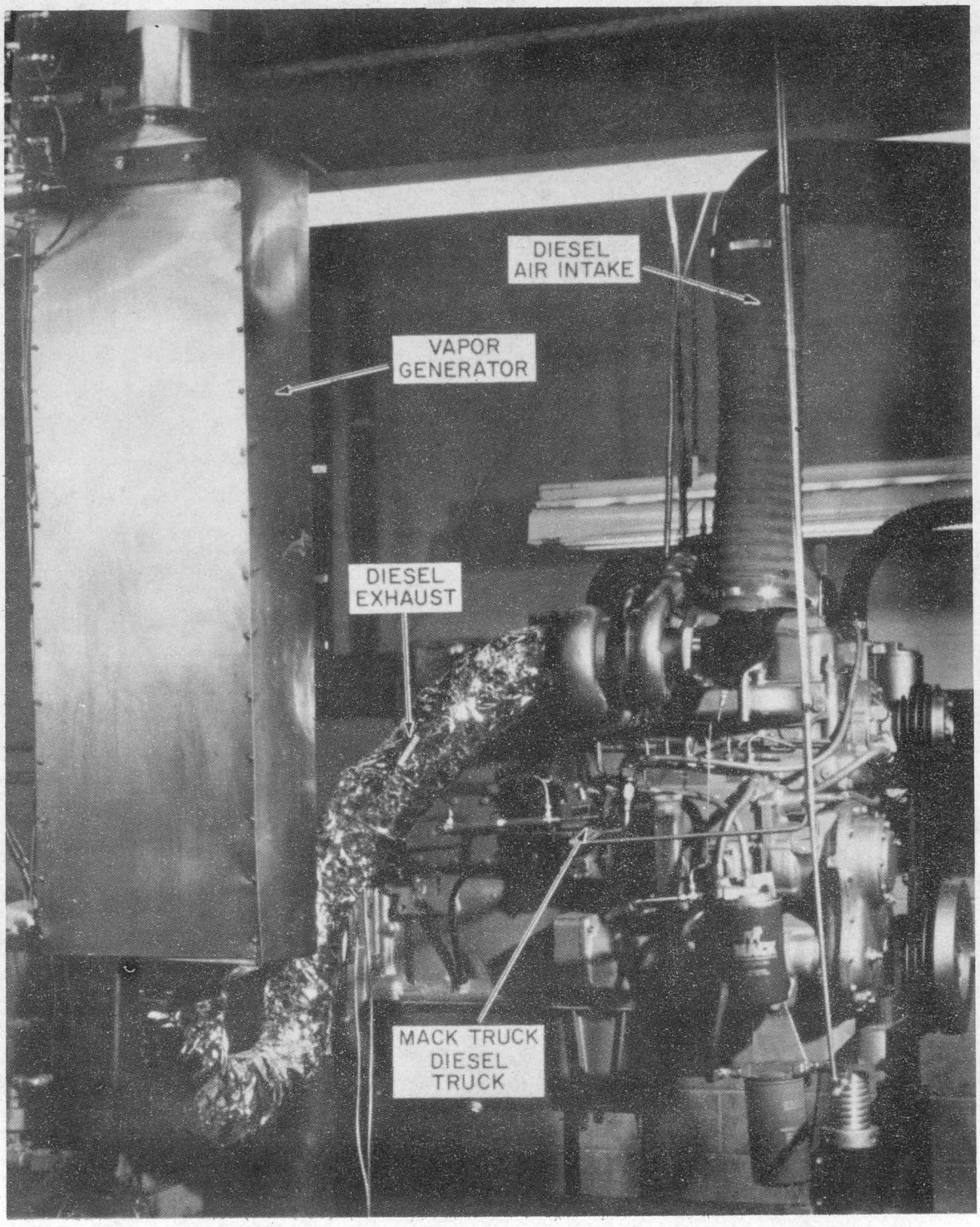

Figure 3.3 Vapor Generator Used in Diesel-ORCS Feasibility Demonstration Tests

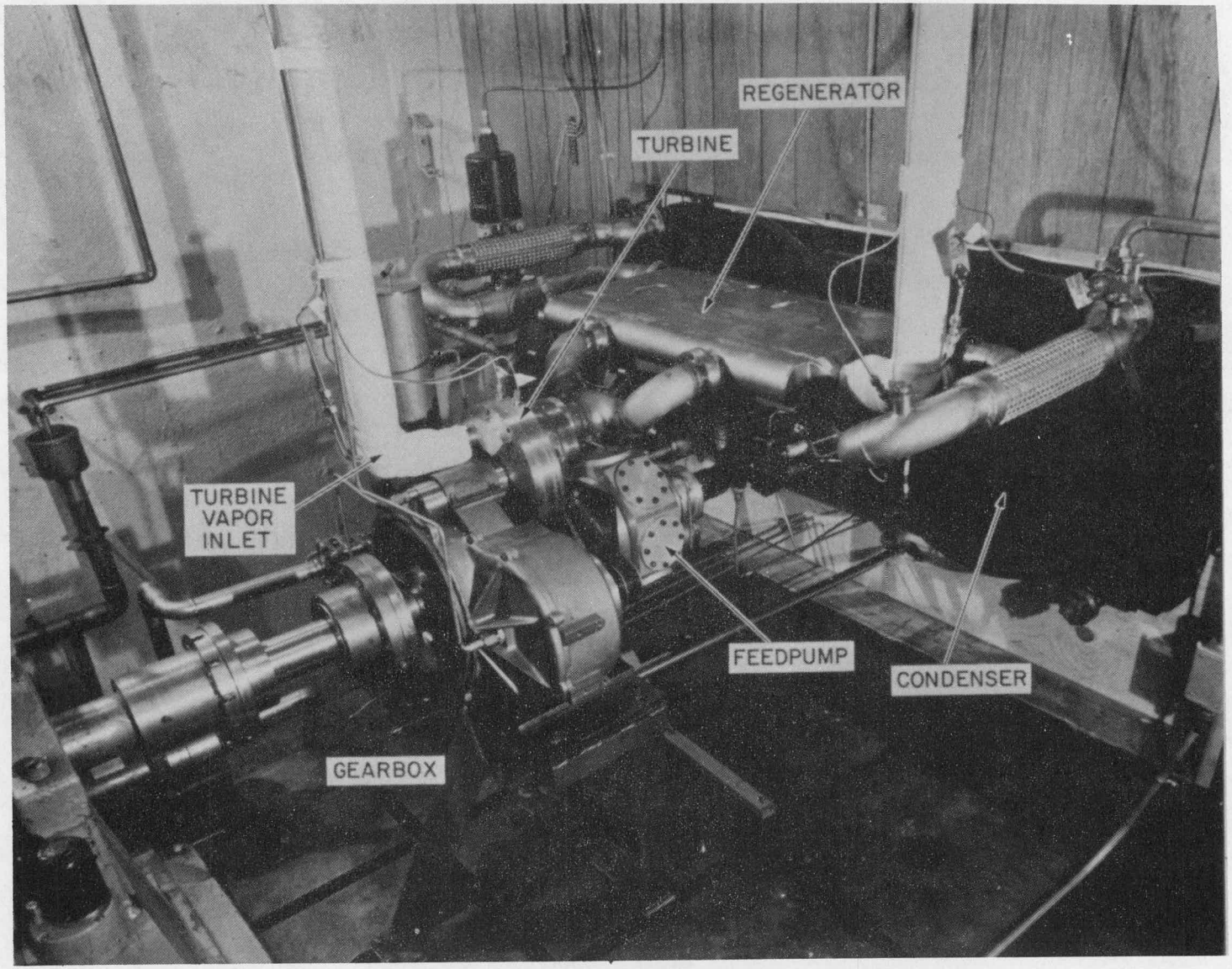

Figure 3.4 ORCS Components Installed in Test Facility

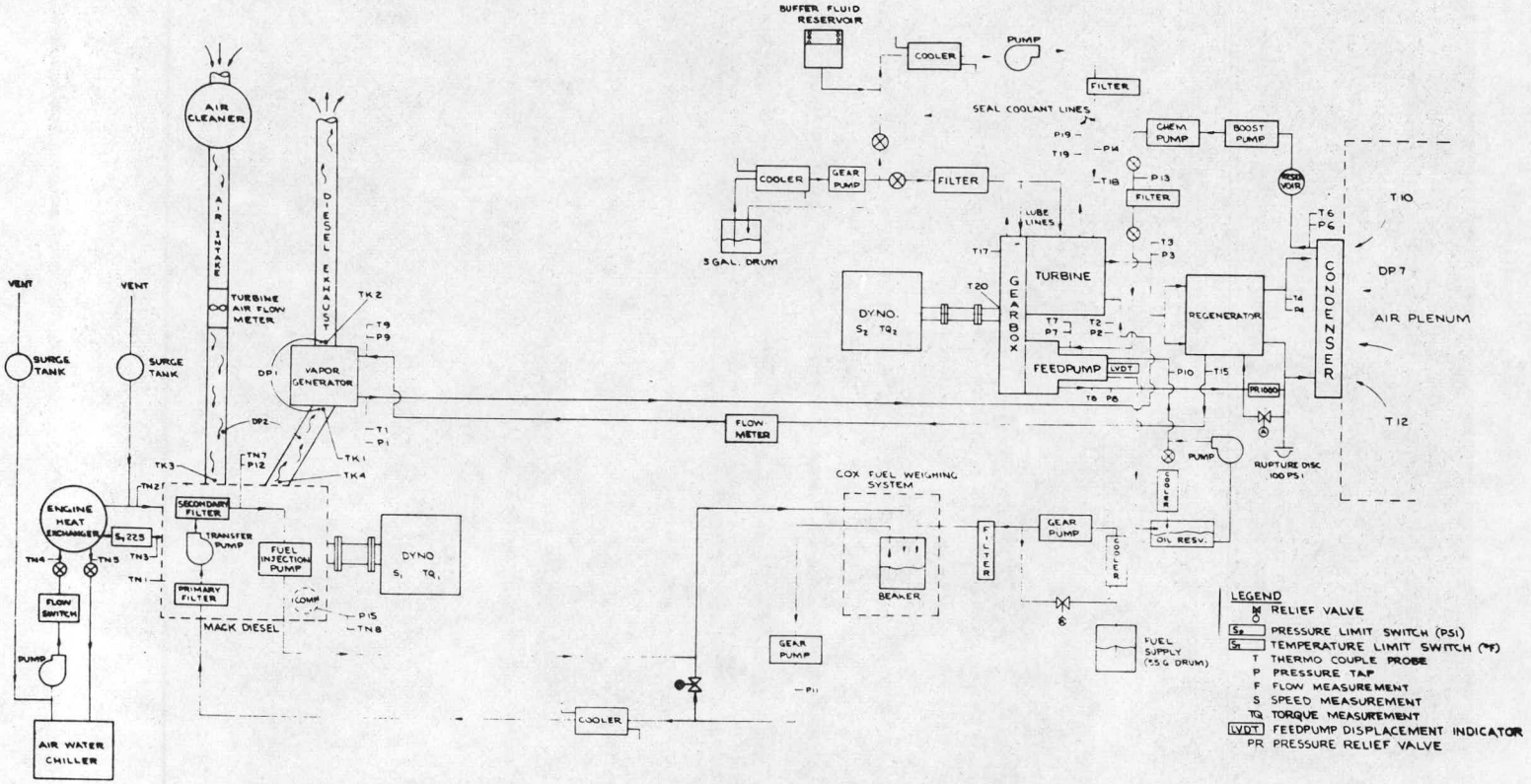

Figure 3.5 Truck Bottoming Demonstration Loop - Schematics

analog multiplexers complete with address selection decoding and output buffer amplifiers combined with an analog-to-digital converter which gives a digital output for a maximum of 47 measurements. This digital output is then recorded on a medium-speed, ink-impression line printer designed specifically for use with digital-type measurement instruments. One Rikadenki and three Honeywell strip recorders were used primarily during the transient study test phase. The Rikadenki multi-pen recorder is capable of continuously recording as many as six simultaneously occurring variables on one chart paper with full-width traces crossing each other. Each Honeywell recorder is a two-pen recorder with full-width traces on both channels. These instruments were used to monitor and continuously record data during the transient tests.

THIS PAGE
WAS INTENTIONALLY
LEFT BLANK

4. SYSTEM TESTS

The purpose of the test program was to demonstrate the feasibility of using an organic Rankine bottoming cycle to increase the efficiency of a heavy-duty diesel truck engine. Both steady-state performance mapping and transient studies were made during this test phase of the program. An important prelude to the actual testing phase of the program was the computer prediction of the system performance. The computer program was used to predict the performance of the ORCS with the actual components used in the test program. These computer results provided a basis for evaluation of the test data and for comparing it with the predictions made for an ORCS having components specifically designed for the application. A computer program was also prepared to translate the data obtained from the tests into the performance of the ORCS and its components and to compare these results with the predictions.

Some initial testing was performed on the system to ensure proper operation of the diesel engine, turbine gearbox, other components of the diesel-ORCS, controls, and instrumentation. During these initial tests, the ratio of the turbine gearbox to the diesel speed was varied. Then it was set for all other tests at 2 to 1 for diesel speeds up to 1800 rpm (3600 rpm on the turbine gearbox) and at a constant 3700 rpm for diesel speeds from 1800 rpm to the maximum speed of 2100 rpm.

Steady-state performance was then measured over the normal operating range of the diesel truck engine. The condenser pressure for these tests was set at the design conditions of the truck as

determined from the condenser design which was shown in the Task I Interim Report. For each setting of diesel engine speed and fuel flow rate (diesel power output), the organic fluid flow rate was adjusted to achieve the maximum power output from the ORCS.

At the completion of the steady-state performance tests, transient tests were conducted to gain a better understanding of the control requirements of the system. These transient tests provided data which will be useful for the design of the organic fluid flow rate control to be used in the final ORCS.

Two types of transient tests were made, and the more critical system parameters were continuously recorded. The first group of tests consisted of holding the diesel-engine speed and turbine-gearbox speed constant while making a step change in fuel flow rate. At the same time, a step change in organic fluid flow rate was made according to a previously determined schedule. These tests were conducted for both increasing and decreasing flow rates. In the second group of tests, both the fuel flow rate and the organic fluid flow rate were held constant, and a step change was made in the diesel-engine speed and the turbine-gearbox speed. These tests were conducted for both increasing and decreasing speeds.

During these tests, over fifty hours of operation were accumulated on the combined diesel-ORCS without any serious breakdowns or mechanical problems. The TGU was never disassembled and no degradation in performance was observed during the entire period of testing.

4.1 DATA REDUCTION

A data-reduction program was prepared to reduce the test data obtained and evaluate the performance of the ORCS and its components. The input data to the program include temperatures, pressures, flow rates, and power measurements (diesel and TGU dynamometer output power). The program computes the following information:

1. State-point conditions entering and leaving each component (temperature, pressure, and enthalpy).
2. Power train calculations from gross turbine power to net system-power output including all the various losses.
3. Cycle efficiency and system flow rates.
4. Component efficiencies, heat loads, and pressure drops.
5. Diesel operating conditions including fuel flow, brake horsepower, and exhaust gas flow.

The net ORCS power is calculated by accounting for all losses which occur in the system power train. Figure 4.1 shows the power distribution for the diesel-ORCS and indicates the parasitic power drain on the turbine, which include:

1. Windage losses - Power loss due to drag on the turbine wheel.
2. Seal losses - Power consumption of high-speed shaft seal.
3. Gearbox losses - High-speed gearbox power losses.
4. Feedpump power requirement - This power drain was determined by performance data established at TECO.

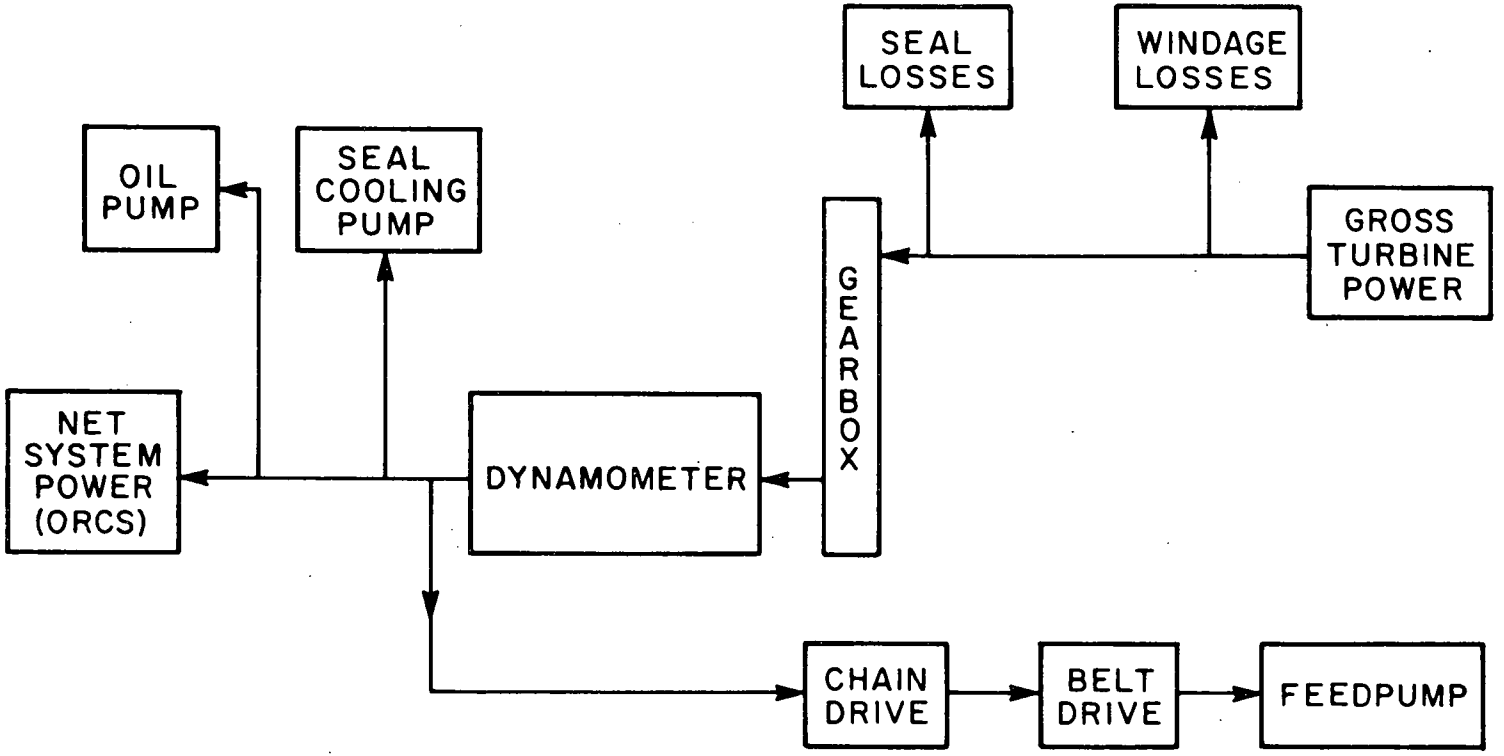

Figure 4.1 Power Distribution for Diesel ORCS

5. Drive losses - Belt and chain transmission losses in the feedpump drive.

6. Oil pump losses - Power consumption of oil pump used for seal cooling and gearbox lubrication.

The gross turbine power is determined by adding the known windage, seal, and gearbox losses to the measured dynamometer power. The net ORCS power output accounts for all the power losses which occur after measuring the dynamometer power. These losses include the feedpump with associated drives and the oil and seal cooling pumps for the turbine-gearbox unit.

4.2 STEADY-STATE TESTS

The steady-state performance mapping consisted of running a total of twenty-six tests over the normal operating range of the diesel engine. These tests consisted of running four fuel rates at a diesel speed of 1000 rpm, six fuel rates at 1200 rpm, six fuel rates at 1600 rpm, six fuel rates at 1800 rpm, and four fuel rates at the maximum diesel speed of 2100 rpm. At each of these test conditions the organic flow rate was set to yield the maximum ORCS power output. Condenser pressure was set at the design value corresponding to each test condition. Both system performance and component performance were measured during these tests, and the results are presented in the following sections.

4.2.1 System Test Results

Steady-state performance test results for the diesel-ORCS compound engine are presented in Table 4.1. Both operating

TABLE 4.1

STEADY-STATE PERFORMANCE TEST RESULTS

Test No.	Diesel						ORCS System											
	Fuel Flow (lb/hr)	Speed (rpm)	Power (hp)	Exh. Gas Flow (lb/hr)	Exh. Gas Temp. (°F)	BSFC	Turbine Inlet Temp. (°F)	Turbine Inlet Press. (psia)	Turbine Outlet Press. (psia)	Condenser Temp. (°F)	F-50 Flow (lb/hr)	TGU Speed (rpm)	TGU Power (hp)	TGU Efficiency (%)	ORCS Power (hp)	ORCS Heat Input (BTU/hr)	ORCS Cycle Eff. (%)	Power Imprvmt (%)
1	32.4	1012	95.4	912.0	843	0.3402	365.8	179.7	4.40	84.5	438.2	2000	6.98	33.17	3.95	145,922	6.89	4.14
2	48.2	1007	135.17	1050.0	1050	0.3562	423.3	289.7	4.70	83.5	672.6	1999	11.46	37.55	8.26	222,453	9.45	6.11
3	57.1	1005	155.0	1152.4	1132	0.3683	438.3	334.7	5.70	83.8	767.5	1999	13.18	39.20	9.89	254,212	9.90	6.38
4	77.9	1007	191.74	1367.8	1259	0.4064	520.7	449.7	7.90	84.6	995.5	2000	18.71	41.73	15.17	337,368	11.44	7.91
5	41.3	1193	126.52	1182.2	864	0.3266	423.5	236.5	5.80	81.3	548.9	2397	11.49	45.50	7.65	200,433	9.71	6.04
6	50.7	1197	154.53	1287.4	950	0.3279	499.0	294.7	6.50	82.4	665.1	2398	14.60	45.76	10.65	233,425	11.62	6.90
7	61.4	1202	178.51	1456.1	1023	0.3442	423.3	362.7	7.70	85.9	870.7	2401	16.50	46.40	12.38	288,852	10.91	6.93
8	69.0	1205	202.36	1604.3	1068	0.3408	459.3	416.7	8.00	80.2	977.0	2401	19.19	46.70	14.96	327,171	11.64	7.39
9	73.1	1202	215.13	1661.8	1095	0.3399	463.0	454.7	8.60	82.4	1060.4	2402	20.99	47.96	16.66	354,871	11.95	7.74
10	84.6	1204	245.29	1875.2	1136	0.3450	484.3	534.7	9.70	81.1	1248.0	2400	25.17	49.32	20.63	416,432	12.61	8.41
11	50.4	1596	142.22	1661.3	812	0.3542	413.0	299.6	6.00	92.0	722.0	3198	17.01	50.81	11.55	-	11.50	8.12
12	62.5	1600	180.0	1948.4	839	0.3471	422.0	359.6	6.35	95.0	869.0	3200	21.10	56.08	15.51	290,443	13.59	8.61
13	66.1	1599	198.5	2081.1	904	0.3329	460.1	389.5	5.70	85.1	889.4	3199	22.99	54.87	17.30	307,802	14.30	8.71
14	80.4	1600	230.92	2395.7	939	0.3481	442.4	486.74	7.90	82.7	1185.7	3200	26.77	53.97	20.80	394,907	13.41	9.01
15	92.3	1600	261.08	2588.1	979	0.3536	476.1	567.7	8.00	79.4	1353.1	3200	31.52	54.02	25.34	454,779	14.18	9.71
16	95.2	1590	278.83	2692.6	1002	0.3416	487.5	594.7	9.70	79.0	1421.2	3201	34.22	57.59	27.94	476,649	14.92	10.02
17	54.8	1799	145.58	2053.4	752	0.3767	406.1	319.8	6.30	83.3	756.4	3599	18.22	51.39	12.01	256,012	11.94	8.25
18	64.9	1800	176.5	2292.4	803	0.3679	439.0	389.8	6.90	84.3	907.7	3600	22.50	54.24	16.15	309,237	13.29	9.15
19	77.5	1800	213.86	2506.2	854	0.3625	469.8	464.8	9.00	86.5	1069.3	3600	26.75	56.99	20.23	364,428	14.13	9.46
20	81.6	1801	232.84	2675.0	887	0.3506	491.2	514.8	9.00	83.9	1162.9	3599	30.38	58.70	23.73	399,857	15.11	10.19
21	98.0	1800	265.61	2891.3	928	0.3688	508.0	569.8	9.30	74.7	1310.5	3600	34.09	58.17	27.28	449,460	15.45	10.27
22	103.1	1797	288.09	-	956	0.3578	546.0	619.7	8.80	120.0	1403.6	3591	38.64	58.11	31.63	501,296	16.06	10.98
23	62.3	2100	147.54	2524.8	770	0.4223	429.1	384.7	6.90	78.7	909.5	3700	22.58	54.79	16.07	309,608	13.21	10.89
24	81.2	2100	202.72	2920.9	848	0.4008	487.8	489.8	8.70	72.8	1142.0	3699	29.90	58.33	22.34	390,907	14.55	11.02
25	88.4	2105	228.46	3132.7	887	0.3868	524.9	549.7	7.10	74.9	1201.4	3700	33.71	57.49	26.83	428,090	15.95	11.74
26	109.5	2100	279.49	-	998	0.3917	556.0	687.7	11.30	126.0	1532.8	3702	42.97	61.45	35.55	542,858	16.67	12.72

conditions and performance data are given for the diesel engine and the ORCS. Table 4.2 summarizes the same twenty-six test points and compares the measured ORCS power with the predicted ORCS power. The measured ORCS power was consistently higher than the predicted ORCS power at all diesel power levels and speeds tested. The measured and predicted ORCS power output also are plotted in Figure 4.2 as a function of diesel power for various speeds over the normal operating range of the diesel engine. The maximum power output from the ORCS was 35.6 horsepower obtained at the wide-open-throttle diesel condition of 279 horsepower and 2100 rpm.

The "NAPCA Control Route," a representative truck driving cycle, was used in the evaluation of the ORCS performance. It is a composite of typical driving, including stop and go, over a route with hills and curves. Mack Trucks, Inc., provided computed data on fuel consumption, diesel speed, and power for a truck driven over this route with a gross weight of 72,000 pounds. Figure 4.3 shows the actual improvement in power output (which is defined as the ratio of ORCS power to diesel power) as a function of the diesel power level over the normal operating range from 1000 rpm to 2100 rpm. Cross-hatched regions on this graph show the percentage of fuel consumed over the NAPCA duty cycle for a range of diesel speeds and powers. Improvements of 10 percent to 12.7 percent were measured over the region where 84 percent of the fuel is consumed.

4.2.2 Turbine Performance

A major reason for the increased power output of the ORCS was the high performance of the turbine-gearbox unit measured during these tests. The overall TGU performance is compared with the

TABLE 4.2

DIESEL-ORCS TEST SUMMARY

Test Points	Fuel Flow (lb/hr)	Diesel		Predicted ORCS Power (HP)	Measured ORCS Power (HP)	
		HP	RPM			
1	32.4	95	1000	3.5	4.0	
2	48.2	135	1000	7.3	8.3	
3	57.1	155	1000	9.1	9.9	
4	77.9	192	1000	13.3	15.2	
5	41.3	127	1200	6.4	7.7	
6	50.7	155	1200	9.5	10.7	
7	61.4	179	1200	11.8	12.4	
8	69.0	202	1200	14.5	15.0	
9	73.1	215	1200	15.9	16.7	
10	84.6	245	1200	19.1	20.6	
11	50.4	142	1600	8.8	11.6	
12	62.5	180	1600	12.5	15.5	
13	66.1	199	1600	14.8	17.3	
14	80.4	231	1600	18.2	20.8	
15	92.3	261	1600	21.7	25.3	95% of fuel consumed over NAPCA duty cycle in this range
16	95.2	279	1600	24.0	27.9	
17	54.8	146	1800	10.9	12.0	
18	64.9	177	1800	14.1	16.2	
19	77.5	214	1800	18.1	20.2	
20	81.6	233	1800	20.5	23.7	
21	98.0	266	1800	24.5	27.3	
22	103.1	288	1800	27.8	31.6	
23	62.3	148	2100	14.0	16.1	
24	81.2	203	2100	20.7	22.3	
25	88.4	228	2100	23.6	26.8	
26	109.5	279	2100	31.6	35.6	

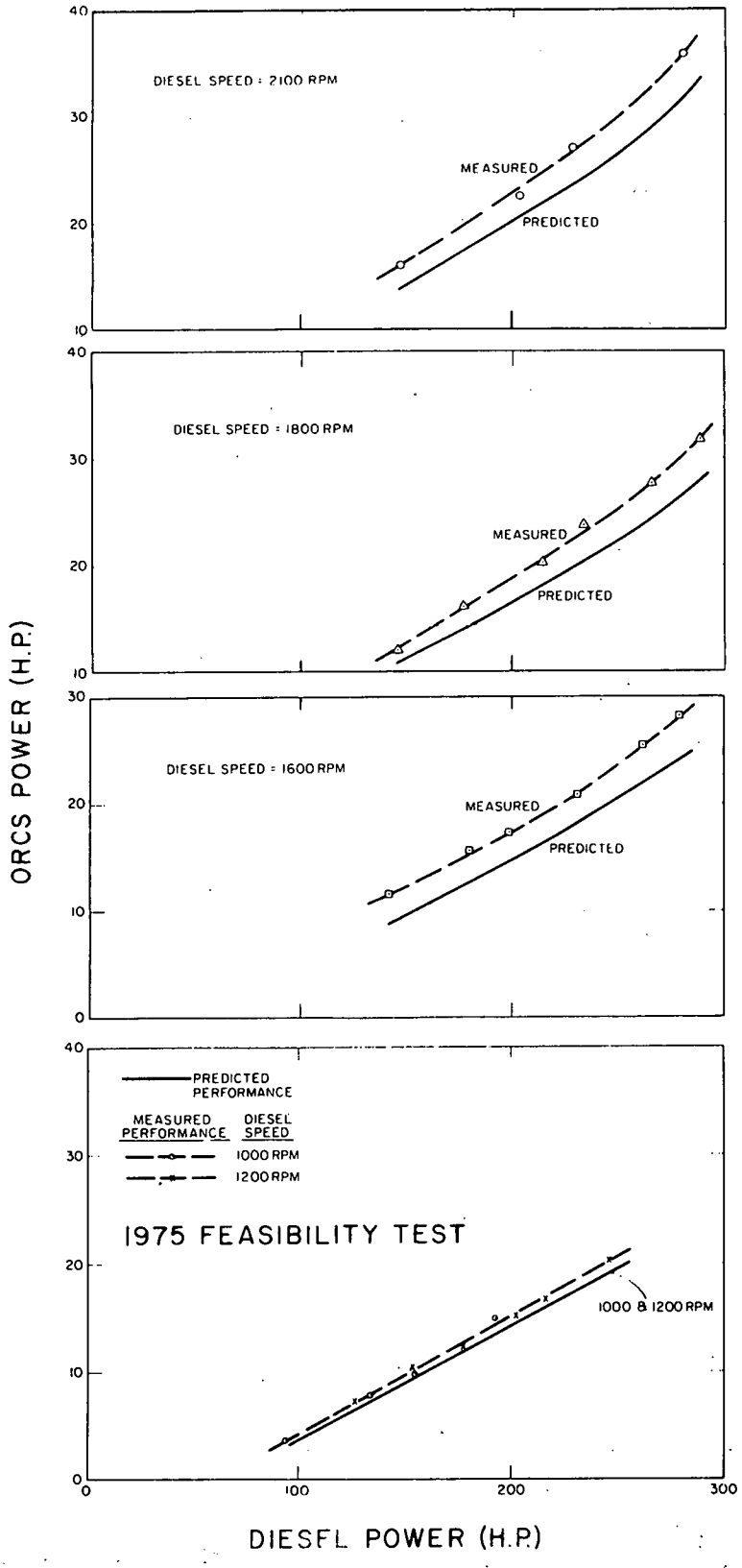

Figure 4.2 ORCS Power versus Diesel Power

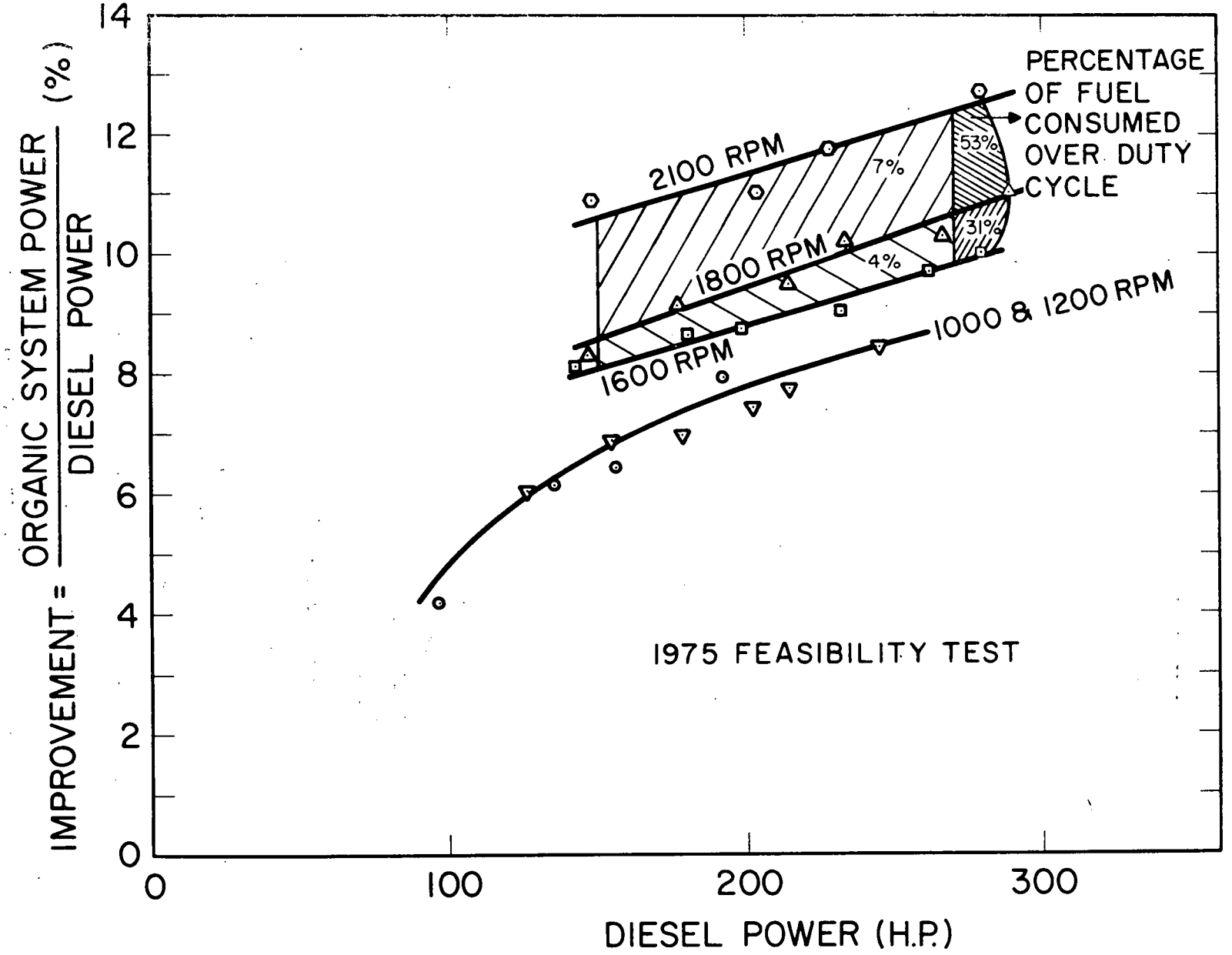

Figure 4.3 Measured Improvement versus Diesel Power Showing Truck Duty Cycle Operating Regions

predicted performance in Figure 4. 4 at various speeds and power levels as a function of organic fluid flow rate. The overall efficiency of the TGU was consistently higher than predicted for tests made at the speeds and power levels indicated. At the maximum ORCS power condition, a TGU efficiency of 61. 5 percent was measured as compared with the predicted value of 54. 8 percent. This improved performance was due to turbine modification made in adapting this machine to this particular application as previously described in Section 2. 2.

4. 2. 3 Vapor Generator Performance

During the initial tests on the diesel-ORCS, a temperature variation existed at the outlet of the three parallel circuits of the vapor generator. Metering valves were installed at the inlet of each circuit of the vapor generator. These valves were adjusted during subsequent tests until the outlet temperatures were balanced. There were no more temperature balancing problems encountered in the vapor generator in any of the subsequent testing, and installation of these valves proved to be a simple and effective solution to the problem.

Analysis of the heat transfer data showed that the performance of the vapor generator agreed with the predicted performance at low to medium power levels, while it was somewhat below the predicted performance at higher power levels. Although the vapor generator did not fully achieve the expected performance, the total heat transfer was close to the predicted levels as shown in Figure 4. 5 which presents vapor generator heat transfer rate as a function of exhaust gas flow rate. The expected heat transfer was achieved as a result of the higher-than-expected diesel exhaust gas temperatures

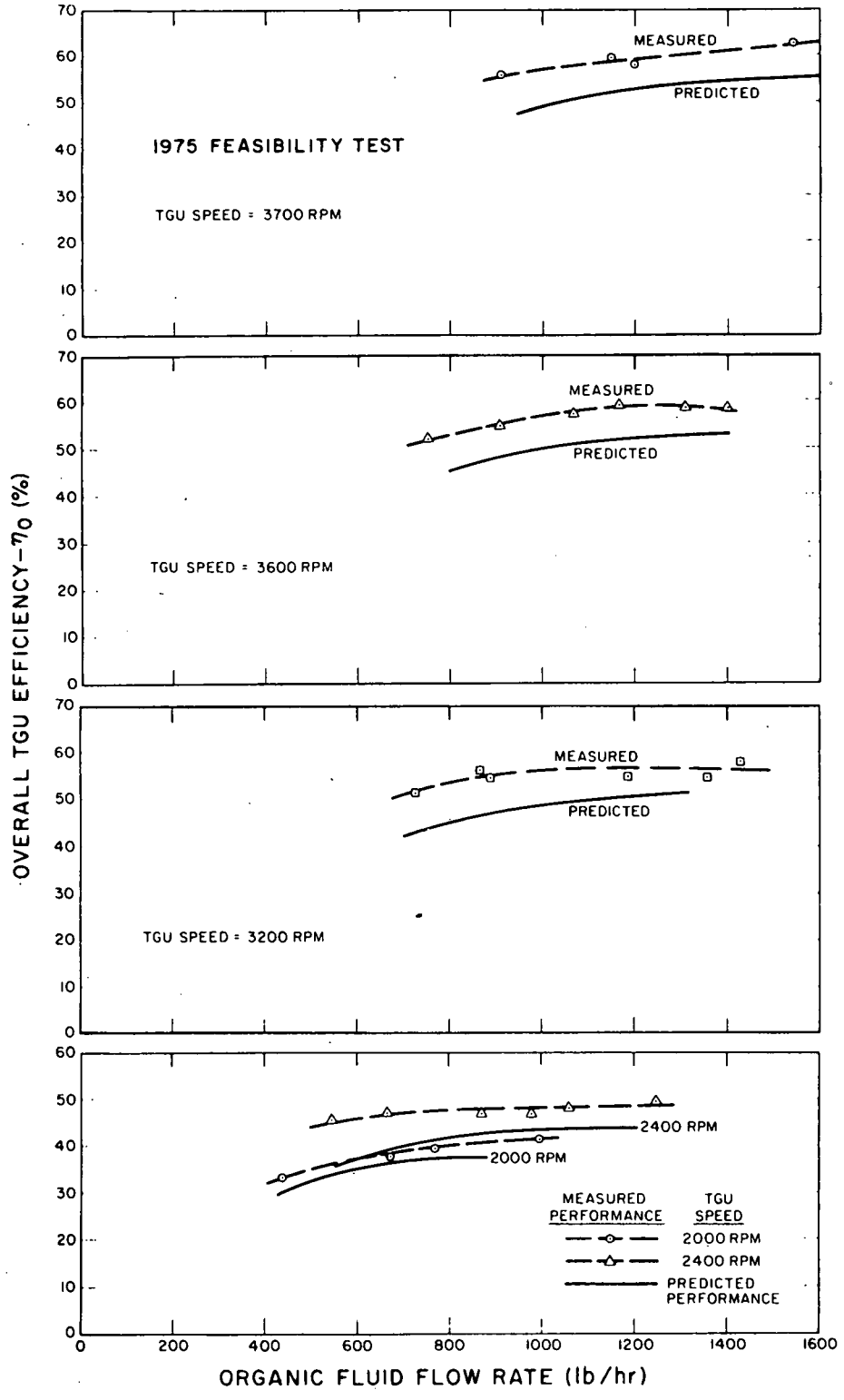

Figure 4.4 Overall Turbine Gearbox (TGU) Performance

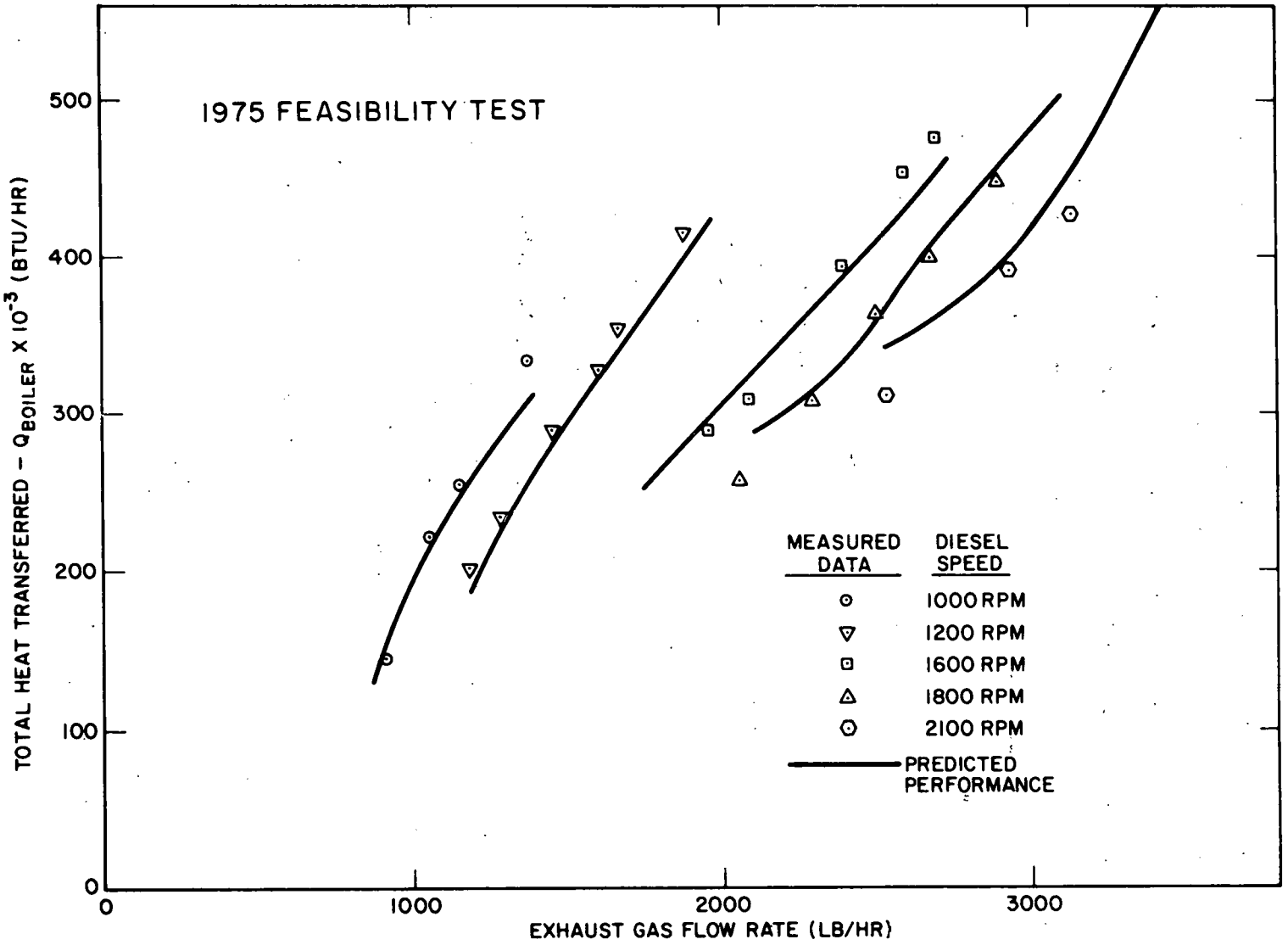

Figure 4.5 Vapor-Generator Heat Transfer Versus Exhaust Gas Flow Rate

measured in these feasibility tests. (Diesel performance data are presented in the following paragraph.) Because of the higher exhaust gas temperatures, the organic flow rate required to achieve the expected ORCS power levels was more than attainable and contributed to increased performance of the ORCS. Figure 4.6 shows organic fluid flow rate as a function of fuel flow rate for the tests compared with the predicted relationship.

4.2.4 Diesel Engine Performance

The brake horsepower, exhaust gas flow rate, and exhaust gas temperature of the diesel engine were measured as a function of speed and fuel flow rate. Figures 4.7 through 4.9 show these measurements made at TECO compared with Mack data as a function of fuel flow rate for 1000, 1200, 1600, 1800, and 2100 rpm diesel speeds. Brake horsepower and exhaust gas flow rate are in excellent agreement at all power levels and speeds tested. The exhaust gas temperatures measured at TECO were consistently higher than those measured at Mack at all power levels and speeds although shielded thermocouples were used in both sets of measurements. Further investigation led to the conclusion that the temperature measurements were made accurately at both TECO and Mack. The reasons which could account for the difference in the exhaust gas temperature measurements are:

1. The diesel engine used at TECO is physically different from the one used at Mack, although it is the same model (a Mack ENDT 676).

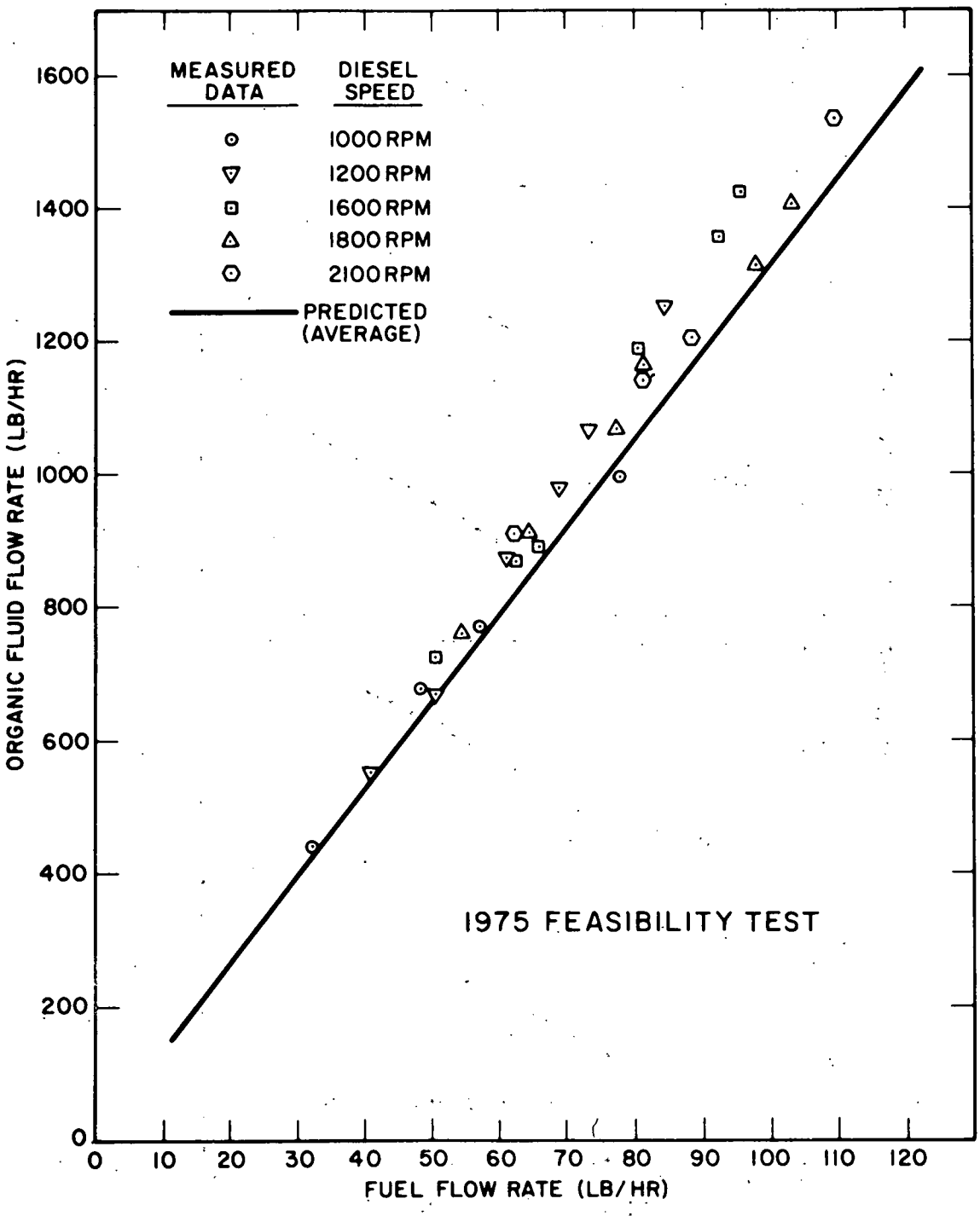

Figure 4.6 Organic Fluid Flow Rate Versus Fuel Flow Rate

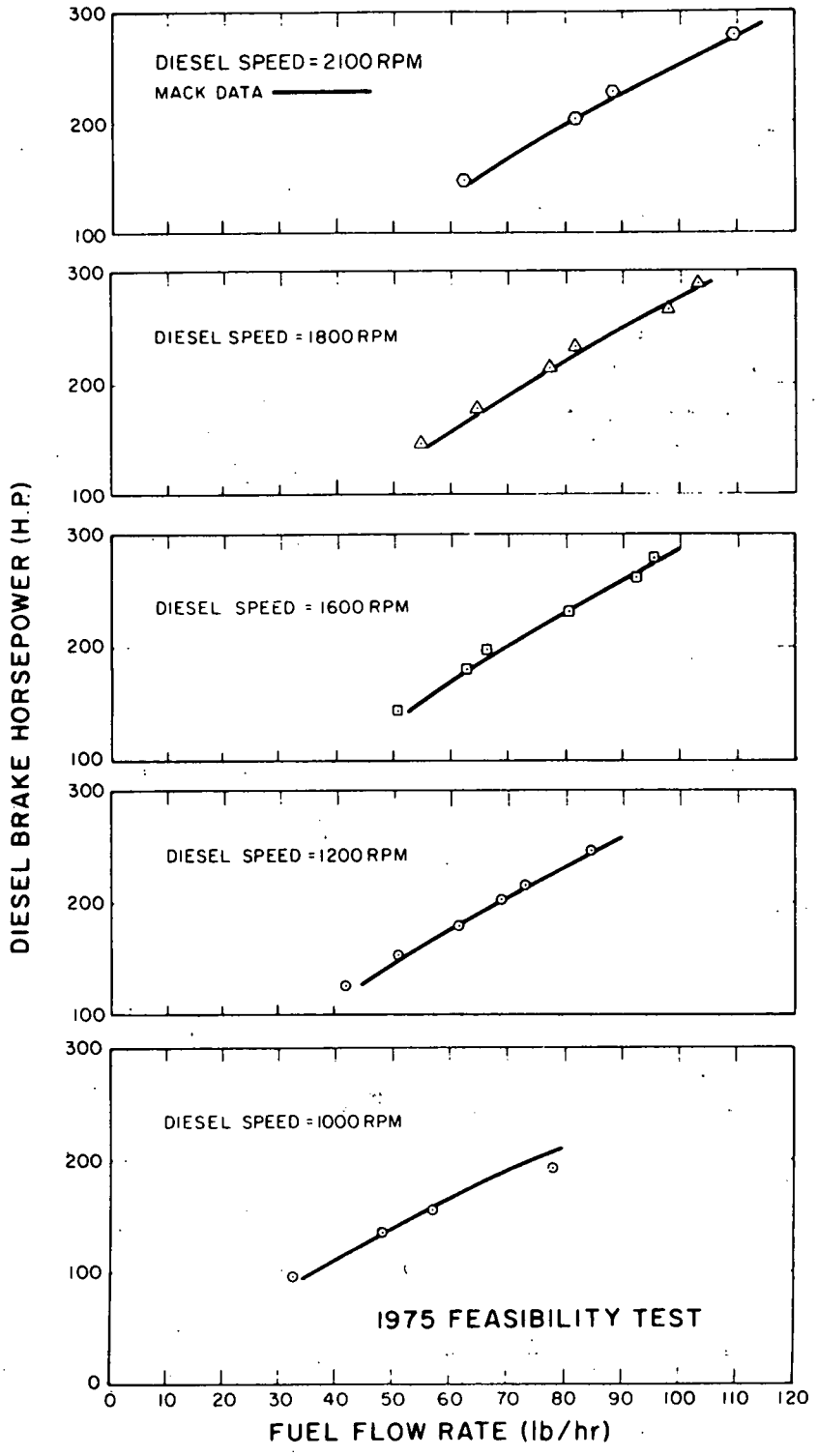

Figure 4.7 Diesel Power versus Fuel Flow Rate

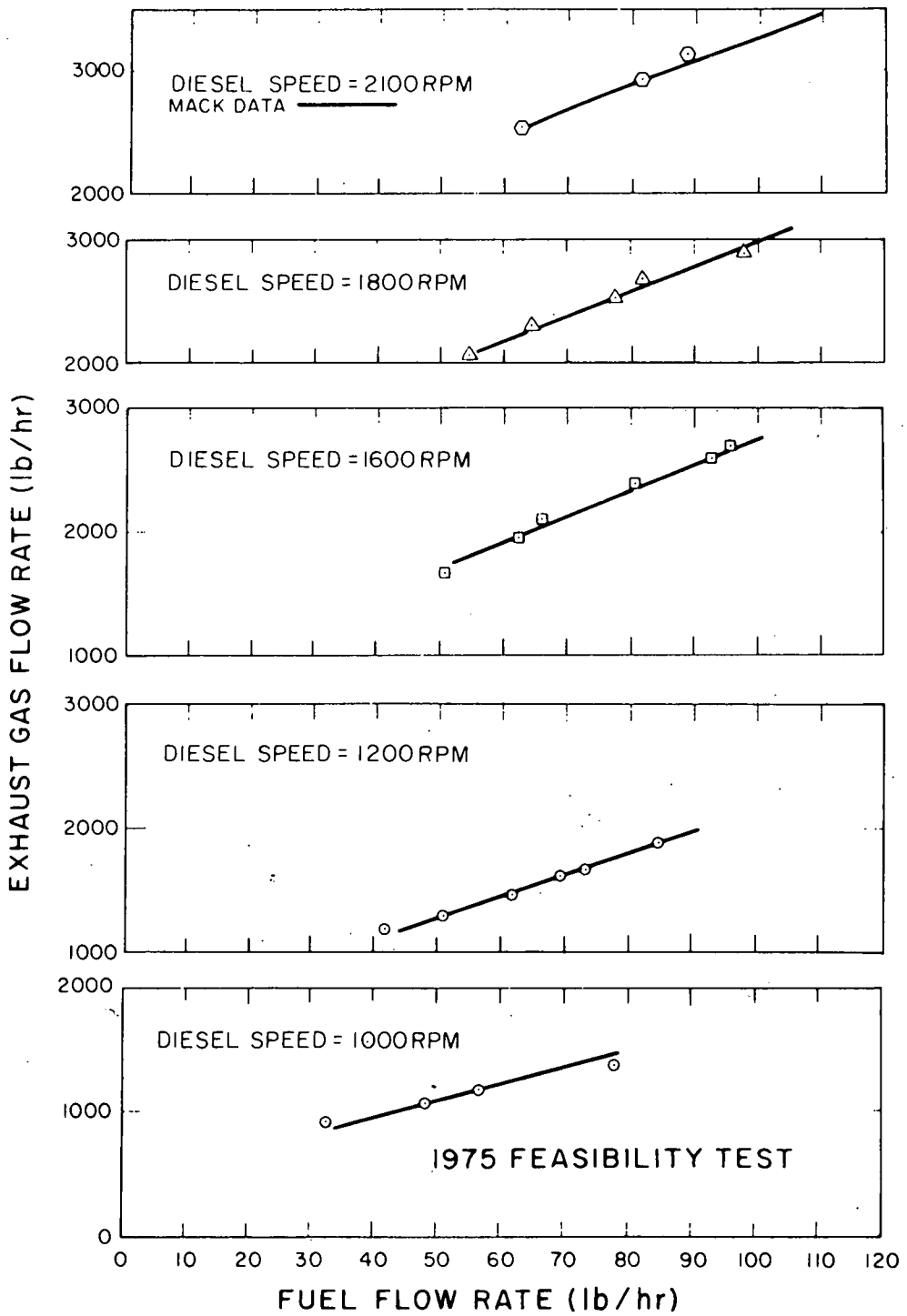

Figure 4.8 Exhaust Gas Flow Rate versus Fuel Flow Rate

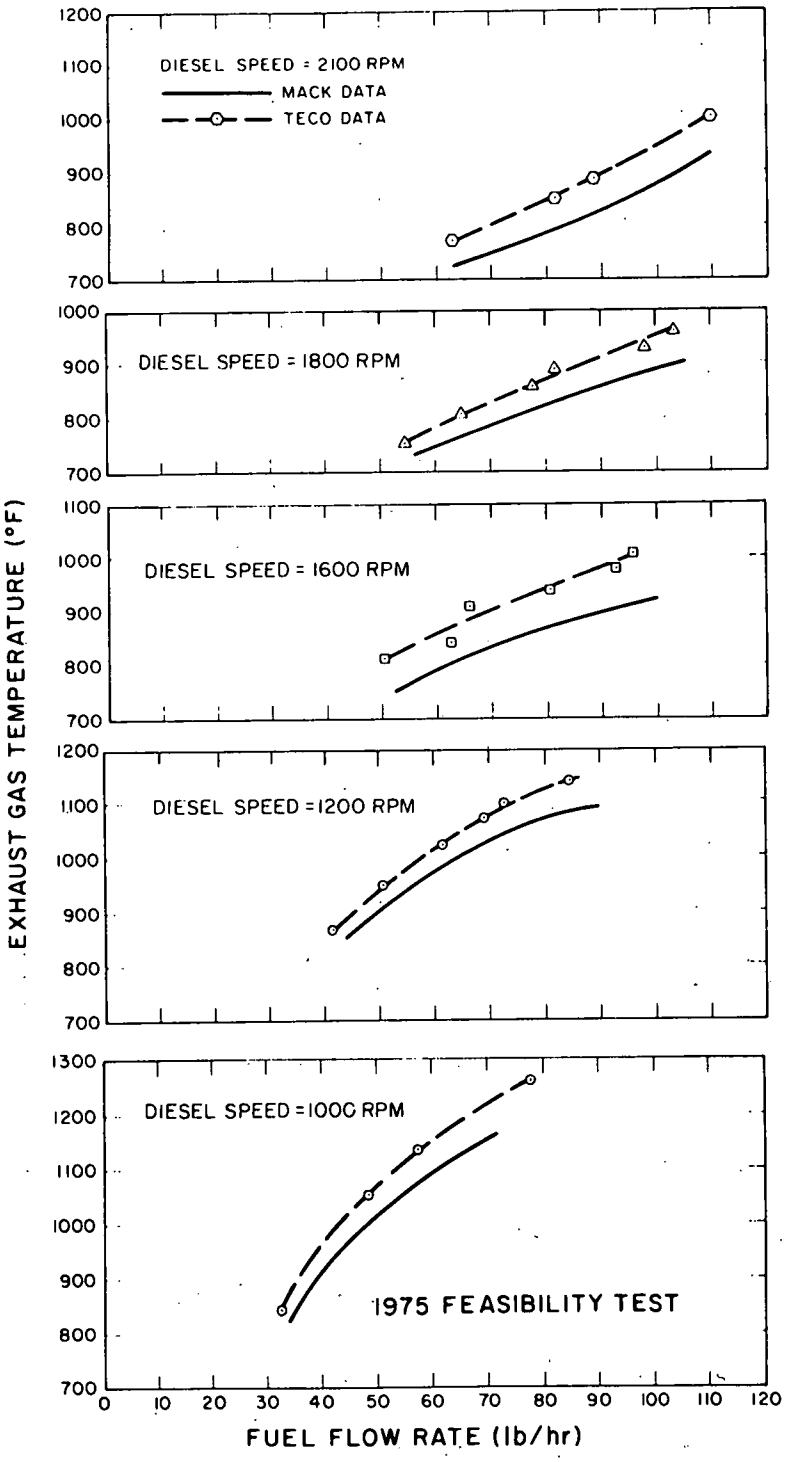

Figure 4.9 Exhaust Gas Temperature versus Fuel Flow Rate

2. The exhaust line from the diesel engine to the vapor generator in the TECO system is insulated; the Mack tailpipe was uninsulated.

3. The Mack data were measured with a maximum back pressure of 1.5 inches of Hg; most of the TECO data were taken at back pressure levels higher than 1.5 inches of Hg but less than the Mack recommended maximum of 3.0 inches of Hg.

4.3 TRANSIENT TESTS

Tests were performed on the diesel-ORCS to study the transient response characteristics of the demonstration hardware and to evaluate the test results for use in the design of the prototype system controls. The prototype control schematic is given in Figure 4.10. The prototype system will use a variable displacement feedpump similar to the one used in these demonstration tests. The pump is used to vary the organic flow rate which is the prime ORCS control parameter. The key element of the control system is the flow rate control which takes the fuel flow rate as an input and sets the proper organic flow rate. The fuel flow rate is measured by the rack position and speed of the diesel engine. The organic flow rate, in turn, is controlled by varying the displacement of the feedpump at a given pump speed. Since the feedpump speed is directly proportional to the diesel speed, displacement of the pump is a unique function of the rack position, and the two will be directly coupled in the prototype system. A more comprehensive and detailed description of the complete control system for the prototype diesel-ORCS is given in the Task I Interim Report attached as an Appendix.

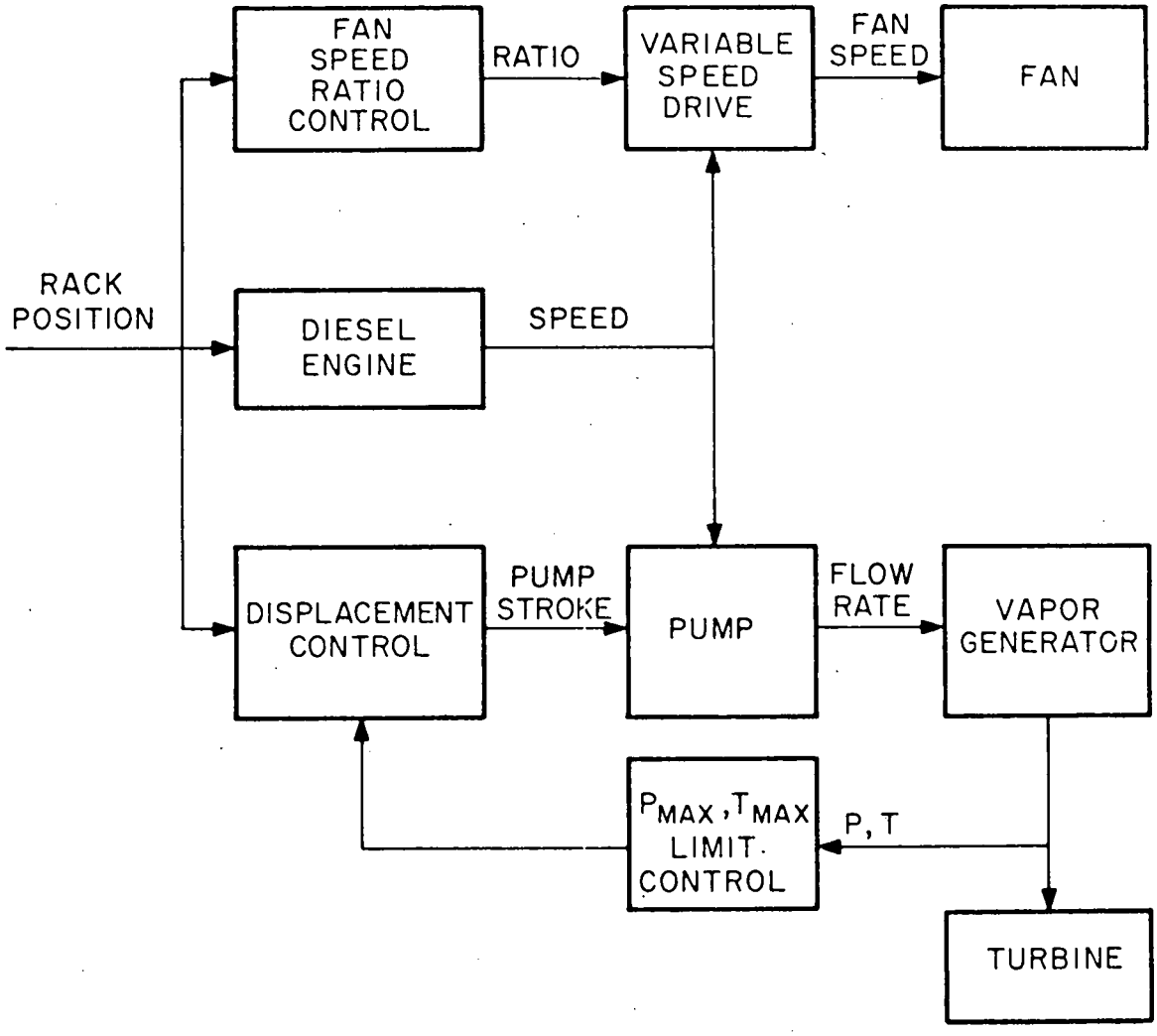

Figure 4.10 Diesel-ORCS Compound Engine - Control Schematic

The transient studies consisted of conducting two types of tests on the demonstration system. The first set of transient tests was made at constant diesel and turbine-gearbox speeds with step changes in fuel and organic flow rates. The second group of transient tests was performed at constant fuel and organic flow rates with step changes in diesel and turbine-gearbox speeds. Figure 4. 11 shows graphically the type and specific transient tests which were performed. The constant speed transient tests were made for both increasing and decreasing fuel flow rate, and the constant flow rate tests were made for both increasing and decreasing speed.

Data were continuously recorded during these transient tests to study the effect on various parameters. Data taken during the constant speed transient tests are shown in Figures 4. 12 and 4. 13. These tests correspond respectively to tests S3 and S4 as shown in Figure 4. 11. These tests were made at a constant diesel speed of 1800 rpm and a constant turbine-gearbox speed of 3600 rpm. Figure 4. 12 represents a test where the fuel flow rate was increased with a corresponding increase in organic flow. Figure 4. 13 represents a decreasing flow rate transient. All the important parameters were monitored during the tests, and these sample outputs show the response of various temperatures and pressures as well as flow rates, torques, and speeds of both the diesel and turbine-gearbox unit. In these particular tests the diesel-fuel flow rate and organic flow rate were controlled independently. The other parameters followed the changes made in flow rate without any excessive excursions and stabilized to the steady-state end condition fairly rapidly.

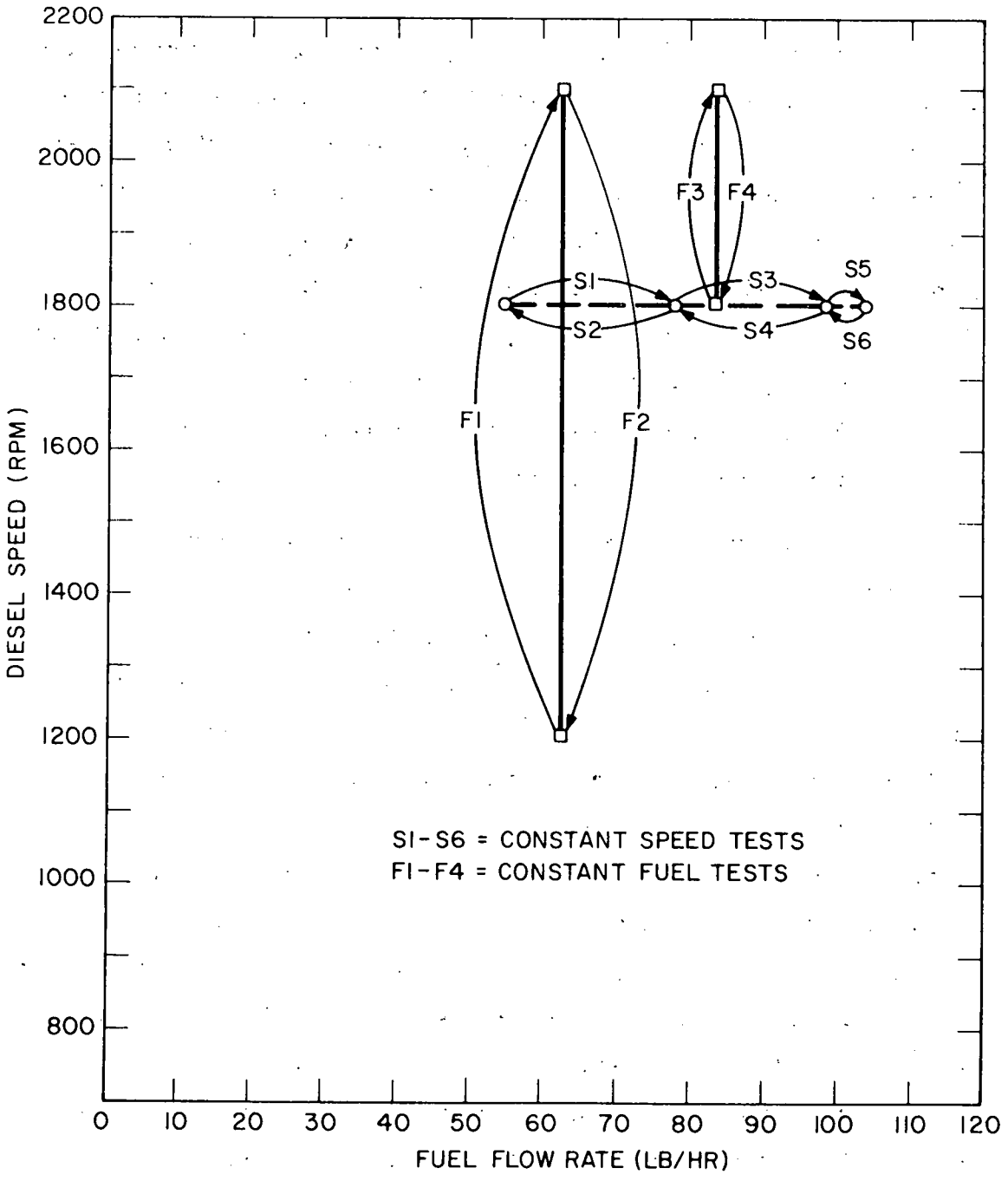

Figure 4.11 Diesel-ORCS Transient Tests

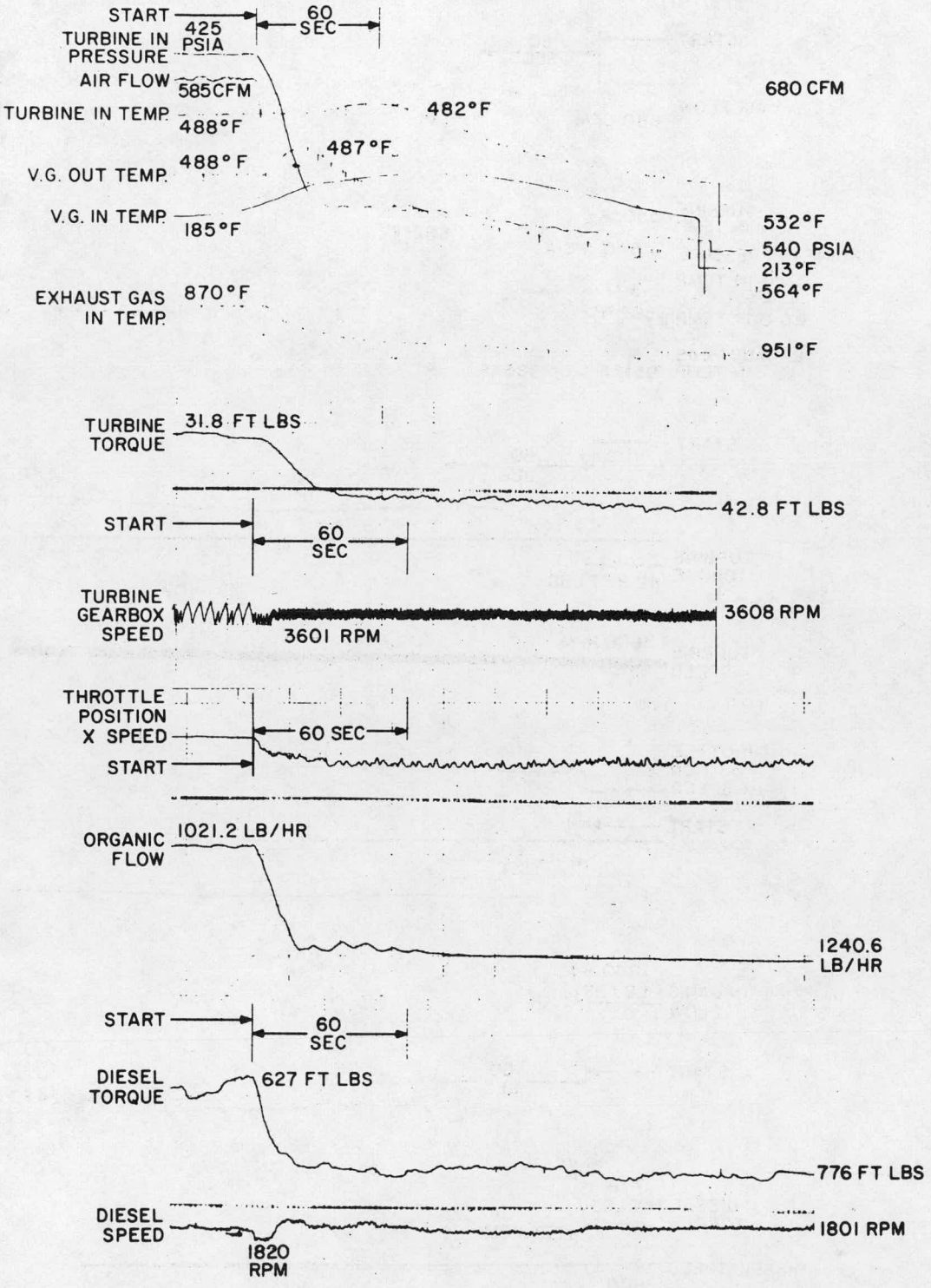

Figure 4.12 Constant-Speed, Increasing-Flow Transient Test S3

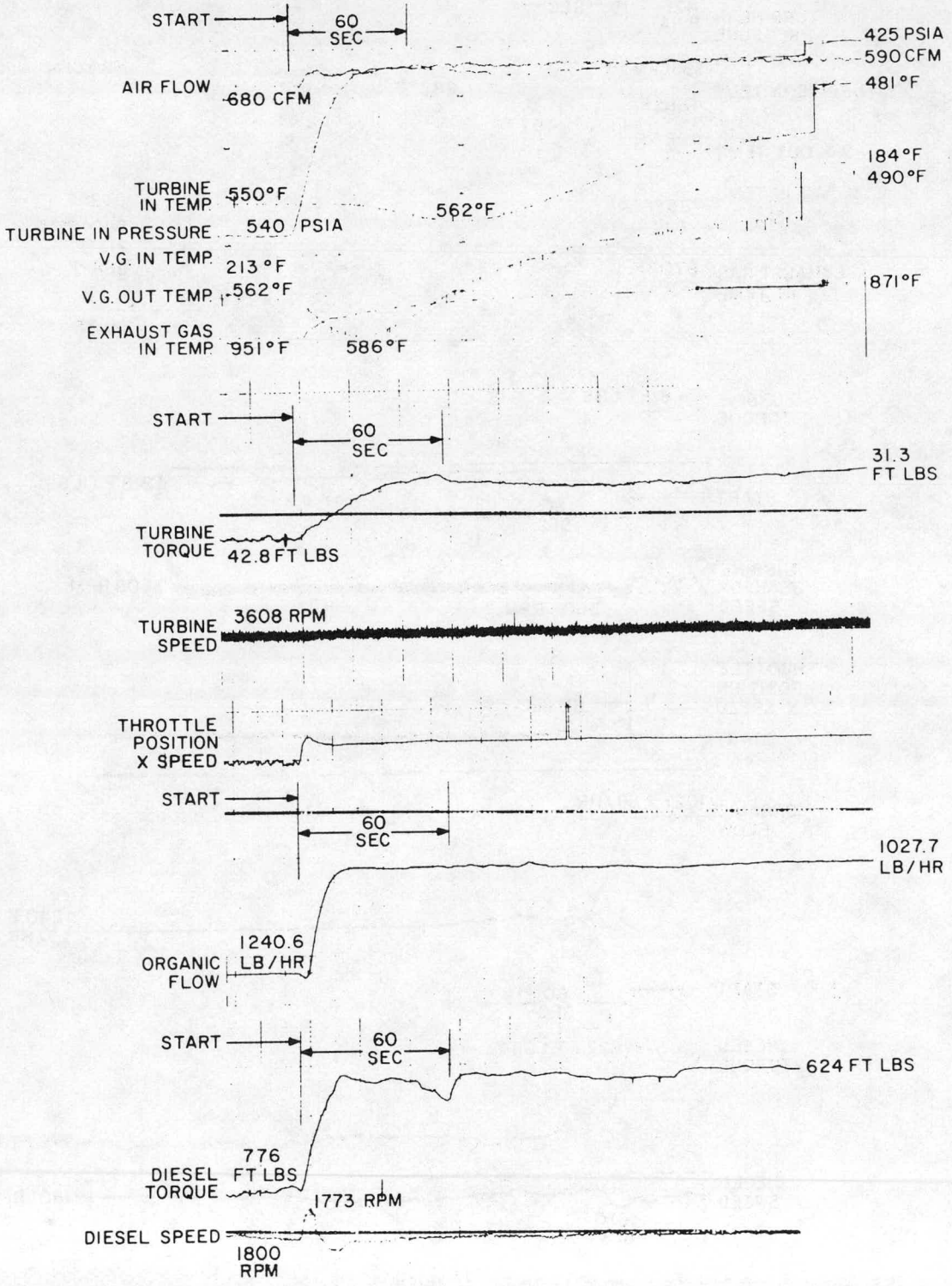

Figure 4.13 Constant-Speed, Increasing-Flow Transient Test S4

Figure 4. 14 is a graph showing the constant-flow rate, variable-speed, transient test shown in Figure 4. 11 as Test F1. The flow rates were held constant while the speed was increased from 1200 to 2100 rpm on the diesel and from 2400 rpm to 3700 rpm on the turbine-gearbox unit. Data from test F2 in Figure 4. 11 are presented in the sample output of Figure 4. 15. This test was made at the same flow rate conditions but with decreasing speed. These test data also show no excessive excursions in any of the parameters measured. The data do show that the change in turbine speed was accomplished in half the time required to make the change in diesel speed and torque. This effect was due to the independent manual control of each of these parameters in the demonstration tests. The behavior of temperatures, pressures, and other parameters of the system indicates that the control for the organic flow will be very manageable for the prototype system. This fixed, power-variable speed test is representative of what typically occurs when a truck is driving up a grade for the decreasing speed case.

The data for these variable speed tests also show a change in the trace of fuel flow which actually did not occur. The transient trace of fuel flow was obtained by multiplying the diesel throttle position by the diesel speed. This method was used because the throttle position is easily measured as well as the speed, whereas the actual diesel rack position is not easily accessible. The relationship between diesel throttle position and rack position was treated as linear for the purpose of the transient tests. As indicated by the steady-state fuel flow at the start and end of these transient tests, this relationship is not a linear one. Since the rack position and

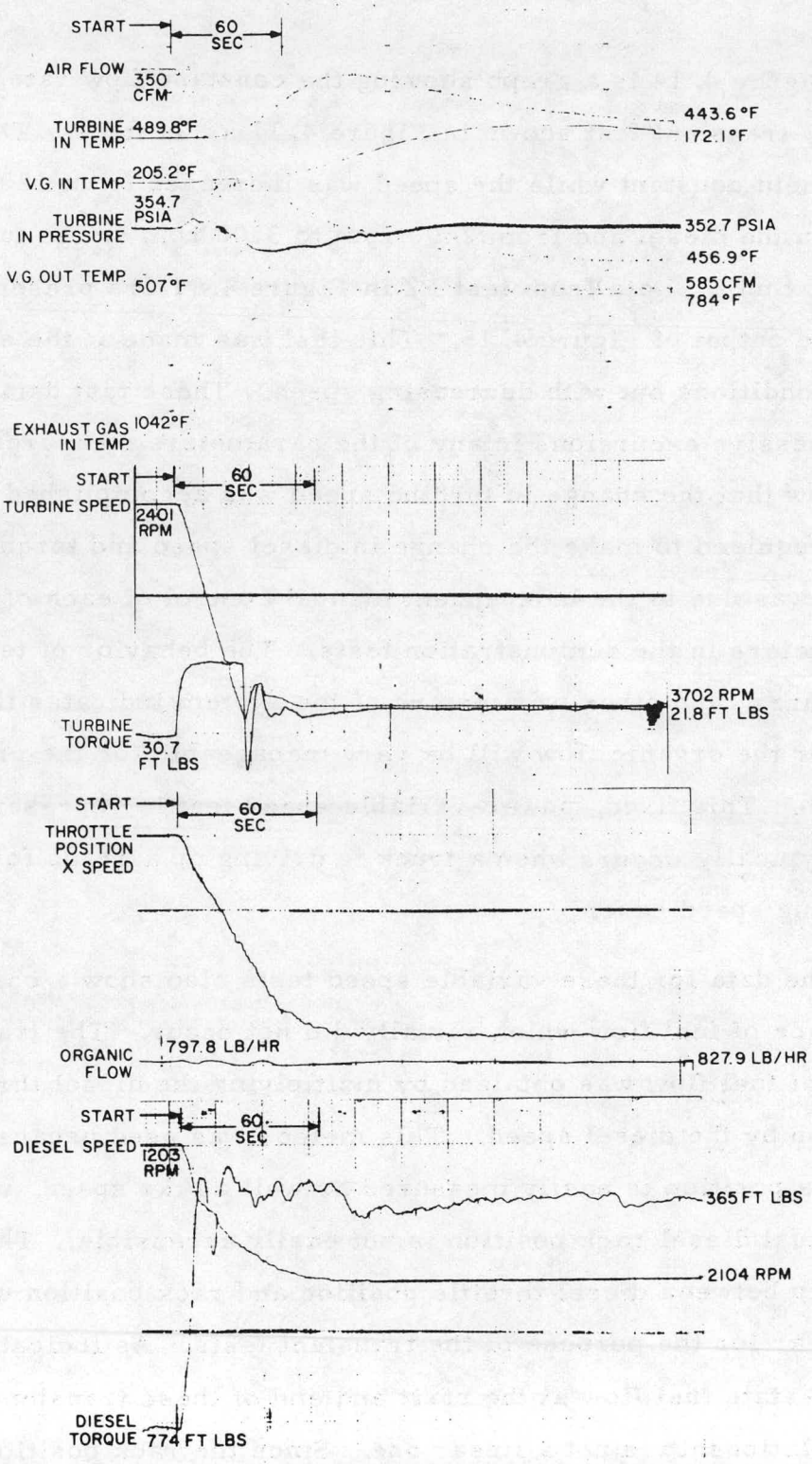

Figure 4.14 Constant-Flow, Increasing-Speed Transient Test F1

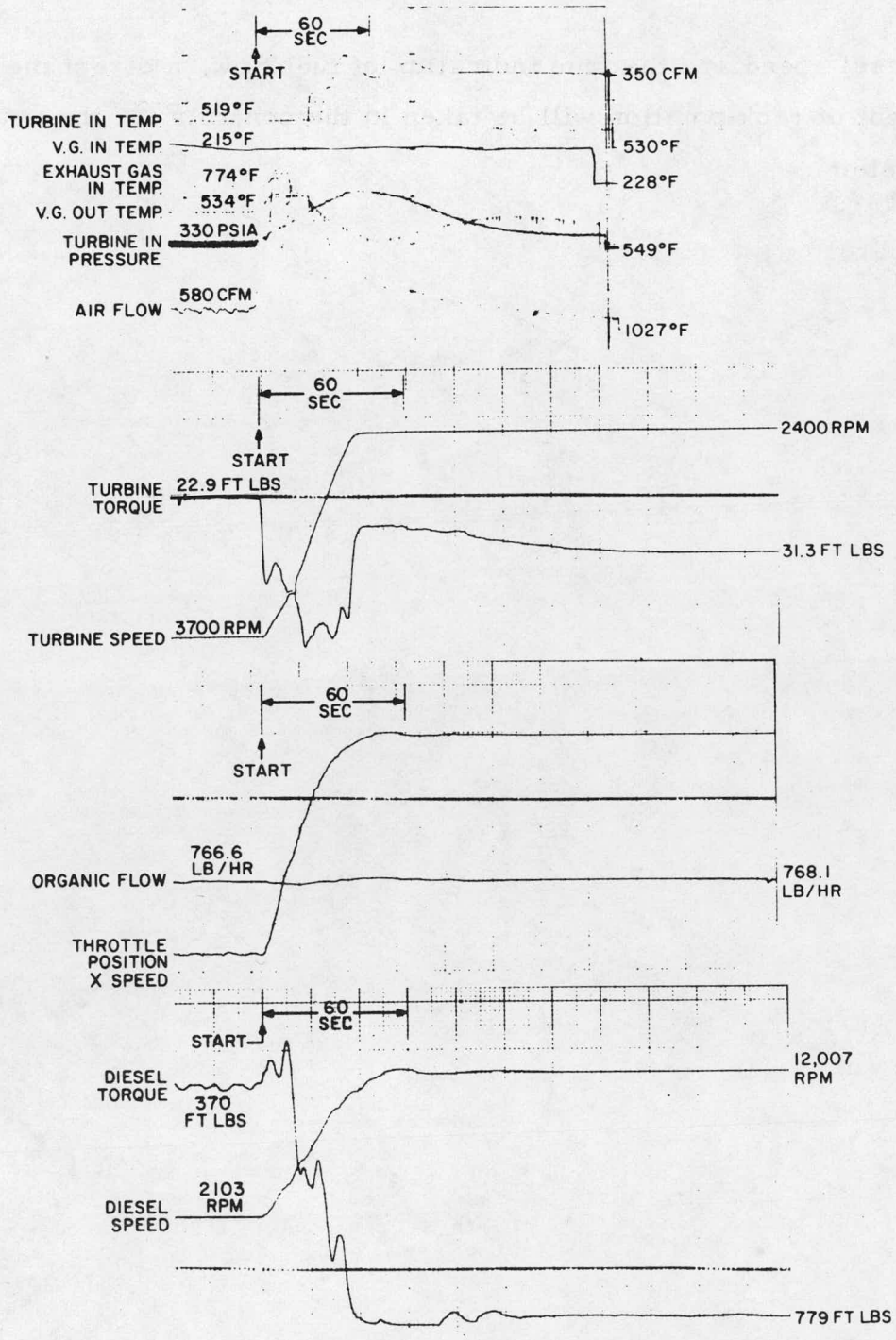

Figure 4.15 Constant-Flow, Decreasing-Speed Transient Test F2

diesel speed are the true indication of fuel flow, a direct measurement of rack position will be taken in the controls for the prototype system.

5. CONCLUSIONS

By utilizing wasted energy associated with the exhaust gases, the Organic Rankine bottoming cycle provides a viable solution for fuel economy improvement in long-haul diesel trucks. The demonstration tests have proven the feasibility of the diesel-ORCS compound engine and have shown the potential of the prototype system. The feasibility tests have been successful in demonstrating and accomplishing the following:

1. The efficiency of a diesel truck engine has been increased with an organic Rankine cycle system (ORCS) to recover waste heat.

2. Existing hardware has been used at the TECO test facility to achieve an early demonstration of the feasibility of the diesel-ORCS compound engine.

3. Steady-state tests have been performed over the normal operating range of the diesel engine which yield better performance results than those initially predicted for the diesel-ORCS.

4. The transient response characteristics of the demonstration hardware have been evaluated for the diesel-ORCS and indicate a simple and manageable prototype control system.

5. The test results from the feasibility demonstration of the diesel-ORCS have provided useful information which will be used in the final design of the prototype system.

APPENDIX

TASK I INTERIM REPORT

CONCEPTUAL DESIGN STUDY
ON
COMPOUNDING THE INTERNAL COMBUSTION ENGINE
FOR AUTOMOTIVE VEHICLES

TABLE OF CONTENTS

TABLE OF CONTENTS (continued)

LIST OF ILLUSTRATIONS

LIST OF ILLUSTRATIONS (continued)

LIST OF ILLUSTRATIONS (continued)

LIST OF ILLUSTRATIONS (continued)

LIST OF ILLUSTRATIONS (continued)

1. INTRODUCTION

Increasing emphasis on improving both fuel economy and emissions provides a strong incentive for development of systems that convert currently wasted energy in automotive vehicles to useful power.

The major portion of the waste energy in an internal combustion engine is associated with the exhaust gases. This exhaust energy is available at temperatures in the range from 700°F to 1500°F at full load, depending upon the type of internal combustion engine. However, at the off-design power levels encountered in typical duty cycles the exhaust gas temperature drops significantly. Thus the maximum temperatures available for use in the waste heat recovery process are limited. For automotive application, the sink temperature would correspond to the maximum ambient temperature at which the system is expected to operate. Therefore, any practical waste heat utilization system would have to perform efficiently in a relatively low temperature range.

The organic Rankine-cycle system (ORCS) offers the best potential for utilizing the internal combustion engine exhaust energy due to its relatively high cycle efficiency at moderate peak cycle temperatures of 550°F to 650°F. The thermodynamic properties of the proposed organic fluid, Fluorinol-50 (50 mole percent trifluoroethanol and 50 mole percent water), which has a low latent heat requirement, make it possible to extract the maximum heat at the highest possible pressures and temperatures for a given exhaust temperature. In a thermodynamic sense, this means that the temperature difference between the exhaust gas and the organic fluid is held to a minimum during the heat addition

process, thereby reducing the thermodynamic irreversibilities.

The organic Rankine bottoming cycle can be considered for various automobile and truck applications. The most attractive use, however, is in large, heavy-duty diesel trucks for long distance hauling. Here, the engine load and speed requirements are nearly constant over a large portion of the operating hours, and high mileages are accumulated. Thus, the potential fuel savings are sufficient to justify the added cost of a bottoming cycle system.

In this study, a detailed state point analysis of the ORCS was carried out for a reference diesel truck. Parametric studies were made to determine the sensitivity of the ORCS net power to the performance of various ORCS components. Part load performance was also computed, and duty cycle fuel economy projections were made. Conceptual design and system integration studies, including coupling the Rankine cycle expander to the diesel engine, were conducted to determine an optimum configuration for the compound engine. A conceptual design and a layout for each component were also prepared.

2. REFERENCE TRUCK-DIESEL ENGINE DESCRIPTION

For the evaluation and design of the compound system, a 676 CID Mack Truck diesel engine was selected. This engine is rated at 288 bhp at 2100 rpm. This engine has excellent brake specific fuel consumption (BFSC) characteristics and was selected because its horsepower rating is representative of the typical engine used for this application. Mack Trucks, Inc. provided the prototype engine data in July 1974. This is shown in Figure 2.1. These characteristics were used in optimizing the Organic Rankine Cycle System (ORCS) for this application. Subsequently, in November 1974 Mack Trucks, Inc. measured data on a production engine similar to the one that will be used for the demonstration tests. These data are shown as solid lines on Figure 2.1. The production engine showed higher exhaust gas energy due primarily to higher temperature and lower BSFC characteristics than the prototype engine. Because of the schedule problem, optimization studies were not repeated for the new characteristics. In turn, performance of the components was evaluated corresponding to the production engine characteristics to project fuel economy improvements due to ORCS. The performance measurements of the production engine at Mack Trucks, Inc. are shown in Appendix A.

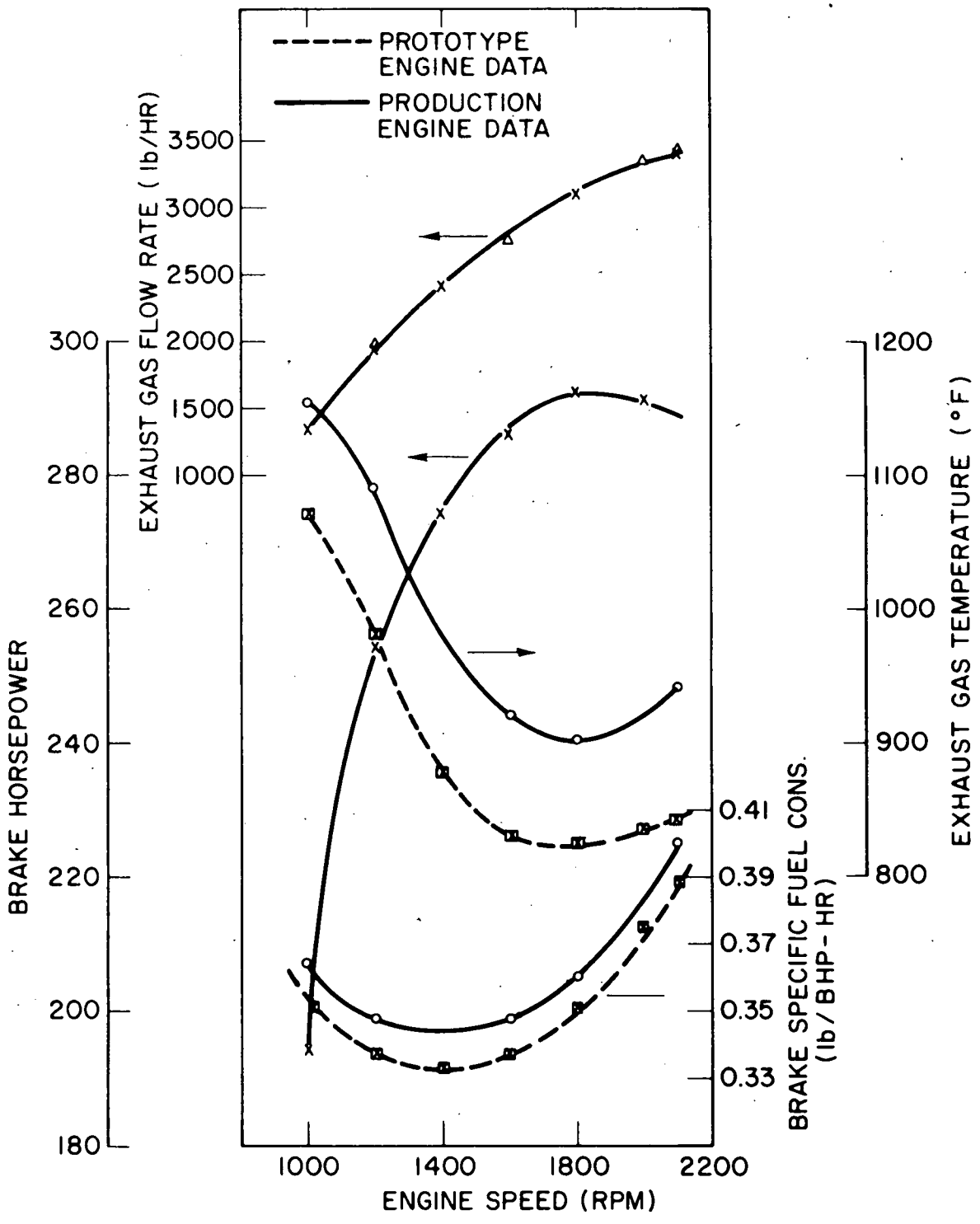

Figure 2.1. Performance Data, Mack ENDT 676 Engine.

3. ORCS - DIESEL COMPOUND ENGINE DESCRIPTION

A schematic of an ORCS-Diesel compound engine is shown in Figure 3.1. The working fluid used is Fluorinol-50, which is a mixture of 50 mole percent trifluoroethanol and 50 mole percent water. The characteristics of Fl-50 are shown in Table 5.1. The selection of the working fluid was based on the conclusions of an optimization study discussed in the next section. The design point was selected to be the maximum power point at 2100 rpm. The working fluid conditions and flow rates were also derived from the various optimization studies described in the next section.

The thermodynamic cycle of the working fluid is shown on T-S and P-H diagrams at the design point in Figures 3.2 and 3.3. In these figures (1) - (2) is the feedpump work, (2) - (3) the regenerator liquid heating, (3) - (4) the vapor-generator heating, (4) - (5) the vapor expansion in the turbine, (5) - (6) the vapor partial sensible cooling in the regenerator and (6) - (1) the vapor heat rejection and condensation in the condenser.

There are three interfaces between the ORCS and the diesel engine:

- The vapor-generator represents an exhaust gas interface with the diesel engine. While the exhaust gas undergoes heat interaction with the working fluid, it also incurs a pressure drop which reflects in terms of higher back pressure of the turbine of the turbocharger. The vapor generator serves the dual function of a heat exchanger and a noise muffler. Thus any pressure drop over and

above that of the muffler is attributed to the vapor generator and any degradation in the diesel performance due to this additional pressure drop is charged to ORCS.

- The second interface is the cooling interface between the condenser and the diesel radiator. In order to make use of one fan for both the condenser and the radiator heat rejection, the radiator and condenser were integrated. The condenser is mounted upstream of the radiator. This is done to take advantage of higher ORCS efficiency with lower sink temperature. The air entering the radiator is preheated due to condenser heat rejection. This also keeps the radiator temperature variation in a narrow range in spite of a larger variation in the ambient temperature, which is desirable from the standpoint of the diesel engine. The system was designed to meet the heat rejection and temperature specifications for the radiator provided by Mack Trucks, Inc. The fan power requirements for the current radiator fan were provided by Mack. The ORCS was charged with the power required by the cooling fan over and above that of the diesel fan.

- The third interface is the mechanical interface where the ORCS power is fed into the diesel shaft. Mack offers an optional gearbox to take off power for any auxiliary drive system such as a cement mixer, etc. It is planned to couple the turbine gearbox to this P. T. O. gearbox, which already exists. The problems associated with this coupling such as torsional vibrations, etc. are discussed in later sections of this report.

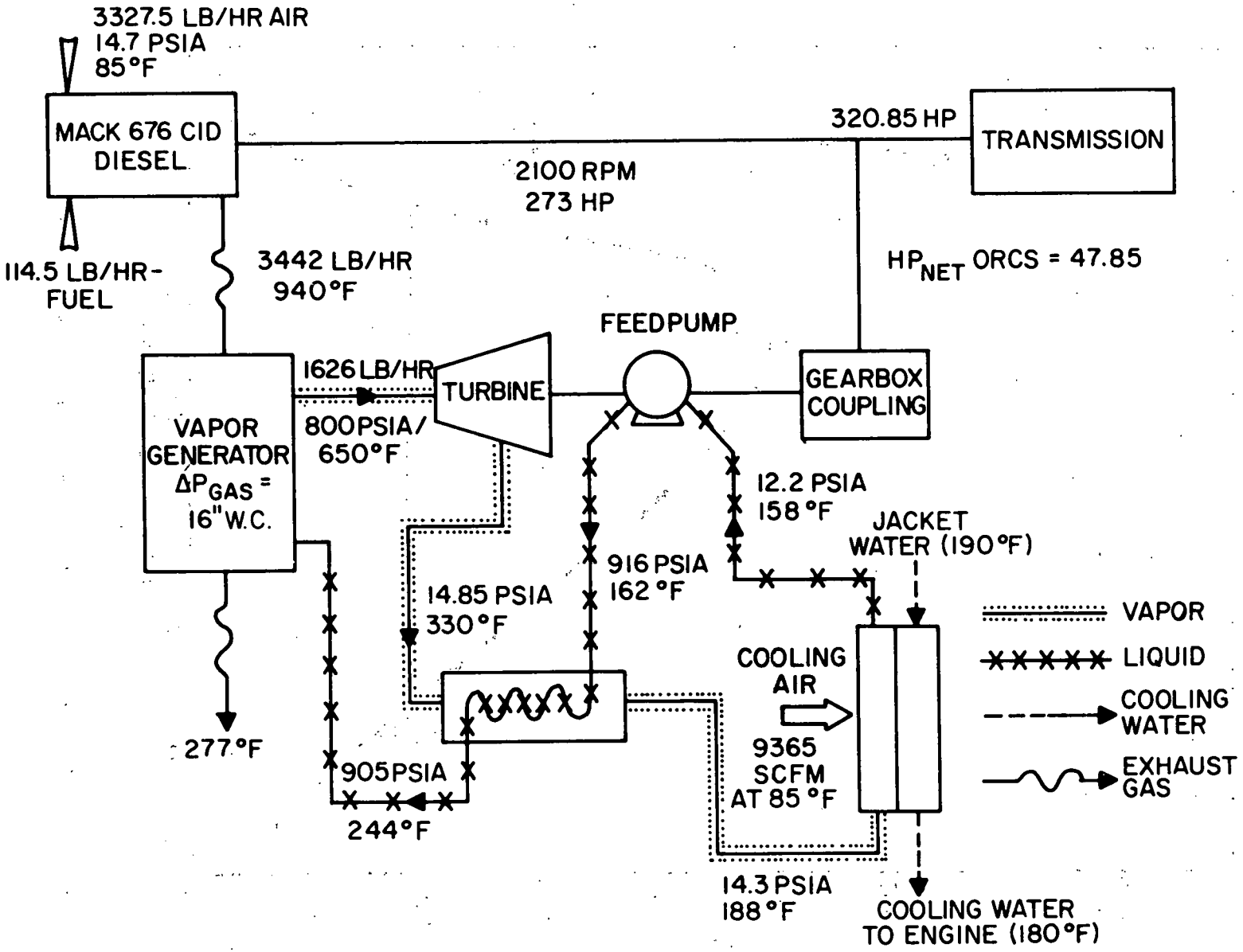

Figure 3.1. Diesel-Organic Rankine-Cycle Compound Engine Flow Schematic.

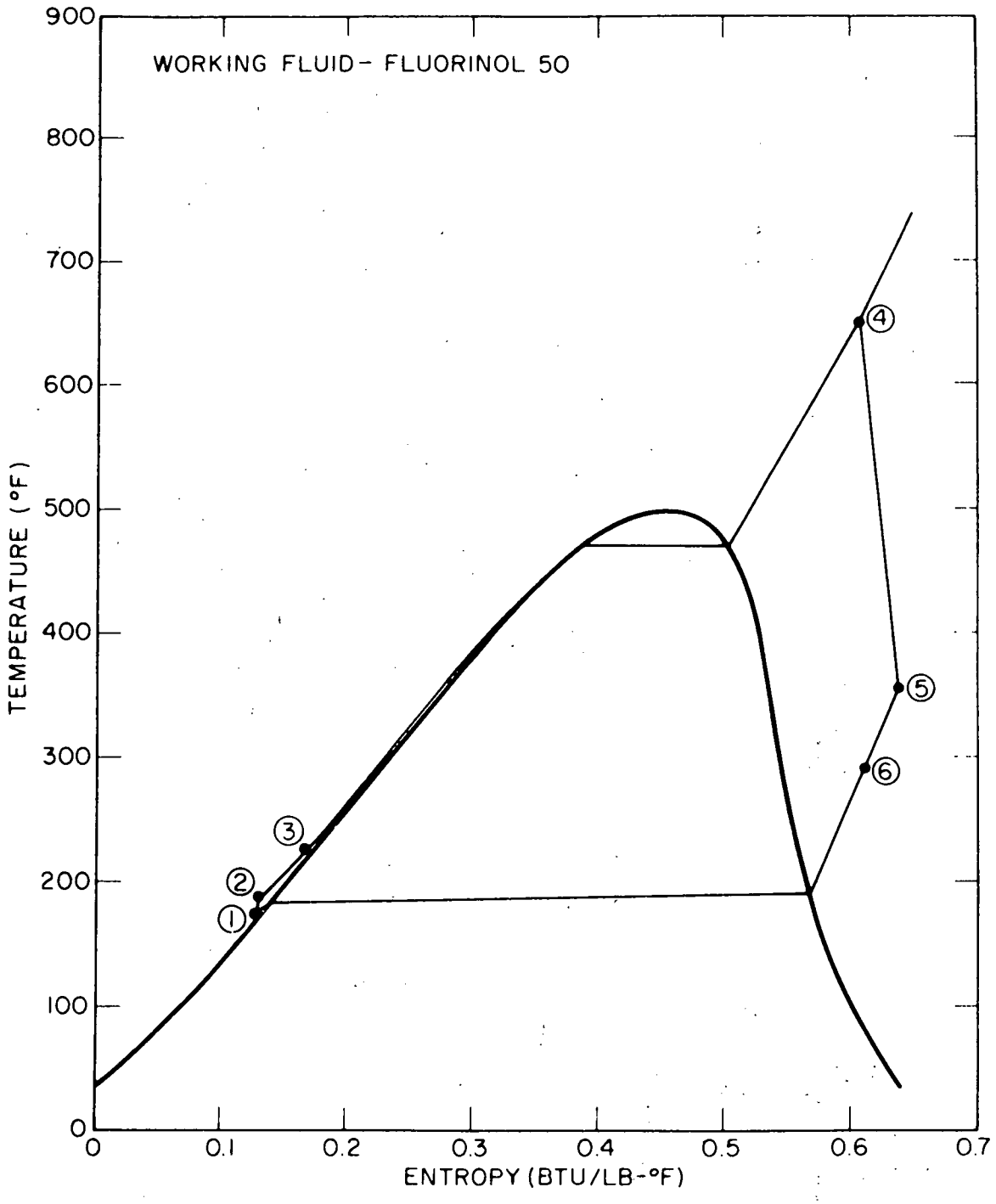

Figure 3.2 T-S Diagram for ORCS at Design Point

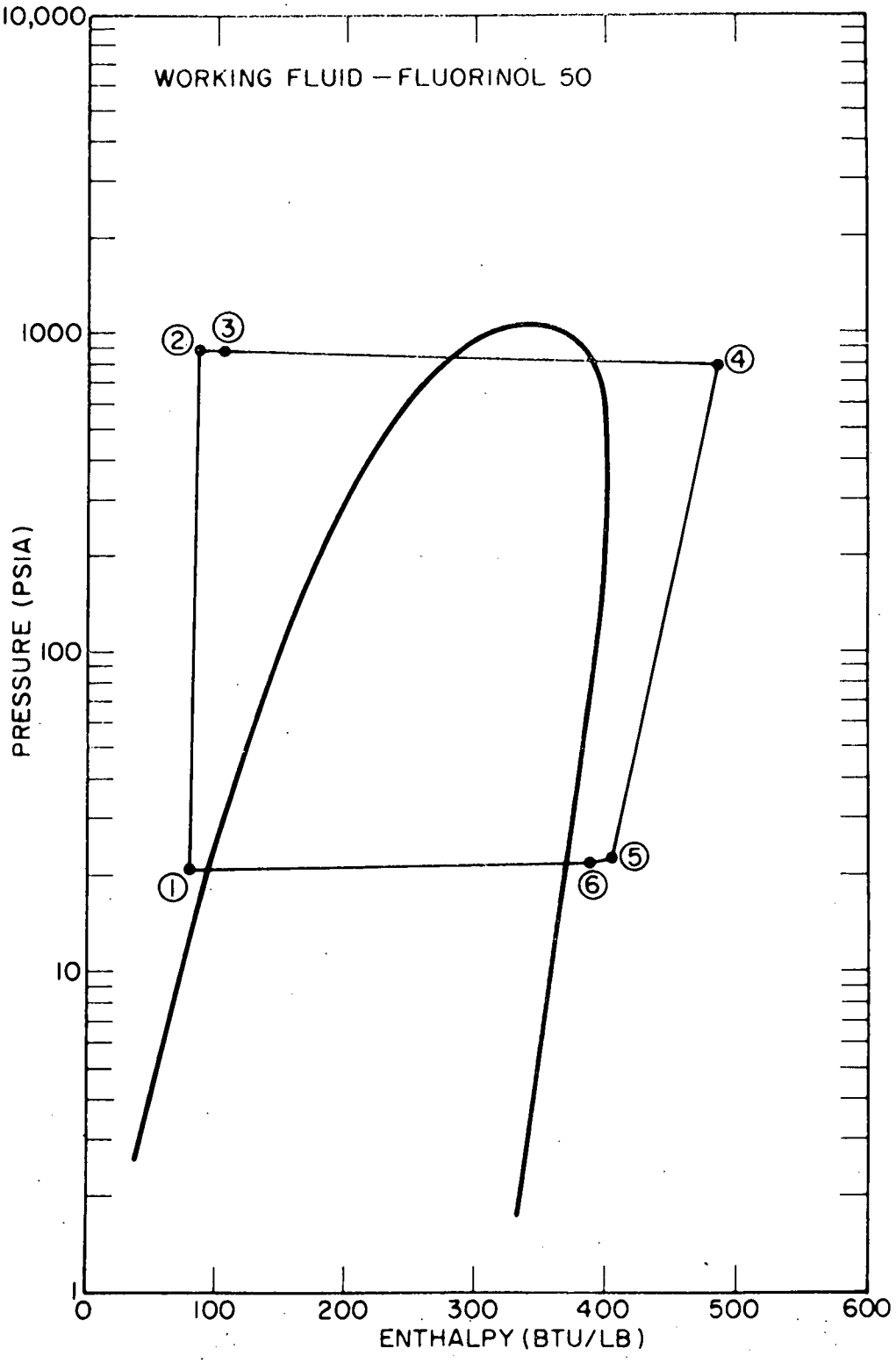

Figure 3.3 P-H Diagram for ORCS at Design Point

4. ORGANIC RANKINE CYCLE SYSTEM OPTIMIZATION STUDIES

4.1 SELECTION OF OPTIMUM WORKING FLUID

The maximum useful work which can be obtained from a relatively low temperature gas from a cyclic device while exchanging heat with an isothermal energy reservoir, i.e., the environment, is derived in Appendix B. The maximum work corresponds to a reversible cyclic heat engine operating with all the heat interactions taking place at zero ΔT (idealized). The work that is recovered from an actual system would be reduced by the irreversibilities of these systems. For a Rankine-cycle engine, this includes inefficiencies in the expander, feedpump and pressure losses. These losses prevent the engine from being internally reversible. In addition, the actual systems do not have external reversibility because of the temperature difference between the exhaust gas and the working fluid in the vapor-generator and the working fluid and the environment in the condenser of the Rankine-cycle power plant. The internal irreversibilities are mild functions of the working fluid. However, the working fluid has a strong influence on external irreversibilities. This is illustrated in Figure 4.1 which compares the characteristics of water and organic. Water has a much larger heat of vaporization compared to the organics. As a result, steam temperature varies widely from the gas temperature whereas the organic temperature follows the gas temperature closely. Thus the organic leaving the vapor-generator has higher availability than water.

Organics are inherently more efficient for this application than water. A search was therefore conducted to find the optimum

organic fluid. In addition to thermodynamic characteristics, other factors involved are:

- Thermal stability
- Compatibility
- Safety
- Cost
- Physical characteristics

The working fluids which were found to have a unique combination of desirable characteristics are mixtures of trifluoroethanol ($CF_3 CH_2 OH$) and water. Two strong working fluid candidates for this application were found to be Fluorinol-85 (85 mole percent of TFE and 15 mole percent water) and Fluorinol-50 (50 mole percent of TFE and 50 mole percent water). An analytical study was conducted to compare these two fluids. A computer program was developed to compute the net ORCS power for given characteristics of the Rankine cycle components. For the purposes of comparison the efficiency of turbine, feedpump, and cooling fan were assumed to be equal and independent of working fluid. Also equal size vapor-generator and equal size regenerator plus condenser/radiator were assumed. The regenerator was grouped with the condenser/radiator since both are of plate fin construction and thus the cost/ft^3 of the heat exchanger would be approximately the same. This allows each fluid to operate with near optimum component characteristics: e.g., Fl-85 may be allowed to have a larger regenerator with smaller condenser/radiator and vice versa for Fl-50.

Because of these constraints the analysis yielded a comparison for equal system cost. The results are shown in Table 4.1. Both fluids were analyzed for the maximum operating temperature

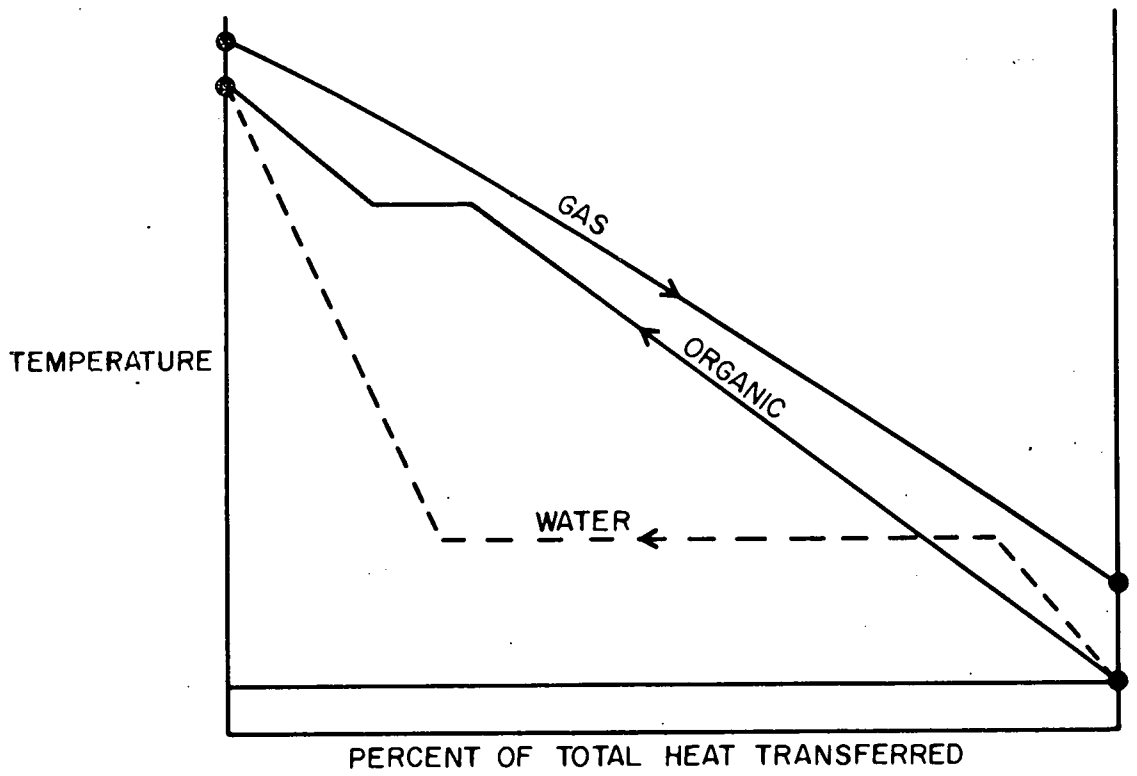

Figure 4.1 Schematic of Vapor-Generator Temperature Profiles for Organic and for Water Working Fluid.

TABLE 4.1

COMPARISON OF WORKING FLUIDS AT DESIGN POINT

Diesel Engine		
Exhaust Gas Flow Rate (lbs/hr)		3397
Exhaust Gas Temperature (°F)		840
BHP (hp)		288
Net Power (hp)		273
RPM		2100
ORCS	**Fl-85**	**Fl-50**
Organic Flow Rate (lbs/hr)	1828	1305
Vapor Generator		
Volume (ft^3)	2.7	2.7
UA (Btu/hr °F)	5197	5197
Heat Transfer Rate (Btu/hr)	458615	470600
Gas Side Pressure Drop (inches of W. C.)	16	16
Gas Outlet Temperature (°F)	333	316
Organic Inlet Temperature (°F)	308	266
Organic Inlet Pressure (psia)	770	870
Organic Outlet Temperature (°F)	625	650
Organic Outlet Pressure (psia)	700	800
Turbine/Gearbox	**Fl-85**	**Fl-50**
Efficiency	.741	.741
No. of Stages	3	3
Speed (rpm)	42000	51880

TABLE 4.1 (continued)

	F1-85	F1-50
Power (hp)	37.04	38.28
Maximum Diameter (inches)	2.86	2.80
Regenerator		
Effectiveness	0.8	0.8
Volume (ft^3)	.1199	.0807
UA (Btu/hr °F)	1366	919
Heat Transfer Rate (Btu/hr)	114500	53500
Condenser/Radiator		
Volume (ft^3)	3.566	3.605
Frontal Area (in^2)	1400	1400
UA (Btu/hr °F)	21048	21284
Condenser Heat Rejection Rate (Btu/hr)	363000	371000
Condensing Temperature (°F)	190	190
Radiator Heat Rejection Rate (Btu/hr)	456000	456000
Radiator Average Temp. (°F)	185	185
Fan Efficiency (%)	34.5	34.5
Fan Power	9.34	9.23
Feedpump		
Efficiency	0.7	0.7
Flow (gpm)	2.913	2.14
HP	1.83	1.53
Auxiliary Gearbox		
Efficiency	0.96	0.96
Overall ORCS Net Power (hp)	35.93	37.51

permissible from the standpoint of thermal degradation. This analysis was performed on the basis of prototype engine data. The results of the analysis can be summarized as follows:

- Fl-50 yields 4.4% more power than Fl-85 system.
- Fl-50 system requires 28.6% less flow than Fl-85 system, permitting the use of smaller lines.
- Fl-85 turbine design speed is 20% lower than that needed for Fl-50 system, resulting in a lower stress design.

Conclusion

Because of a higher power output, Fl-50 was selected as the reference working fluid. However, the system will be designed for the interchangeability of the working fluid, as far as possible.

4.2 OPTIMIZATION OF ORCS PARAMETERS

Having selected the reference working fluid, optimization of the performance of various ORCS components was carried out. Various trade-offs such as performance, size and packaging were considered. All optimization studies were performed at the design point corresponding to the prototype engine data.

4.2.1 Expander Efficiency

A turbine expander was selected in preference to a reciprocating expander, primarily because of the nature of the application. The long-haul, over-the-road, heavy duty trucks generally operate over a narrow speed and horsepower range; e.g., over a typical duty cycle, 85% of the total fuel is consumed in a 270-300 hp range and at 1600-2100 rpm range. A turbine can maintain high efficiency over a narrow

speed range and lends itself to this application. In addition, it offers lower weight and volume compared to a reciprocating expander.

A high efficiency turbine-gearbox system was designed. The number of stages and the design speed were selected to optimize its efficiency. The details of these tradeoffs are discussed in Chapter VIII. The turbine-gearbox design does not offer any significant packaging tradeoffs.

4.2.2 Feedpump Efficiency

A high efficiency, variable displacement feedpump similar to the automotive ORCS feedpump will be used. The system performance is not very sensitive to the feedpump efficiency since the feedpump requires less than 5% of the expander power. There are no significant tradeoffs in the design of the feedpump.

4.2.3 Condensing Temperature

An integrated condenser/radiator with one fan was designed to meet the heat rejection requirements of the condenser and radiator. Whereas the radiator specifications, in terms of heat rejection rate and temperature, remained constant, the condenser specifications are a function of condensing temperature. Since the condenser is mounted upstream of the radiator, and air is preheated coming into the radiator, the radiator design is influenced by the condensing temperature; e.g., a higher condensing temperature would require increased radiator thickness and reduced condenser thickness.

Lowering the condenser temperature results in the following:

a) Higher cycle efficiency and higher expander power output at the rate of approximately 0.5% per °F reduction in condensing temperature.

b) Reduced temperature difference (Δ T) between air and condensing vapor and hence higher air flow and fan power, roughly as the cube power of the ΔT ratio.

Since these two effects are opposite, an optimum is expected. The analysis was carried out for constant condenser/radiator overall size. The split between the two was, however, allowed to vary. Thus the condensing temperature was optimized for a fixed heat exchanger size. Sizes of the regenerator and vapor-generator were also held constant in this analysis. The design of the vapor-generator for each condensing temperature was modified to match the heat transfer requirements by varying the flow area and gas side pressure drop for fixed volume. The ORCS was charged for the reduction in diesel horsepower due to this increased back pressure. As shown in Figure 4.2 the fan efficiency was held constant in this analysis at 34.5%, which is typical for automotive fans. It is noteworthy that fan efficiency influences the optimum condensing temperature. A higher efficiency fan would push the optimum condensing temperature to a lower value.

The results of the study show a well-defined optimum condensing temperature of 150 °F, as shown in Figure 4.3.

4.2.4 Regenerator Effectiveness

In the regenerator, vapor undergoes partial sensible cooling before entering the condenser. The heat is transferred to liquid which becomes preheated before entering the vapor-generator. Regenerator effectiveness is a measure of the percent of the maximum sensible

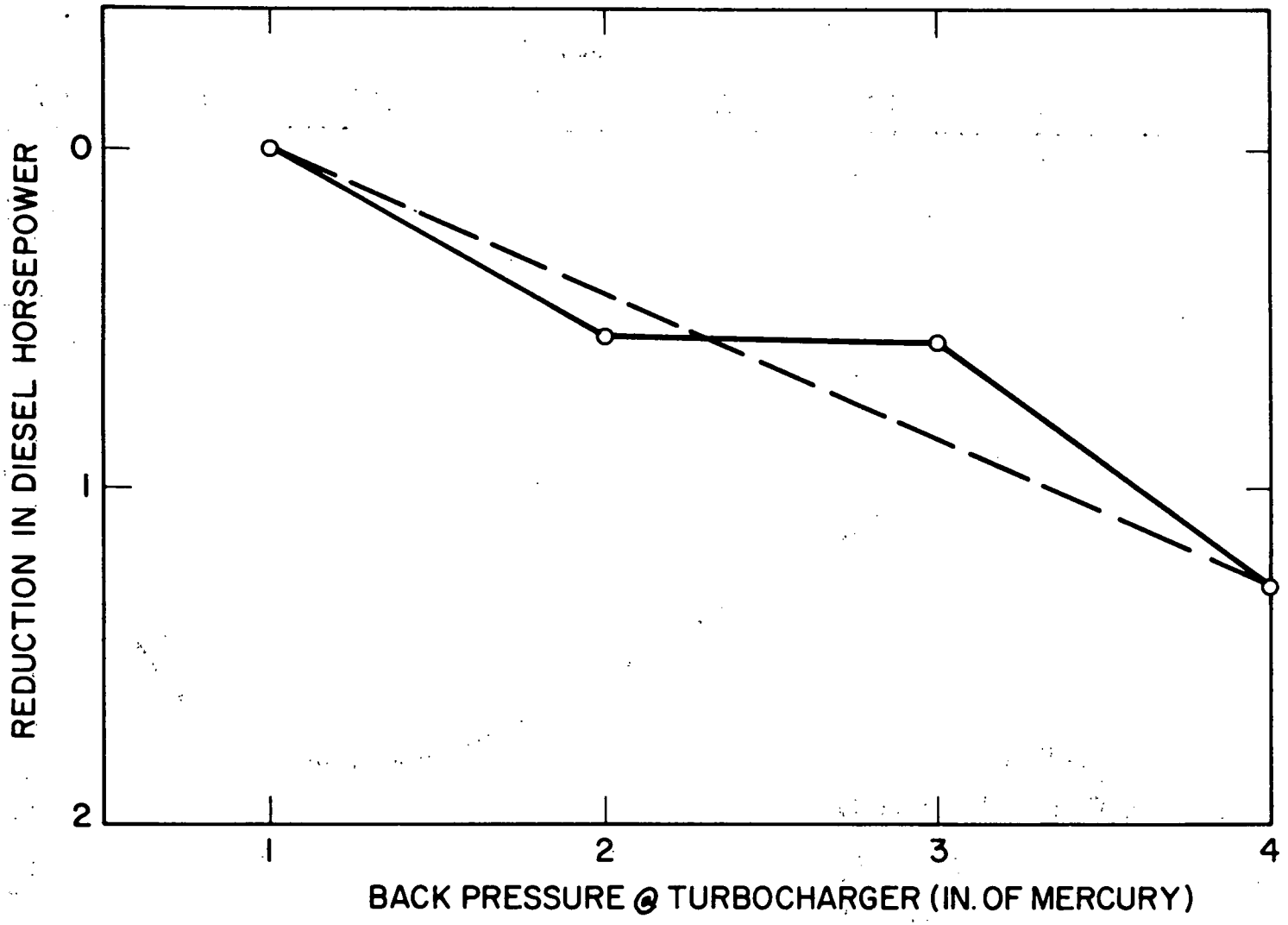

Figure 4.2. Effect of Turbocharger Back Pressure on Diesel Performance at Design Point.

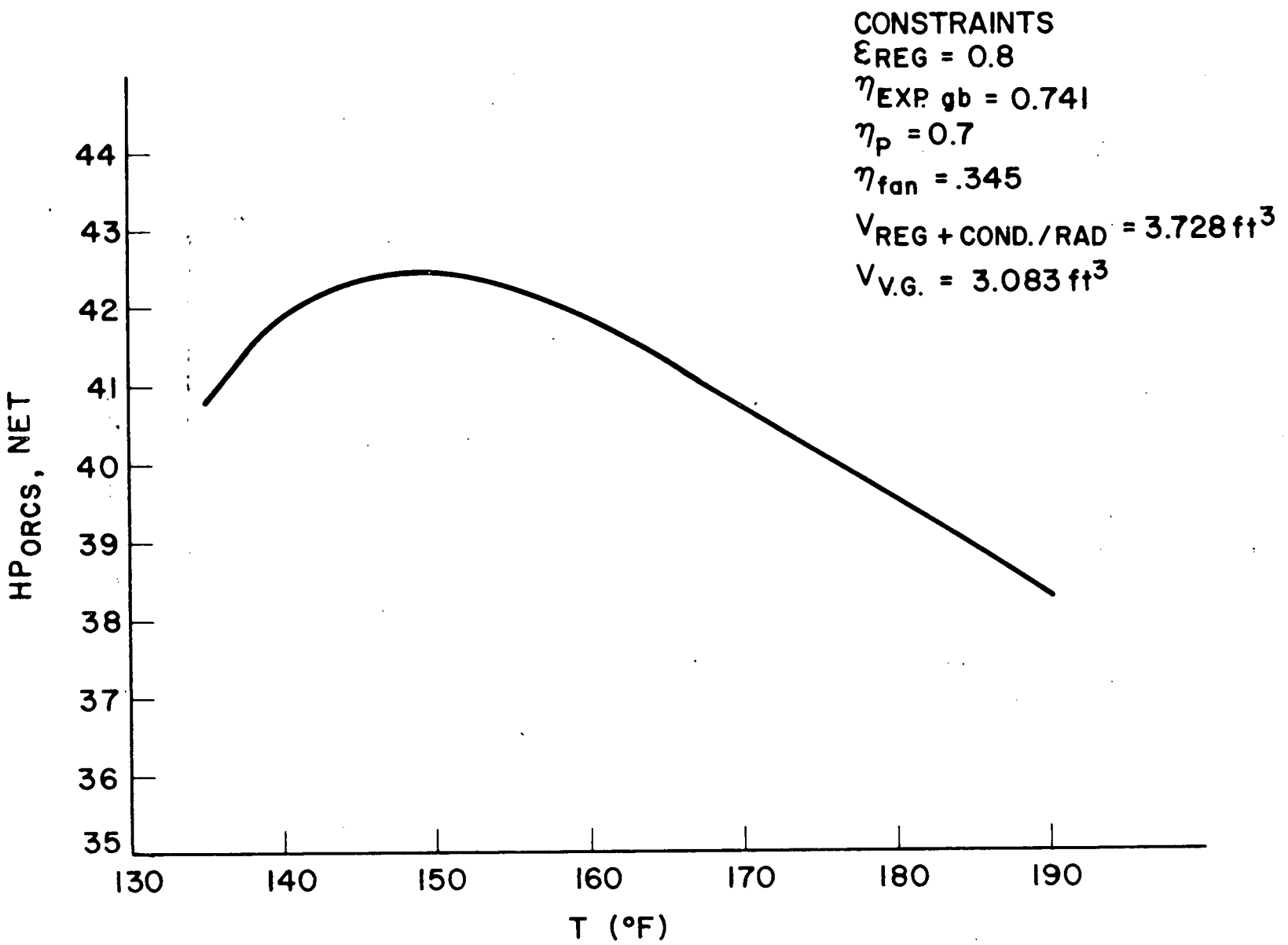

Figure 4.3. Condenser Temperature Optimization.

cooling that the vapor could have undergone. Increasing the regenerator effectiveness results in the following:

- Higher cycle efficiency
- Reduced condenser heat rejection requirements
- Higher liquid temperature entering vapor generator
- Reduced heat recovery from the exhaust gas

Although higher cycle efficiency would translate into higher power at the same heat input, this is counteracted by the reduced heat recovery from the exhaust gas in the vapor-generator. Therefore, an investigation was carried out to see if an optimum exists.

The study was made for a fixed overall volume of the condenser/radiator plus the regenerator. These units were lumped into one group because both are plate-fin heat exchangers and cost/core volume is expected to be approximately equal. The vapor side pressure drop was input in the regenerator design. Therefore, when the regenerator effectiveness is raised, a larger volume regenerator is needed; however, this is allowed at the expense of smaller condenser/radiator volume. This, in turn, results in lower condenser/radiator effectiveness, although the condenser heat rejection requirement is also lower. The fan speed is therefore adjusted to maintain optimum condensing temperature and the new fan power is computed. The vapor-generator design is also adjusted by changing the gas side pressure drop to satisfy the "UA" requirement. The resulting change in diesel power (Figure 4.3) is charged to the ORCS.

The results of this optimization study are shown in Figure 4.4. The study does not offer a well-defined optimum from the standpoint of the net ORCS power. In the limit, of course, as regenerator

effectiveness approaches unity, the regenerator size will become very large at the expense of the smaller condenser/radiator with very high fan power requirements, and the net ORCS power will drop rapidly.

The regenerator effectiveness of 0.9 at the design point was selected. An intangible effect of selecting high regenerator effectiveness is the higher liquid temperature entering the vapor-generator, which minimizes the chances of moisture condensation and the attendant corrosion in the vapor-generator.

4.2.5 Vapor Generator Effectiveness

As the vapor-generator "UA" increases, the gas temperature leaving the vapor-generator approaches the inlet fluid temperature at the design point. The vapor-generator was assigned a volume from the packaging standpoint. Maximum fin density was dictated by the diesel exhaust service. Therefore for fixed heat transfer area of the vapor generator, "UA" can be changed by varying the pressure drop. Higher "UA" results in the following:

- Higher heat recovery from the exhaust gas
- Higher heat rejection requirement in the condenser
- Higher back pressure of the diesel engine

Higher heat recovery from the exhaust gas results in higher expander power output. However, the larger heat rejection requirement in the condenser calls for greater fan power. Also, higher back pressure results in lower diesel power output (Figure 4.2). Because of these counteracting effects, an investigation was carried out to search for an optimum vapor generator "UA."

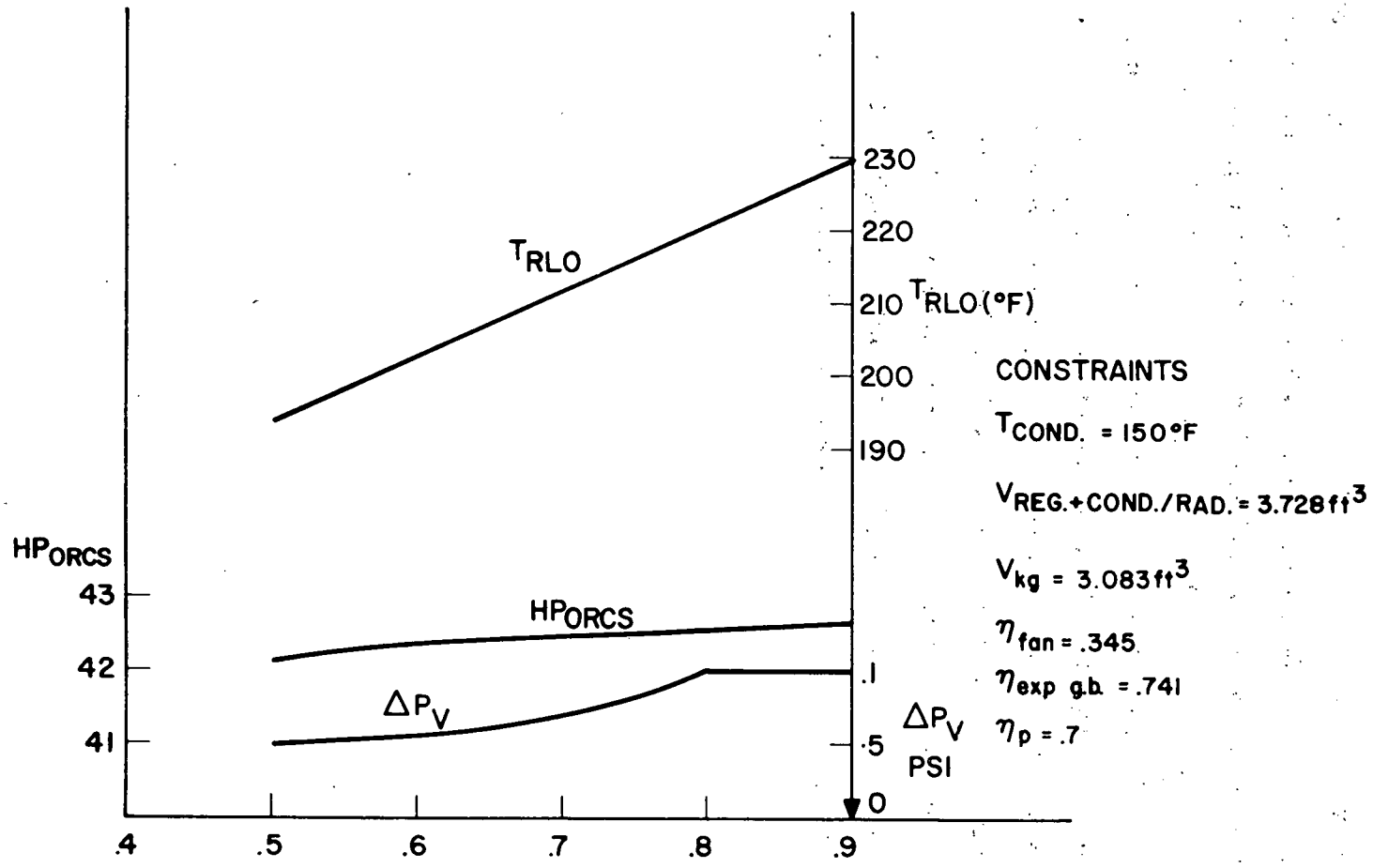

Figure 4.4. Regenerator Effectiveness Optimization.

The results are shown in Figure 4.5. The vapor-generator heat transfer characteristics cannot be listed in terms of effectiveness since effectiveness is different in the preheating, boiling and superheating portions of the vapor-generator. "UA," however, is a measure of the effectiveness. Net ORCS power was found to increase in the range of investigation. However, the slope was very shallow; e.g., the net ORCS power increases by only 1% for every 10% increase in the vapor generator "UA." Higher "UA" values were not investigated because that would call for a lean and tall vapor-generator which would violate the packaging constraint on height. Thus, the maximum permissible "UA" packaging and clogging constraints were used.

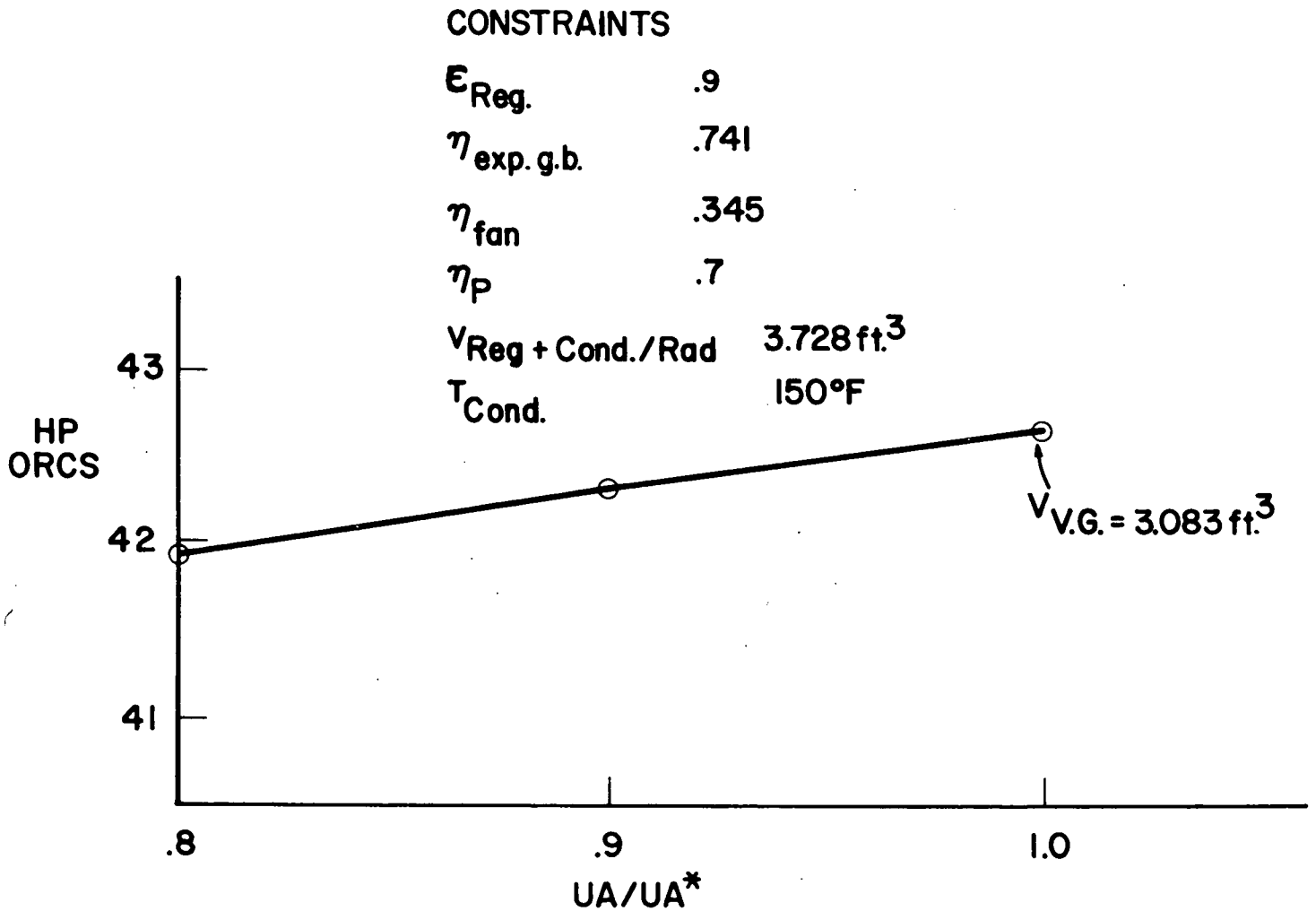

Figure 4.5. Vapor Generator Size Optimization.

5. DESIGN POINT FUEL ECONOMY IMPROVEMENT DUE TO ORCS

The optimization studies described in Chapter 4 are based on earlier prototype engine data. Later in the program Mack made measurements on the production engine that will be actually used in the demonstration testing. Due to modifications made to the prototype engine to meet emission standards, the exhaust gas temperature measured was higher for the production engine, as shown in Figure 2.1. Because of the schedule problems, the component designs were not re-optimized for the new design point. Instead, the revised component performance at the new design point was computed using an off-design performance prediction program. Therefore, the ORCS performance projection may not be optimum but should be conservative.

The design point characteristics of the Diesel-ORCS compound engine are listed in Table 5.1. The ORCS contributes 17.51% additional power to the diesel shaft before the transmission at zero additional fuel cost. This is after all the additional parasitic losses incurred in the system (such as additional fan power, losses in the P. T. O. gearbox, etc.) are charged to the ORCS.

TABLE 5.1

DESIGN POINT CHARACTERISTICS OF ORCS FOR DIESEL TRUCK BOTTOMING APPLICATIONS

WORKING FLUID	Fluorinol-50
TURBINE INLET TEMPERATURE/PRESSURE	650°F/800 psia
TURBINE/GEAR BOX EFFICIENCY	72.85%
REGENERATOR EFFECTIVENESS	90%
AVERAGE CONDENSING TEMPERATURE	163°F
RADIATOR AVERAGE TEMPERATURE	185°F
COOLING FAN EFFICIENCY	34.5%
PUMP EFFICIENCY	79.26%
VAPOR GENERATOR (MIN. TEMP. DIFF.)	33°F
GAS	
Flow Rate	3442 lbs/hr
Inlet Temp.	940°F
Outlet Temp.	277°F
P.T.O. EFFICIENCY TO DIESEL SHAFT	96%
NET ORCS POWER (AFTER ALLOWING FOR ACCESSORIES)	47.85 hp
DIESEL NET H.P. (AFTER ALLOWING FOR ACCESSORIES)	273 hp
IMPROVEMENT IN FUEL ECONOMY	17.51%

6. FUEL ECONOMY IMPROVEMENT IN OTHER TRUCK DIESEL ENGINES

The diesel engines made by various manufacturers differ in their exhaust gas characteristics. In order to evaluate the impact of compounding the diesel with an ORCS on an industry-wide basis, design-point fuel economy improvement was computed for various makes of engines to determine whether the improvement obtained with the reference Mack engine is also typical for other engines. The same design-point organic cycle was used for all systems; i. e., net ORCS power/heat transferred in the vapor-generator was the same for all engines. The results are shown in Table 6. 1. The improvement in the fuel economy of the reference engine is below the median improvement projected for all engines. The Caterpillar engine showed the lowest fuel economy improvement, but this may be due to the definition of design point, which may not be the maximum horsepower condition at maximum speed. Table 6.1 also shows the improvement in fuel economy due to compounding a spark ignition (S. I.) engine with an ORCS. This design-point improvement is higher because the S. I. engine is inherently less efficient than the diesel engine and has higher exhaust energy available. However, over a duty cycle the improvement may be reduced substantially because the spark ignition engine typically runs at a fraction of its design power where the available energy of the exhaust gas drops sharply.

TABLE 6.1

DESIGN POINT FUEL ECONOMY IMPROVEMENT DUE TO ORCS

ENGINE	HP_{NET}	W_G	T_{GI}	ORCS HP_{NET}	PERCENT
Mack 676	273	3442	940	47.85	17.51
Mack 675	218	2720	948	39.7	18.20
Saab Scania	334.6	3726	1040	61.8	18.47
Caterpillar	266.4	3108	842	38.1	14.30
Cummins NTC-290	268.3	3144	1016	53.5	19.96
Spark Ignition	111.9	1176	1430	29.41	24.91

- HP and Gas Flow Data for Diesel Engines from Mack Trucks. Inc.
- All Engines Evaluated for Constant ORCS Efficiency

7. SENSITIVITY ANALYSIS

The fuel economy improvement projection listed in Chapter 5 is based on the design point characteristics of the system. In this section the sensitivity of the fuel economy improvement to the performance of each ORCS component is studied. In this analysis the net ORCS power was computed as one component's performance was reduced below design value while all other components performed according to the specifications. The results are as follows.

7.1 SENSITIVITY TO TURBINE EFFICIENCY

The net ORCS power was computed assuming the turbine operated at an efficiency lower than design value. A less efficient turbine results in lower gross power in direct proportion to the turbine efficiency. It also results in a higher heat rejection requirement which calls for increased fan power, reducing the net ORCS power further. The regenerator, however, offsets the latter effect somewhat by higher heat recovery. The overall effect is shown in Figure 7.1a. When turbine efficiency dropped to 80% of the design value, the ORCS net power dropped to 79% of the design value, indicating that increased heat rejection requirement is mostly offset by higher heat recovery in the regenerator. But for that, the effect would be linearly proportional.

7.2 SENSITIVITY TO CONDENSER/RADIATOR PERFORMANCE

In this analysis, the "UA" value of the condenser/radiator was assumed to be lower than the design value, while its pressure drop was the same as the design value. The resulting lower effectiveness yields a higher condenser temperature as well as a higher

radiator temperature. The radiator temperature specification provided by Mack was not allowed to be exceeded; therefore, the fan speed had to be increased to maintain the radiator temperature. The higher fan speed translates into higher fan power, reducing the net ORCS power. The condenser temperature, however, is still higher than the design value, resulting in lower cycle efficiency and lower gross power. The overall effect on the ORCS power is shown in Figure 7.1b. For a 20% reduction in condenser/radiator "UA," the ORCS net power drops off by 8%, becoming 92% of the design value.

Although the ORCS net power is moderately sensitive to condenser/radiator performance, it is noteworthy that the heat transfer surface selected is a louvered fin surface widely used in the automobile industry; therefore, confidence level in the condenser/radiator design is very high.

7.3 SENSITIVITY TO VAPOR GENERATOR PERFORMANCE

In this analysis the effect on the ORCS net power of having the vapor-generator "UA" value lower than the design value was studied; all other components performed as per specifications. The gas side pressure drop was assumed to remain constant. A lower "UA" of vapor-generator results in lower effectiveness which in turn results in lower organic flow rate and reduced heat recovery from exhaust gas. This naturally results in lower ORCS power; however, the effect is somewhat offset by the reduction in fan power required to reject less heat into the condenser. The fan power varies approximately as cube function of the heat rejection rate.

The results of this analysis are shown in Figure 7.1c. The ORCS net power is found to be relatively insensitive to the vapor-generator performance. For 20% lower "UA" of the vapor-generator, the system power drops off by less than 2%. Hence the net ORCS power is weakly sensitive to the vapor-generator performance.

7.4 SENSITIVITY TO FEEDPUMP EFFICIENCY

The impact on the ORCS net power of having feedpump efficiency lower than the design value was evaluated. The feedpump work represents less than 5% of the expander; therefore, the effect of feedpump efficiency is rather small (e.g., if the feedpump operates at 20% lower than design efficiency, the ORCS net power drops by about 1%), as shown in Figure 7.1d.

The feedpump design has been thoroughly tested and evaluated at Thermo Electron and the confidence level is very high.

7.5 SENSITIVITY TO REGENERATOR PERFORMANCE

The effect on the ORCS net power of having the regenerator "UA" lower than the design value was studied. Lower value of regenerator "UA" results in lower effectiveness and, hence, lower cycle efficiency; however, this effect is offset somewhat by higher heat recovery from the exhaust gas due to lower inlet fluid temperature. The net effect is shown in Figure 7.1e, which shows that for 20% reduction in the regenerator "UA," the overall effect on the ORCS net power is less than 1%. It may be concluded that the ORCS net power is nearly insensitive to the regenerator performance.

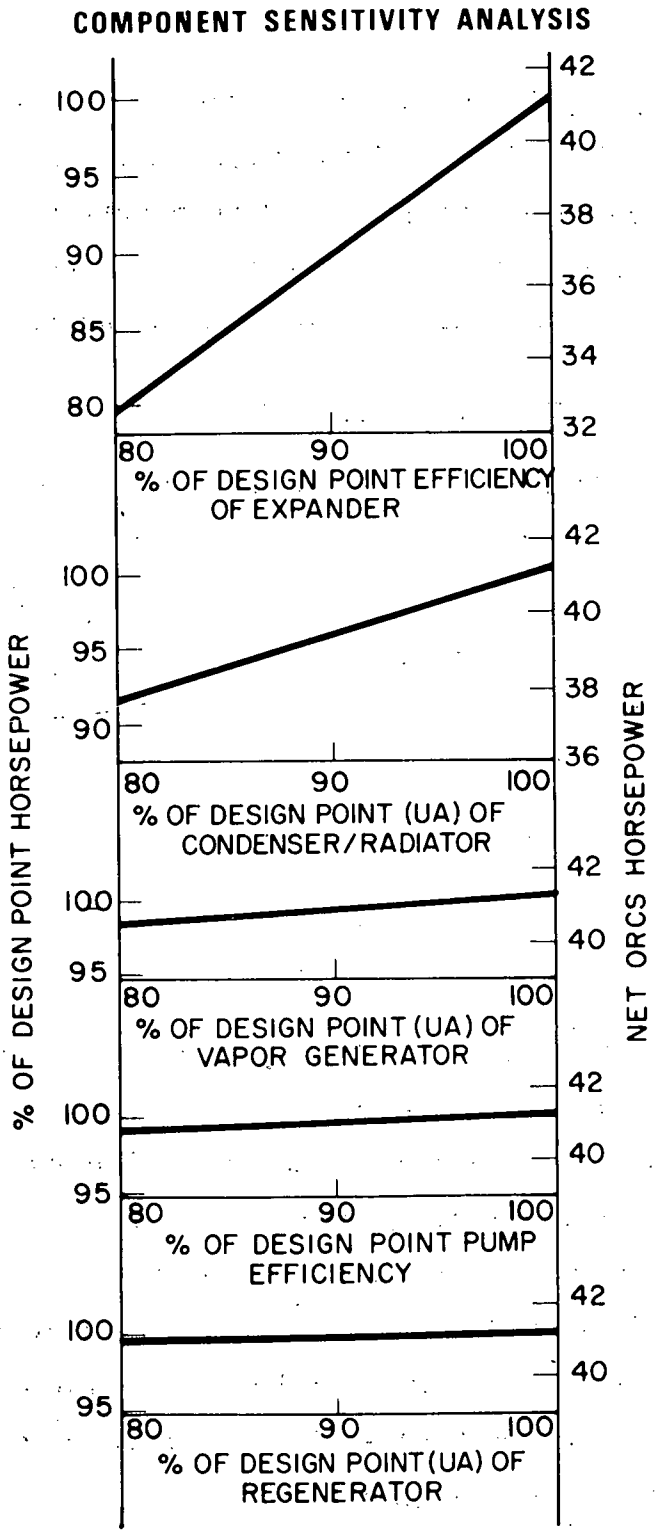

Figure 7.1a

Figure 7.1b

Figure 7.1c

Figure 7.1d

Figure 7.1e

Figure 7.1. Component Sensitivity Analysis.

7.6 CUMULATIVE SENSITIVITY

In this analysis, it was assumed that all components were performing at a fixed percent level below the design value, simultaneously, and their cumulative effect on the ORCS net power was evaluated. The results are shown in Figure 7.2, which indicates that for a 10% simultaneous reduction in the performance of each component the ORCS net power drops off by approximately 12%, whereas a 20% drop in component performance results in a 28% drop in the ORCS net power. It is, however, highly unlikely that such a situation will occur.

In conclusion, the ORCS net power is the most sensitive to the expander efficiency, moderately sensitive to the condenser/radiator and almost insensitive to the vapor-generator, feedpump, and regenerator. Thus, the turbine is the most critical of all ORCS components and great care should be exercised in its design.

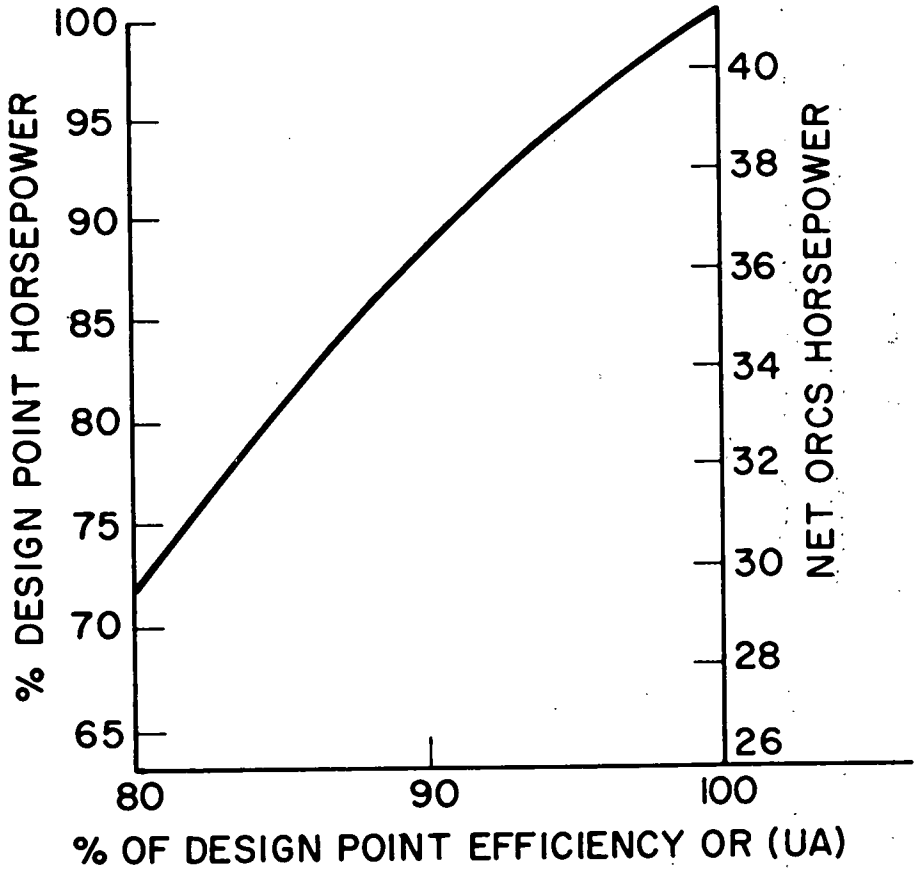

DESIGN POINT VALUES

$\eta_{EXPANDER\ g.b} = 0.727$

$\eta_{PUMP} = 0.7$

$(UA)_{VAPOR\ GENERATOR} = 6195\ \frac{BTU}{hr\,°F}$

$(UA)_{REGENERATOR} = 1915\ \frac{BTU}{hr\,°F}$

$(UA)_{CONDENSER/RADIATOR} = 22930\ \frac{BTU}{hr\,°F}$

Figure 7.2. Cumulative Sensitivity Analysis.

8. COMPONENT DESIGN

8.1 TURBINE DESIGN

8.1.1 Turbine Design Conditions

Power output of the ORCS is very nearly a direct function of the expander efficiency so that it is important for the expander to have the highest practical efficiency. Early in the program, preliminary design conditions were established for the purpose of selecting both the type and configuration of expander that best fit this application. These design conditions are based on prototype engine data. The maximum power condition was chosen for the preliminary design point, and the range of operating speeds for the expander was defined as follows:

- Inlet Pressure - 800 psia
- Inlet Temperature - 650°F
- Exhaust Pressure - 11.0 psia
- Flow Rate - 1324 lbs/hr
- Diesel Engine Design Speed - 2100 rpm
- Normal Operating Speed Range - 1200-2100 rpm
- Idle Speed - 300 rpm
- Maximum Overspeed - 3000 rpm

A turbine type expander was selected for this application because the operational requirements for the expander are closely matched to the characteristics of a turbine. Most importantly, as will be discussed in the section on duty cycle analysis, high efficiency is required over a relatively narrow range of speed and power. In

addition, the power level is high enough so that acceptable efficiency can be achieved when using Fluorinol-50 as the working fluid. A turbine with a speed reduction gearbox results in a relatively compact package, particularly when the expander must operate efficiently at a very high pressure ratio.

These design conditions were used for the evaluation of the various turbine configurations that will be discussed. In addition, a number of other considerations and practical limitations were also placed on the turbine design. These are summarized below:

- Operational and Mechanical Reliability
- Maximum Practical Overall Efficiency Including Bearings, Seals, and Gearbox Losses
- Critical Speeds to be Below the Normal Operating Speed Range and Above the Maximum Overspeed
- Maximum Shaft Seal Surface Speed of 250 Ft/Sec at the Design Speed
- Turbine Safe at Runaway Speed
- Minimum Blade Height of 0.1 Inch
- Low Wheel Stress
- Maximum Gearbox Ratio of 35

Basic mechanical and aerodynamic aspects of the turbine design were studied to define these design limits and then each type of turbine was evaluated within these practical boundaries. The intent is to achieve maximum overall TGU efficiency by using hardware based on state-of-the-art technology.

Critical speeds should be either above the maximum operating speed or between idling and operating speed. Critical speeds were estimated for each configuration that was considered. The maximum diameter of the shaft, an important parameter in calculating the critical speed, is limited by the shaft seal, since the surface speed of the seal face should be held below 250 ft/sec to assure reasonable life. A large seal also increases the seal loss which is proportional to surface speed and diameter. The bearing design also places limits on the turbine design speed. Thus, it is necessary to check each design to be sure it is within the mechanical design limits.

It is desirable to keep the gearbox ratio below 35 so that only two reduction stages will be required and so that the gear design is within the state of the art. The TGU is connected to the diesel engine through a power take-off unit (PTO). This is available with a reduction ratio of either 1 to 1 or 1.43 to 1.

A blade height of 0.1 inch is used to avoid excessive losses in and around the blades. This will also assure a reasonable nozzle throat size.

8.1.2 Comparison of Possible Turbine Configurations

Axial and radial turbines with various numbers of stages were evaluated, and the results are summarized in Table 8.1 and Figure 8.1. A single-stage turbine has very low efficiency, while a two-stage turbine has critical speed problems apart from a comparatively low efficiency. A three-stage, axial turbine not only gives better performance but also improves reliability. Increasing the number of stages beyond three will show further

TABLE 8.1

TRUCK BOTTOMING CYCLE TURBINE SELECTION

Type of Turbine	Fluorinol-50				
	Overall Efficiency OA	Diam Inches	Speed RPM	Blade Height Inches	Remarks
Single Stage, Axial, Overhung	.65	2.75	70,000	.44	Efficiency Low Seal Speed High G. B. Ratio Limited Design
2 Stages, Axial, Overhung	.66		50,000		Critical Speed in Operating Range
2 Stages, Axial, Both Ends Supported	.699	2.45 2.75	70,000	.2145	G. B. Ratio Limited Design Low Efficiency High Seal Speed
3 Stages, Axial, Both Ends Supported	.727	2.25 2.25 2.7	60,000	.1 .1 .209	Higher Cycle Efficiency Selected
3 Stages, Radial, Supported at Both Ends	.678	2.12 2.5 3.35	70,000		Low Efficiency High Leakage High Windage Loss Interstage Losses High

η_{OA} = Overall Efficiency of Turbine + Gearbox, All Losses Included.

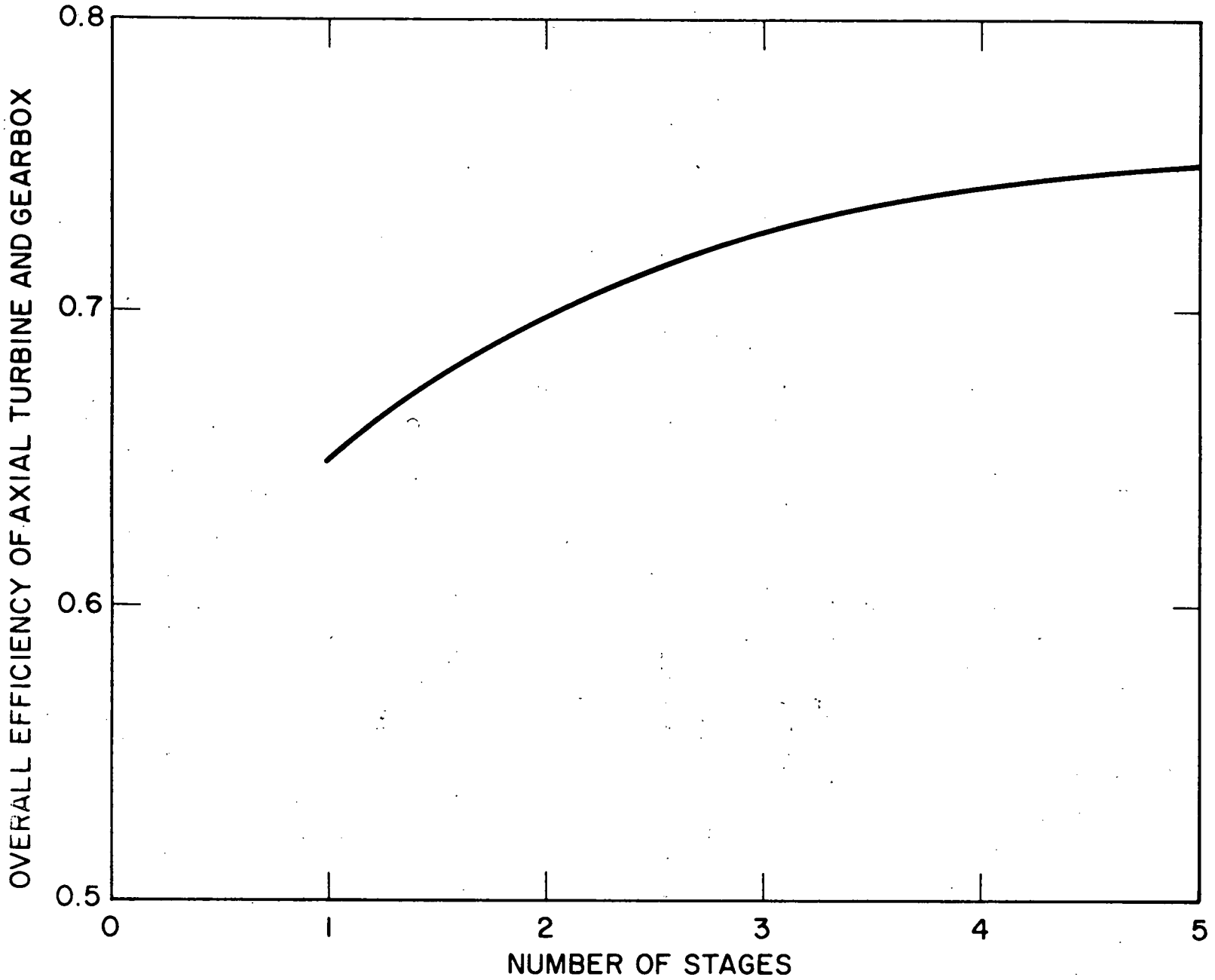

Figure 8. 1. Overall Turbine and Gearbox Efficiency vs Number of Stages.

improvement, but the net gain will not be enough to justify the complexity of more stages. A multi-stage radial design may be cheaper to manufacture than an axial turbine, but the overall performance is not as good because of leakage and windage losses.

8.1.3 Discussion of Selected Turbine Design

The three-stage axial turbine supported at both ends was selected, and the aerodynamic and mechanical details were checked in greater depth. The head is equally split between three stages. The first stage is a partial admission stage which is used to get reasonable blade height. The second stage is identical to the first stage aerodynamically and physically, except it is a full admission stage. This reduces the development effort without sacrificing performance. The last stage has some reaction to improve performance. Ideally, there should be no reaction at the blade root and maximum reaction at the blade tip which minimizes the net thrust load. Unfortunately, this may be difficult to achieve because of the relatively small blade height. Care was taken to avoid operation in the transonic region. Performance penalties due to a high aspect ratio for either the nozzles or blades are eliminated by using a three-stage turbine which has a low pressure ratio across each stage. Low rotor stresses make it possible to shroud the rotor; this minimizes leakage losses and vibrations. Relevent data on axial turbines are shown in Table 8.2. The small turbine data measured at Thermo Electron can be compared with the predictions for the first two stages of the proposed turbine. The data developed by NASA for units with slight reaction actually gave better performance than that predicted for the last stage.

TABLE 8.2

LOW POWER TURBINE DATA

Stages	Reference	η_{TS}	PR_{Stage}	Speed	Diam.	Power	Vel. Ratio
1	TECO Axial Overhang	.69	16	70,000	2.42"	6 HP	.408
2	NASA TND-4388	.826	1.226	12,000	9.75"	10 KW	.46
10	NASA TMX-52892	.83	1.4	15,000	3"-5.572"	10-15 HP	.45

η_{TS} = Total to Static Efficiency of Turbine Stage

This Data Can be Compared with Last Stage Efficiency of Proposed Turbine for Truck Bottoming Cycle

Details of the design are summarized in Table 8.3. No pressure recovery was expected from the first stage exhaust because of redistribution losses. Credit was not taken for any gain in performance from the diffuser. Overall turbine efficiency of 78.3% is expected.

A preliminary layout of the three-stage turbine is presented in Figure 8.2. The rotor is straddle-mounted between two journal bearings with a buffered shaft seal on the rotor side of each bearing. These seals with a pressurized buffer space between each sealing face prevent working fluid from leaking out, air from leaking in, and mixing of lubricant with the working fluid. Any small leakage across the seal faces is buffer fluid leaking into the working fluid or lubricant. The buffer fluid is compatible with both. Journal bearings have been selected for long life and reliability.

Interstage leakage must be kept low, particularly between the first and second stage, in order to achieve high efficiency. A number of different seals were considered before selecting a non-contact carbon seal with a metal band around it to control the leakage gap when the temperature varies. Data on these seals from various manufacturers were used to estimate the interstage leakage for the performance calculations.

A simple stack-up assembly procedure can be used with this design. No special assembly or mechanical problems are expected. This design approach is quite flexible, and minor changes to improve performance can be accomplished easily during development.

Seal loss, bearing loss, and gearbox loss are major mechanical losses. Mechanical efficiency of 93% is expected which will give TGU overall efficiency of 72.7%.

TABLE 8.3

THREE-STAGE TURBINE DESIGN DETAILS

	FIRST STAGE	SECOND STAGE	THIRD STAGE
Tip Diameter (in.)	2.2	2.2	2.96
Blade Height (in.)	0.1	0.1	0.207
Pressure Ratio	4.21	4.13	4.18
Relative Mach No.	1.15	1.165	0.852
Velocity Ratio	0.407	0.418	0.587
Tip Speed (ft/sec)	576	576	775
Total to Static Efficiency	0.67	0.735	0.815
Total to Total Efficiency	0.71	0.80	0.83
Nozzle Angle (degrees)	16	16	16
Leakage (%)	0	2	1

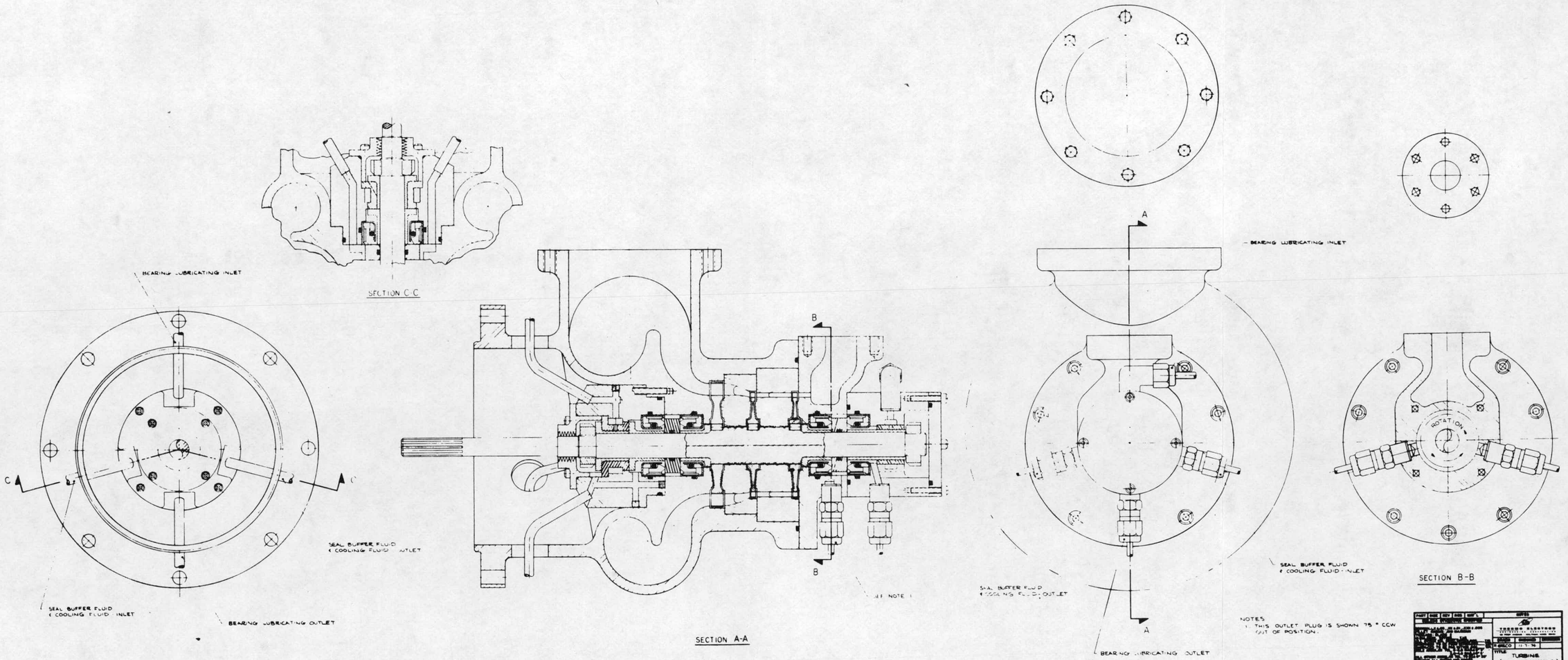

Figure 8. 2. Preliminary Layout of Three Stage Turbine.

8.1.4 Independent Turbine Analysis

Since the turbine expander is an important key component in the Rankine cycle system, verification of the predicted performance is desirable. Barber-Nichols Engineering Company was hired as an independent consultant to analyze the performance and to suggest an alternate design. Their performance analysis predicted a combined TGU efficiency of 0.71 as compared to the Thermo Electron value of 0.727. The small discrepancy is due mostly to a difference in the estimate of interstage leakage. Barber-Nichols suggested a double cantilever configuration for the three-stage turbine. The preliminary layout for this design and the details of the analysis are given in Appendix C. This configuration, by overhanging the wheels from both sides of the gearbox, eliminates two bearings and any leakage between the first and second stages. On the other hand, there will be flow transfer loss between the first and second stage. A key feature of this design is that all critical speeds can be above the maximum operating speed if care is taken in the details of the design. The shaft seals are mounted concentric with the journal bearing in order to reduce the overhang. A comparison of the two approaches is made in Table 8.4.

8.1.5 Computer Model for Turbine Part-Load Performance

A standard technique to evaluate turbine performance is used. No control valve of any type between the boiler and the turbine is considered. First stage nozzles will be choked and, for a given flow, the nozzles will determine the inlet condition.

TABLE 8.4

COMPARISON OF THREE-STAGE TURBINE APPROACHES

	TECO	B/N
Type of Configuration	Straddle Mounted	Double Cantilever
Overall TGU Efficiency	0.727	0.730
Design Speed	60,000 rpm	62,000 rpm
First Critical Speed	> Idle < Operating Speed	> Max. Speed
Second Critical Speed	> Max. Speed	> Max. Speed
Packaging	Longer Package	Extra Plumbing, Two Less Bearings
Seal, Bearing	State of Art	Combined Seal and Bearing Design
First Stage	Partial Admission Impulse	Partial Admission Impulse
Second Stage	Full Admission Impulse	Partial Admission Impulse
Third Stage	40% Reaction	40% Reaction

The first two stages are assumed to operate at design pressure ratio and the last stage is assumed to operate at the available pressure ratio. Partial admission loss of the first stage is included in the stage efficiency. No recovery is expected from the first stage exhaust because of redistribution losses. Second stage exhaust energy is expected to be recovered. No gain from the diffuser after the last stage is assumed.

Anticipating that the pressure ratio would remain relatively constant at various loads, the effect on performance of under-expansion and over-expansion is neglected. Based on TECO data, a curve of normalized efficiency versus relative velocity ratio was prepared to predict off-design stage efficiency (Figure 8.3). The efficiency is fairly constant within a velocity ratio of 30% near the peak efficiency point. With a relatively constant pressure ratio and a narrow operating speed range, the relative velocity ratio does not vary significantly, and the exact shape of the curve has little effect on the prediction of stage efficiency.

The gearbox and seal losses are predicted at the design point, based on TECO experimental data. These losses are assumed to be linear functions of speed based on available test data.

8.2 GEARBOX

The primary requirement of a high-speed gearbox is to transmit the power from the organic turbine to the input drive shaft to the Mack Diesel. For convenience, the power take-off shaft on the diesel was used for the input power shaft from the high-speed gearbox.

The gearbox housing satisfies a secondary function by providing the mounting structure for the turbine and feedpump to the PTO housing of the diesel.

The gearbox design point was at the maximum organic turbine power output and the maximum turbine operating speed. The gross turbine horsepower is 51.9 at 60,000 rpm at the design point. The turbine output speed is reduced down to 3000 rpm at the gearbox output shaft to the diesel PTO. The PTO gearing reduces the speed down to the maximum operating diesel speed of 2100 rpm. The gearbox contains an auxiliary drive shaft geared off the output power shaft to drive the feedpump at 2100 rpm and 1.92 horsepower. The gearbox design life is 10,000 hours.

The gearbox design was patterned after the automotive turbine gearbox. The design point characteristics are listed in Table 8.5.

Ball bearings are selected over journal type bearings to limit the developmental effort. A considerable amount of design, engineering, and testing would be needed to design journal bearings which would operate over the required speed range. Thermo Electron has had experience with high-speed ball bearings on the automotive turbine. In order to meet the scheduled development time required for the truck bottoming system, it is desirable to use ball bearings.

ABEC class 7 bearings are used on the high- and intermediate-speed shafts. ABEC class 5 bearings are used on the output shaft and the pump auxiliary drive shaft. The high-speed pinion shaft is shown on the gearbox layout (Figure 8.4) as the pinion gear cantilever off of two duplex pair bearings. To obtain the design life

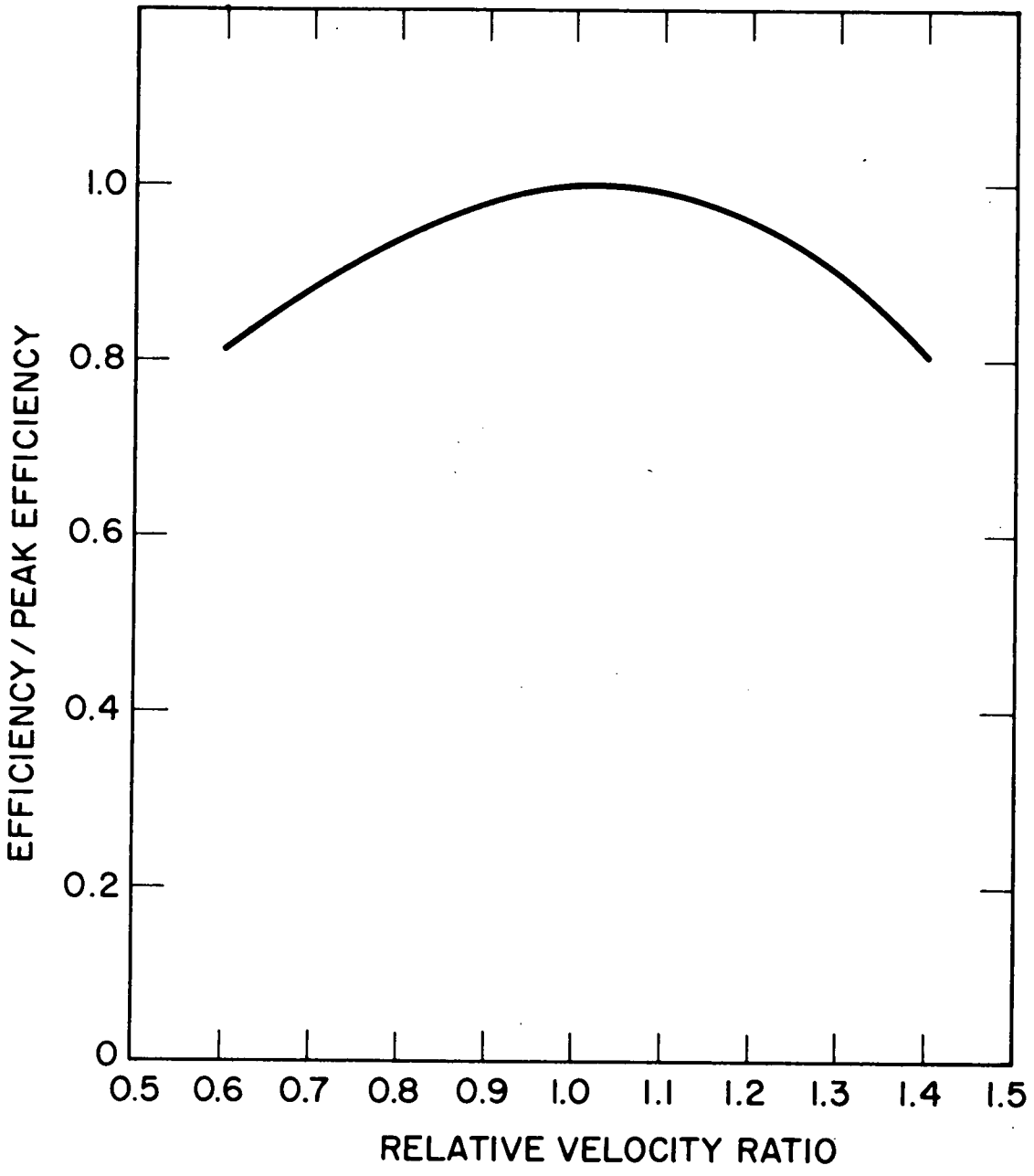

Figure 8.3. Partload Performance of Turbine.

TABLE 8.5

GEAR DESIGN POINT CHARACTERISTICS

Gear No.	Pitch	Pitch Dia. In.	No. Of Teeth	AGMA Class	Hardness RC	Pitch Line Velocity FPM	AGMA* Bending Stress psi	AGMA** Contact Stress psi	Tooth Contact Force #/in
1	32	.8125	26	12	58	12,762	33,301	168,812	179.6
2	32	4.0625	130	12	55	12,762	33,301	168,812	179.6
3	20	1.2500	25	12	58	3,927	40,171	195,304	397.5
4	20	5.0000	100	12	55	3,927	40,171	195,304	397.5
5	20	3.0000	60	8	38	2,356	4,746	59,918	35.6
6	20	4.3000	86	8	38	2,356	4,746	59,918	35.6

*AGMA Bending Stress Formula

**AGMA Surface Contact Stress

$$\sigma = \frac{W^t K_o}{K_v} \times \frac{P}{F} \times \frac{K_s K_m}{J}$$

$$\sigma_H = C_p \sqrt{\frac{W^t C_o}{C_v} \frac{C_s}{DF} \frac{C_m C_t}{I}}$$

σ = corrected bending stress, psi

W^t = transmitted load, lb

K_o = overload correction factor

K_v = dynamic factor

P = diametral pitch

F = face width, inch

K_s = size correction factor

K_m = load-distribution correction factor

J = geometry factor

C_p = elastic coefficient

C_o = overload factor

C_v = velocity factor

C_s = size factor

D = pitch diameter, inch

F = face width, inch

C_m = load-distribution factor

C_t = surface condition factor

I = geometry factor

* Shigley, J. E., "Mechanical Engineering Design," Chapter 11, McGraw-Hill Book Company, Inc. (1963).

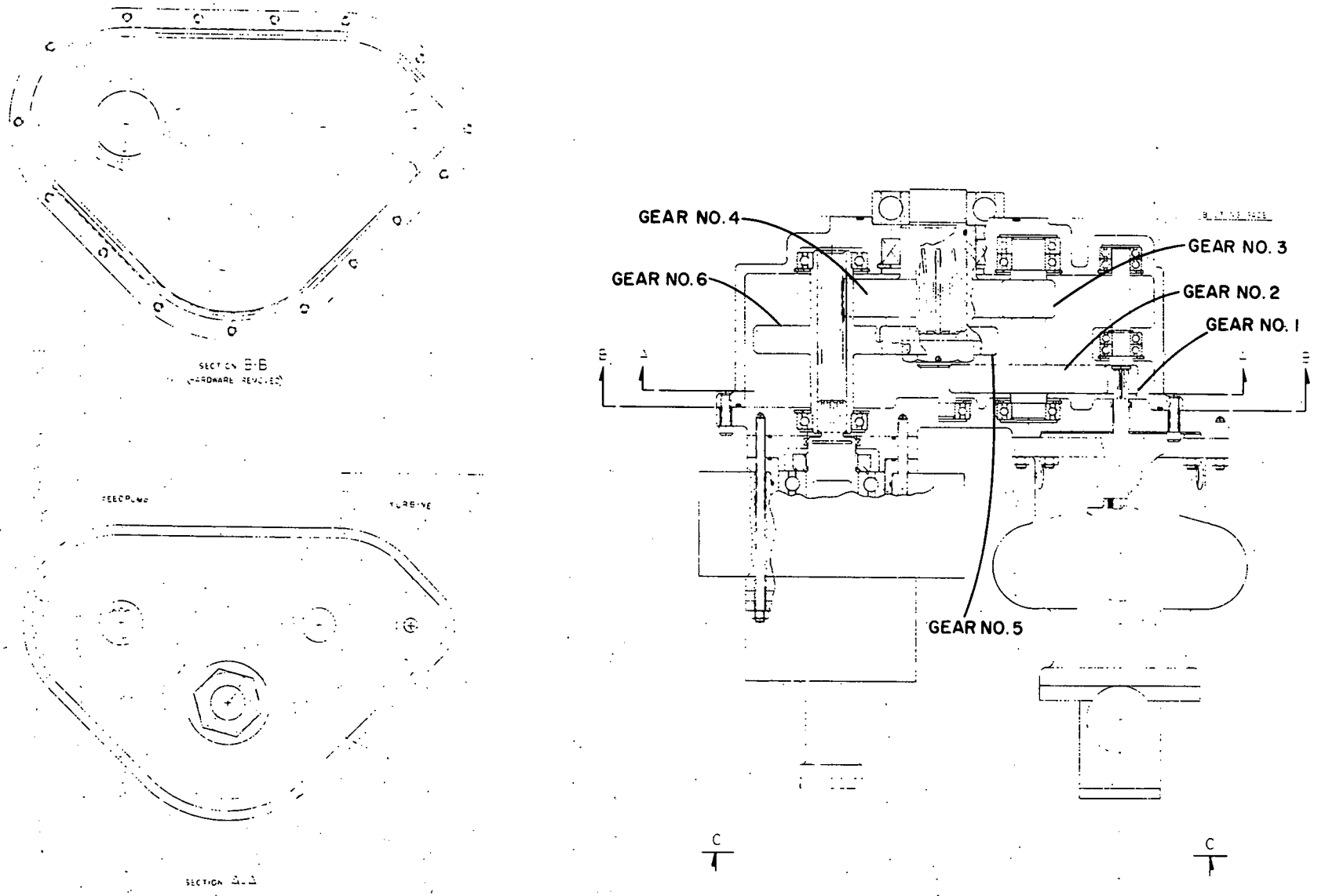

Figure 8.4. Gearbox Layout.

of 10,000 hours, it is necessary to equalize the loading on the duplex bearings by rearranging the duplex bearings to straddle the high-speed pinion.

The high-speed duplex bearings will be spray lubricated directly with provision on the outboard side of the bearings to remove the oil to prevent stagnant oil buildup. The high-speed gear mesh will be spray lubricated and cooled directly. The oil mist in the gearbox is expected to be sufficient for lubrication of the other gears and bearings, using centrifugal impellers to pull the oil mist through the bearings and return it to the sump.

The question of lubrication will be studied further to determine the final system requirements. There is a question as to whether the turbine and gearbox could use the same lubricant; if so, one oil pump and filter built into the gearbox is proposed. The question of whether there is a need for an oil cooler has yet to be resolved.

This gearbox compares favorably with the automotive high-speed turbine gearbox already developed. The automotive gearbox has been run with the pitchline velocity between 11,309 and 11,938 fpm with a tooth contact force of more than 242.85 lbs per inch with over ten million pinion tooth contacts made. No surface fatigue has been observed and it is not likely that surface fatigue would occur after more than ten million cycles. The design calculations indicate high gear tooth contact stresses for the truck bottoming gearbox, but these stresses are less than the stresses on the automotive gears. The design point tooth contact force on the truck high-speed pinion is 73% less than the experienced running condition of the automotive gearbox pinion. The conservative comparison of the

truck to automotive gearbox substantiates the engineering calculation and provides a high degree of confidence in the proposed gearbox design with further engineering effort devoted to the design.

8.3 FEEDPUMP

Many of the design requirements for the ORCS feedpump are similar to those of the seven-cylinder radial pump developed for the Automotive Rankine Power System. These similar requirements are: low NPSH, variable piston displacement to control flow rate, high pressure, compactness and reliability. However, there are the two pump differences; the truck bottoming feedpump has a 2.55 gpm maximum flow versus 16.0 gpm for the automotive pump, and it has three radial pistons, versus seven for the automotive pump. The truck bottoming components which are the same as those used in the automotive pump are the valving, the pistons, the piston rings, the variable displacement mechanism, and the eccentric radial piston drive. TECO experience gained in the development of the automotive pump will assist in the development of the truck bottoming pump.

The proposed pump is illustrated in Figure 8.5 which shows the pump diameter to be approximately seven inches and 5.12 inches from the end cover to the actuator interface. Between the actuator interface and the end of the actuator measures 4.7 inches. The input drive shaft will pilot into the pump drive off of the turbine gearbox. At the center portion of the pump is the Z-shaft. The Z-shaft axial position is controlled to change the eccentric throw, thereby changing the piston stroke.

The actuator is electro-mechanical. The actuator drive is a 1/100 horsepower, 24 volt dc reversible gear motor. The power to the motor is from the electrical power supply of the truck. The gear motor drives the gear, which is mounted on the "Saginaw" ball screw nut. The ball screw nut rotates to displace the ball screw axially. The ball screw nut is held axially in thrust roller bearings and the ball screw is held from rotating by the anti-rotation pin riding in the slot of the actuator housing. The motion of the ball screw is transmitted through the rotary joint to displace the Z-shaft axially.

The displacement setting of the pump is obtained from the feedback potentiometer driven off the gear mounted on the ball screw nut. When the feedback signal is within the control bandwidth of the control signal, the actuator is in position. If the feedback signal is out of the control signal bandwidth, the electric control will set the gear motor turning in the desired direction until the feedback signal is within the control signal control bandwidth.

Currently, the response of the actuator to change the pump displacement from zero to full is 3.5 seconds. The response time is only an engineering guess and will therefore have to be confirmed by the control system analysis. The gear motor and mechanical drive could be modified easily to accommodate any future response needs.

To obtain the predicted pump characteristics shown in Table 8.6, the pump efficiency, volumetric efficiency and minimum required NPSH were based on the automotive pump and 3 kw pump test results. Two design points were selected for the pump; one at the maximum operating speed of 2100 rpm where the maximum flow

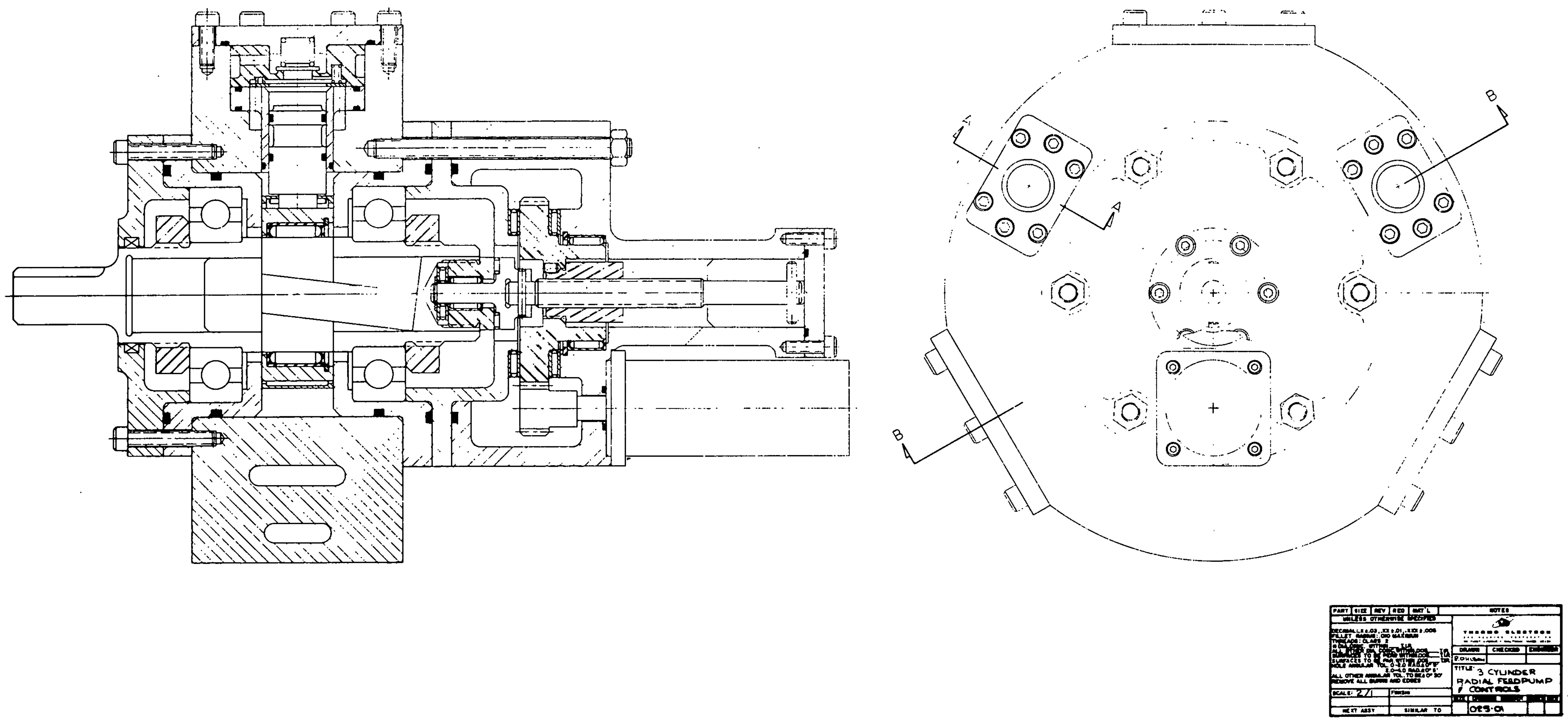

Figure 8.5 Proposed Truck Bottoming Pump.

TABLE 8.6

THREE-CYLINDER RADIAL PUMP

RPM	Pump Eff. η_p	Vol. Eff. η_v	Req'd Min. NPSH	C. I. D. $In^3/rev.$	HP	Outlet Pressure psi	Bore In.	Stroke In.	Max. Flow gpm
2100*	71%	80%	9	.355	1.91	916	.816	.226	2.55
1200**	79%	87%	5	.405	.84	628	.816	.258	1.81

* 2100 rpm maximum operating speed and flow

** 1200 rpm maximum pump displacement

of 2.55 gpm occurs, and the other at 1200 rpm where the maximum displacement of 0.405 cubic inch occurs. At 2100 rpm, the pump horsepower is 1.91, which is 4.6 percent of the organic power. It is believed that with additional engineering and design effort the proposed pump will meet the truck bottoming pumping and flow control requirements.

The part load characteristics of this pump are assumed to be the same as those of the automotive feedpump and are shown in Figures 8.6 and 8.7. These characteristics were the basis of the prediction of the part load performance characteristics of the ORCS.

8.4 VAPOR GENERATOR

The design point characteristics of the vapor-generator are shown in Table 8.7. The vapor-generator can be subdivided into three distinct zones of heat transfer. Subcooled organic liquid enters the vapor-generator and undergoes preheating until the saturation temperature is reached. The saturated liquid undergoes boiling in the next zone until the state of saturated vapor is attained. The vapor undergoes superheating in the third zone. The organic flows in a multipass cross-counterflow arrangement with respect to gas. The number of passes, however, is large and the overall design approaches the true counterflow design.

A computer program was made to study the influence of various parameters on the design of the vapor-generator. Among the parameters studied were:

- fin density
- tube diameter
- tube spacing
- organic side pressure drop
- gas side pressure drop
- number of circuits.

All these parameters were studied for the basic geometry of a finned-tube arrangement. Strip fins rather than solid fins were used, as shown in Figure 8.8a and 8.8b. The fin surface is marketed under the commercial name of ESCOA turb-x strip fin. Because of frequent interruption of the boundary layer, the heat transfer characteristics of the surface are excellent. Also, the two dimensional movement of the fins, due to thermal expansion, leads to good dirt shedding characteristics and high fouling resistance. The surface is widely used in the power-generation industry. The fins are spot-welded to the tubes.

The highest fin density permissible within the clogging constraint of the diesel exhaust service was selected; this leads to the compact design. An in-line tube arrangement was selected. Gas side pressure drop was selected so that the overall gas side pressure drop of the vapor-generator will be the same as that of the present muffler system it replaces. Thus the diesel engine does not incur any horsepower penalty.

The tube diameter and spacing decided upon were selected to achieve an attractive design from the packaging standpoint. Maximum height and width constraints were set after consultation with Mack, and the final design was selected to meet these restrictions.

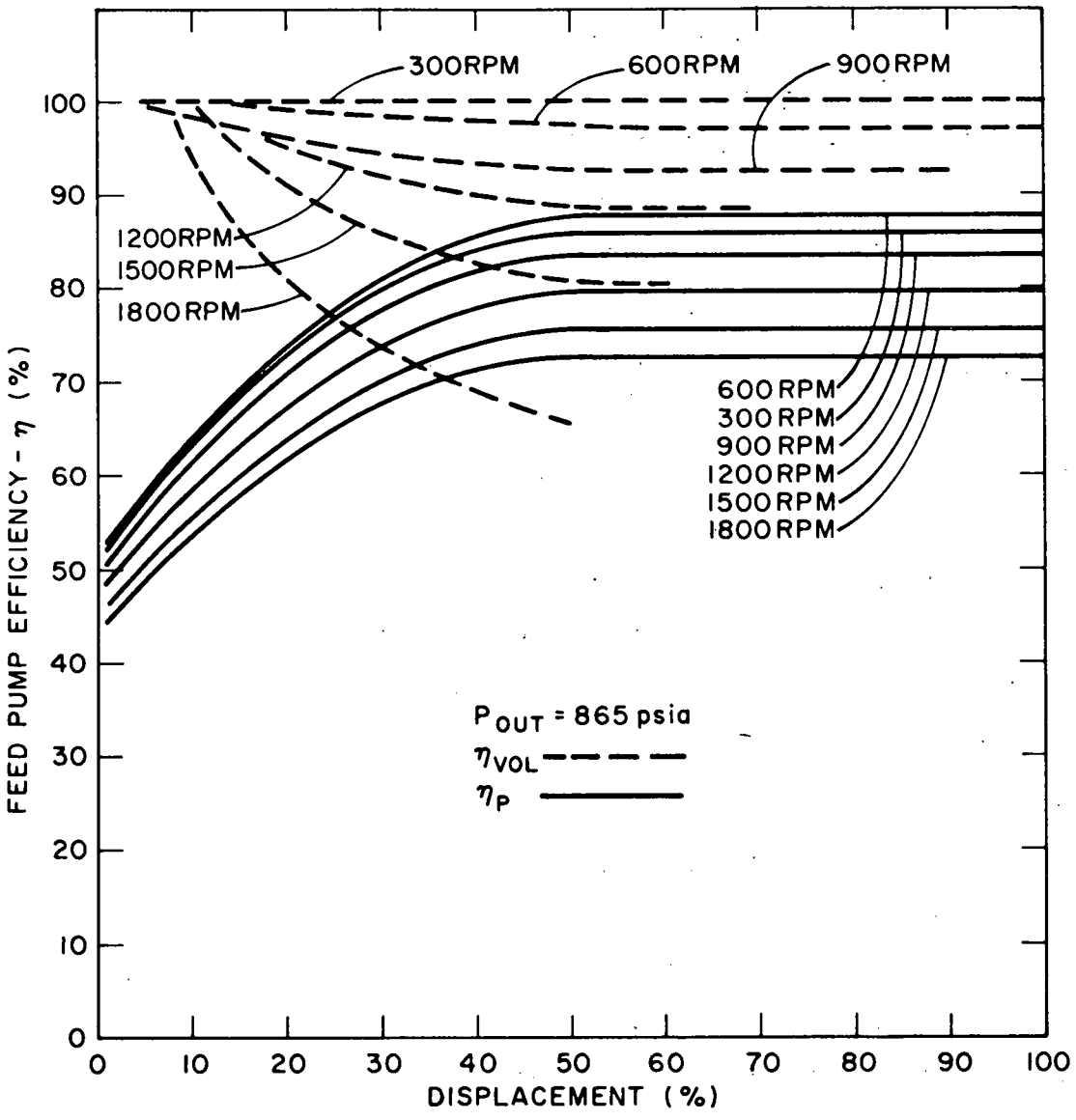

Figure 8.6. Efficiency vs Displacement of Radial Feedpump.

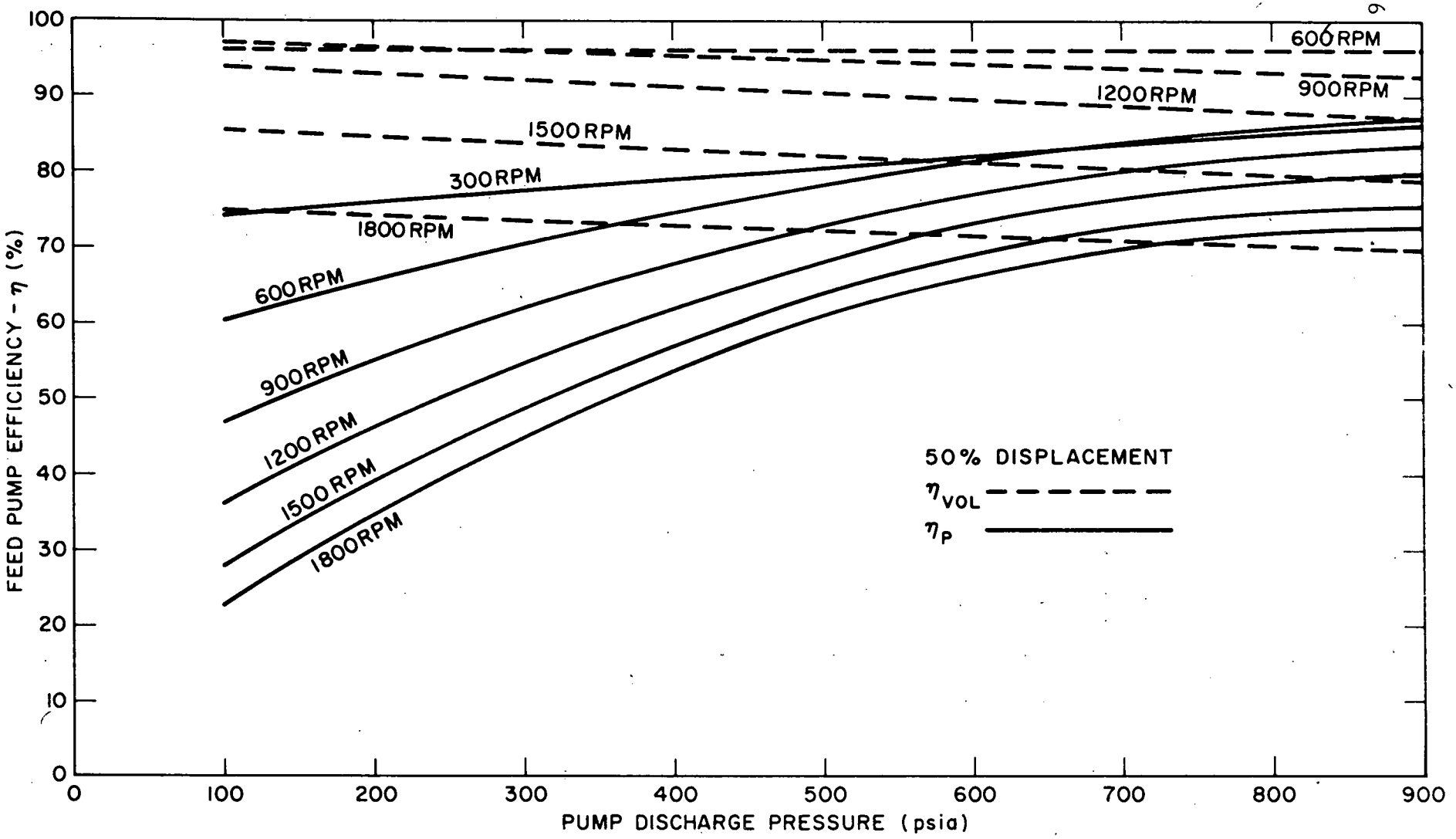

Figure 8.7. Efficiency vs Pump Discharge Pressure of Radial Feedpump.

TABLE 8.7

DESIGN POINT CHARACTERISTICS

OF THE VAPOR GENERATOR

1. Performance Characteristics	
Heat Transfer Rate	605400 Btu/hr
Working Fluid - Fluorinol-50	
Flow Rate	1626 lbm/hr
Inlet Temperature	244.7 °F
Inlet Pressure	906 psia
Outlet Temperature	650 °F
Outlet Pressure	800 psia
Diesel Exhaust Gas	
Flow Rate	3442 lbm/hr
Inlet Temperature	940 °F
Outlet Temperature	278 °F
Pressure Drop	8 in. WC
2. Salient Features	
Type of Flow	cross-counterflow
Type of Construction	banks of finned tubing in-line arrangement
Number of Parallel Circuits	12
Number of Passes	56
3. Dimensions	
Tube	
Outside Diameter	.375 in.
Inside Diameter	.305 in.
Fin	
Type	ESCOA Turb X 5/64" segment

TABLE 8.7 (continued)

Fin (continued)	
Thickness	.012 in.
Height	.125 in.
Pitch	10 FPI
Transfer Area/ft of Tubing	.38 ft^2/ft
Tube Spacing	
Transverse XT	.75 in.
Longitudinal XL	1.0 in.

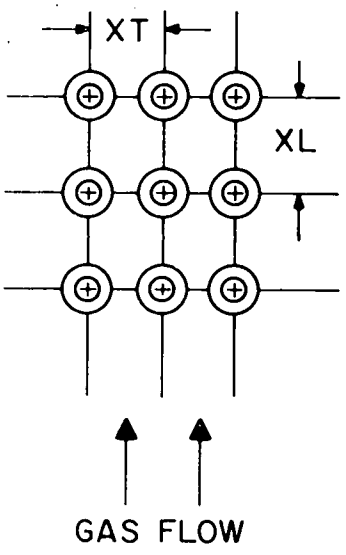

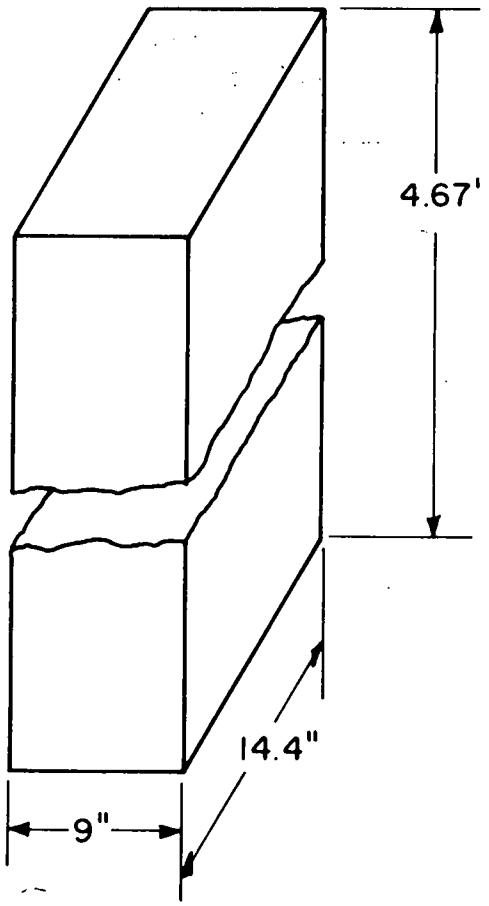

TABLE 8.7 (continued)

DESIGN POINT CHARACTERISTICS

OF THE VAPOR GENERATOR

4. Heat Transfer Characteristics		
Effectiveness		
Preheat Region	.895	
Boiling Region	.713	
Superheat Region	.388	
"UA"		
Preheat Region	4493	Btu/hr °F
Boiling Region	1146	Btu/hr °F
Superheat Region	557	Btu/hr °F

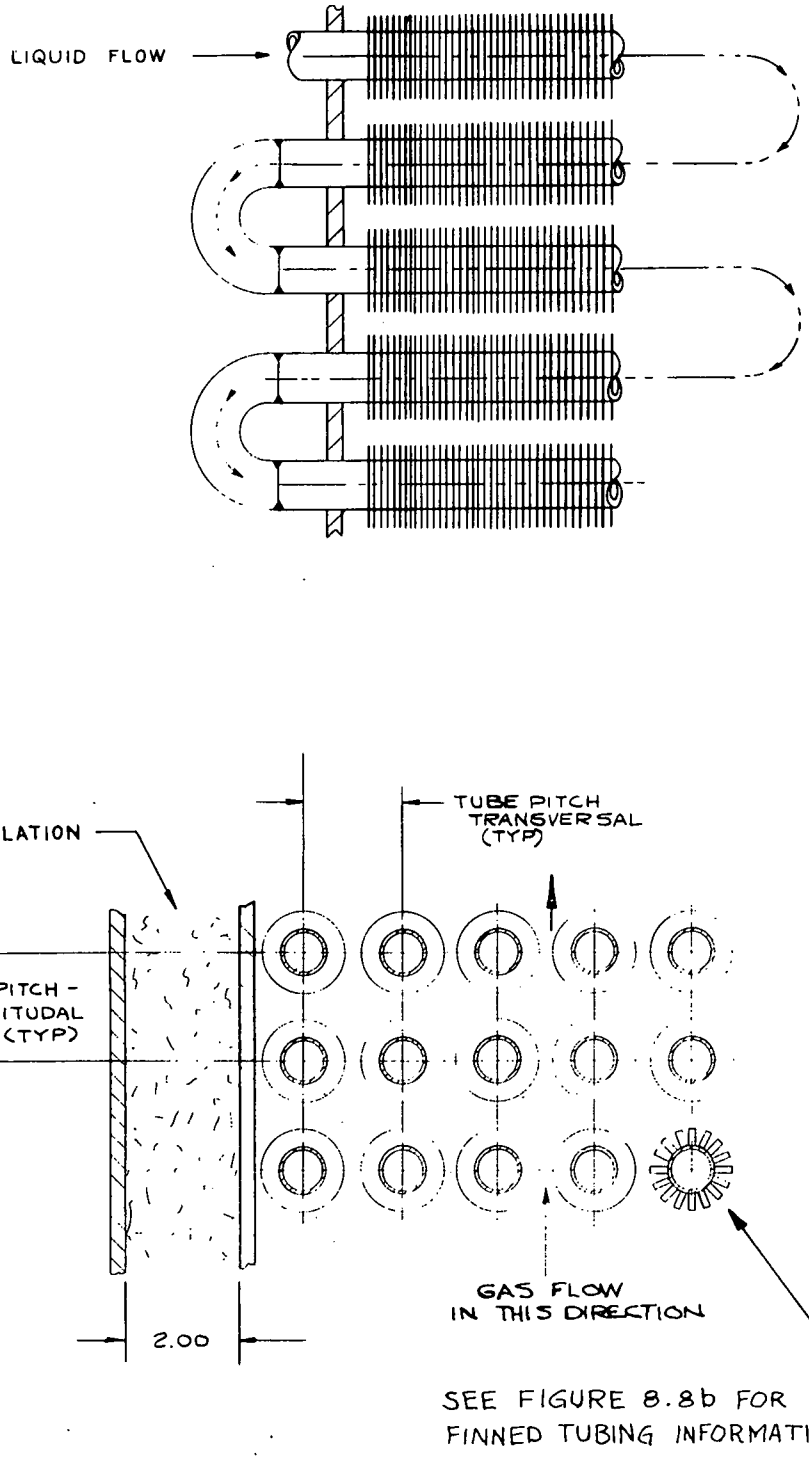

Figure 8.8a. Section Details Illustrating Finned Tube Geometry.

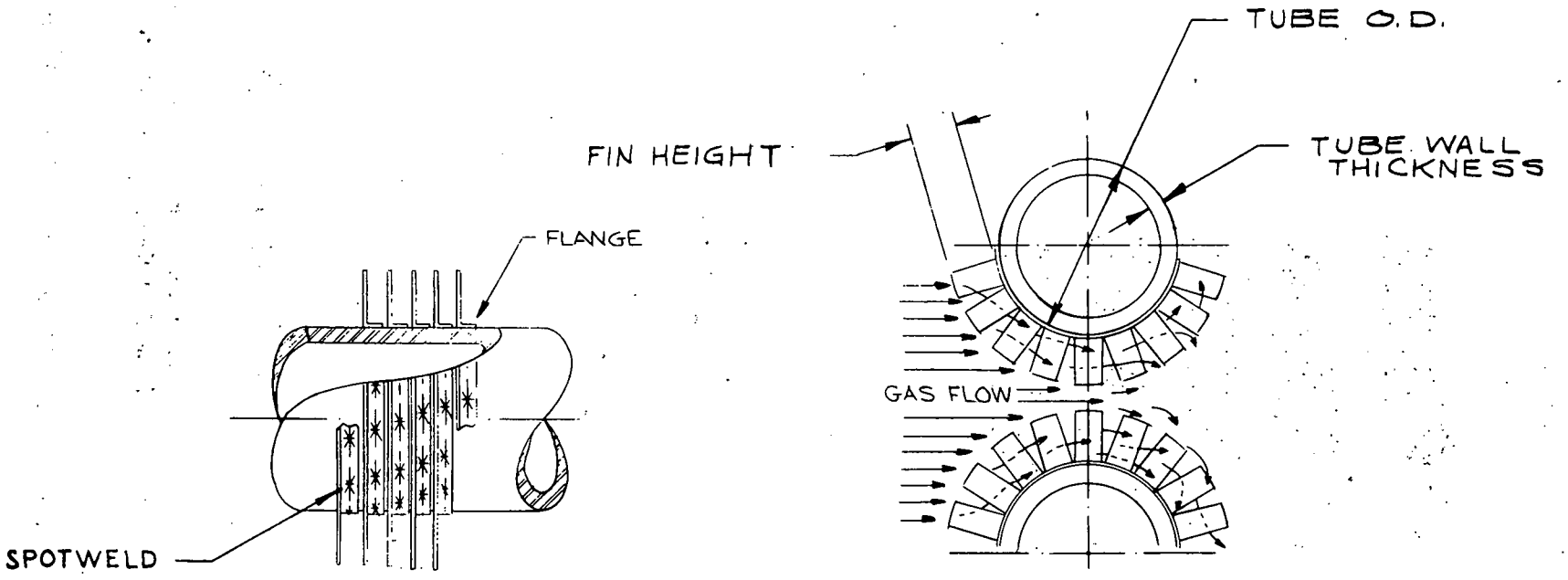

Figure 8.8b. **Illustration of Finned Tube Geometry.**

A multiparallel circuit design was selected for the organic side to keep the pressure drop low. Also, it permits the use of small diameter tubes and allows a more compact design. An analysis was made for flow stability in multi-channel flow. The pressure drop on the organic side was assumed to be given by the homogeneous flow model in the two phase region. No flow instability was discovered as per Ledinegg criterion. The organics are inherently less prone to parallel flow instability than water. This is because of lower heat of vaporization and a much lower specific volume change between the liquid and vapor phases compared to water. In order to make the design even more conservative, inlet orifices are incorporated into the design. The attendant inlet pressure drop has further stabilizing influence on the vapor-generator performance.

The detailed design and characteristics of the vapor-generator that will be used in the demonstration testing in the next phase are described in Chapter XIII.

The organic and gas temperature profiles at the design point are shown in Figures 8.9 and 8.10. The preheat region represents nearly 72% of the total vapor-generator size, although it represents only 42% of the total heat transfer rate. The vapor-generator has a very high effectiveness design, and the exhaust gas temperature leaving the vapor-generator is only 32.8°F greater than the incoming organic liquid temperature.

The part load characteristics of the vapor generator are shown in Figure 8.11. The "UA" of the vapor-generator decreases as 0.59 power of the exhaust gas flow rate. This model of the vapor-generator is used to evaluate the part load characteristics of the

ORCS. The vapor-generator temperature profile at an off-design condition is shown in Figures 8.12 and 8.13. The minimum temperature difference between the organic and gas stream no longer occurs at the gas outlet location, but at the point where boiling begins. This point is also referred to as the "Pinch Point." The boiling region now represents the largest fraction of the heat transfer rate, as well as the "UA."

8.5 CONDENSER/RADIATOR

The heat rejection rate of the ORCS is comparable to that of the diesel engine alone. In order to use a single fan for the entire cooling requirement, it was decided to integrate the condenser and radiator. The existing truck radiator uses most of the available height; however, significantly more width is available. Mack specified the maximum frontal area that could be used conveniently for the heat exchanger. A depth was chosen which was consistent with the existing truck dimensions and which allowed sufficient room for a fan and shroud.

The design point characteristics of the condenser/radiator are shown in Table 8.8. The radiator heat rejection and temperature specifications were given by Mack. For this exchanger, it was necessary to find an efficient and compact surface. A search for such a surface had been made earlier for use in automotive Rankine-cycle condensers. On the basis of that research a perforated fin surface manufactured by Air Research was selected. For the present application this surface was compared with the louvered fin surface used by Ford Motor Company in their automobiles.

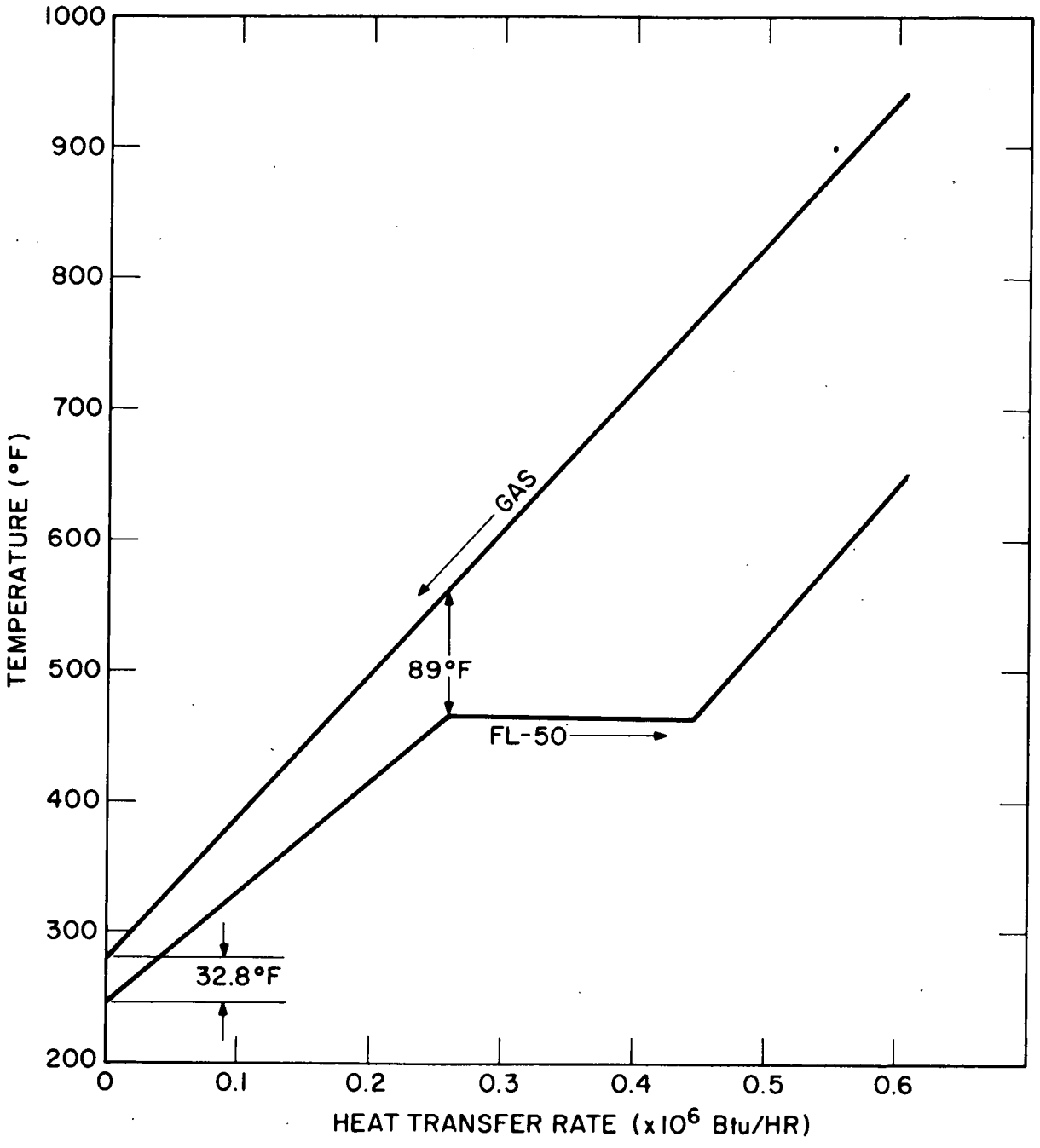

Figure 8.9. Design Point Temperature Profile Vs. Vapor Generator Heat Transfer Rate.

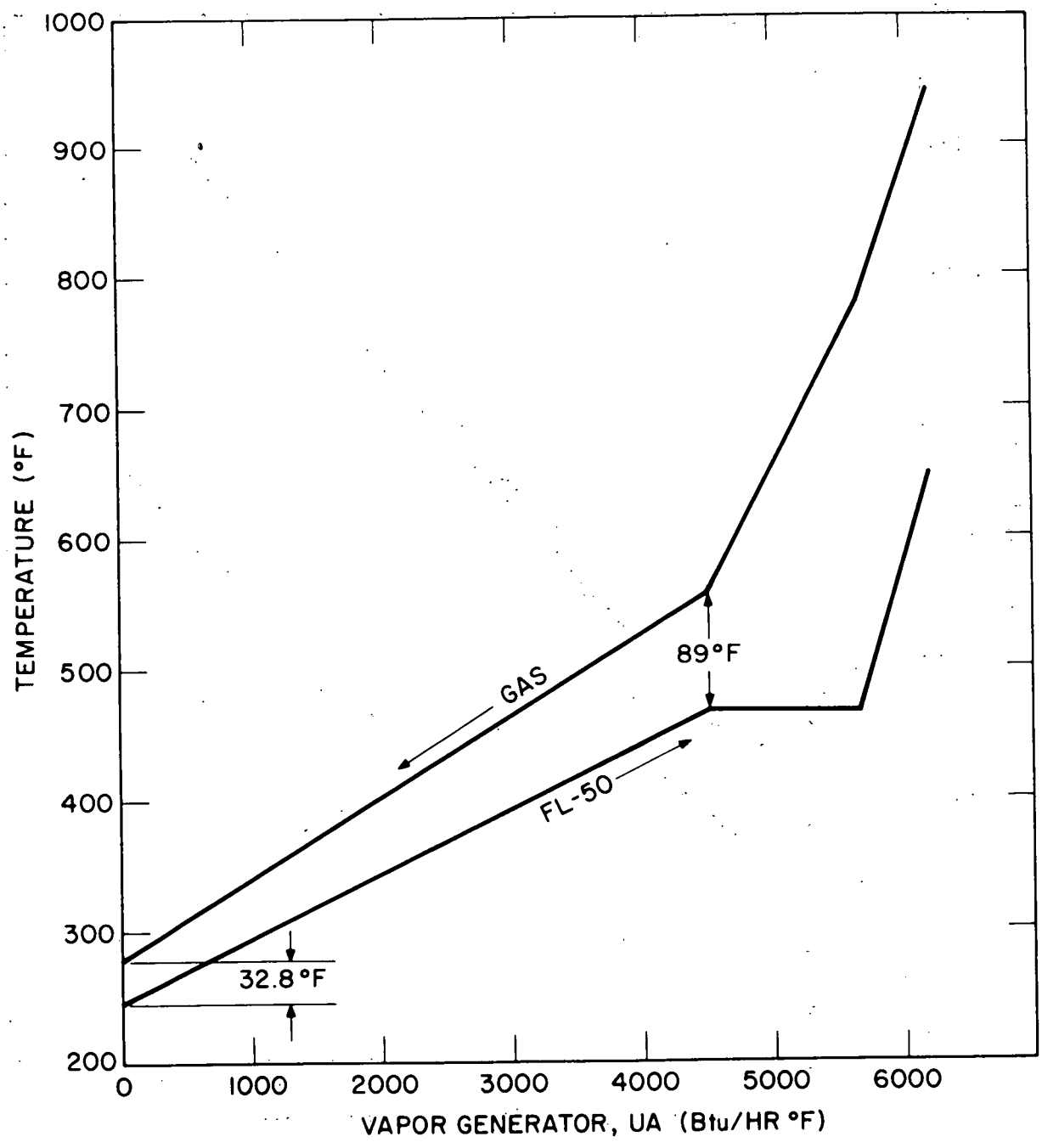

Figure 8.10. Design Point Temperature Profile vs. Vapor Generator "UA" Btu/hr °F.

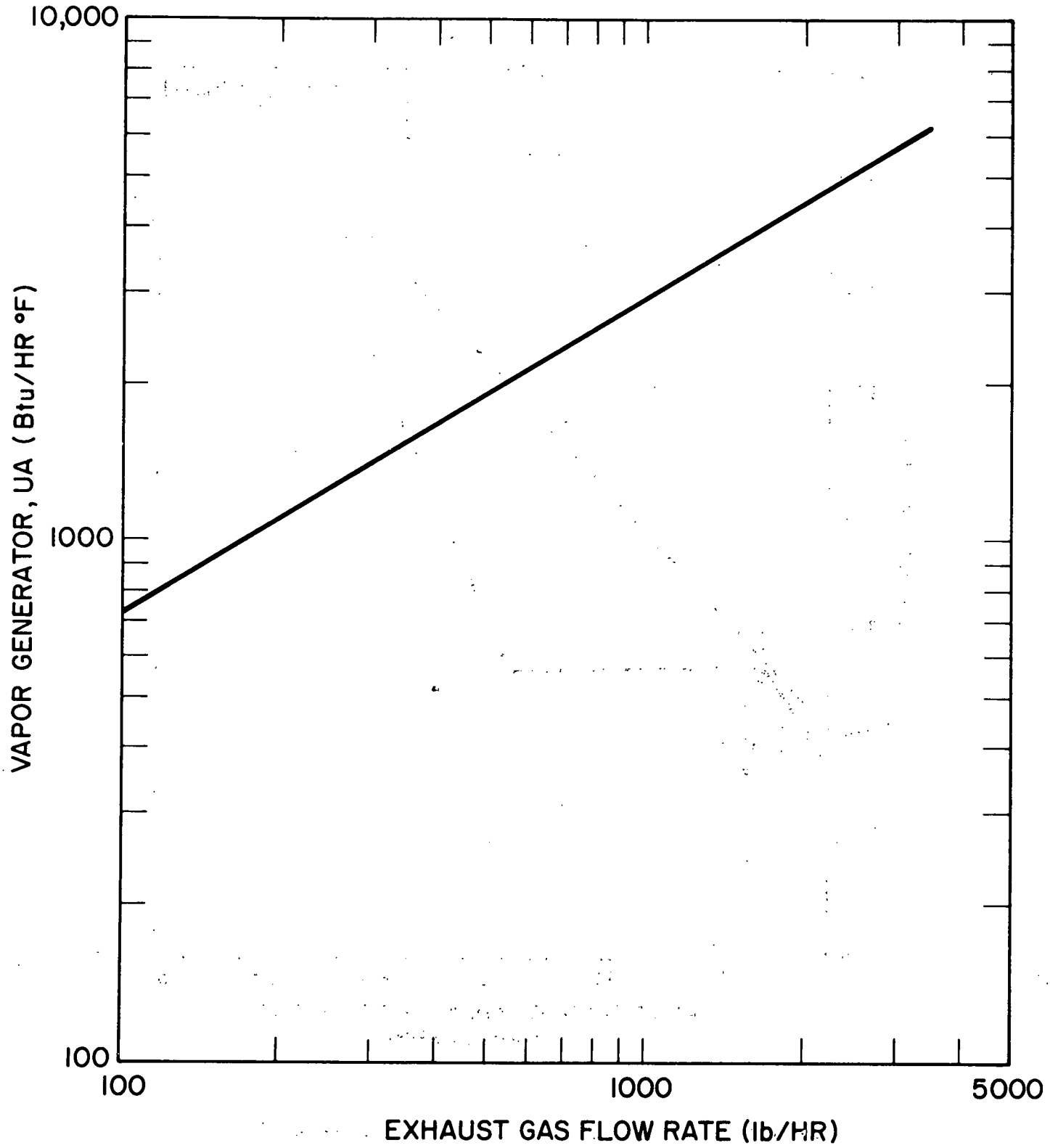

Figure 8.11. Vapor Generator "VA" vs. Exhaust Gas Flow Rate.

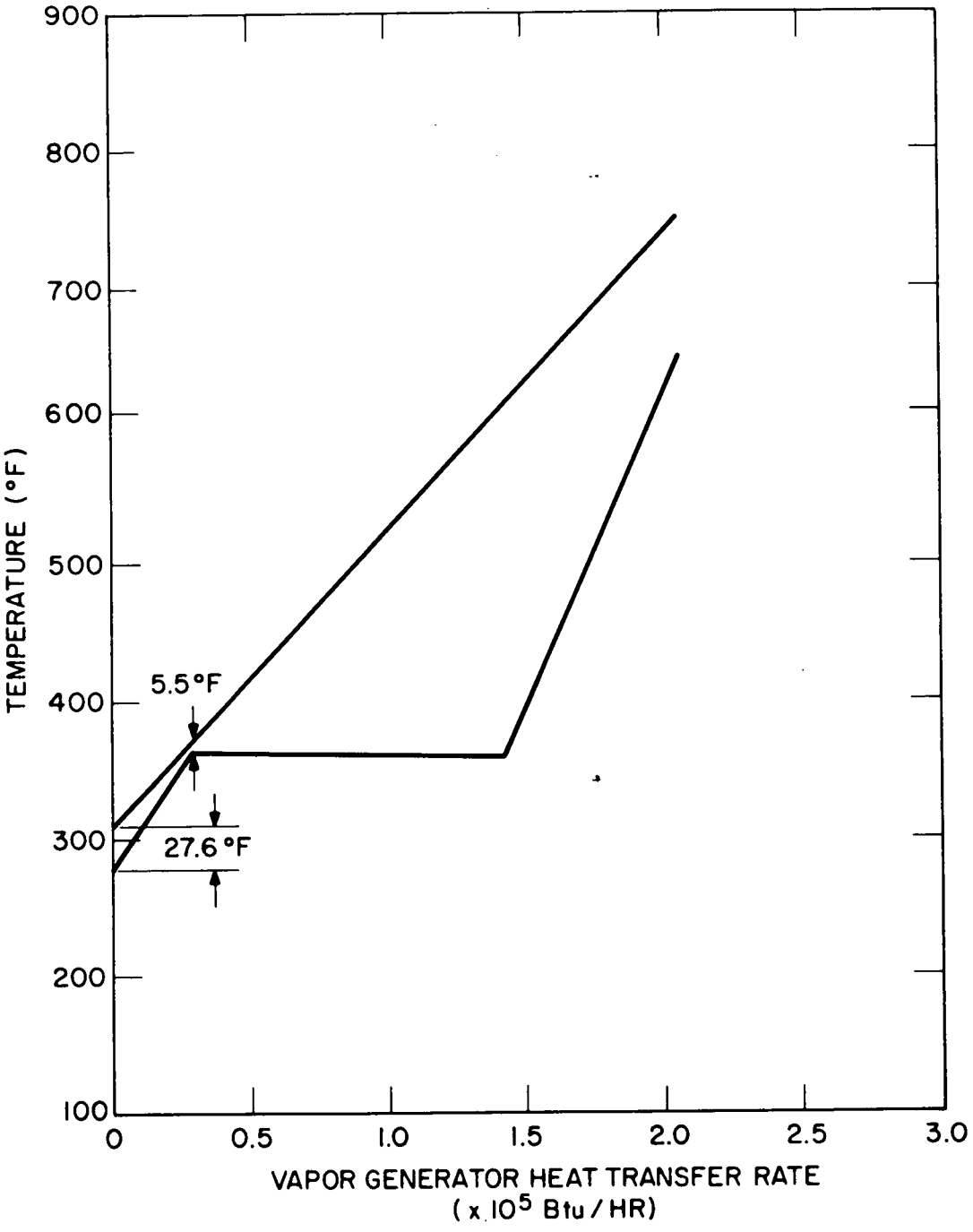

Figure 8.12. Temperature Profile vs. Vapor Generator Heat Transfer Rate at Part Load.

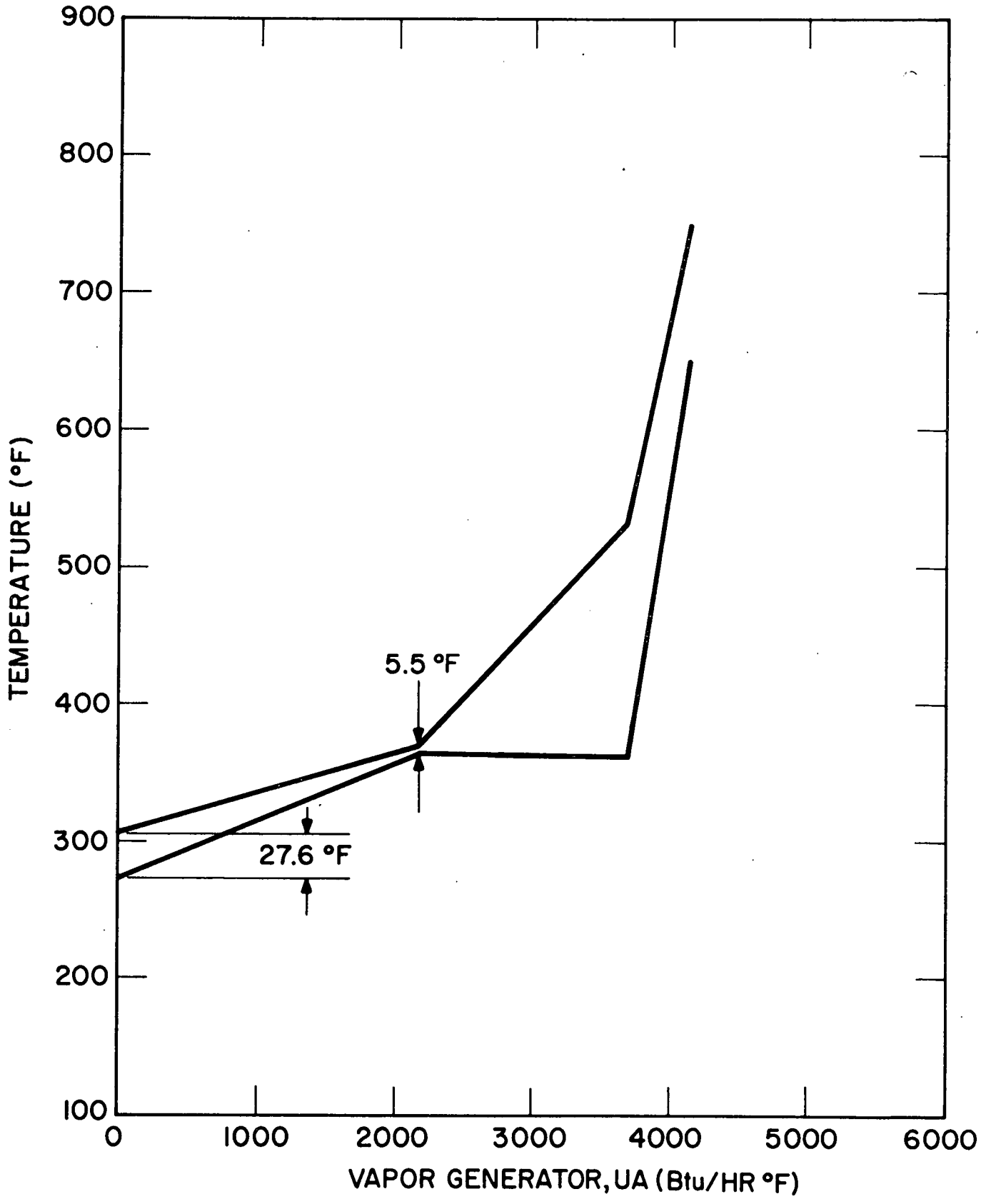

Figure 8.13. Temperature Profile vs. Vapor Generator "UA" at Part Load.

TABLE 8.8

CONDENSER-RADIATOR CHARACTERISTICS

1. Performance Characteristics	
Heat Transfer Rate	
Condenser	468,100 Btu/hr
Radiator	392,200 Btu/hr
Flow Rate	
Air	40,944 lbm/hr
Water	51,900 lbm/hr
Fluorinol	1,626 lbm/hr
Condensing Temperature	163°F
Water Temperature (average)	185°F
Air Temperature	
Inlet	85°F
Outlet	172.2°F
Pressure Drop	
Air	core 1.17 in. WC overall 2.35 in. WC
Water	2.9 psi
Fluorinol	1.5 psi
2. Physical Characteristics	
Type of Flow	Crossflow
Type of Construction	fin and tube Ford 13 FPI EC7 louvered fin core
Core Dimensions	
Height	30 in.
Width	46.6 in.
Depth	
Condenser	2.39 in.
Radiator	1.91 in.

TABLE 8.8 (continued)

CONDENSER-RADIATOR CHARACTERISTICS

Fin Dimensions		
Height	0.50	in.
Thickness	0.0025	in.
Pitch	13	fpi
Material	Copper	
Tube Dimensions		
Width	0.076	in.
Depth	0.625	in.
Air Side Transfer Area/Total Volume	312.79	
Water and Fluorinol Side Area/Total Volume	37.77	
3. Heat Transfer Characteristics		
Number of Transfer Units		
Condenser	0.936	
Radiator	1.4105	
Average Transfer Coefficient		
Air	37.36	Btu/hr-ft^2-°F
Water	2370	Btu/hr-ft^2-°F
Fluorinol	377	Btu/hr-ft^2-°F
Heat Transfer Resistance Ratio		
Condenser Rf/Ra	1.09	
Radiator Rw/Ra	0.09	

From the standpoint of the overall volume and pressure drop, there was a virtual standoff between the choice of which surface to use. However, a louvered fin surface was selected for two reasons: (1) it has a lower fin density (13 fpi compared to 22 fpi required for the perforated fin surface) and also has better clogging characteristics and lower weight, and (2) the surface has been accepted from the standpoint of automotive duty requirements and the heat exchanger can be fabricated with a very high level of confidence for this application.

A layout of the condenser/radiator and fan assembly is shown in Figure 8.14. Although the heat exchanger is constructed as a single unit, it is essentially two separate heat exchangers with separate tanks and tubes, operating in series in the air stream. The condenser is mounted upstream of the radiator to keep the condensing temperature as low as possible, thus operating the ORCS at the highest possible efficiency. Also, this results in preheating of the air entering the radiator and helps to maintain the average jacket water temperature within a relatively narrow range for fairly wide variations in ambient temperature. This is desirable from the diesel standpoint.

The fan was selected to provide adequate flow with no ram assist required at the design point. Sufficient head has to be provided to overcome the compartment losses in addition to the core loss. The characteristics of the axial fan selected are shown in Figure 8.15. These characteristics were used for evaluating the part load performance of the ORCS. The ORCS was charged for the difference between the actual fan power and the diesel fan power given by Mack. The compartment losses were also provided by Mack. The efficiency of the fan is typical for automotive type fans. The fan power could be reduced substantially by the use of a tube-axial high-efficiency fan.

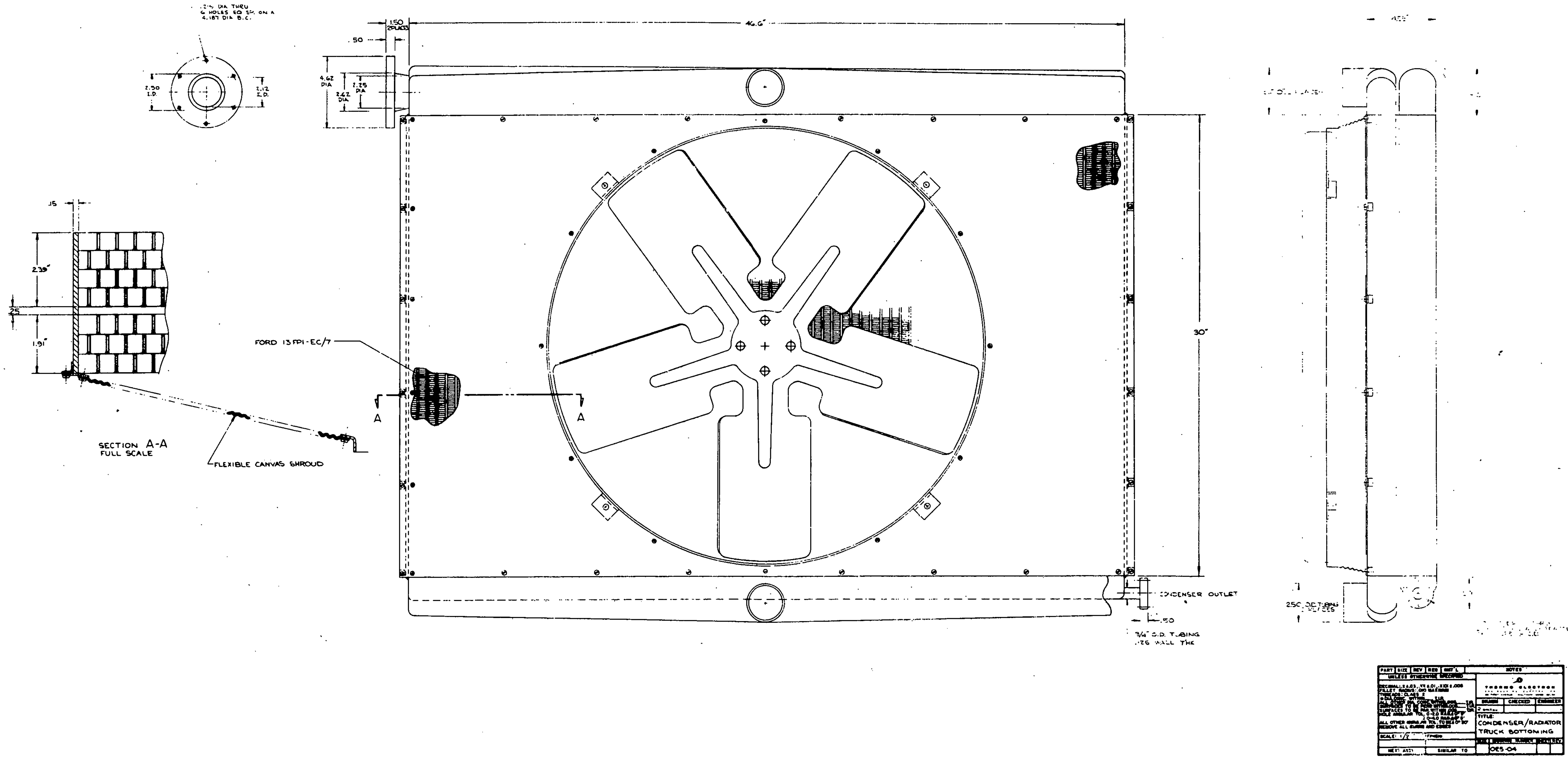

Figure 8.14. Condenser/Radiator and Fan Assembly.

THIS PAGE
WAS INTENTIONALLY
LEFT BLANK

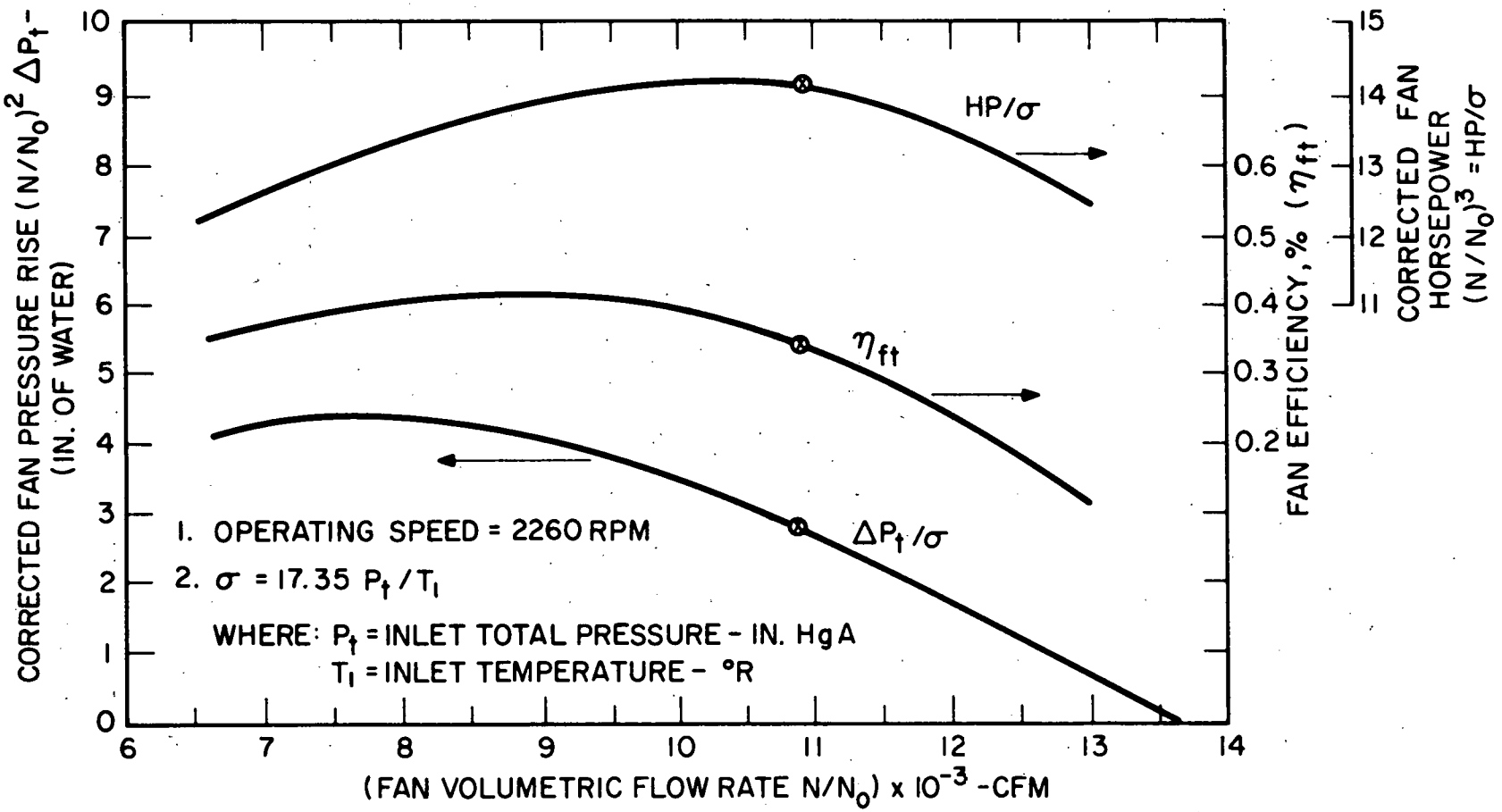

Figure 8.15. Performance of the Condenser/Radiator Fan.

The fan is driven by a diesel engine via a variable ratio drive. Thus, the fan speed/diesel speed is changed in response to the rack position. The fan speed/diesel speed schedule was obtained from the part load optimization study described in the next chapter.

Part load characteristics of the condenser/radiator were also computed. Figure 8.16 shows the effectiveness of the condenser and the radiator as a function of air flow rate. These characteristics were used in the part load program to compute the overall ORCS characteristics.

In this study, the optimization was done to maximize net power. For this reason, the approach of using an intermediate water-cooled condenser (Figure 8.17) was rejected. This approach would, in essence, call for the organic rejecting heat to the water which in turn would reject heat to the ambient air. Since the use of an intermediate heat exchanger would raise the ΔT between the ambient air and the condensing temperature for the same fan power, it would amount to lower cycle efficiency and increased irreversibilities and, hence, lower net power. There is also added parasitic loss associated with the water pump. Also because of the nature of the duty cycle, which is a very high average power/design power cycle, the energy storage feature of the water to augment the performance over fast transients is of little practical use. An intermediate water system does, however, have the attractive feature of replacing a large hermetic condenser with a small hermetic water-cooled exchanger, thus eliminating the need for a flex line between the regenerator and the condenser. There will still be an efficiency penalty associated with this approach, but the hardware simplicity tradeoff may be appealing from the standpoint of fabrication, assembly and testing.

8.6 REGENERATOR

The regenerator provides partial sensible cooling of the exhaust vapor from the turbine and, in turn, preheats the liquid entering the vapor-generator. Thus a higher effectiveness regenerator reduces the condenser heat rejection requirement and the fan power requirement. Although it also improves the cycle efficiency of the ORCS in terms of gross power output/heat input in the vapor generator, this effect is somewhat offset by reduced heat recovery in the vapor generator. These effects were studied in the system optimization studies and an optimum regenerator effectiveness of 0.9 was selected. Regenerator effectiveness is the fraction of maximum sensible cooling undergone by vapor.

The design point characteristics of the regenerator are shown in Table 8.9. The design is a multipass, cross-counterflow, plate fin construction. Low carbon steel was selected as the material of construction with AWS BN-2 as the braze material. Aluminum was first considered because of its high thermal conductivity, low weight and good corrosion resistant properties. However, because of high pressure on the liquid side and moderately high temperature, the stress levels for aluminum were too high and therefore steel was selected.

The ruffled fin surface is used for both the liquid and the vapor side to keep the design simple. This surface is fabricated by U. A. P. and was also used for the automotive regenerator. The liquid flows in a four-pass cross-counterflow arrangement with one vapor pass.

The layout of the regenerator is shown in Figure 8.18.

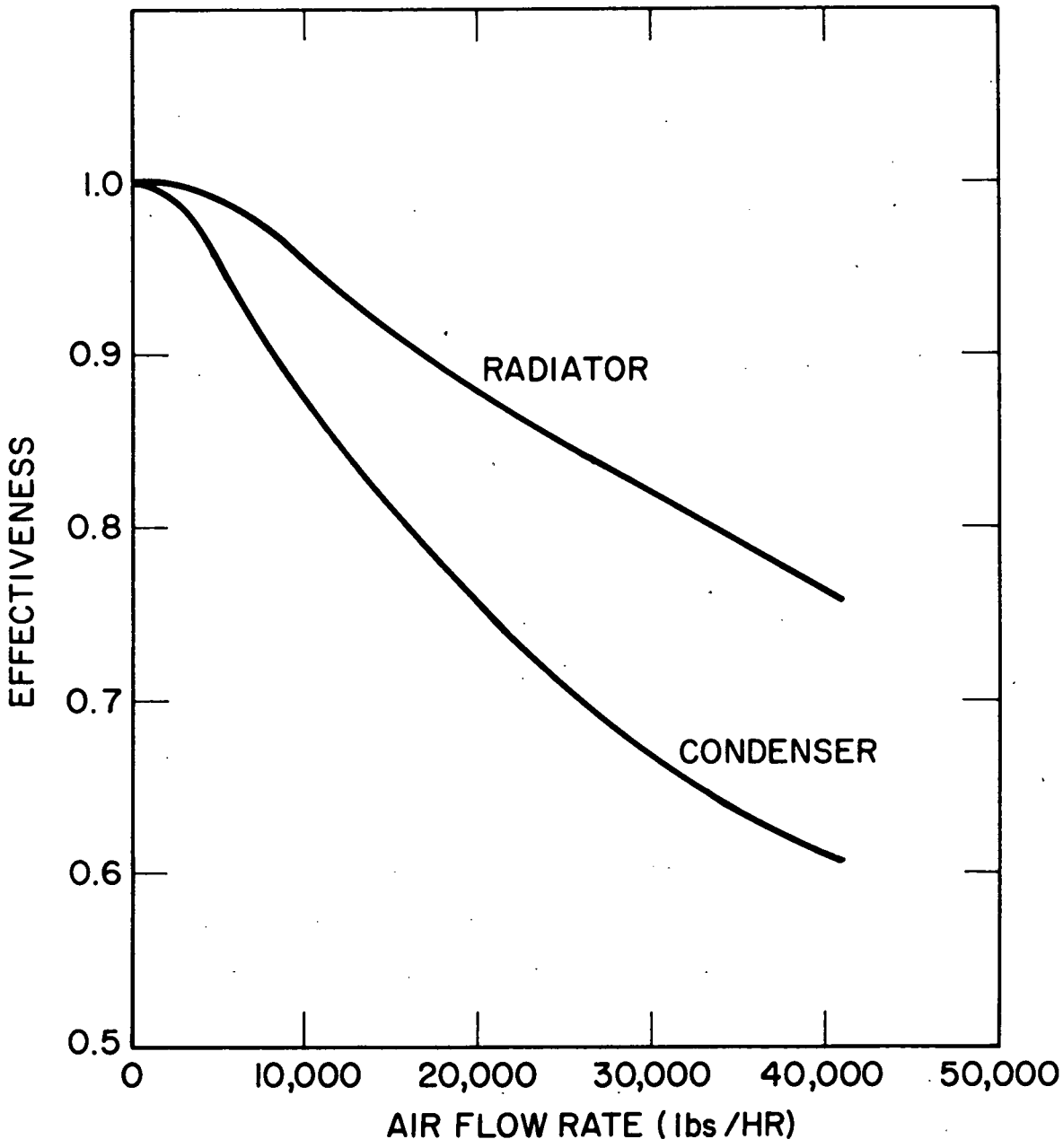

Figure 8.16. Condenser/Radiator Effectiveness vs. Air Flow Rate.

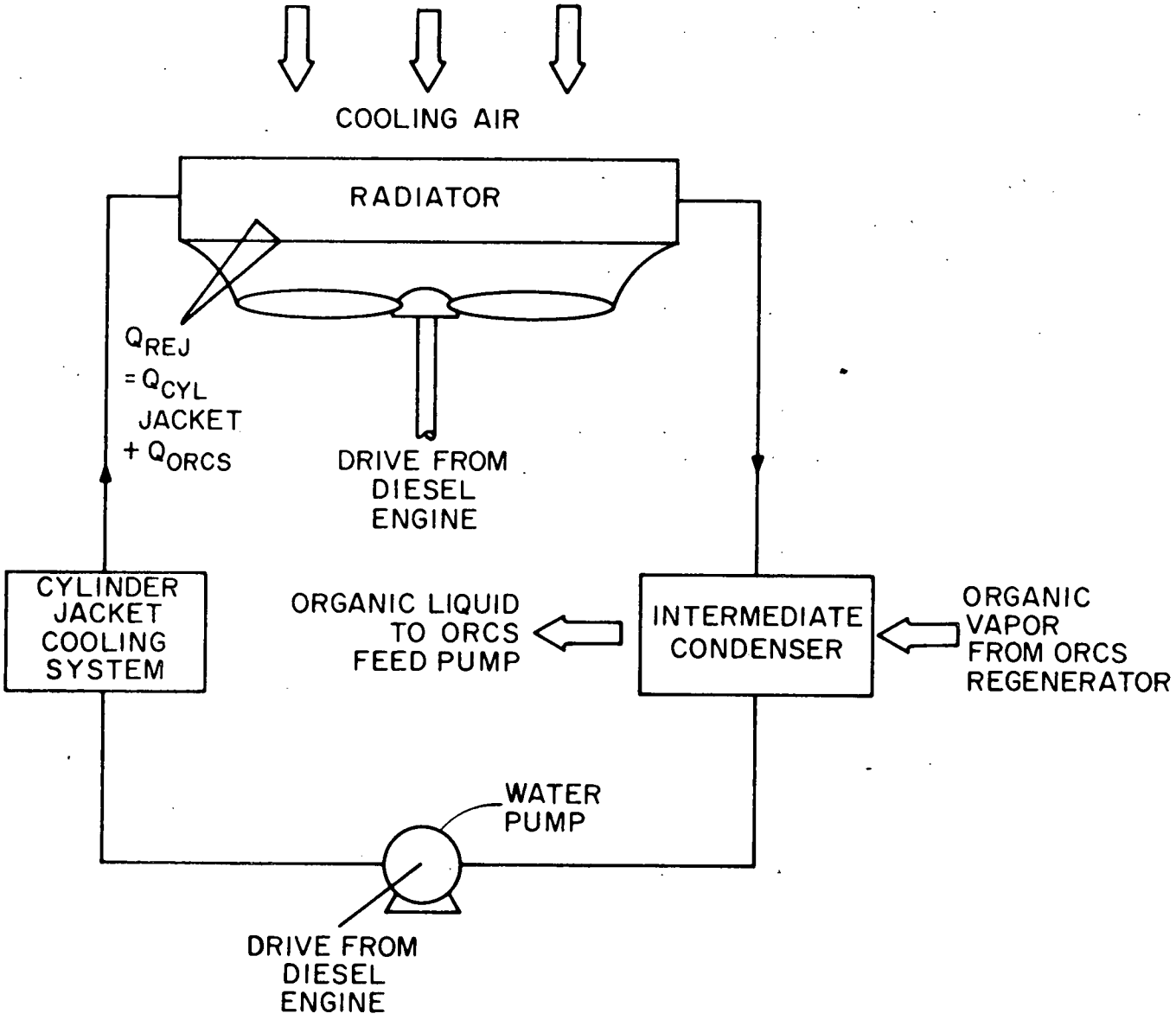

Figure 8.17. Intermediate Condenser with Air-Cooled Radiator Flow Schematic.

TABLE 8.9

DESIGN POINT CHARACTERISTICS OF REGENERATOR

1. Performance Characteristics	
Heat Transfer Rate	60,540 Btu/hr
Effectiveness at 100% load	0.9
Liquid Conditions	
Inlet temperature	162.01 °F
Inlet pressure	916 psia
Outlet temperature	244.7 °F
Outlet pressure	901 psia
Vapor Conditions	
Inlet temperature	330 °F
Inlet pressure	14.85 psia
Outlet temperature	188 °F
Outlet pressure	14.33 psia
Flow Rate	1626 lbm/hr
2. Physical Characteristics	
Type of Flow	Cross-counter flow
Type of Construction	Plate and fin
Material	Low Carbon Steel
Number of layers	
Vapor	11
Liquid	10
Number of Passes	
Vapor	1
Liquid	4
Core Dimensions, Fin	7 x 7 x 5.43 in.

TABLE 8.9 (continued)

DESIGN POINT CHARACTERISTICS

OF REGENERATOR

Type	ruffled fin, UAP U-405649
Pitch	24 fpi
Thickness	0.007 in.
Height	0.233 in.
3. Heat Transfer Characteristics	
Transfer Coefficient	
Liquid	195.7 Btu/hr-ft^2-°F
Vapor	112.4 Btu/hr-ft^2-°F
Transfer Area	
Liquid	38.26 ft^2
Vapor	47.2 ft^2
Fin Efficiency	
Liquid	0.60
Vapor	0.65
Transfer Resistance Ratio Rl/Rv	0.76
Overall UA	1959

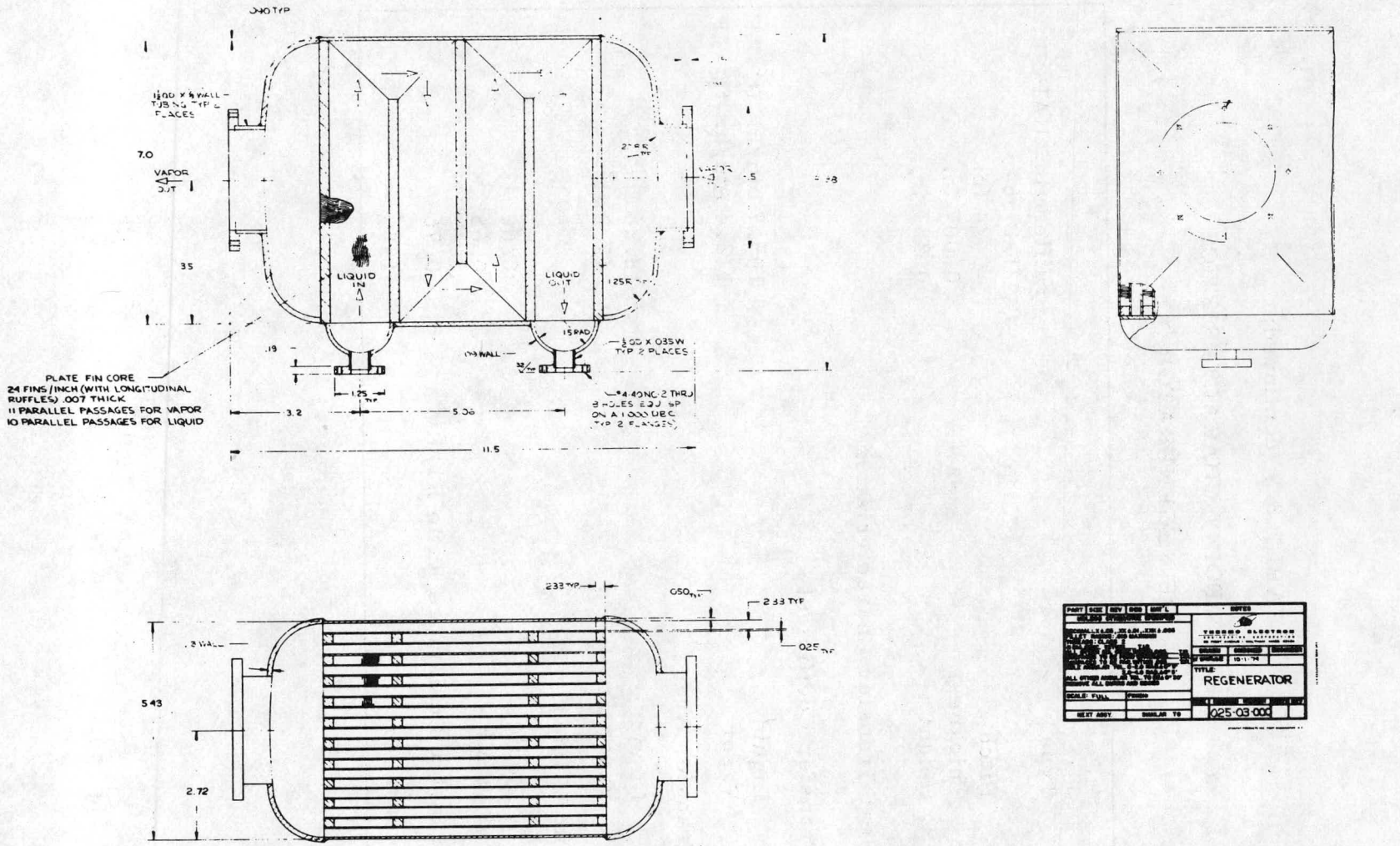

Figure 8.18. Regenerator Layout.

Part load characteristics of the regenerator are shown in Figure 8.19. These characteristics were used to compute the overall ORCS part load performance.

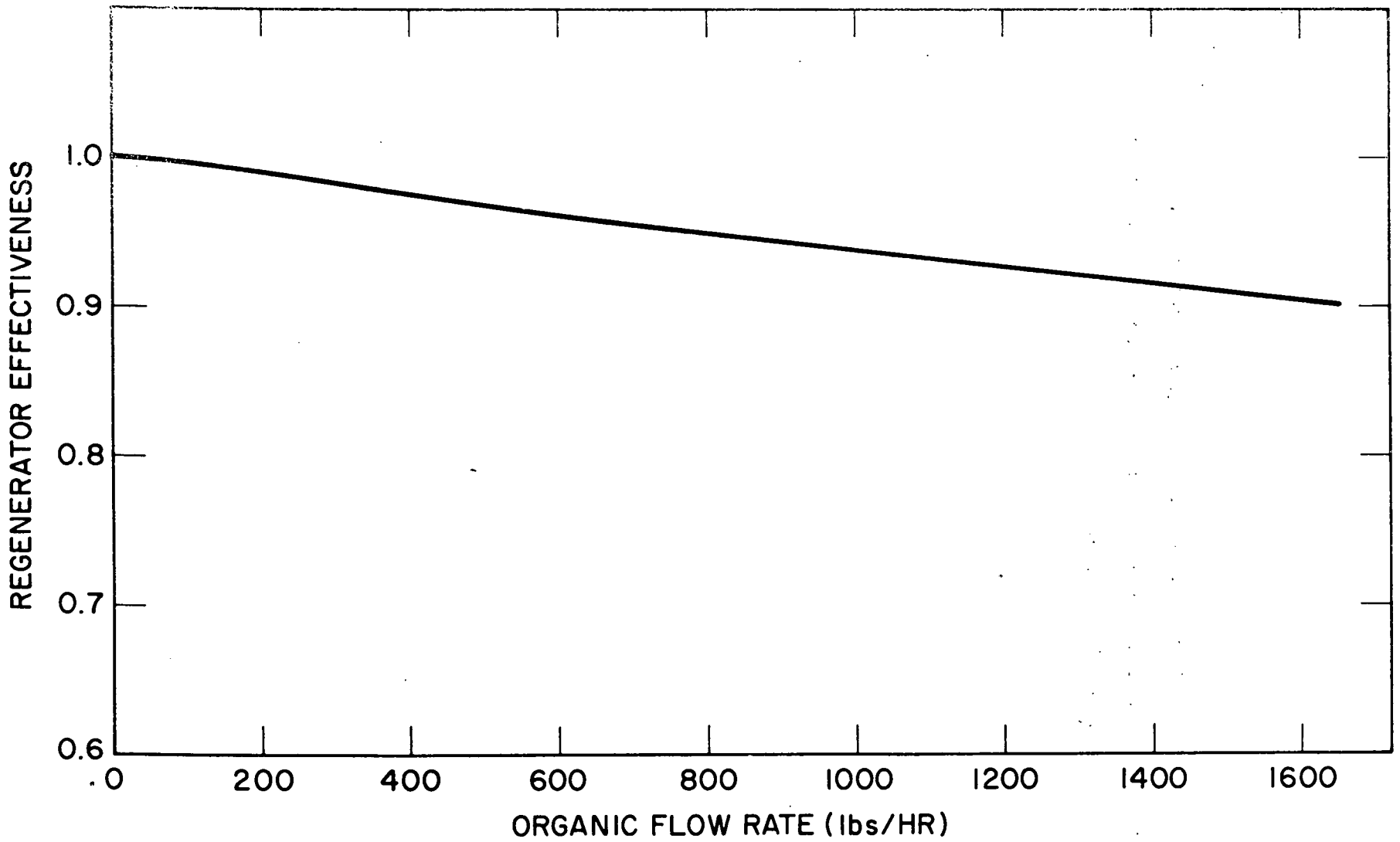

Figure 8.19. Part Load Characteristics of Regenerator.

9. PART LOAD PERFORMANCE OF ORCS

The part load performance of the ORCS was computed to cover the range of operation for a typical duty cycle for the reference diesel engine. The diesel engine performance for the production engine was measured by Mack Trucks, Inc. and the data are shown in Appendix A. The steady-state performance characteristics of the ORCS corresponding to each of the points listed in Table 9.1 were calculated.

A computer program was made to analyze the ORCS. A summary of the program logic is described in Appendix D. Part load characteristics of the major ORCS components are described in Chapter VIII. These were programmed for the ORCS performance evaluation.

The diesel exhaust gas temperature decreases with load. In order to maximize the net power from the ORCS, the pressure level is reduced with load. One simple way to accomplish this is by using a fixed area turbine nozzle block. The flow at the nozzle throat is choked and therefore the pressure level is determined by the flow rate and temperature of the organic.

The organic flow rate and fan speed were treated as parameters for each diesel engine operating point. An iterative procedure was set up for convergence of cycle conditions while satisfying all the part load characteristics. The ORCS net power was computed for a range of flow rate and fan speed for each point and the optimum values of these parameters were selected. The organic temperature at the outlet of the vapor-generator was never allowed to exceed 650°F to control thermal degradation of the fluid. The average

TABLE 9.1

PART LOAD PERFORMANCE OF DIESEL/ORCS COMPOUND ENGINE

Diesel Speed rpm	Diesel BHP	Diesel Fuel Flow Rate lbs/hr	Diesel Exhaust Gas Flow Rate lbs/hr	Diesel Exhaust Gas Temp. °F	Diesel Net Power hp	Organic Flow Rate lbs/hr	Fan Speed rpm	Turbine Efficiency %	ORCS Net Power hp	Compound Engine Net Power hp	% Improvemt.
2100	288	114.5	3442	940	273	1626	2270	72.8	47.8	320.8	17.51
2100	202	82.7	2951	795	187	1025	1570	69.3	37.1	224.1	19.86
2100	146	63.8	2527	727	131	743	940	65.4	30.8	161.8	23.52
1800	292	105.5	3090	903	284	1355	1980	70.3	37.1	321.1	13.04
1800	232	84.5	2668	835	224	1030	1500	68.6	30.9	254.9	13.8
1800	203	74.5	2448	800	195	865	1265	67.1	27.3	222.3	13.96
1800	146	56.5	2100	730	138	630	450	63.9	20.8	158.8	15.03
1600	285	99.5	2739	920	278.6	1255	1895	67.5	32.1	310.7	11.51
1600	229	79.5	2323	865	222.6	945	1405	65.7	27.0	249.6	12.1
1600	142	52.3	1738	750	135.6	555	850	60.9	16.8	152.4	12.39
1200	254	89.0	1958	1090	240.6	1153	1860	58.4	24.3	273.9	9.78
1200	178	61.5	1470	980	173.5	737	1190	56.3	17.0	191.5	10.36
1200	127	44.5	1204	855	123.6	491	810	53.3	11.2	134.8	10.02

radiator water temperature specification of 185°F for 85°F ambient was also never exceeded in selecting the optimum flow rate and fan speed. Figure 9.1 shows the optimization procedure followed. Based on these results, optimum flow rate is 1025 lbs/hr. Lower flow rate will violate the restriction of the maximum F1-50 temperature of 650°F. The optimum fan speed of 1570 rpm is selected. Lower fan speed would violate the constraint of maximum radiator average temperature of 185°F. The higher fan speed, on the other hand, would yield lower ORCS net power. These plots are also typical of the sensitivity of optimum to organic flow rate and fan speed. The net ORCS power decreases by only 0.9% for 8% higher than optimum flow. Thus the flow rate optimum is very shallow; however, a lower than optimum flow rate is not permissible since that would result in violation of the maximum allowable organic temperature constraint. The net ORCS power also decreases by 1.2% for a 10.8% increase in fan speed. This effect is also very weak, but again a lower than optimum fan speed would result in violation of the maximum radiator average temperature constraint.

Based on these optimization studies, optimum organic flow rate and fan speed schedules were derived. These are illustrated in Figures 9.2 and 9.3. The fuel economy improvement due to ORCS at part load is shown in Table 9.1. The lines of constant fuel economy improvement shown in Figure 9.4 are obtained by interpolating between points listed in Table 9.1. An improvement between 10-23% over the range of diesel operation is predicted.

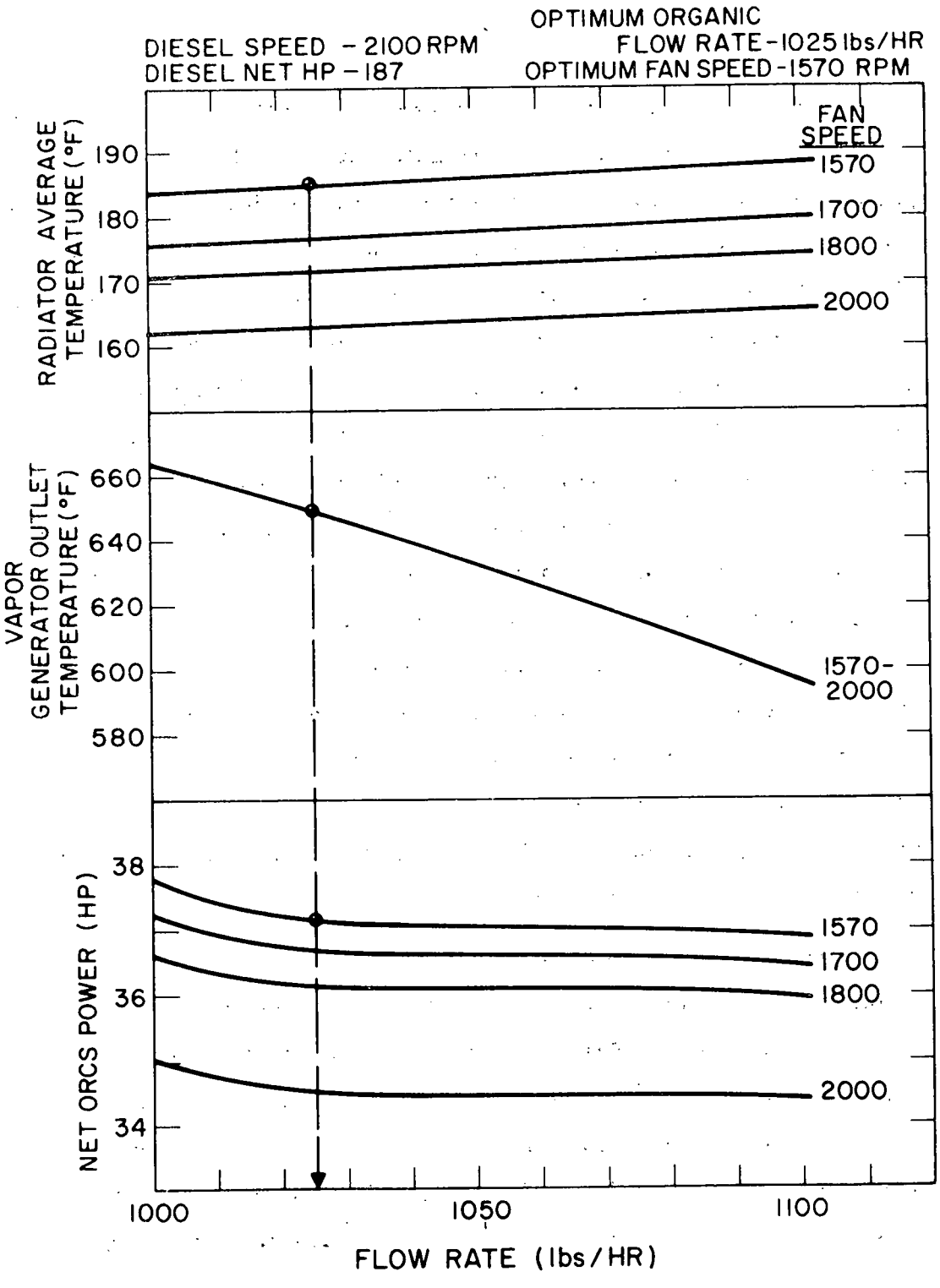

Figure 9.1. Effect of Fan Speed and Organic Flow Rate on Part Load Performance.

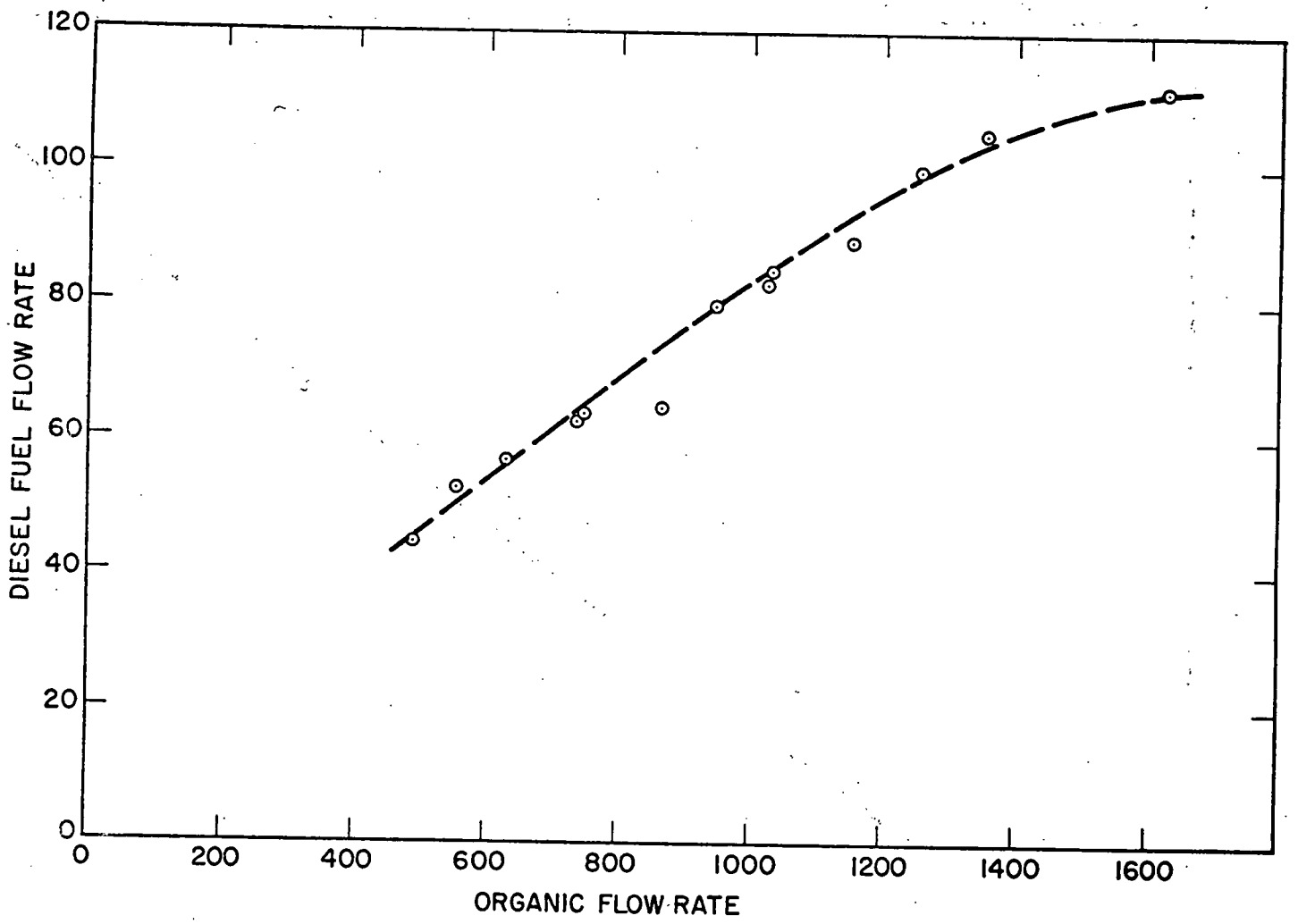

Figure 9.2. Diesel Fuel vs. Organic Flow Rate.

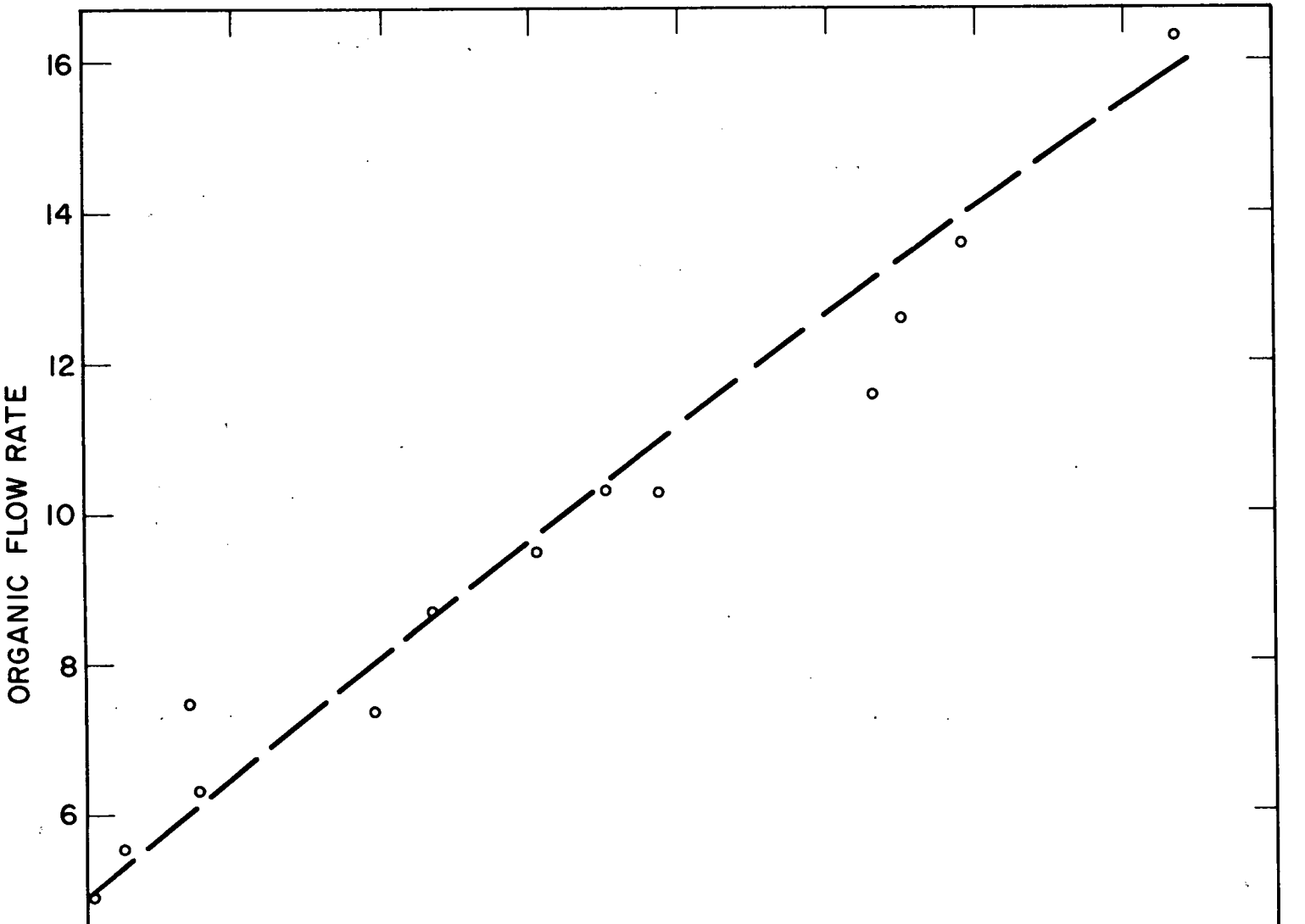

Figure 9. 3. Organic Flow Rate and Fan rpm Relation.

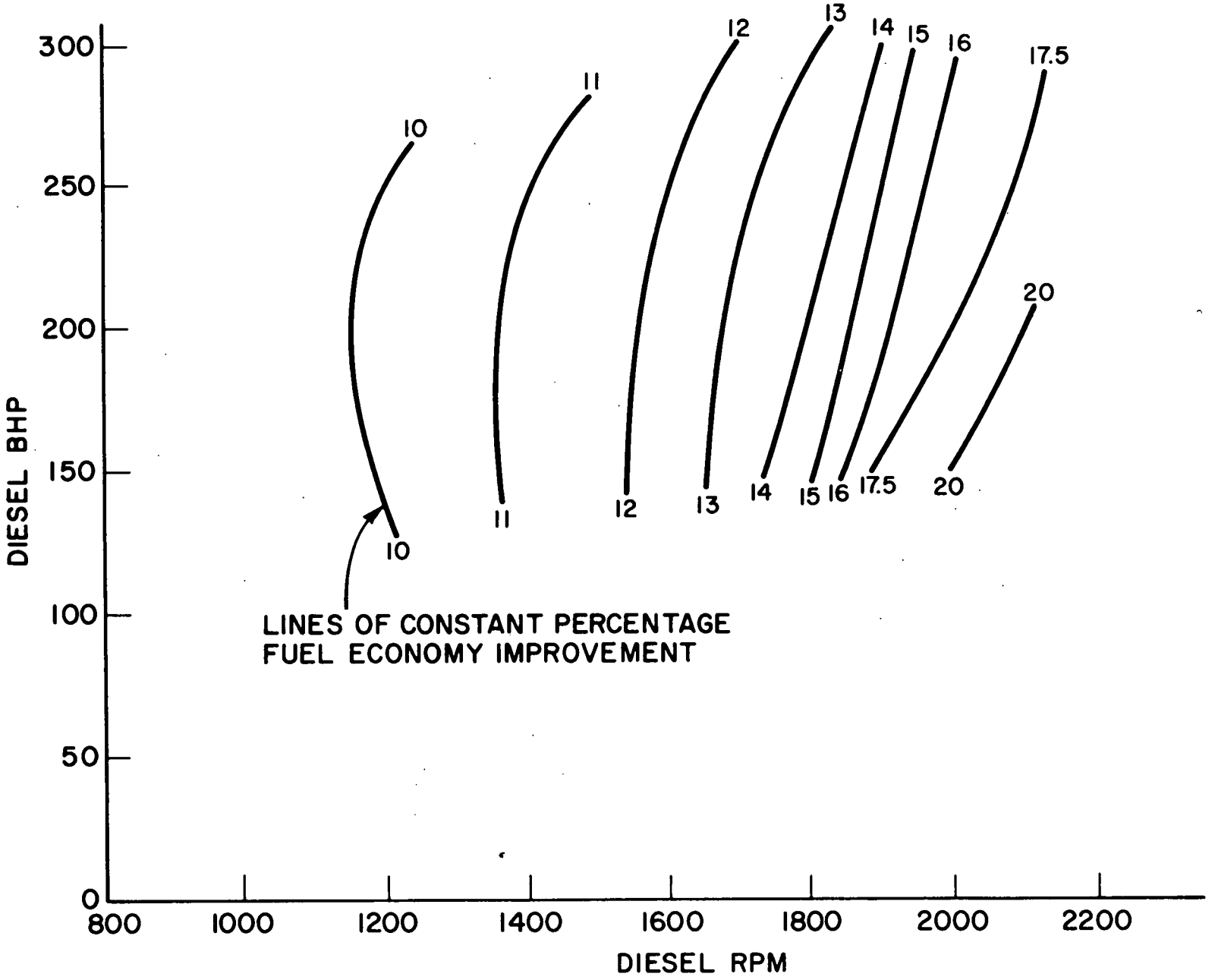

Figure 9.4. Part Load Fuel Economy Improvement.

10. FUEL ECONOMY IMPROVEMENT FOR TYPICAL TRUCK DUTY CYCLE AND IMPACT ON NATIONAL FUEL USAGE

Two representative truck driving cycles are computerized and are available through Mack Trucks, Inc. for evaluation of the ORCS. These driving cycles are known as the "NAPCA Control Route," essentially a "typical composite" of stop and go, and hills and curve types of driving, and the "Denver to Kansas City" route. The reference vehicle and engine (using prototype engine performance data) were put through both driving cycles and the percent time at various speeds and horsepowers is shown in Table 10.1. Figure 10.1 is a bar chart of the information shown in Table 10.1 for the NAPCA Control Route. In addition to speed and horsepower, Figure 10.1 shows the percentage of the total fuel used in the cycle as a function of horsepower. This was calculated by using the percentage time at horsepower and the average brake specific fuel consumption for the entire cycle (0.365 lb/3 Bhp/hr). Figure 10.2 shows the driving cycle result plotted on the part load fuel economy improvement map. This indicates that fuel economy improvement should be of the order of 15% over the NAPCA cycle. The computer programs will be re-run with production engine performance to get base-line economy and then re-run with the ORCS to show the actual improvement for both duty cycles.

It is noteworthy that most of the fuel consumed over the driving cycle is in the speed range of 1650-2100 rpm. Further, the largest percentage of time and fuel consumption is in the 1800-1850 rpm range. The present turbine is designed to maximize its efficiency at the design point as shown in Figure 10.3. In order to improve further

TABLE 10.1

DUTY CYCLE SUMMARY, TWO ROUTES

Gross Vehicle Weight: 72,000 lbs.

Legal Speed Limit: 60 mph

Engine: Mack ENDT 676, 292 Bhp at 1800 rpm

SPEED	PERCENT TIME AT SPEED	
	NAPCA CONTROL ROUTE	DENVER TO KANSAS CITY
1150	0.6	
1200		
1250	0.8	
1300	0.7	
1350	2.3	
1400	2.0	
1450	3.1	
1500	2.9	
1550	1.8	4.8
1600	3.5	7.8
1650	12.7	6.7
1700	3.6	10.5
1750	3.9	10.5
1800	6.4	11.2
1850	20.7	7.7
1900	9.7	7.3
1950	9.8	4.6
2000	9.0	7.3
2050	0.7	0.4
2100	0.9	4.1
2150		
TOTALS	95%	82.9%

TABLE 10.1 (continued)

DUTY CYCLE SUMMARY, TWO ROUTES

HORSEPOWER	PERCENT TIME AT HORSEPOWER	
	NAPCA CONTROL ROUTE	DENVER TO KANSAS CITY
165	0.8	0.2
180		0.1
195	0.6	1.0
210	0.2	0.3
225	0.8	0.6
240	3.1	1.5
255	1.5	5.3
270	4.9	26.3
285	17.0	59.0
300	56.0	
TOTALS	84.9%	94.2%

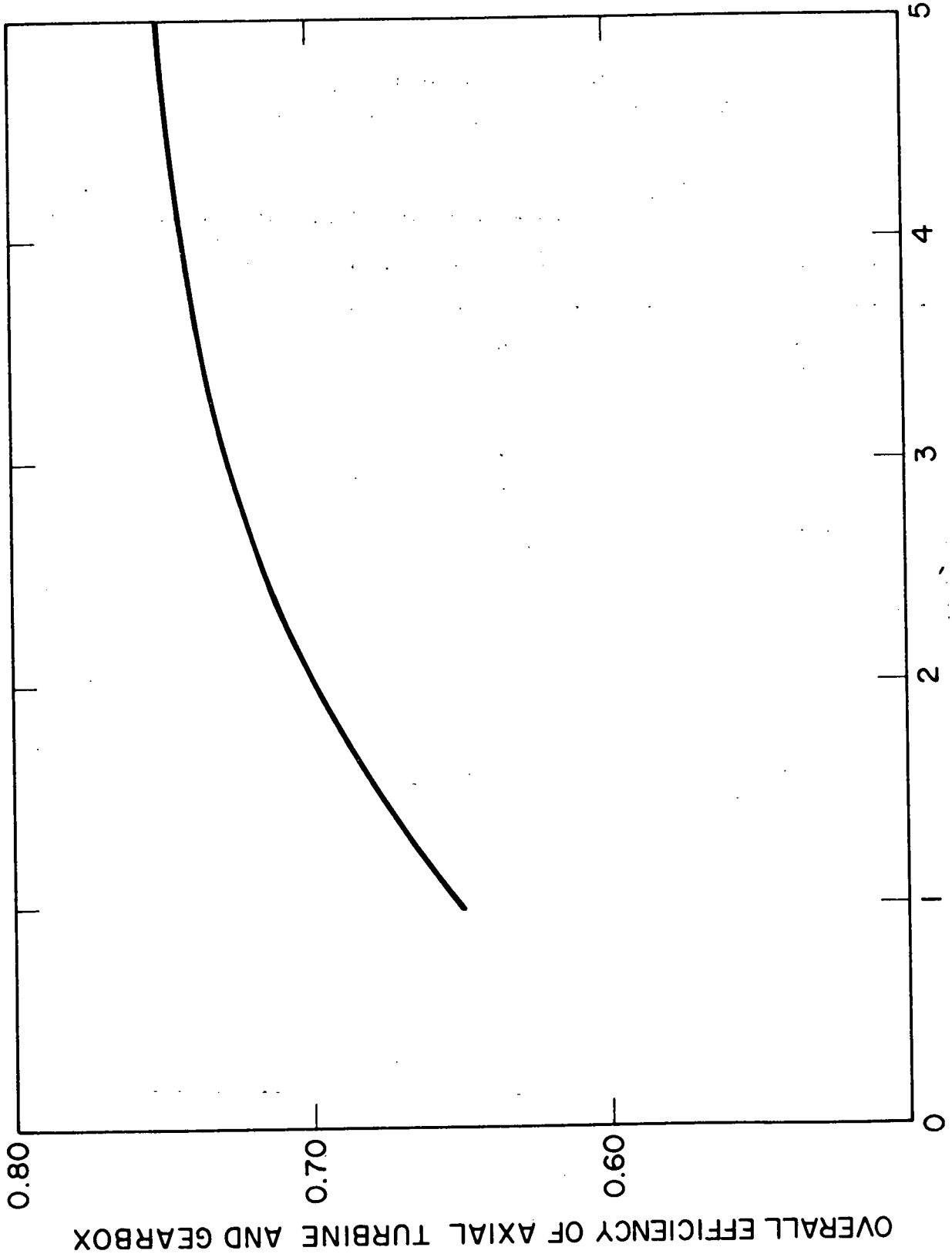

Figure 10.1. Overall Turbine and Gearbox Efficiency vs. Number of Stages.

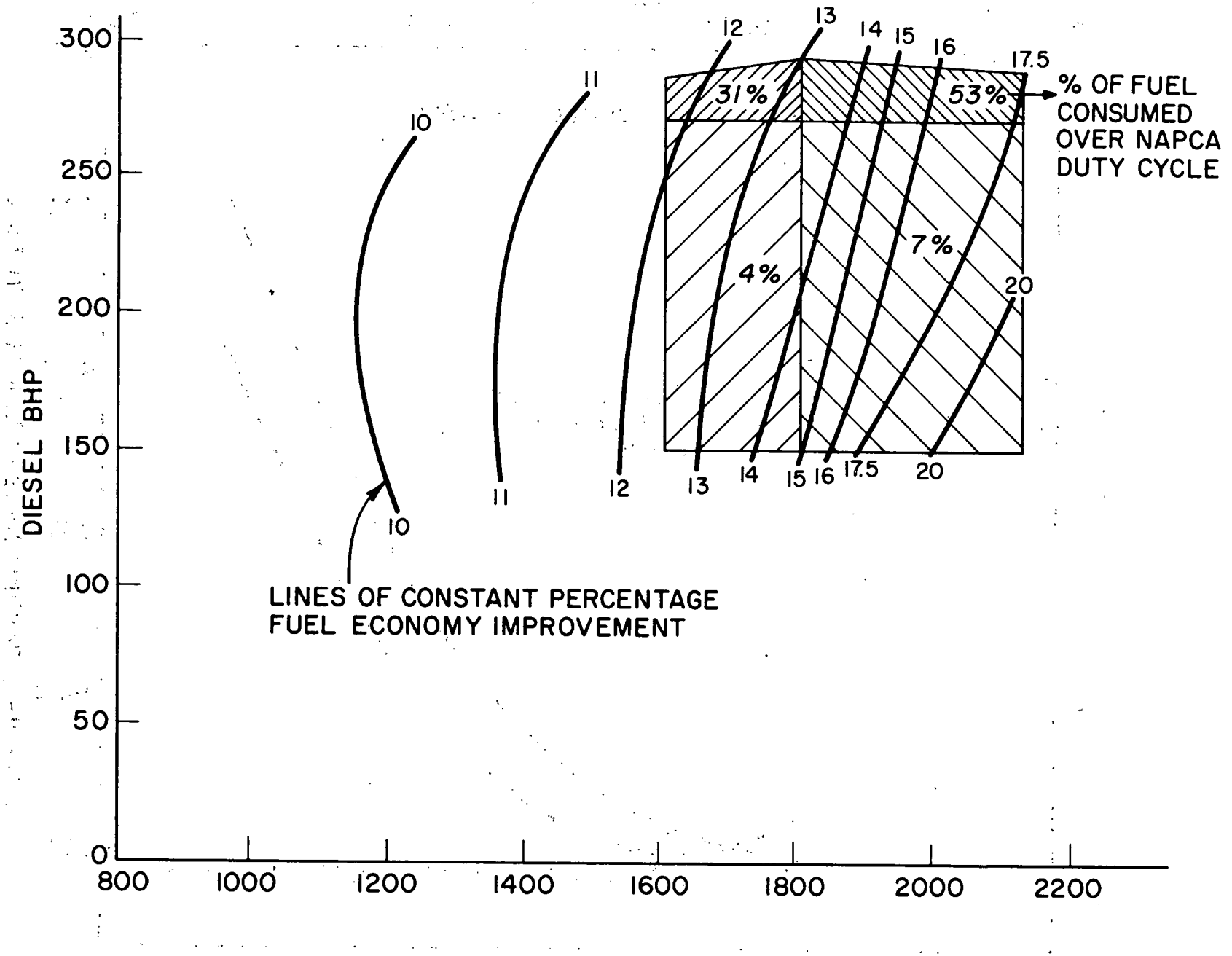
DIESEL BHP
300
250
200
150
100
50
0
800
1000
1200
1400
1600
1800
2000
2200
10
11
12
13
14
15
16
17.5
20
31%
53%
4%
7%
% OF FUEL CONSUMED OVER NAPCA DUTY CYCLE
LINES OF CONSTANT PERCENTAGE FUEL ECONOMY IMPROVEMENT

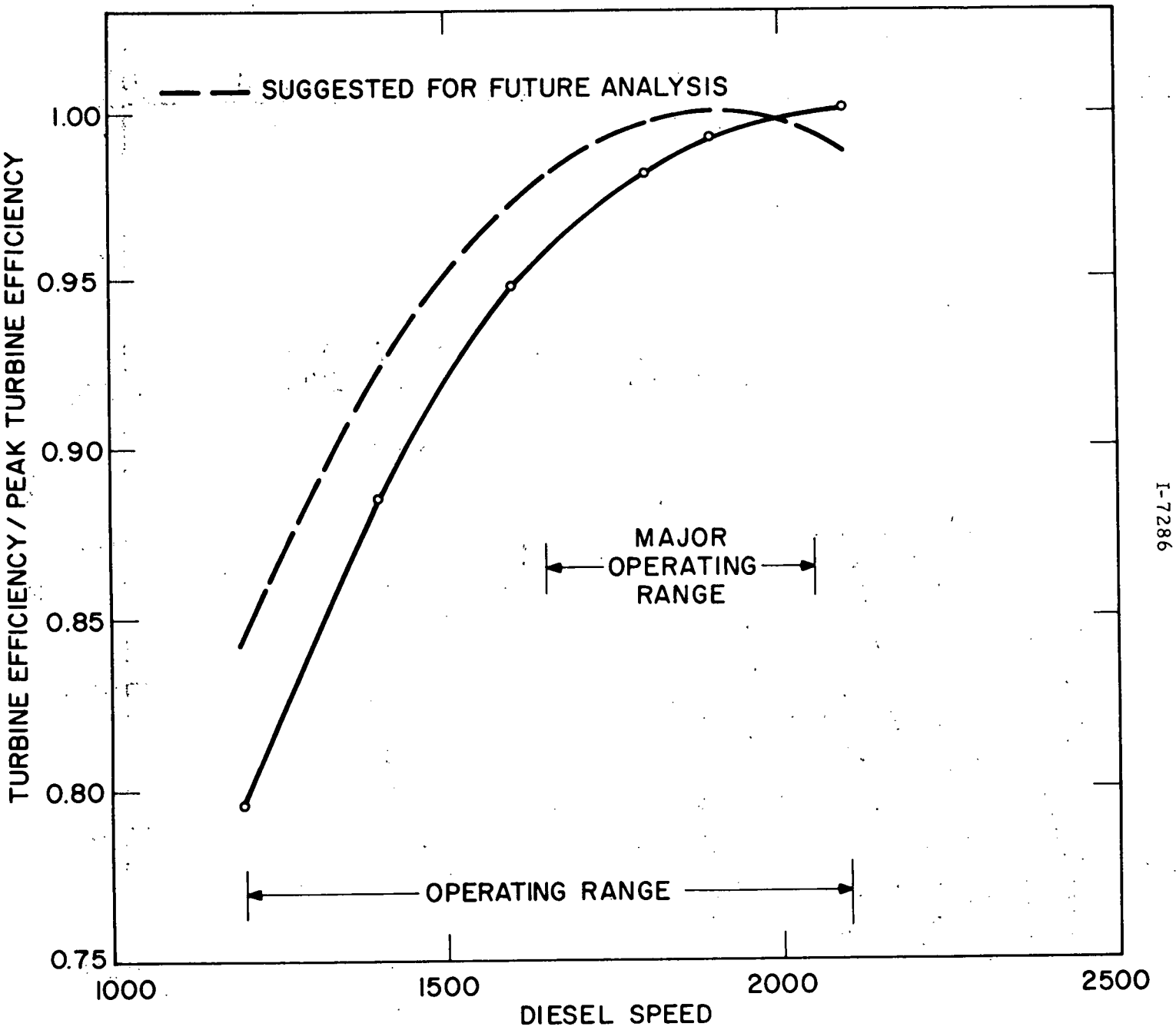

Figure 10.3. Modified Turbine Performance with Diesel Speed.

the fuel economy over the duty cycle, it is recommended that the turbine maximum efficiency should be matched with the diesel speed of 1850 rpm, as shown in Figure 10.3. This will improve the overall turbine efficiency over the duty cycle and result in higher fuel economy.

Based on this estimate of the average fuel economy improvement due to the ORCS, it is possible to estimate the impact of this system on national fuel usage. The following sources were used for the estimate:

1. TC72-T52, "1972 Census of Transportation Truck Inventory and Use Survey," Bureau of the Census, U. S. Dept. of Commerce.
2. "Shipments of Fuel Oil and Kerosene," U. S. Dept. of Interior, Bureau of Mines, Mineral Industry Surveys, Washington, D. C. (see Figure 10.4).
3. "1974 Motor Truck Facts," Motor Vehicle Manufacturers Association of the U. S., Inc., Detroit, Michigan.
4. Mack Trucks, Inc., Private Correspondence.

The Department of Commerce truck census of 1972 (Ref. 1) has defined "long range of operation" as those trucks used principally for over-the-road trips of 200 miles or more one-way. This estimate will assume that all trucks in this classification will be equipped with the bottoming cycle. The 1972 census gives the following figures:

Number of Trucks - 469,000.

Number of miles per truck per year - 52,200.

Therefore, the number of truck-miles per year = 24.5×10^9. Information from Mack indicates that this type of truck averages 4.4 miles per gallon. Therefore, the gallons consumed per year = 5.56×10^9 gallons. In 1972, therefore, long range trucks consumed approximately 133×10^6 barrels of oil. The total consumption of diesel oil on the highway in that year was 189×10^6 barrels. By extrapolation of the data for the annual U. S. highway diesel oil consumption (Figure 10.4) and assuming that long haul trucks retain the same fraction as in 1972,

For 1974 barrels per year = $\frac{133}{189} \times 248 = 175 \times 10^6$.

For 1980 barrels per year = $\frac{133}{189} \times 400 = 282 \times 10^6$.

The improvement in efficiency due to the bottoming cycle for the present diesel truck population is estimated at 15%. The national fuel savings with the bottoming cycle applied to long haul trucks would then be:

At 1974 consumption levels, $\approx 26 \times 10^6$ barrels per year
$\approx 1.1 \times 10^9$ gallons per year.

At 1980 consumption levels, $\approx 42.3 \times 10^6$ barrels per year
$\approx 1.8 \times 10^9$ gallons per year.

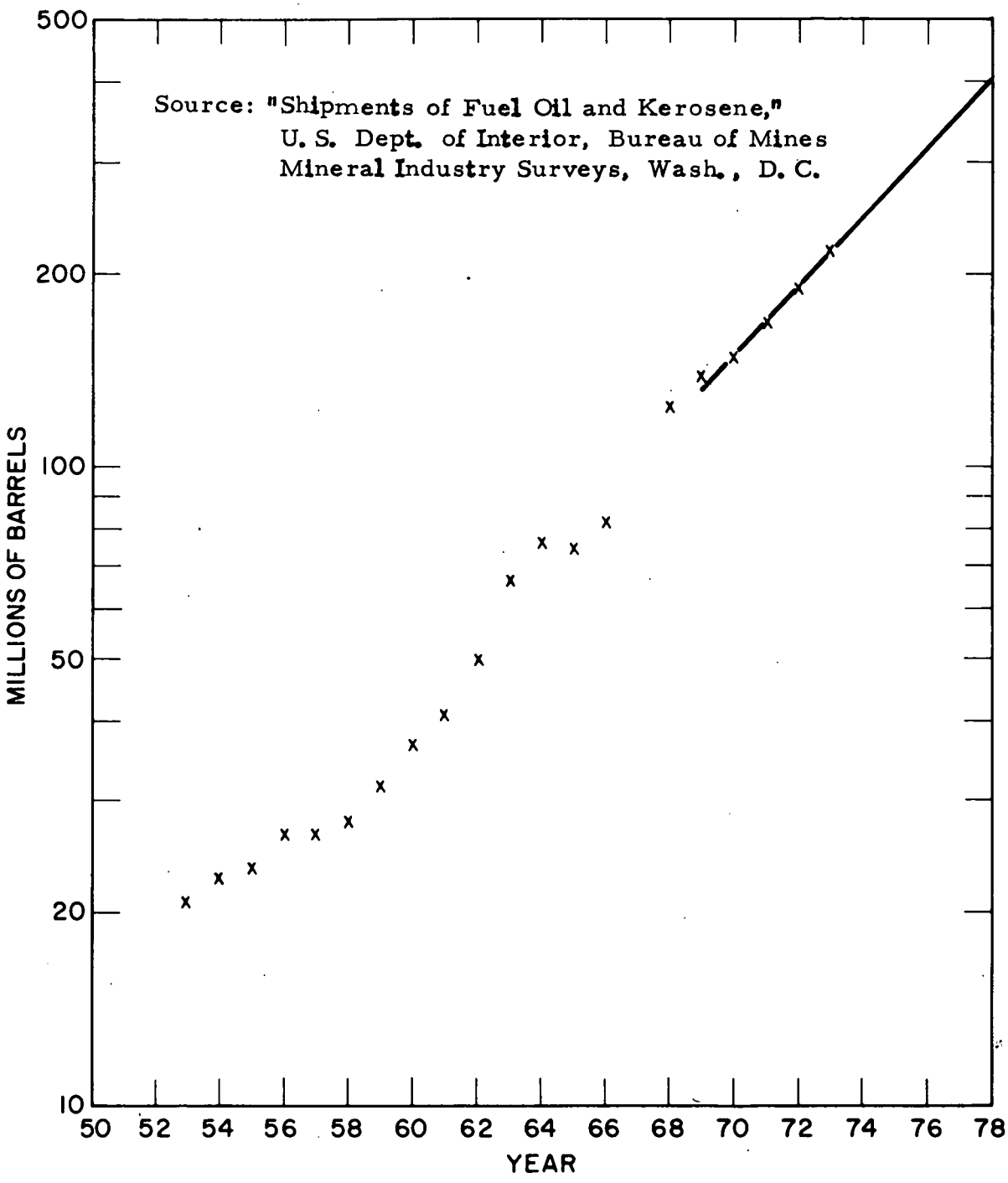

Figure 10.4. Annual U. S. Highway Diesel Oil Consumption.

11. MECHANICAL INTERFACE AND PACKAGING

Very early in the program it became apparent that the logical point at which to couple the output of the ORCS to the diesel was at the diesel engine flywheel, as this was the most stable point with respect to torsional vibrations. Figure 11.1 shows the lumped parameter model of the engine and drive train and includes the inertias and stiffnesses of the various parts. Figure 11.2 is a mass-elastic diagram of the system shown in Figure 11.1 which shows the mode shapes and natural frequencies for the four lowest modes of vibration. This information was provided by Mack Trucks, Inc. It should be noted that this analysis gives only the mode shapes and frequencies; the amplitudes are all relative to the front of the engine. To date, Mack has no information as to the actual amplitude of vibration at various points in the engine-drive train system. Referring to Figure 11.2, only the lowest natural frequency, 11.7 Hz. has a large relative amplitude at, and mode far from, the flywheel. Since the major exciting orders for the engine are the 3, 6, 9, and 12, the highest engine speed which could excite this frequency is 11.7/3 x 60 or 234 rpm, a speed well below the operating range of the engine. One can conclude, therefore, that the ORCS should be coupled at the flywheel. It is also clear that the ORCS system, when coupled to the flywheel, should have its lowest natural frequency well above the highest shown in Figure 11.2 or 190.3 Hz.

After the preliminary layouts of the turbine and the gearbox were completed, a mass-elastic study of the system was performed. The model for this is shown in Figure 11.3. All inertias and stiffnesses were referred to engine speed, which means multiplying by the appropriate speed ratio squared. The lowest natural frequency

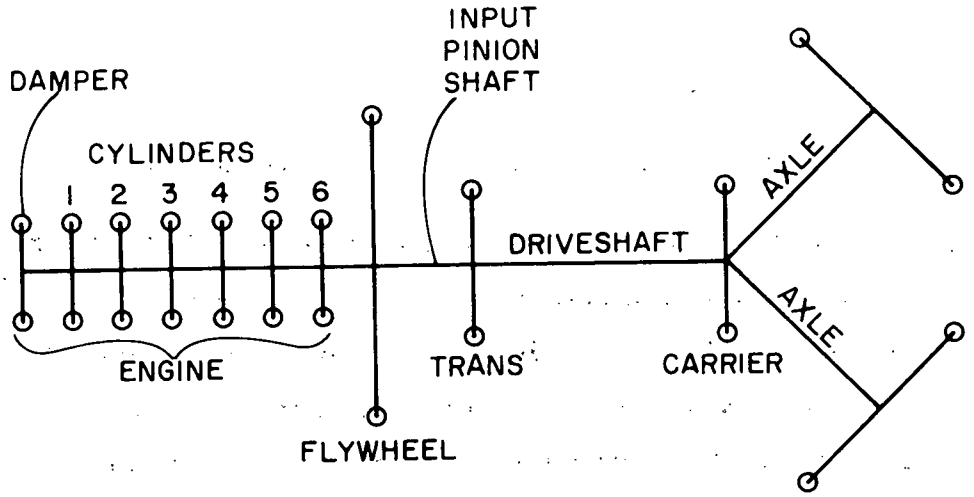

INERTIA AND STIFFNESS DATA

	INERTIAS (in.-lb-sec^2)	STIFFNESSES (In-lb/rad x 10^{-6})
ENDT 676 Engine		
Damper & Hub	1.59	9.850
Cyl #1	1.04	17.099
Cyl #2	0.60	17.099
Cyl #3	1.02	16.697
Cyl #4	1.02	17.099
Cyl #5	0.60	17.099
Cyl #6	1.04	28.379
Flywheel & Clutch	23.93	2.014
Input Pinion Shaft		
TRL 1076 Transmission		
Driveshaft, 9 muA 353A		.819
5th Gear	2.33	
4th Gear	1.16	
3rd Gear	.55	
Carrier, R-170	2.029	
Axle Shaft, Rockwell R170-F6		.760
Wheel, 13QJ179 with 11:22.5 Dual Tires	235.0342	

Figure 11.1. Lumped Parameter Model of Engine-Drive Train System.

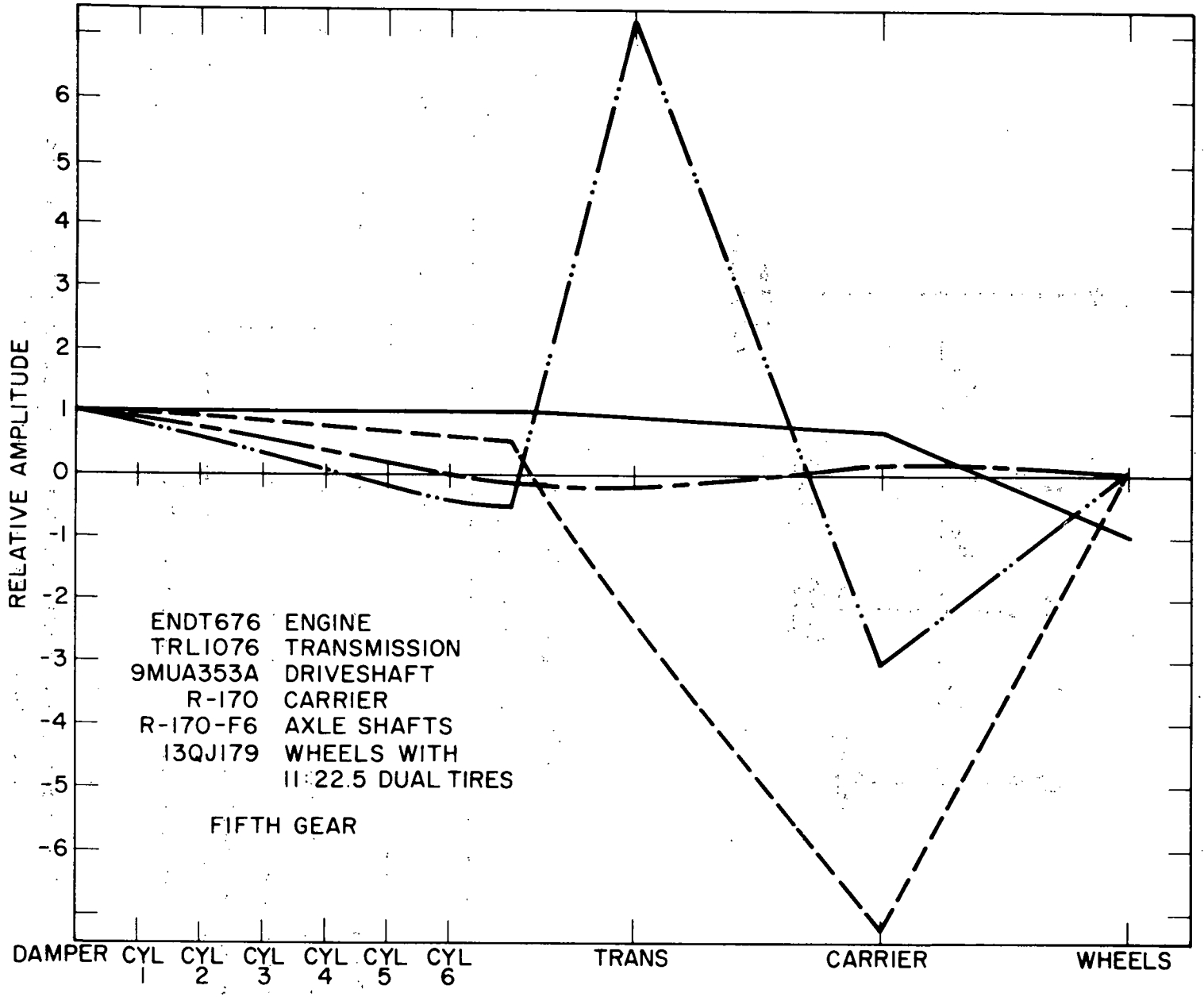

Figure 11.2 Mode Shapes.

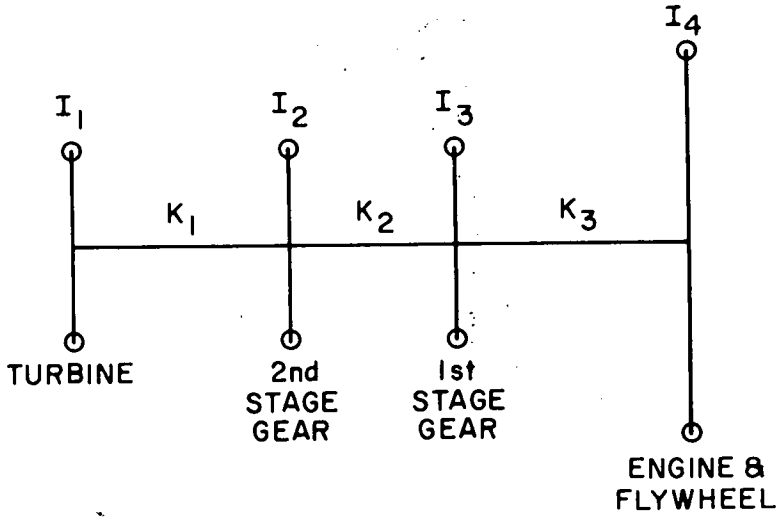

INERTIA AND STIFFNESS DATA

(All Referred to Engine Speed)

	I $(in\text{-}lb\text{-}sec^2)$	K $(lb\text{-}in/rad) \times 10^6$
Turbine	0.65	8.63
Second Stage Gears	0.545	15.6
First Stage Gears	0.248	6.96
Engine & Flywheel	32.14	

Lowest Natural Frequency = 289 kz

Figure 11.3 Mass-Elastic Diagram for ORCS Turbine and Gearbox Coupled to the Diesel Engine at the Flywheel

is 289 Hz, which is well above the 190.3 Hz of the engine-drive train system.

If a prototype system were built, the method of coupling would be to use a standard Mack flywheel power-take-off (PTO) unit. These are normally used to drive cement mixers, fuel unloading pumps, etc. One such arrangement is shown in Figure 11.4 which shows the flywheel, clutch, PTO, and drive to the transmission. Note that the PTO drive is directly off the flywheel through a shaft which is concentric with the drive through the clutch to the transmission. This works out well for the ORCS system since it is essential that it be coupled directly to the engine and not engaged and disengaged with the clutch.

Figure 11.5 shows the Mack 676 engine with the turbine, feed-pump, and gearbox of the ORCS attached to the power take off. The standard five-speed transmission is also shown.

Figure 11.6 shows the complete diesel engine-organic Rankine cycle system. The location of the regenerator is arbitrary, as its exact location in the vehicle has not been determined. These drawings, together with drawings of the various components, have been sent to Mack for review and vehicle packaging feasibility studies.

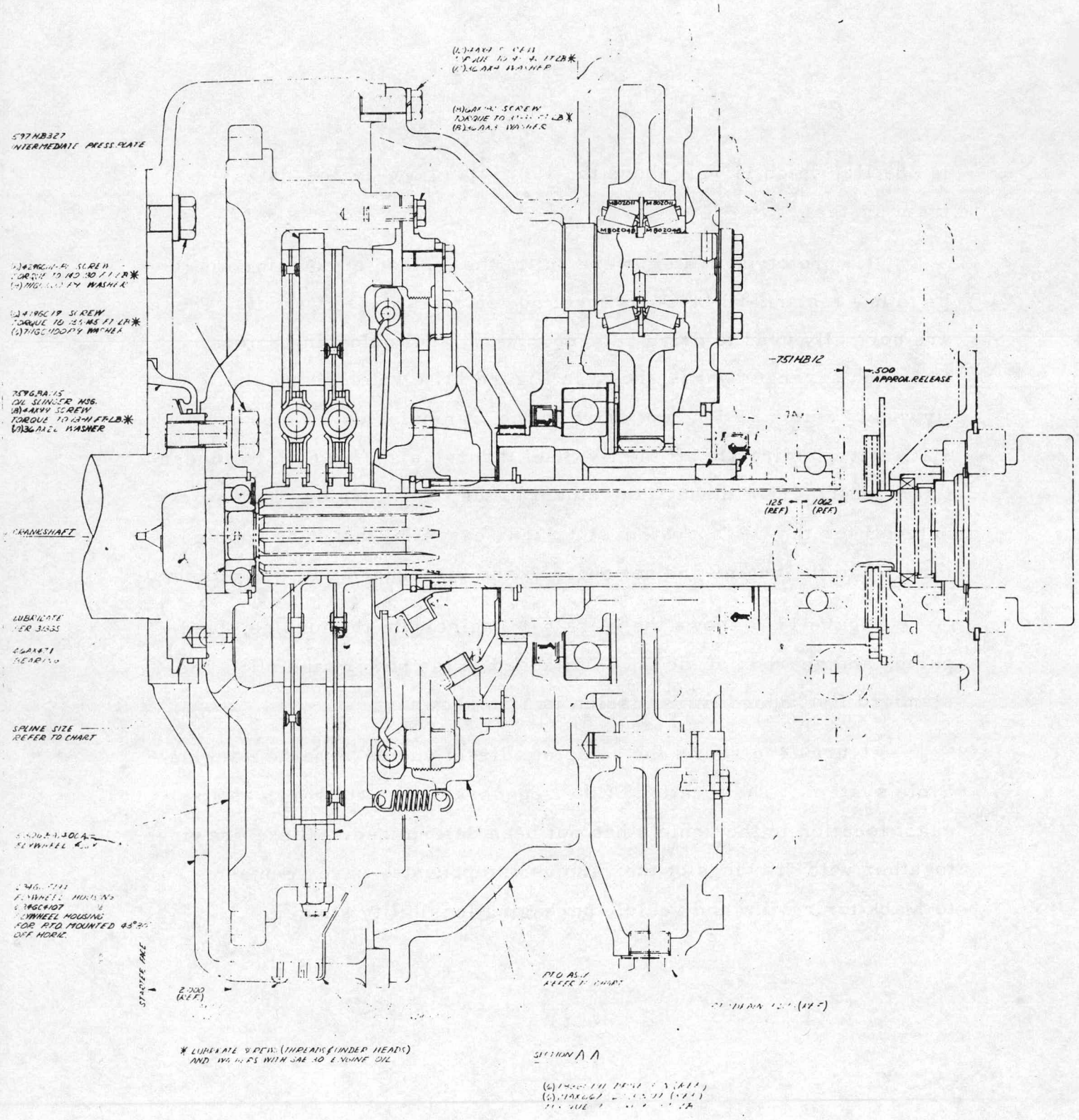

Figure 11.4. Clutch Arrangement with Power Take-off.

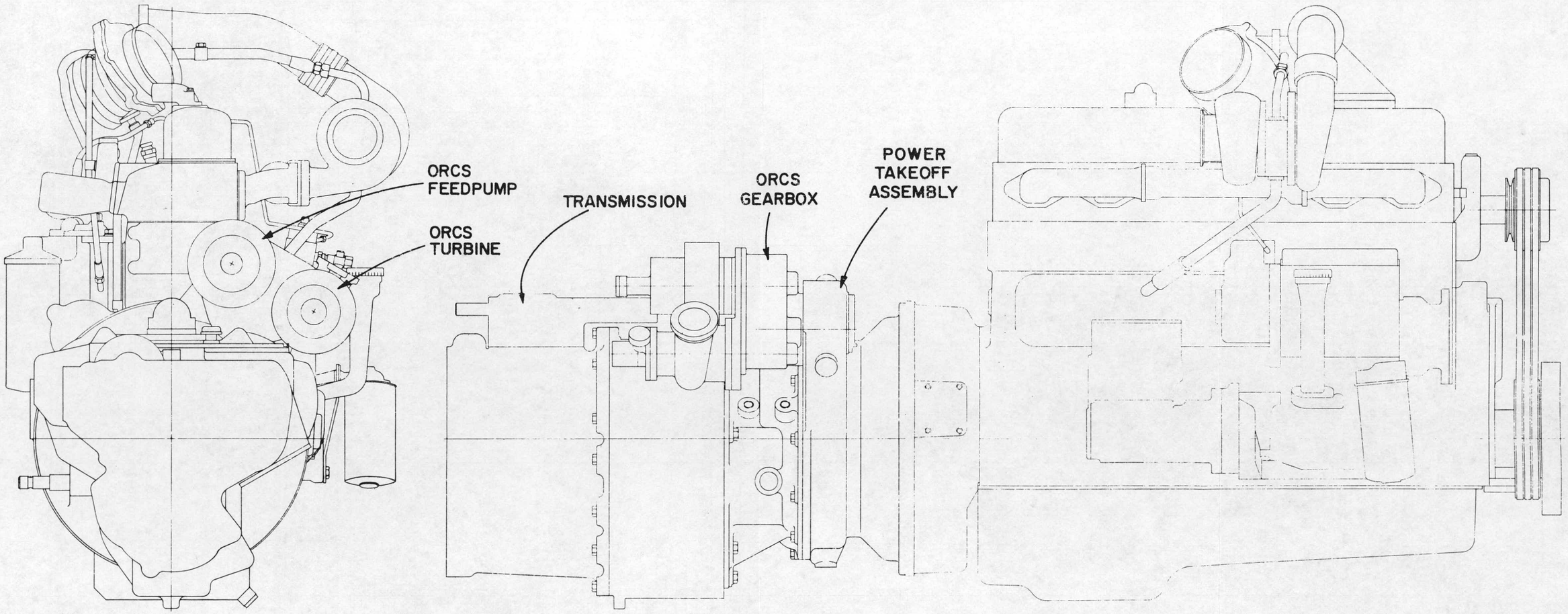

Figure 11.5. Transmission Assembly with Gearbox and Feedpump.

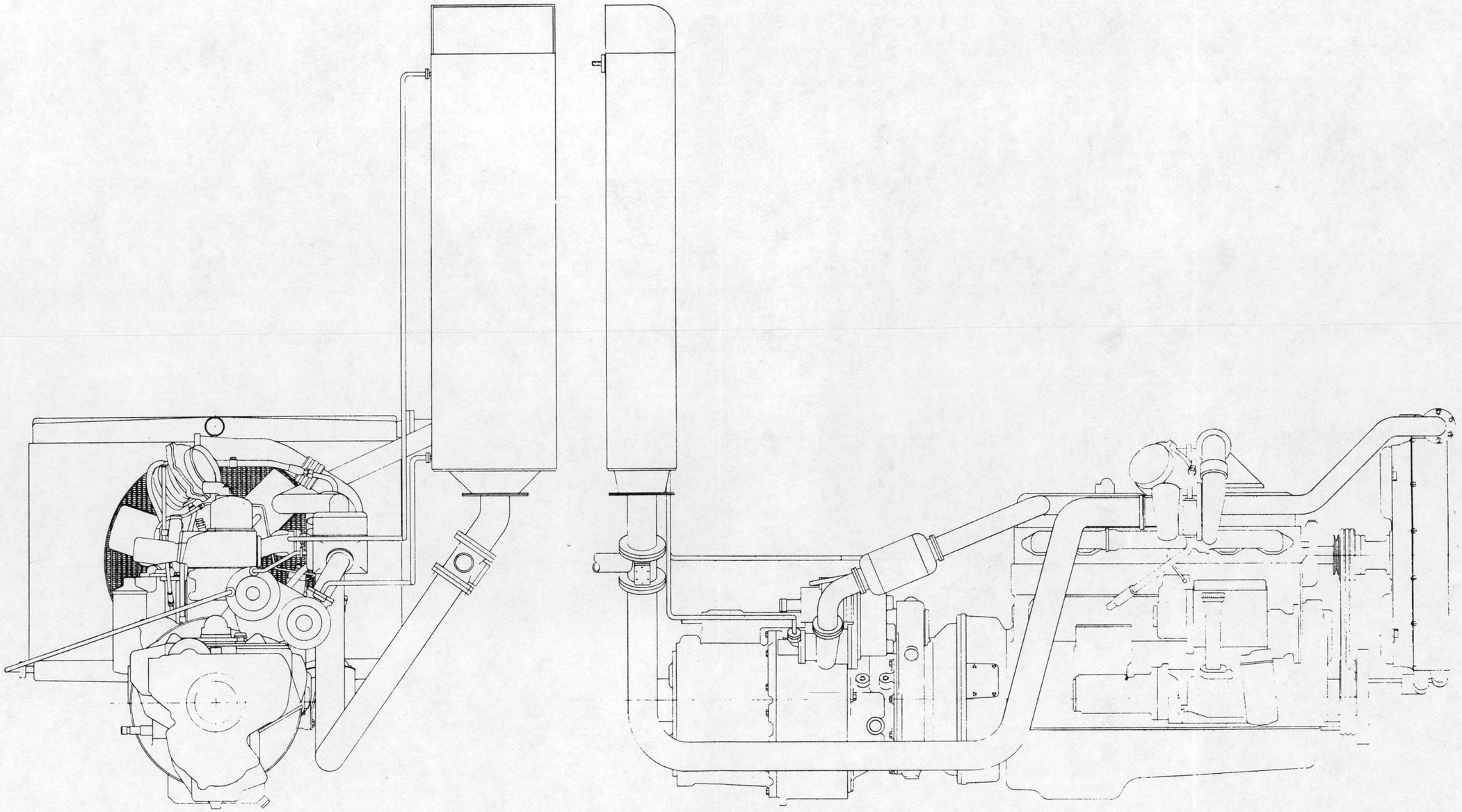

Figure 11.6. Diesel ORC Engine System.

12. ORCS - DIESEL COMPOUND ENGINE CONTROL

The proposed control system is similar in many ways to the automotive control system. The major difference is that the vapor-generator outlet pressure and temperature are allowed to vary with the load. The gas temperature decreases as the load drops off and thus a lower vapor-generator pressure is required to optimize the ORCS power. The organic temperature is also allowed to vary except that it is never permitted to exceed 650°F so that no thermal degradation of the working fluid occurs.

The control logic schematic is given in Figure 12.1. A predictive control system is planned with the prime system control provided by varying the organic flow rate, which is accomplished by means of the variable displacement feedpump similar to the automotive unit developed at TECO. The key element of the control system is the flow rate control, which takes the fuel flow rate as an input and predicts the proper organic flow rate. The organic flow rate schedule as a function of fuel flow rate was derived from the part load optimization studies and is shown in Figure 9.2. The fuel flow rate is measured by the rack position and speed of the diesel engine. The organic flow rate in turn is controlled by varying the displacement of the feedpump at a given pump speed. Since the feedpump speed is directly proportional to the diesel speed, displacement of the pump is a monotonic function of the rack position and the two will be directly coupled. The coupling could be mechanical or electromechanical.

As shown in Figure 9.1, the ORCS net power curve as a function of organic flow rate for given diesel engine conditions presents a rather

shallow optimum. This indicates that the flow rate does not have to be very accurately controlled and flow rate errors up to 10% from the desired schedule would yield net power from the ORCS within 1% from the optimum. Thus the accuracy required from the feedpump displacement control is not very stringent. However, the error on the low side may not be allowed at certain conditions if it permits the organic temperature to exceed 650°F. In such a case, the schedule would be adjusted to ensure that the maximum temperature limit is not exceeded under any operating condition.

The turbine is a 3-stage design with partial admission first stage with a fixed nozzle area. Since the flow is choked, the pressure level at the turbine inlet is controlled primarily by the flow rate of the organic. There is no active pressure control incorporated in the system and it is passively controlled by varying the organic flow rate. The vapor temperature is also not actively controlled but is in turn determined by the exhaust gas flow rate and temperature, the organic flow rate and the pressure level. The only control on the pressure and temperature of the fluid is the safety control to prevent an over-pressure or over-temperature condition from occurring in the event of a malfunction or breakdown. The turbine and feed-pump are both geared to the diesel shaft and their speeds are proportional to the diesel engine speed.

In obtaining the organic flow versus fuel flow rate schedule, the cooling fan speed was independently optimized. The fan speed versus organic flow rate schedule obtained from the part load optimization study is shown in Figure 9.3. The fan is driven by the diesel engine via the variable speed ratio drive. Thus a

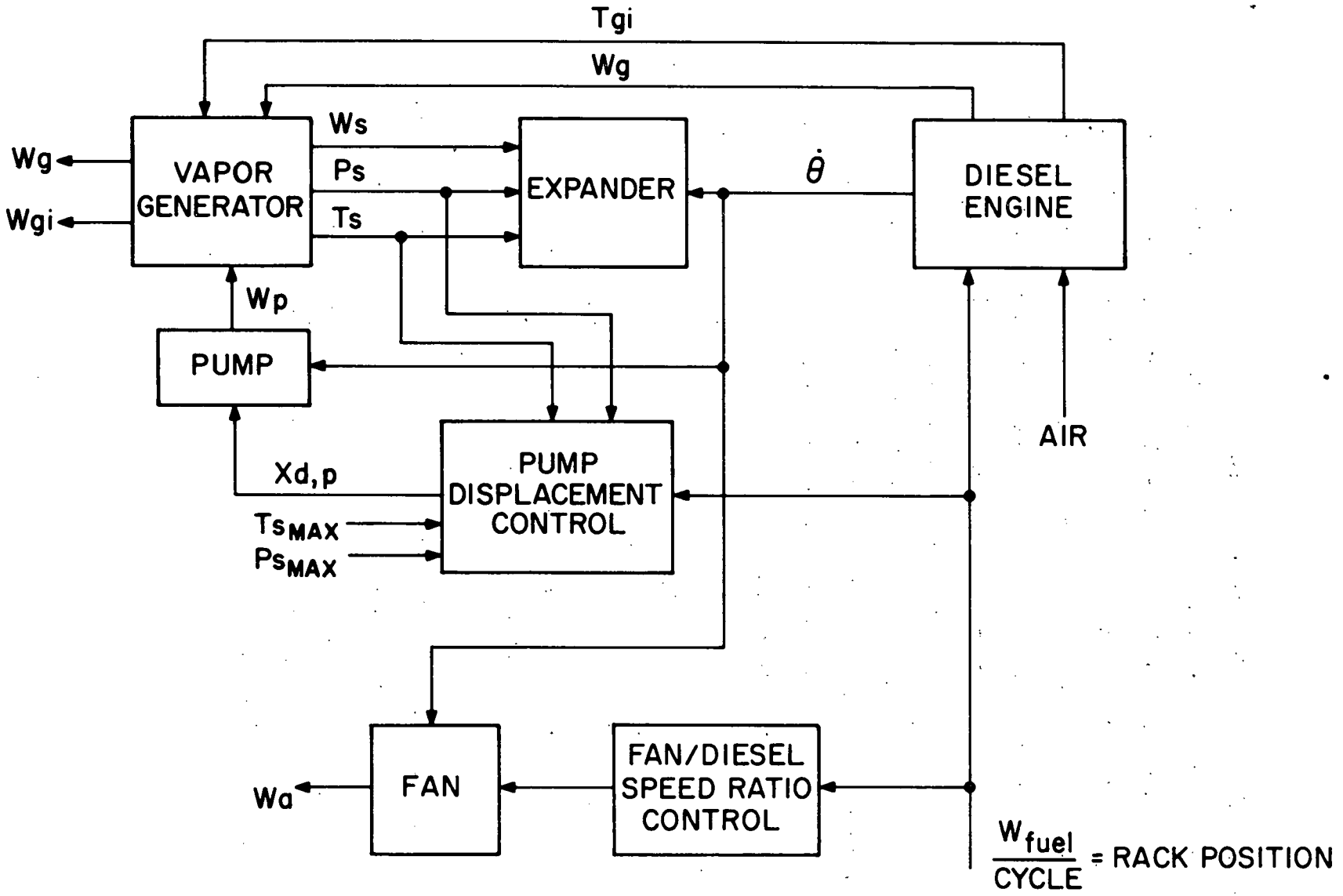

Figure 12.1. ORCS-Diesel Compound Engine Control Schematic.

fan/diesel speed ratio schedule is required corresponding to optimum part load performance. Figure 12.2 shows the dependence of fan/diesel speed ratio on the fuel flow rate with the diesel speed being a parameter. Because maximum heat rejection rate does not decrease appreciably with the diesel speed, the fan/diesel speed ratio has to be correspondingly increased at lower diesel speeds to meet the heat rejection requirements. Figure 12.3 shows the dependence of fan/diesel speed ratio on diesel rpm with fuel flow rate being a parameter. Since both the diesel speed and the fuel flow rate have a strong effect on the fan/diesel speed ratio, the dependence of this ratio on rack position (which is a measure of fuel flow rate/ diesel speed) was investigated. The results are shown in Figure 12.4. Thus, the rack position can be used as an input signal to monitor the fan/diesel speed ratio schedule. The speed ratio is the ratio between driving and driven pulleys, and the ratio may be changed by an electric gear motor with position feedback to match the rack speed versus speed ratio schedule as shown in Figure 12.5. There are other approaches for fan speed control. An attractive alternative is the use of a viscous clutch with a Flex fan design. The viscous clutch results in inefficiency when the clutch is slipping at lower temperature but is self-compensating for lower than design ambient temperatures and also affords ease of packaging. However, the final selection can only be made after studying its effect on the fuel economy improvement.

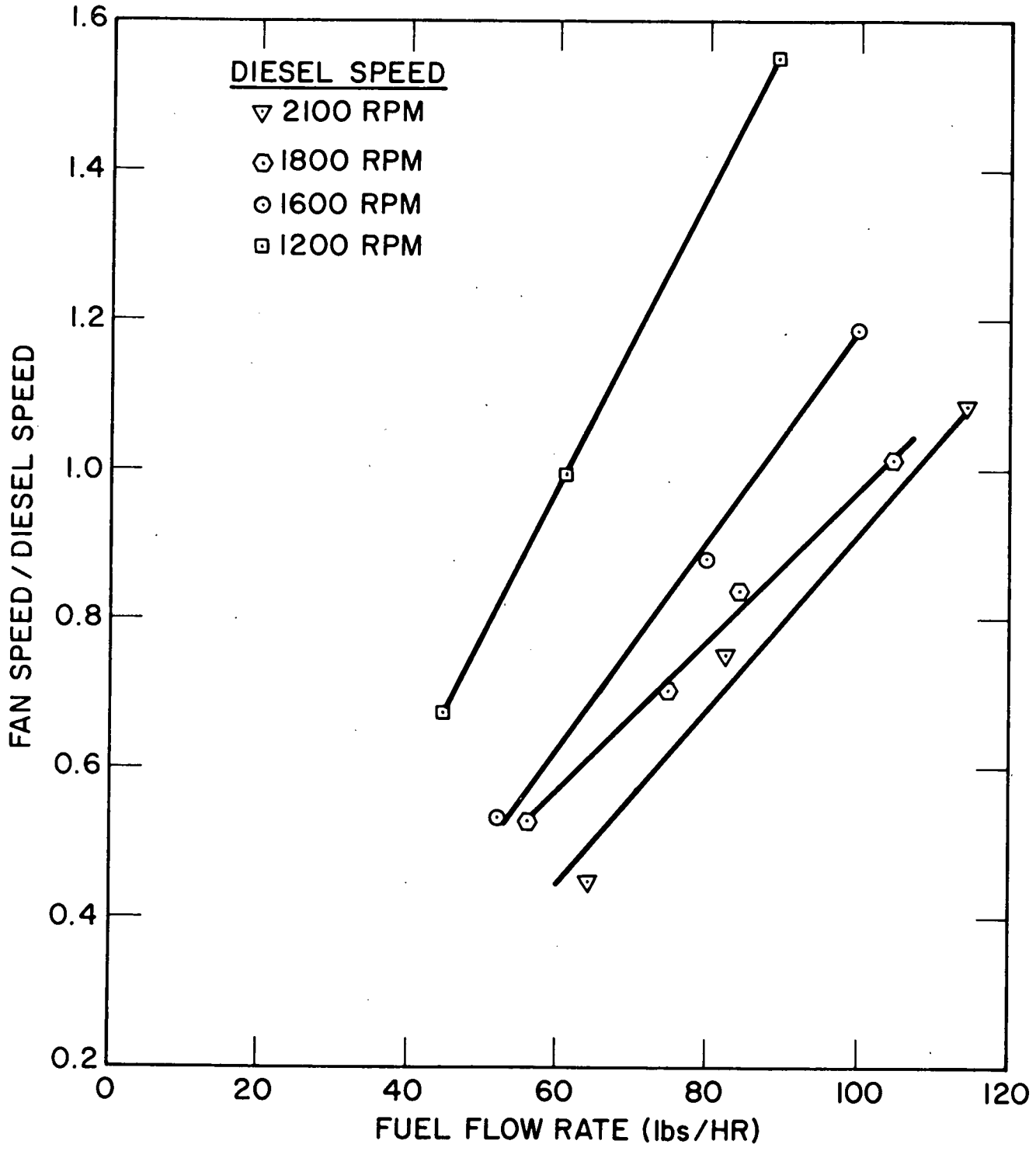

Figure 12.2. Fan/Diesel Speed Ratio vs. Fuel Flow Rate.

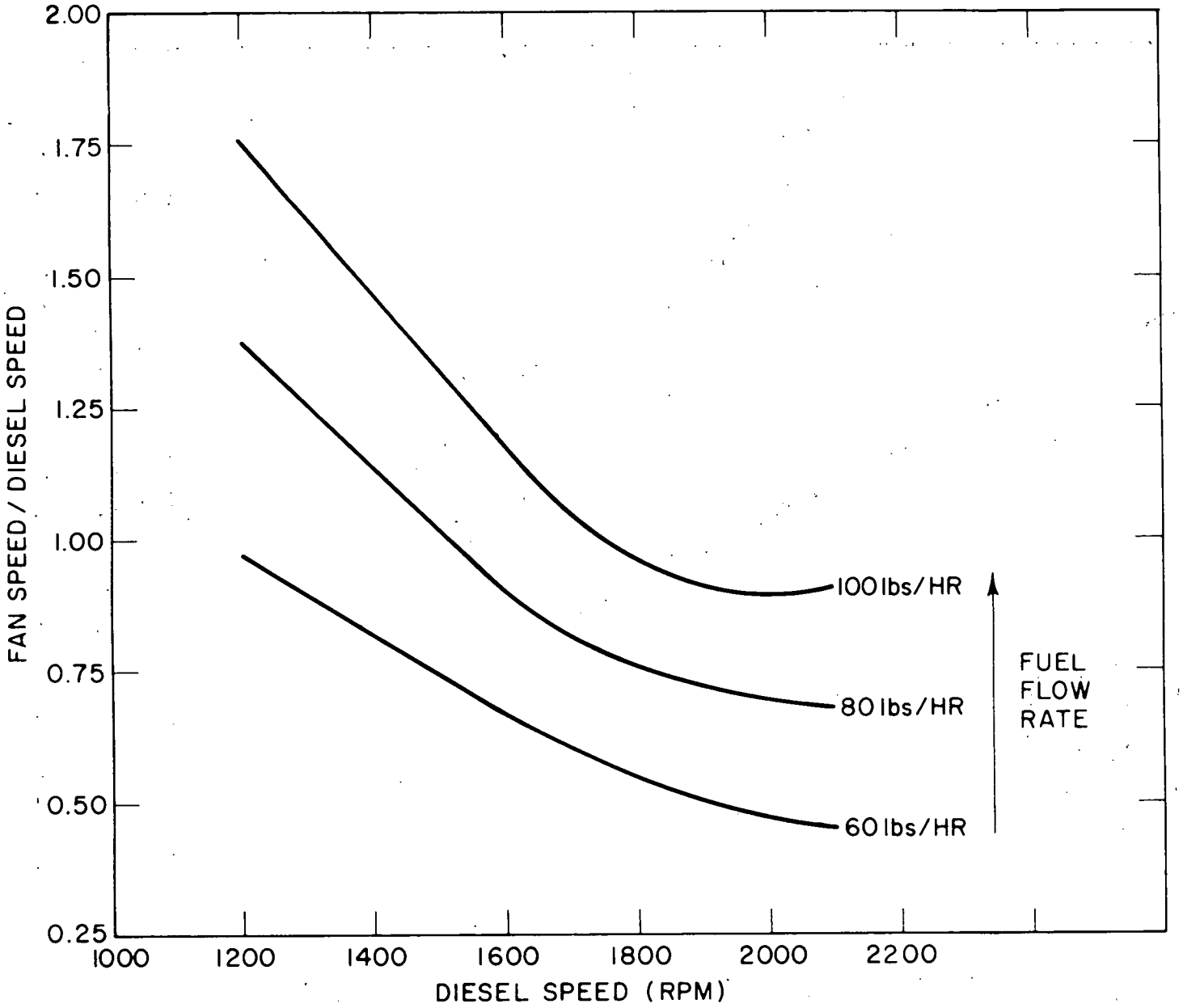

Figure 12.3. Fan/Diesel Speed Ratio Schedule.

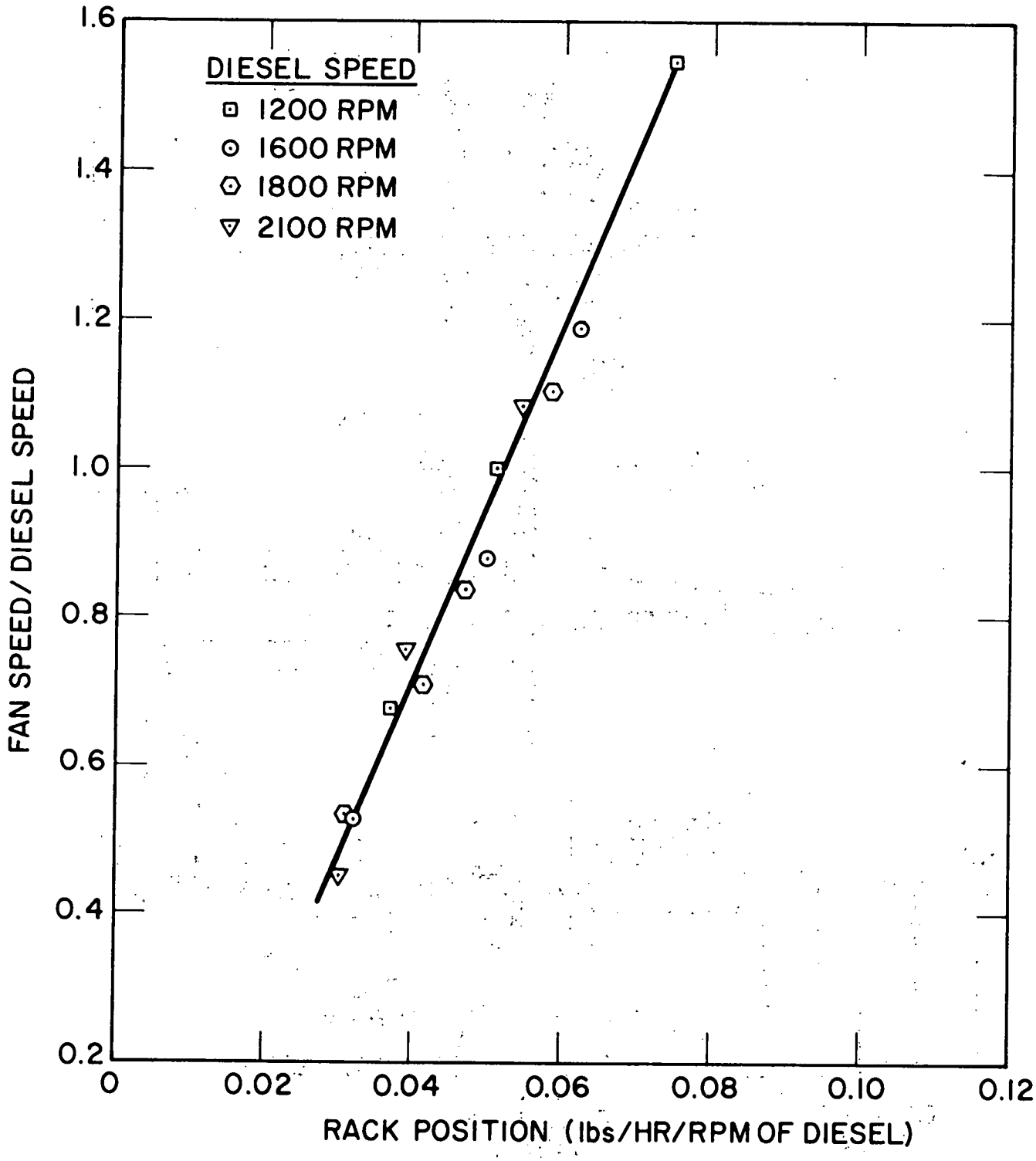

Figure 12.4. Fan/Diesel Speed Ratio Schedule vs. Rack Position.

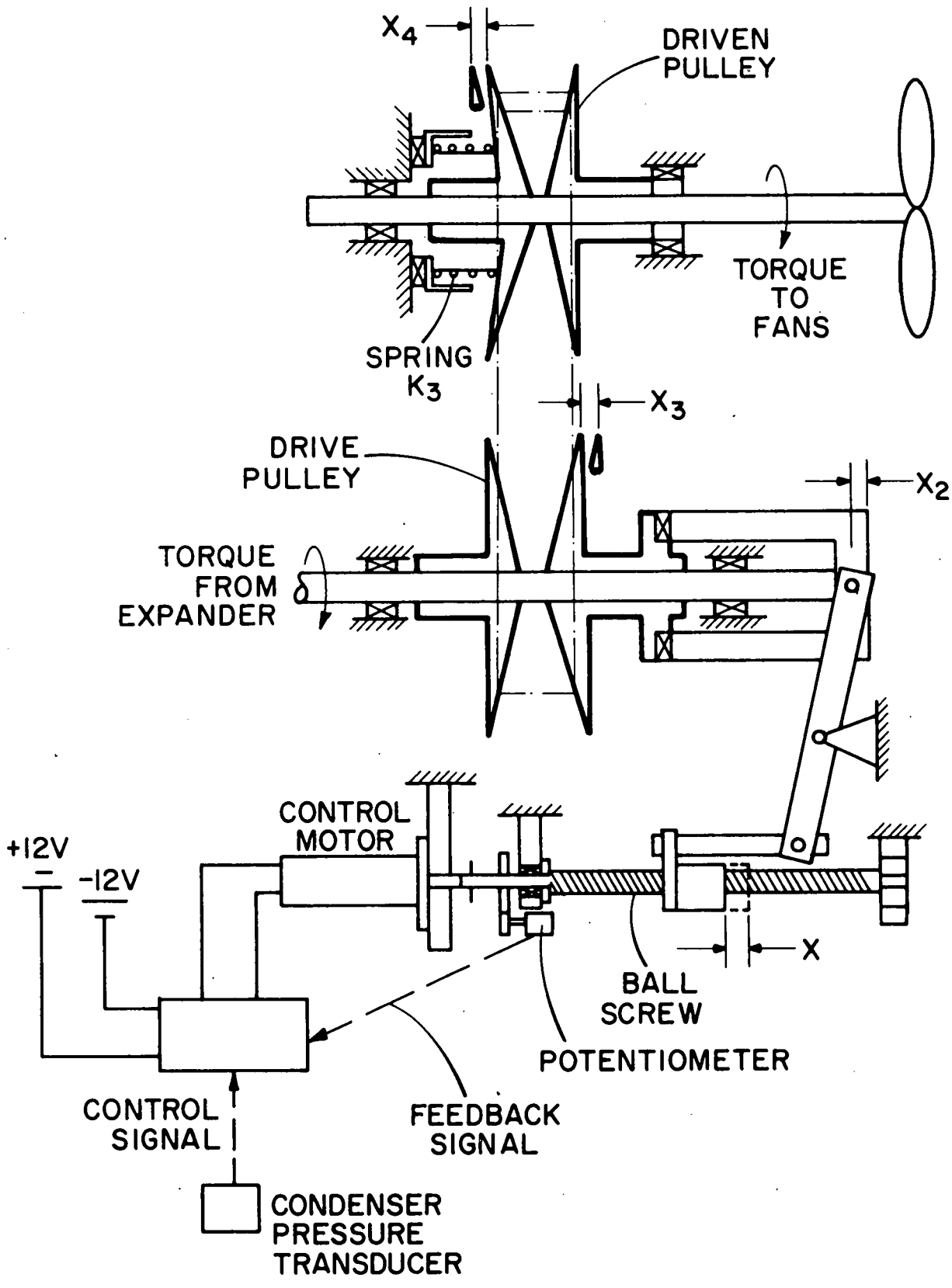

Figure 12.5. Electrically-Controlled Condenser Fan Drive.

13. COMPONENT DESIGNS FOR DEMONSTRATION TEST

In the next quarter, it is planned to run a demonstration test to measure the fuel economy improvement characteristics of an ORCS bottoming a diesel engine. Most of the ORCS components to be used in this test are the same as those fabricated for the automotive Rankine cycle powerplant. This includes a condenser, regenerator, feedpump, boost pump, etc. A 150 hp turbine-gearbox unit designed for the automotive application is also available. However, its nozzle block has to be modified to match the conditions for this application. Also a vapor-generator is required to recover the heat from the diesel exhaust. In this section the designs of the vapor-generator and turbine gearbox are described.

13.1 VAPOR-GENERATOR

Vendor contacts were made to see if the prototype vapor-generator described in Chapter 8 could be made on schedule for the demonstration test. Upon review of their responses, it was concluded that this would not be possible due to several problems that were discovered. First, the ESCOA fin tube surface selected was assumed to be a continuous welded fin tube; however, it was learned that the fins are actually spot welded in the tube size of interest and may present substantial contact resistance. The manufacturer indicated interest in producing a batch of finned tubes with continuous welding for this program; however, it would have involved developmental efforts and delivery could not be met. Also, the U bends required to connect tubes between passes were non-standard and presented delivery problems.

In view of these problems, the vapor-generator was redesigned within the same packaging constraints. This design has a staggered tube arrangement and a tube spacing suitable for a stock return bend. As the tubes are now spaced further apart the height of the fins is increased to compensate for the lower number of tubes. The fins are solid and brazed to the tube. The design point characteristics of the demonstration vapor-generator are shown in Table 13.1. As expected, the heat transfer coefficient for the solid fin is lower than that for the strip fin. However, this is partially offset by the increased gas side heat transfer area. The overall "UA" for this vapor-generator is 5096 Btu/hr °F compared to 6195 Btu/hr °F for the prototype design. The organic flow rate, however, is 1555 lbs/hr which is only 4.4% lower than the design flow rate of 1626 lbs/hr. The difference in the net ORCS power is expected to be about 3% because of the lower fan power requirement.

The design of the vapor-generator was based on the prototype engine test data. The characteristics at the design point corresponding to the production engine test data were evaluated using part load analysis. Because of the higher gas temperature, the maximum wall temperature corresponding to the new design point is calculated to be 730 °F, which exceeds the maximum wall temperature limit of 700 °F for Fluorinol-50. This problem can be solved by increasing the design point flow rate to lower the maximum wall temperature, as well as the cycle temperature, by 30 °F. As shown in the part load optimization study the overall effect on the net ORCS power is expected to be less than 1%.

TABLE 13.1

DESIGN POINT CHARACTERISTICS
OF VAPOR GENERATOR FOR DEMONSTRATION TEST

1. Performance Characteristics	
Heat Transfer Rate	578,700 Btu/hr
Working Fluid - Fluorinol-50	
Flow Rate	1555 lbm/hr
Inlet Temperature	232.6 °F
Inlet Pressure	860 psia
Outlet Temperature	650 °F *
Outlet Pressure	800 psia
Diesel Exhaust Gas	
Flow Rate	3442 lbm/hr
Inlet Temperature	925 °F
Outlet Temperature	286 °F
Pressure Drop	16 in. WC
2. Salient Features	
Type of Flow	Cross-counterflow
Type of Construction	Banks of finned tubing staggered arrangement
Number of Parallel Circuits	3
Number of Passes	52
3. Dimensions	
Tube	
Outside Diameter	0.375 in.
Inside Diameter	0.305 in.
Fin	
Type	Wound, brazed, solid fins
Thickness	0.021 in.
Height	5/16 in.
Pitch	10 fpi
Transfer Area/ft of Tubing	1.256 ft^2/ft

TABLE 13.1 (continued)

DESIGN POINT CHARACTERISTICS
OF VAPOR GENERATOR FOR DEMONSTRATION TEST

Tube Spacing	1-1/8 in. equilateral triangular spacing
4. Heat Transfer Characteristics	
Effectiveness	
Preheat region	.84
Boiling region	.67
Superheat region	.40
UA	
Preheat region	3426 Btu/°F
Boiling region	1157 Btu/°F
Superheat region	512 Btu/°F

3

The unit consists of three sections, individually fabricated and subsequently assembled together. This approach will allow the unit to be disassembled for inspection and cleaning. It has three parallel circuits with each circuit traversing twice in the same pass. The layout is shown in Figure 13-1. The U bends and tubes will be furnace brazed together.

The part load characteristics of this vapor-generator will be used for predicting the fuel economy improvement for the demonstration test.

13.2 TURBINE GEARBOX

A 150 hp turbine gearbox unit (TGU) was built for an automotive application to operate on Fl-85 as the working fluid. This unit will be modified for this application. It is a 5.5-inch diameter, single-stage, partial admission, impulse turbine. The gearbox has a single stage reduction of 9.43. It is designed to operate at output speeds of up to 3700 rpm.

The design conditions are 1550 lb/hr at 800 psia, 650°F inlet and 15 psia exhaust. The nozzle block with 5 nozzles of 7.51 expansion ratio is designed for the pressure ratio and flow desired. There will be no control valve between the boiler and the turbine for part load operation. A partial exhaust with a built-in diffuser was designed to eliminate some of the pumping losses of the rotor. This will improve the performance at low load. The turbine modifications are shown in Figure 13.2. A high-speed seal is installed between the turbine and the gearbox which simplifies turbine

operation but increases the mechanical losses. A smaller seal to reduce this loss is under consideration.

Change of working fluid from Fl-85 to Fl-50, along with a higher pressure ratio, requires higher TGU speed to achieve good efficiency. However, the TGU output speed should be limited to 3700 rpm for stress reasons. The duty cycle study indicates that the TGU peak efficiency should occur at a diesel engine speed of 1850 rpm. Thus the TGU speed will be maintained at twice the diesel speed until it reaches 3700 rpm and then maintained constant. The predicted performance of the TGU at 3700 rpm is 58%.

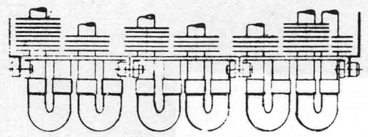

SECTION A-A

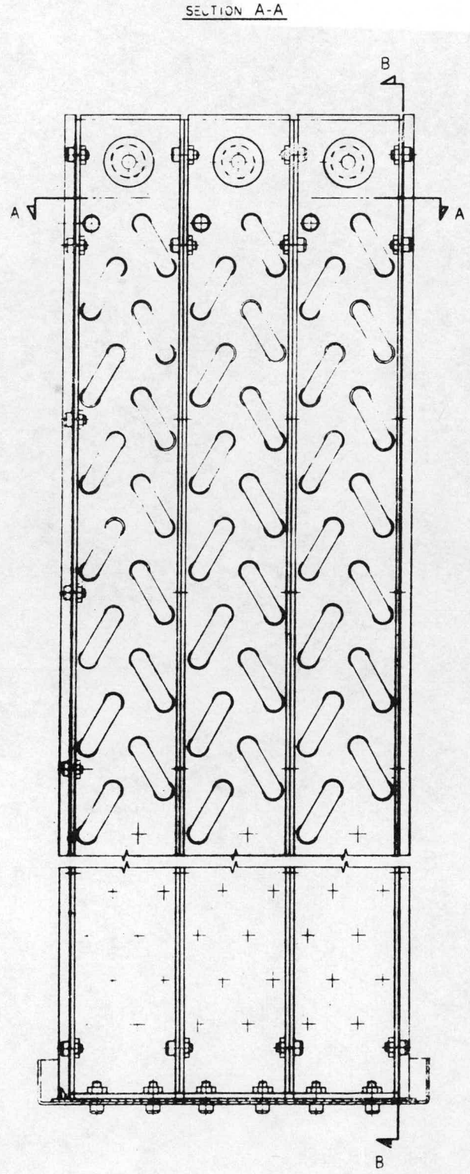

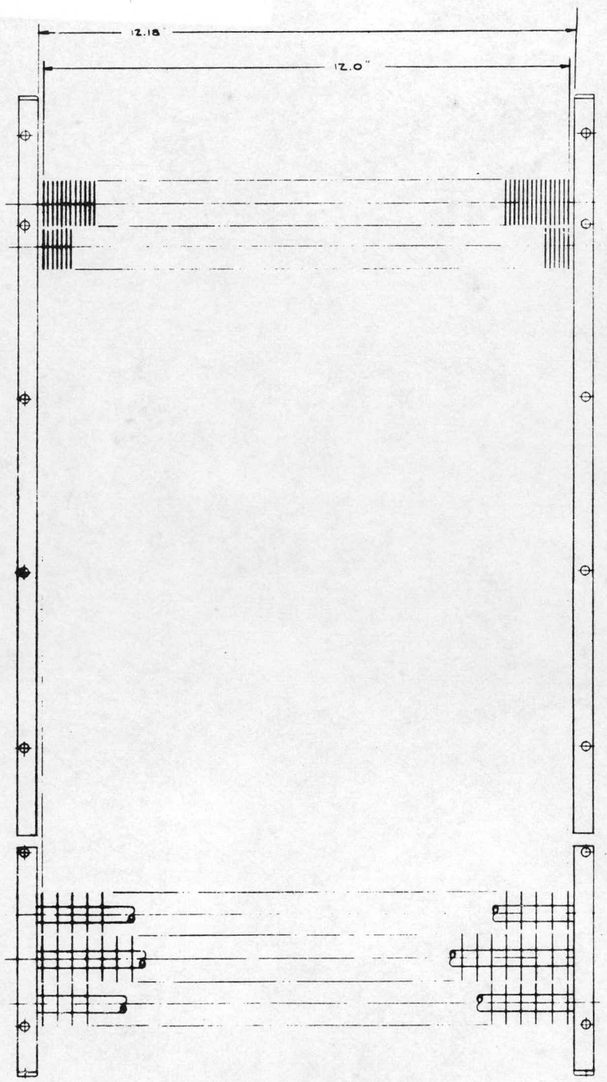

SECTION B-B

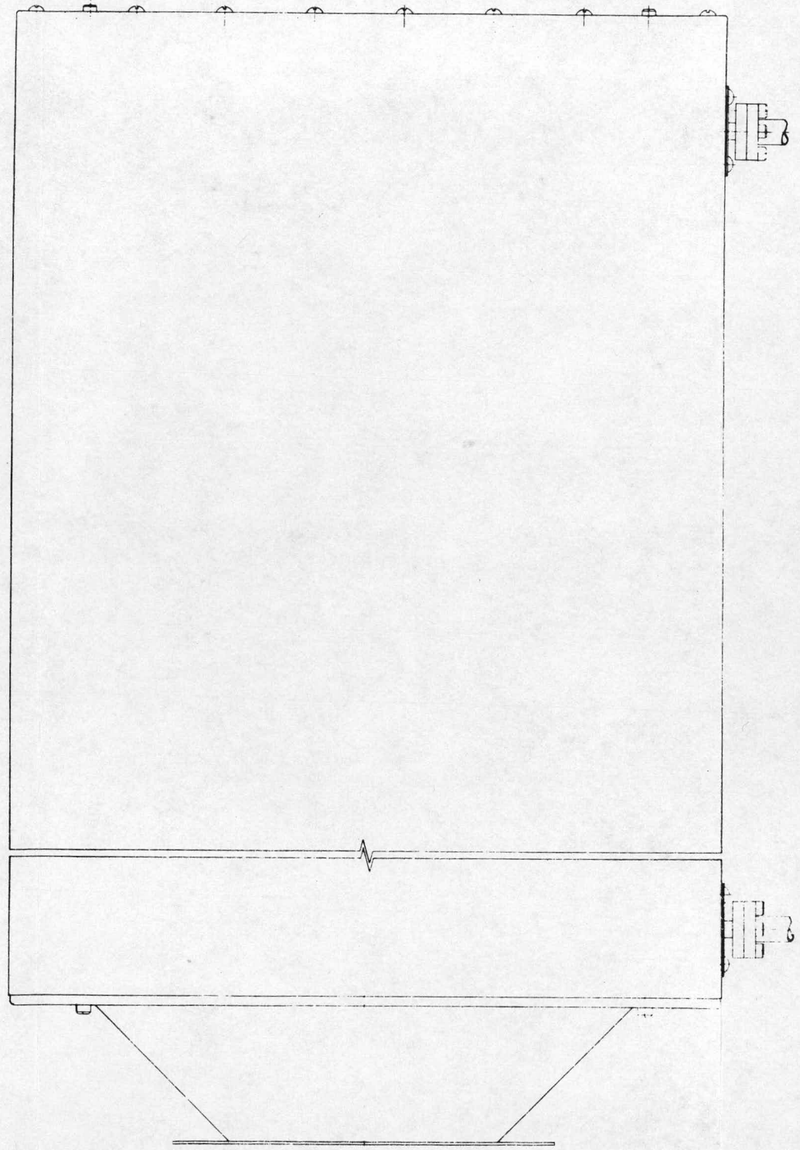

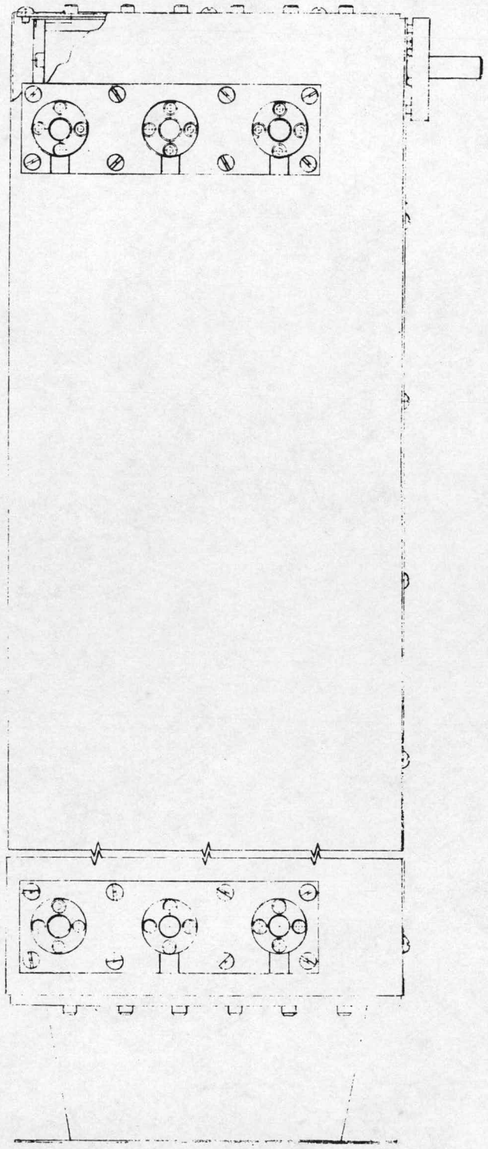

Figure 13.1. Layout of Vapor Generator.

THIS PAGE
WAS INTENTIONALLY
LEFT BLANK

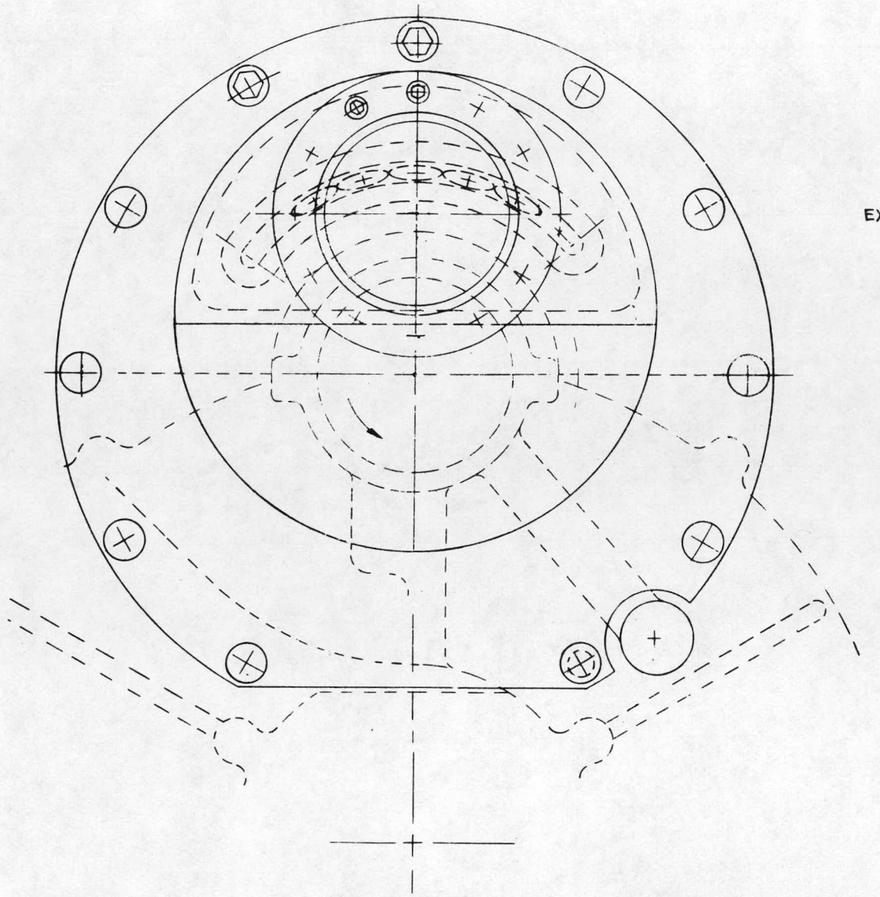

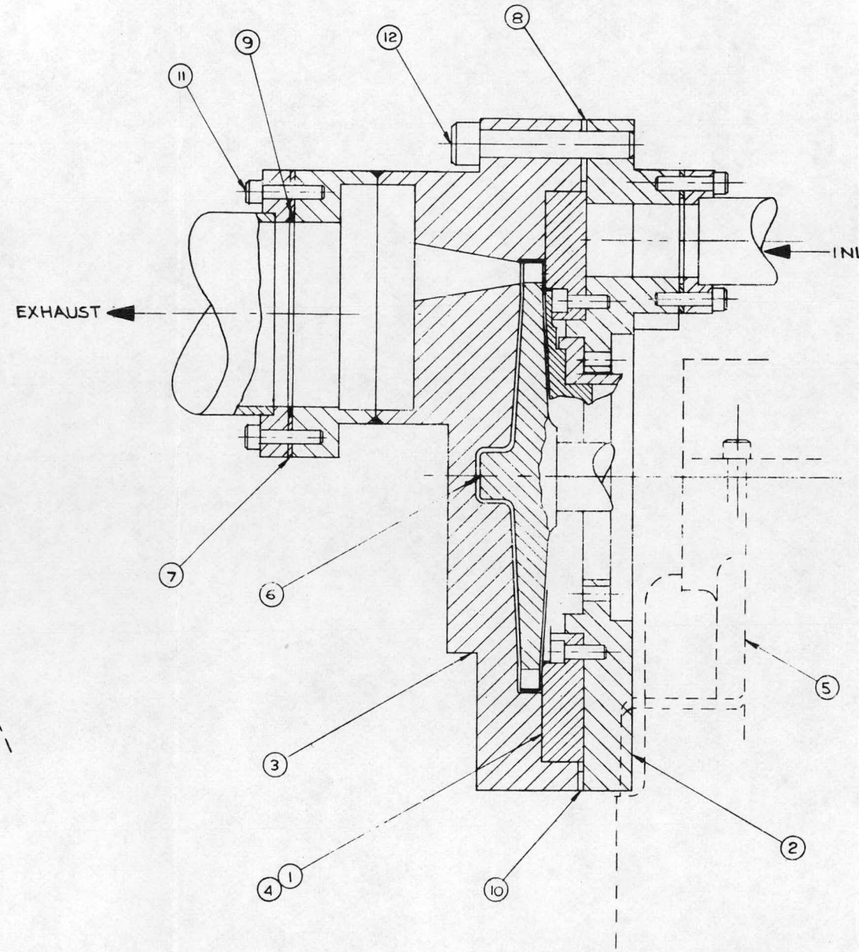

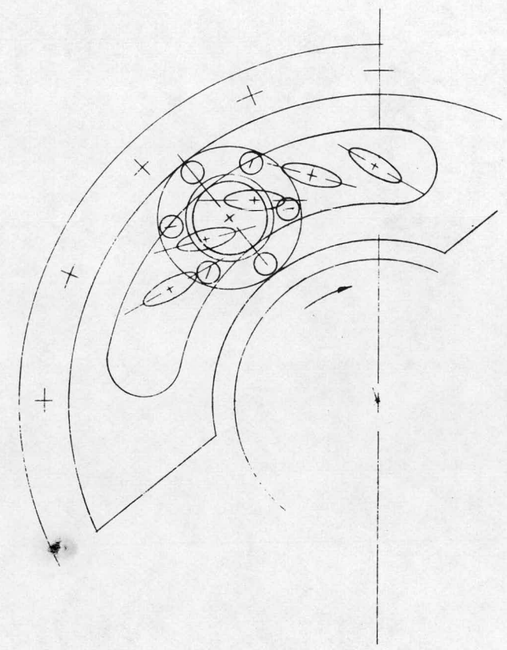

Figure 13.2. Modifications to Auto Turbine to Demonstrate Truck Bottoming Turbine

APPENDIX A

EXHAUST TEMPERATURE MEASUREMENTS ON MACK ENDT 676 DIESEL ENGINE (Performed at Mack Truck Inc.)

The engine testing was conducted to verify initial engine performance data and to determine the tail pipe temperature drop from the turbocharger to a point downstream which simulates a typical muffler mounting location. This location was chosen as the most probable for the organic system vapor generator. The engine performance testing, done to verify the initial data given to TECO, was conducted in a similar fashion to that which produced the initial data. The slight differences in performance arise from a two degree change in injection timing and from slightly different inlet air temperature and exhaust back pressure. The injection timing change was required for emissions. The performance difference is summarized in Figure A-1.

The tail pipe temperatures were taken in a free convection environment; there was no engine fan installed. The testing was done at four different loads, from part load to full load, at five different speeds, from 1000 to 2100 rpm. For each of these specific points, engine performance and tail pipe temperatures were recorded.

The tail pipe temperatures were taken with the axial spacing as shown in Figure A-2. Each succeeding thermocouple was radially disposed 90° from the preceding one. They were mounted in the center of the exhaust flow stream in order to measure the bulk gas temperature. The maximum temperature drop was 70°F, which occurred at full load at 1000 rpm. The minimum temperature drop was 20°F, which occurred at full load at 2100 rpm. Complete engine test data are enclosed. See Figures A-3 to A-15.

Performance Data Corrected to 29.9 in Hg ABS and 85°F
Bore - 4-7/8, Stroke - 6, Displacement 672 in.^{3}

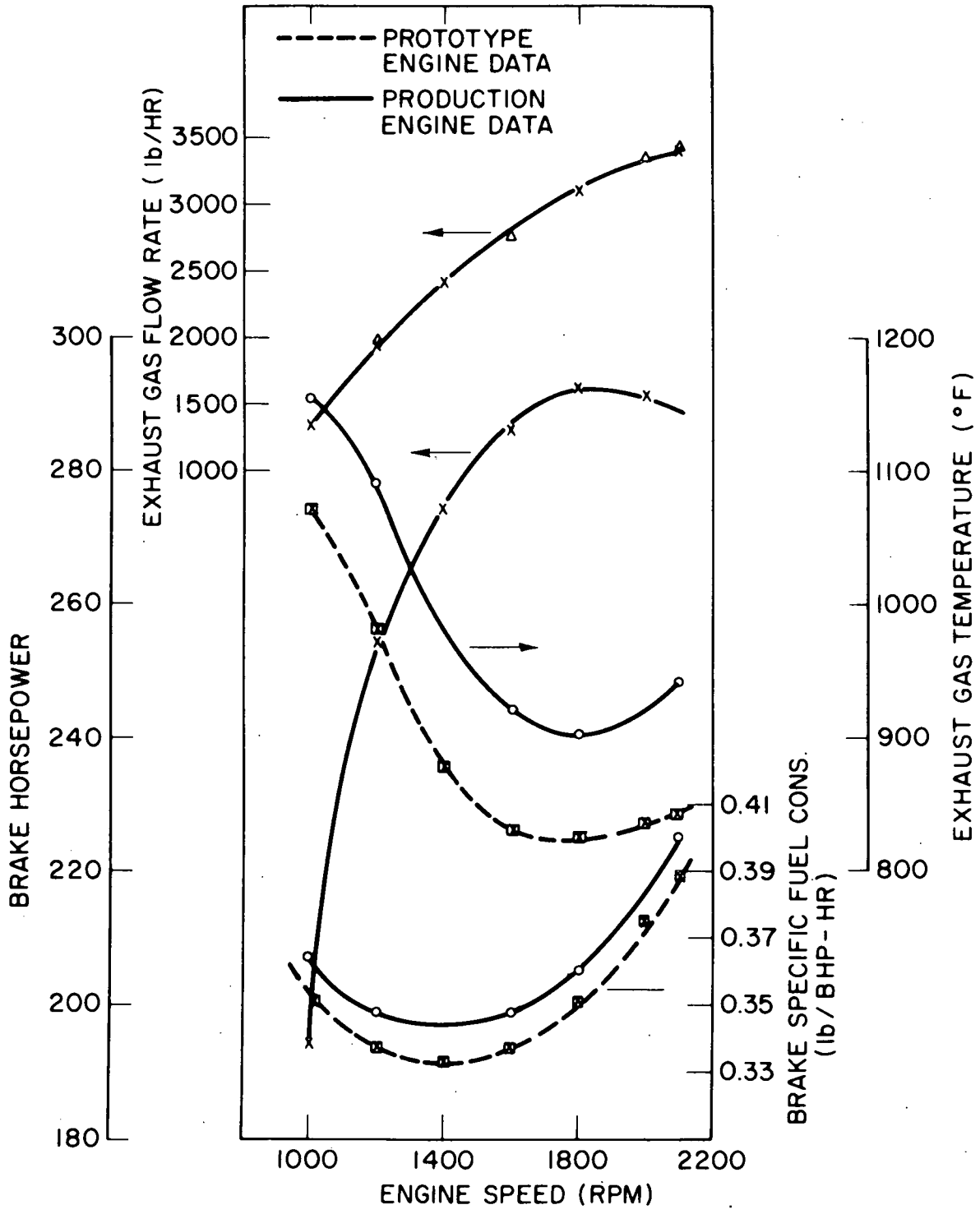

Figure A-1. Performance Data, Mack ENDT676 Engine

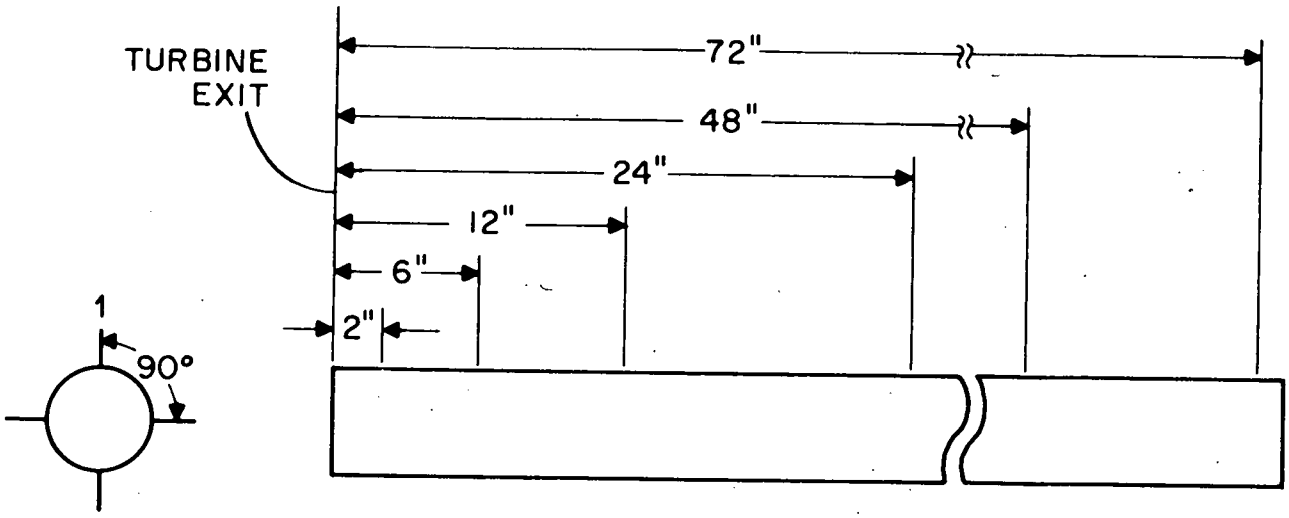

NOTE: ORIENT THERMOCOUPLES
90° FROM THE PRECEDING
ONE STARTING FROM POSITION 1.

T^1 = 2"

T^2 = 6"

T^3 = 12"

T^4 = 24"

T^5 = 48"

T^6 = 72"

Figure A-2. Tailpipe Temperature Measurement
RFT E-358, Proj. #50-00351

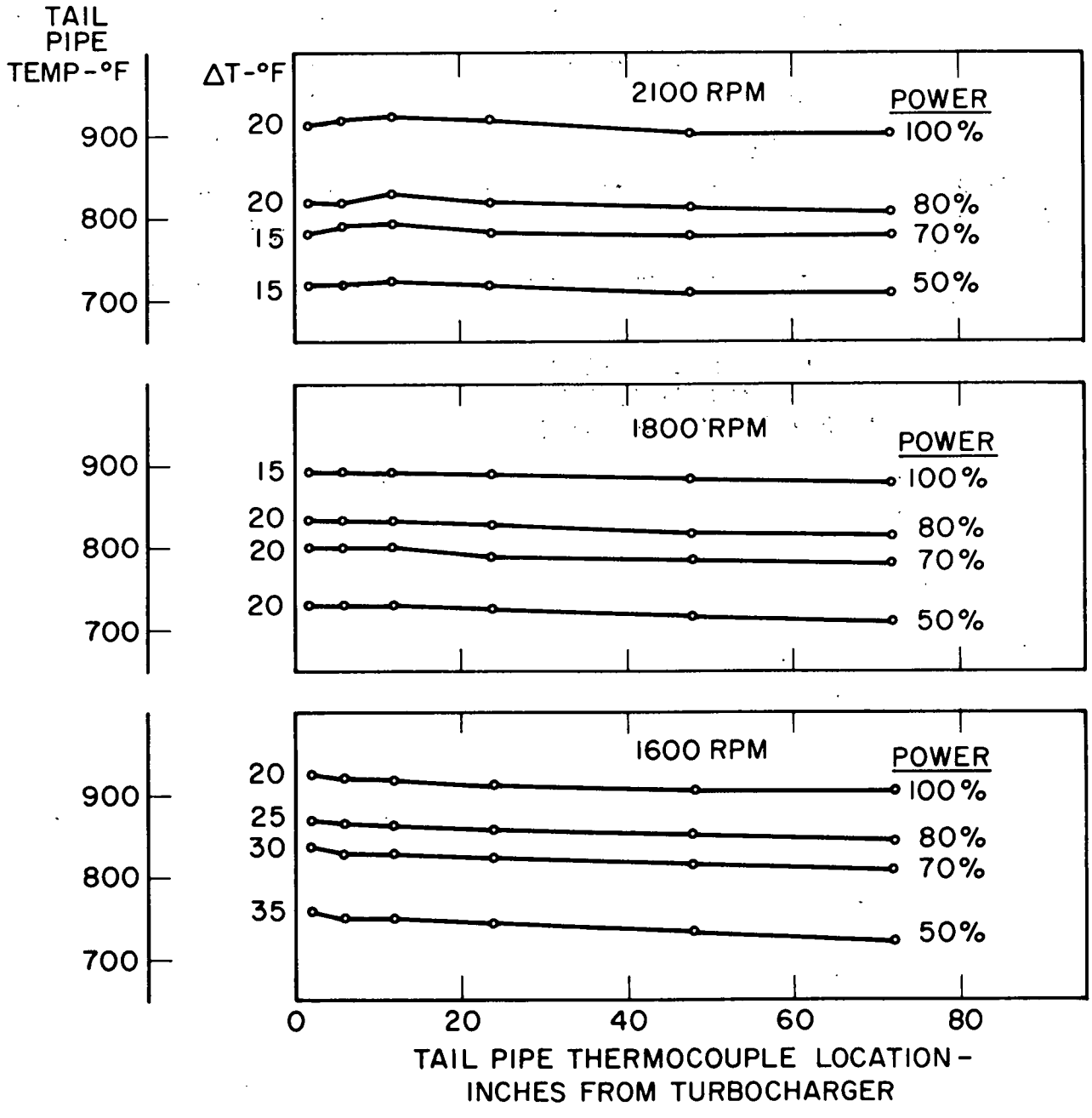

Figure A-3. Performance Data, Mack ENDT676 Engine Exhaust Tail Pipe Temperature - °F vs Length

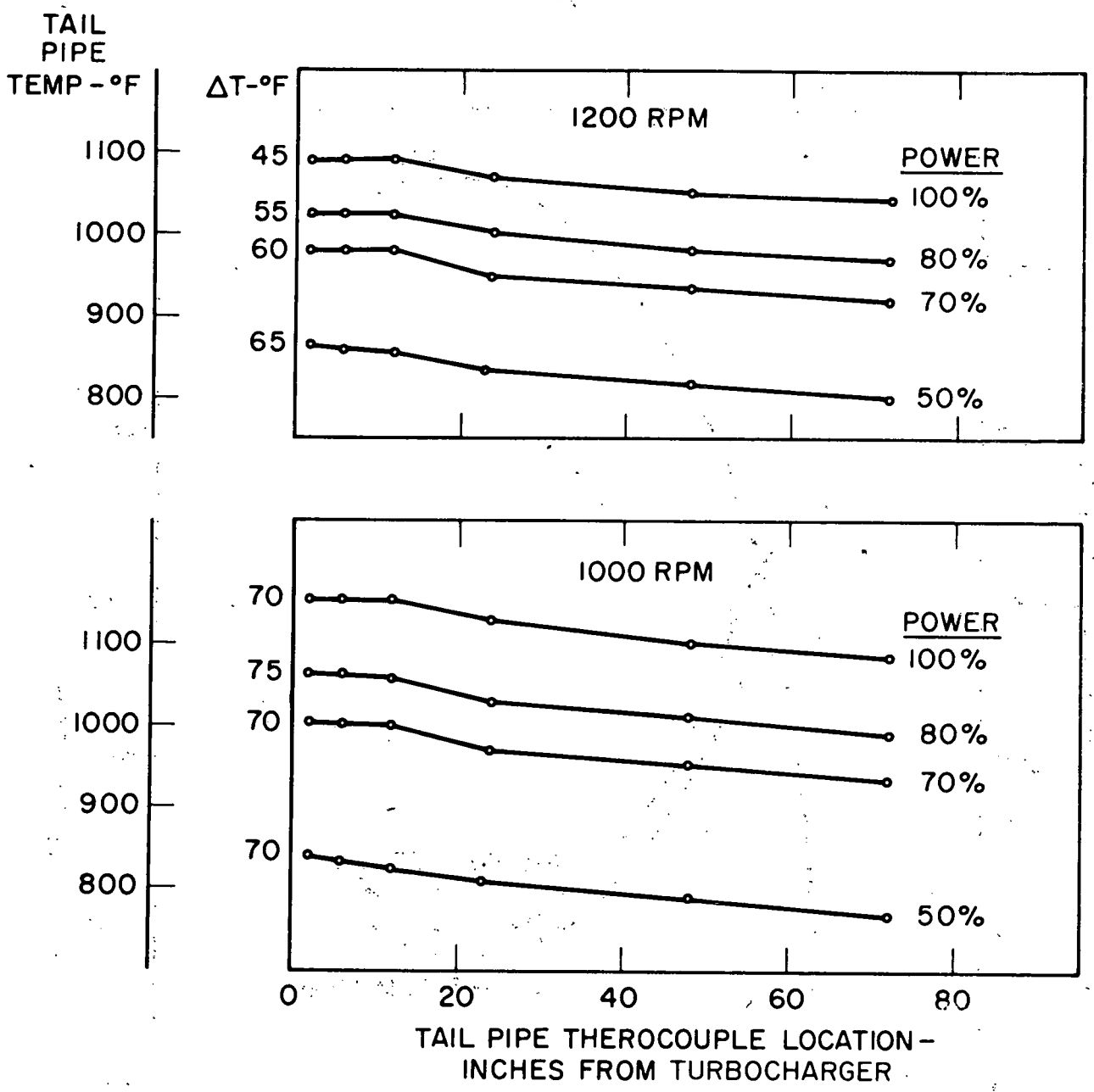

Figure A-4. Performance Data, Mack ENDT676 Engine Exhaust Tailpipe Temperature - °F vs. Length

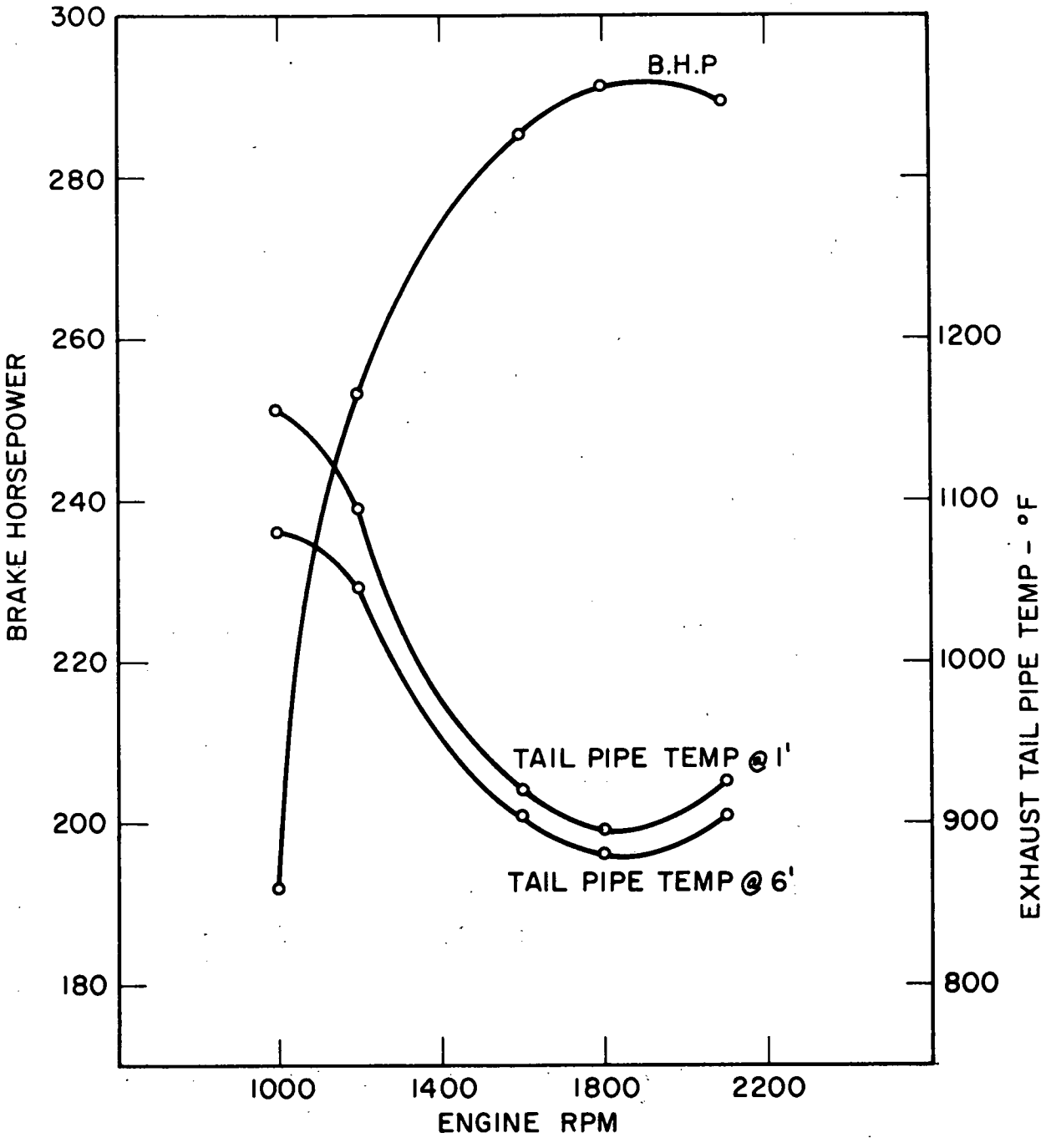

Figure A-5. Performance Data, Mack ENDT676
Engine Performance

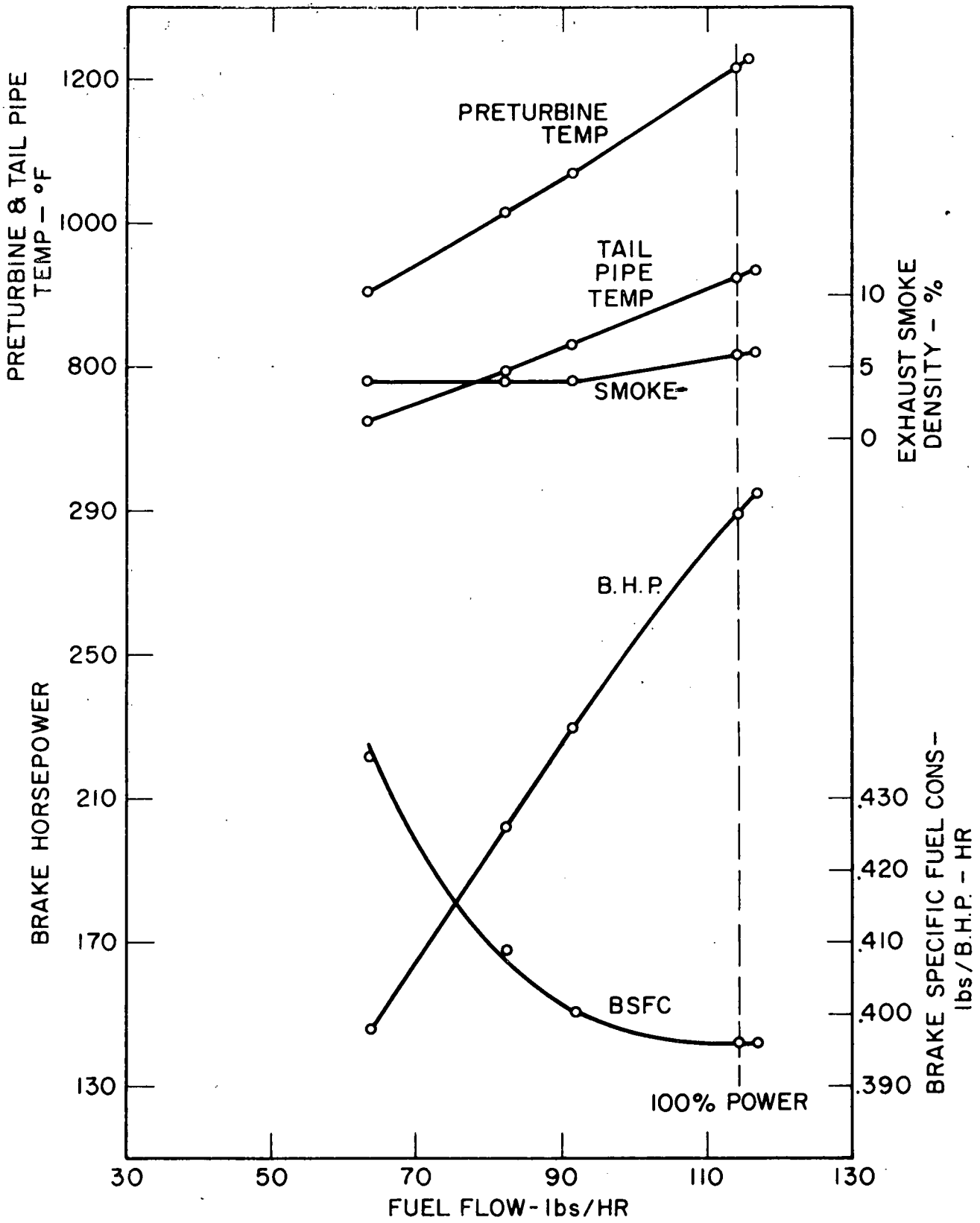

Figure A-6. Performance Data, Mack ENDT676 Engine, Partial Throttle, 2100 rpm

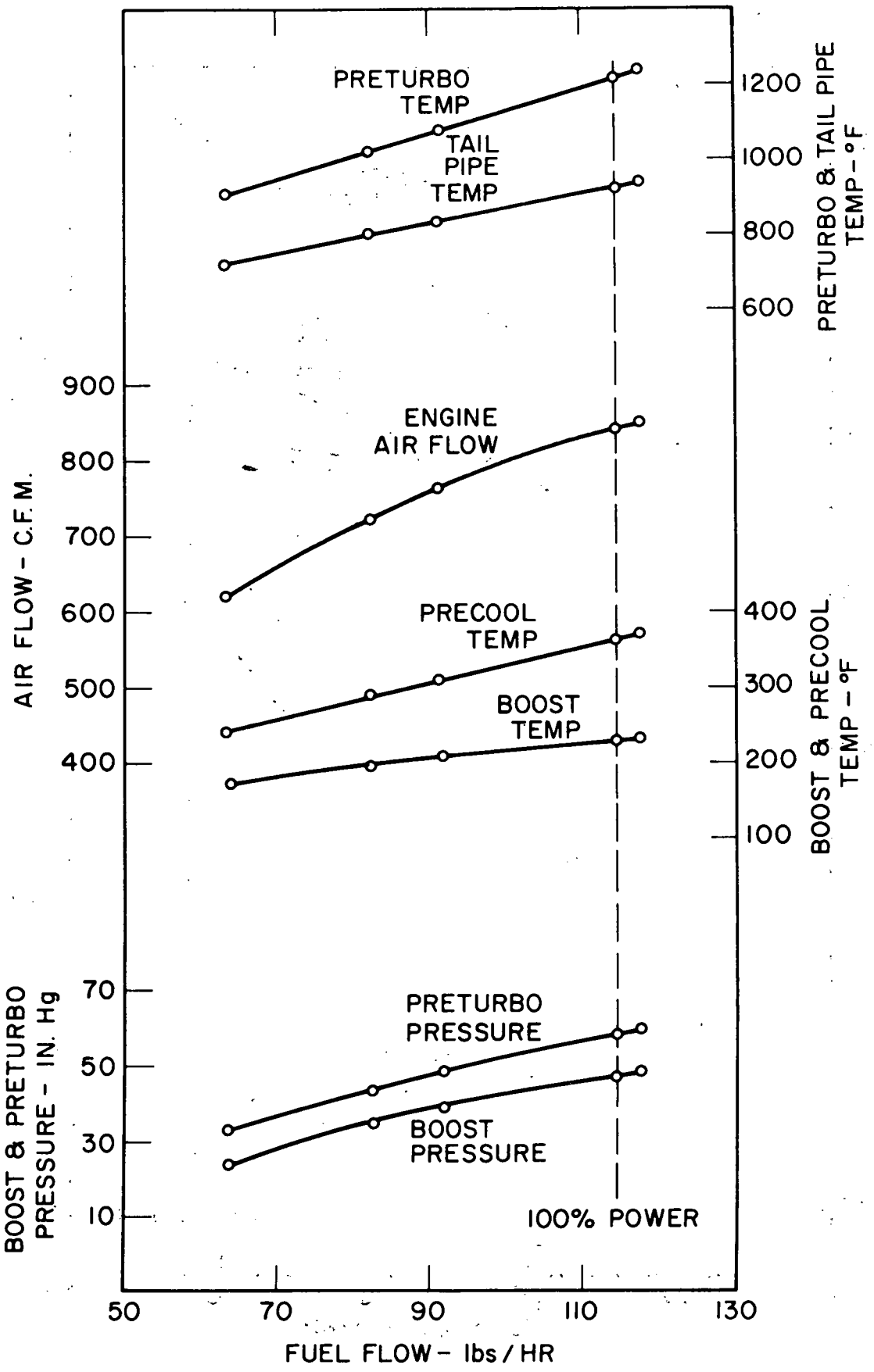

Figure A-7. Performance Data, Mack ENDT676 Engine Partial Throttle, 2100 rpm

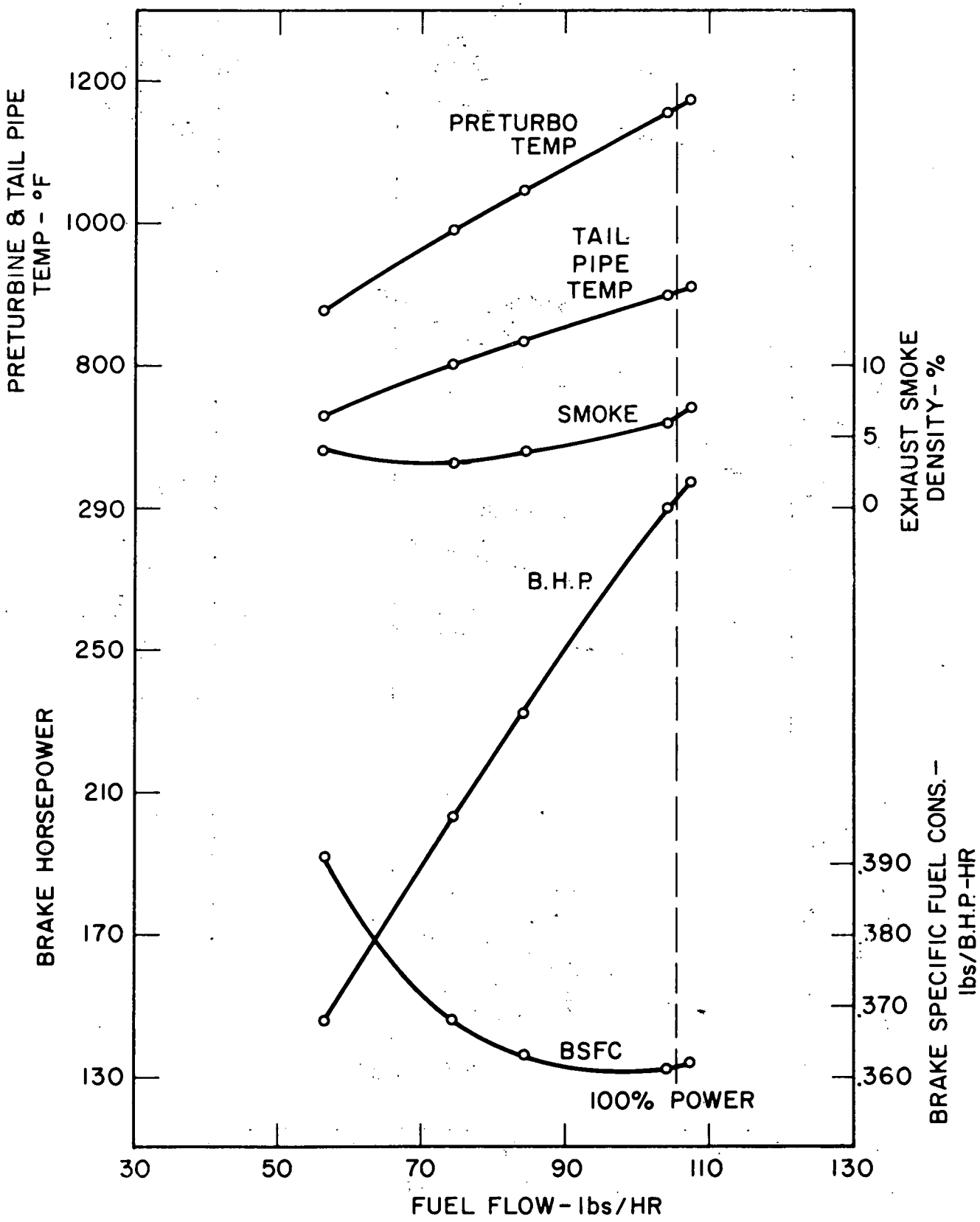

Figure A-8. Performance Data, Mack ENDT676 Engine
Partial Throttle, 1800 rpm

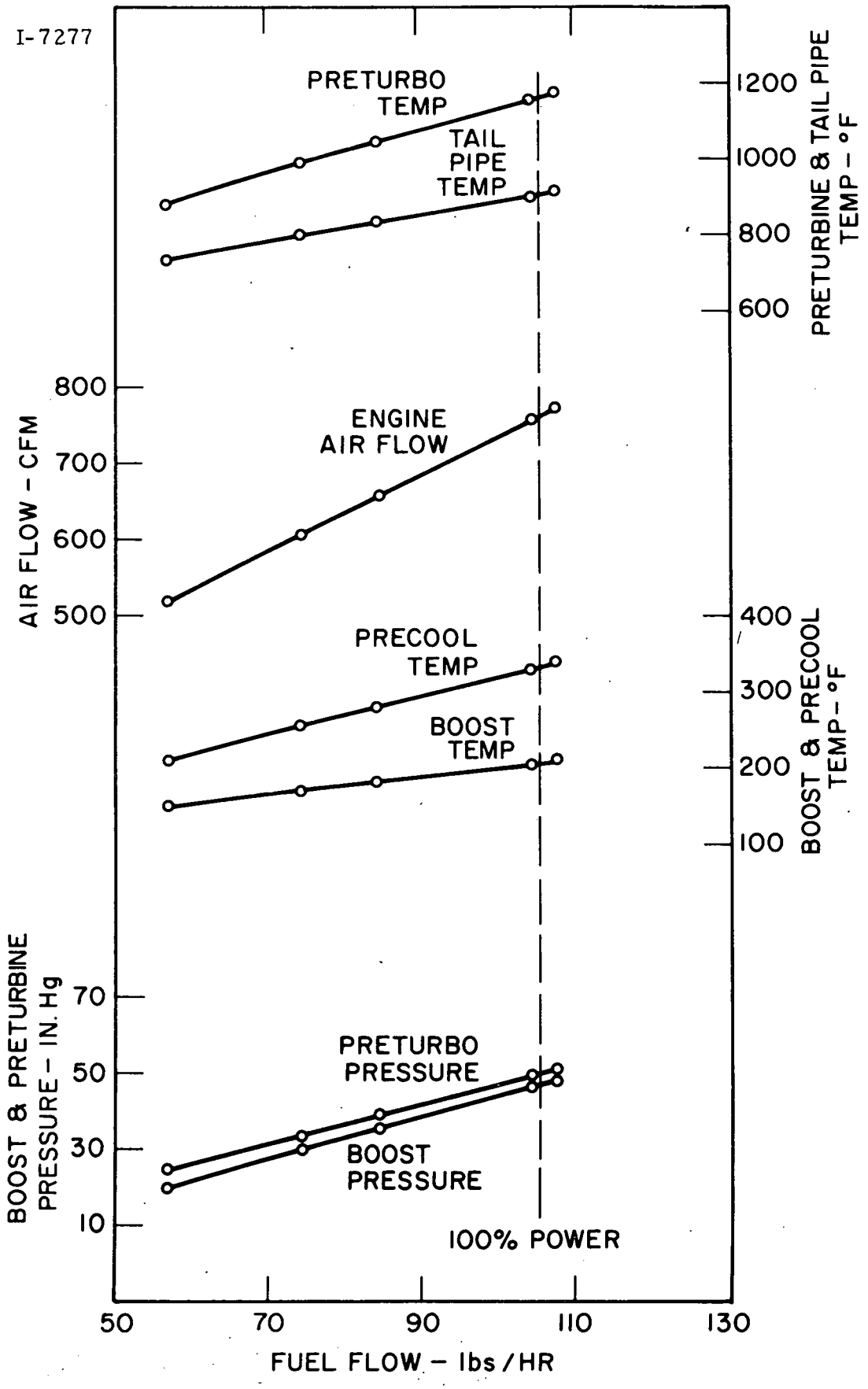

Figure A-9. Performance Data, Mack ENDT676 Engine Partial Throttle, 1800 rpm

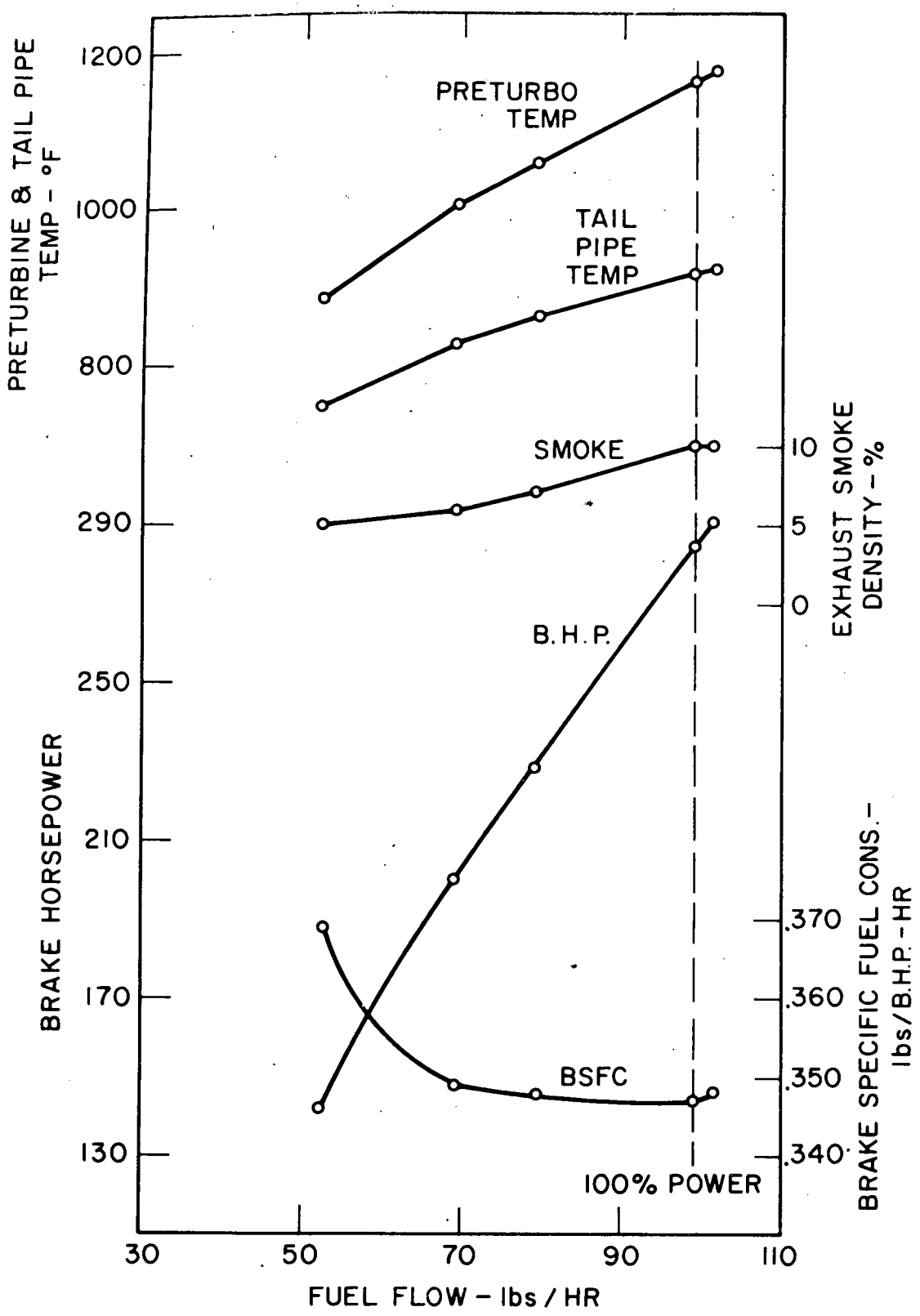

Figure A-10. Performance Data, Mack ENDT676 Engine Partial Throttle, 1600 rpm

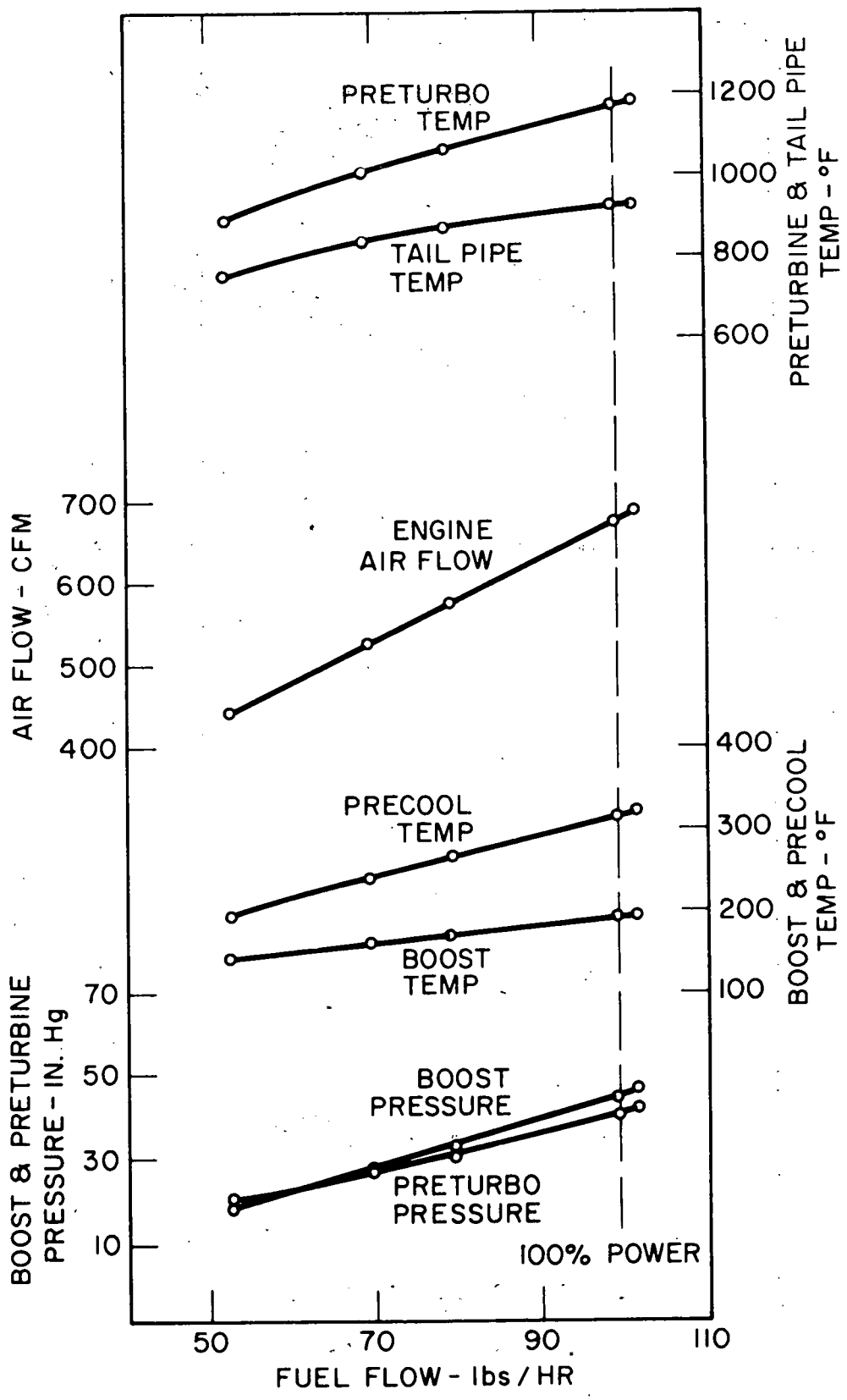

Figure A-11. Performance Data, Mack ENDT676 Engine Partial Throttle, 1600 rpm

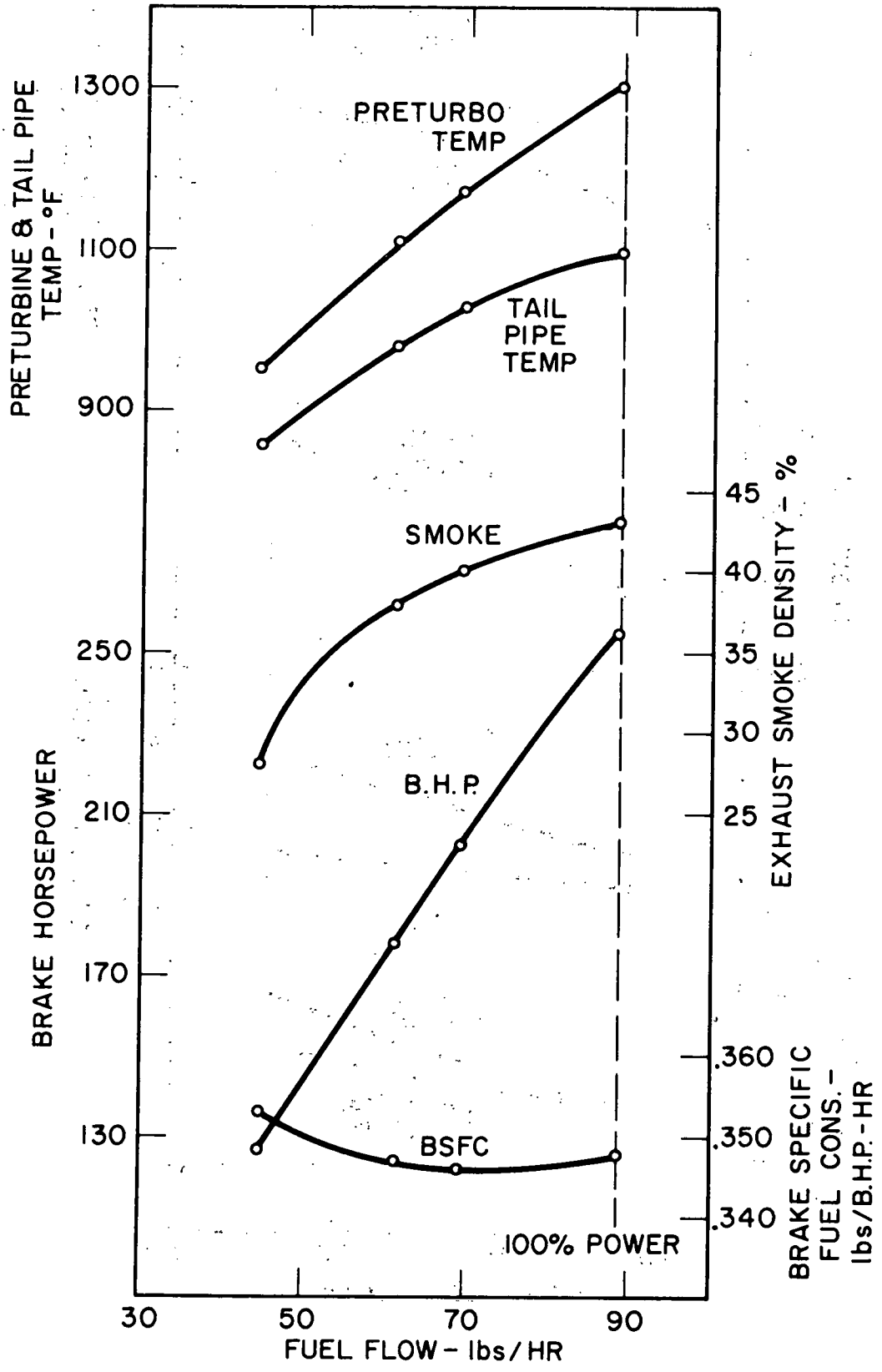

Figure A-12. Performance Data, Mack ENDT 676 Engine Partial Throttle, 1200 rpm

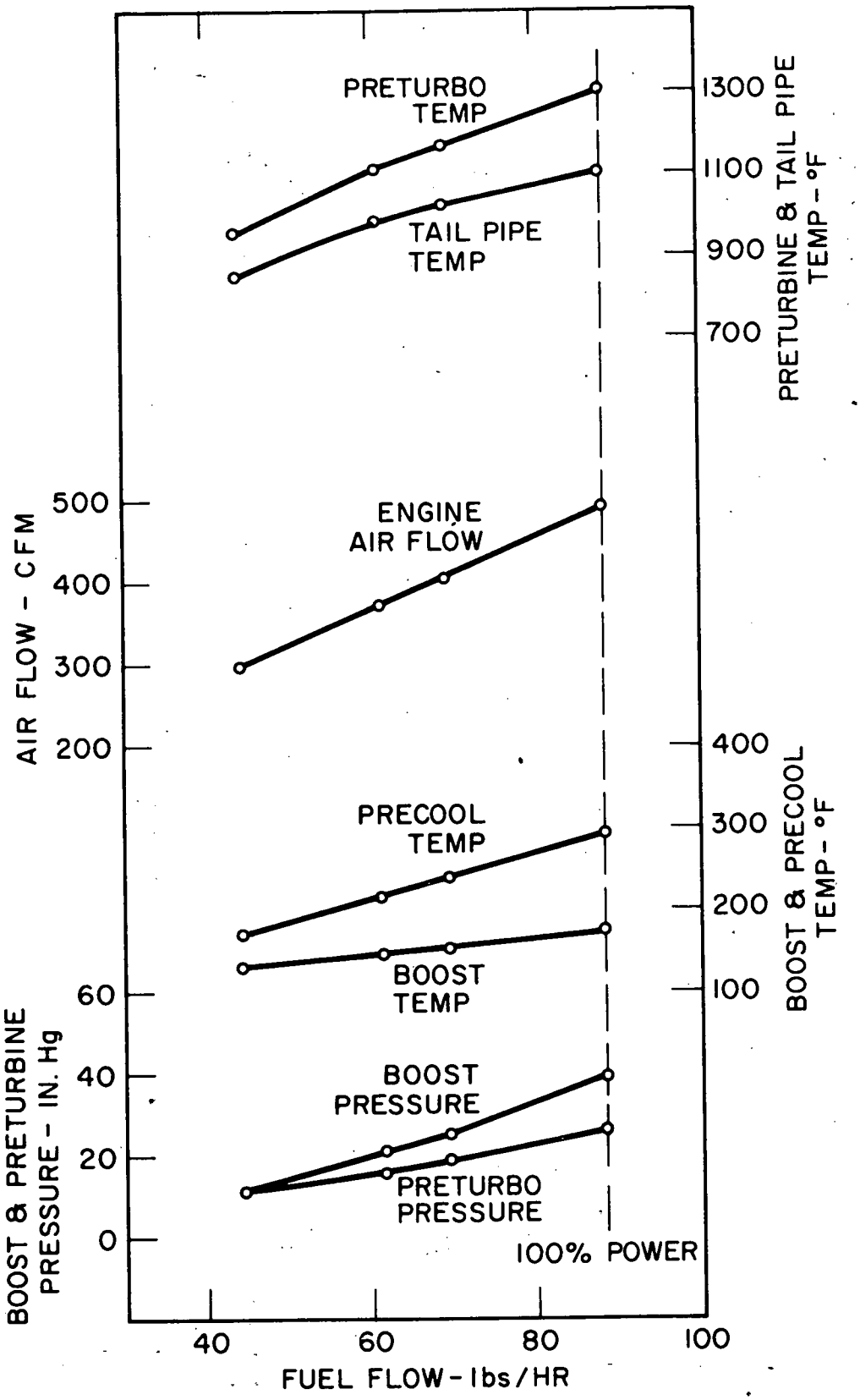

Figure A-13 Performance Data, Mack ENDT676 Engine, Partial Throttle 1200 rpm

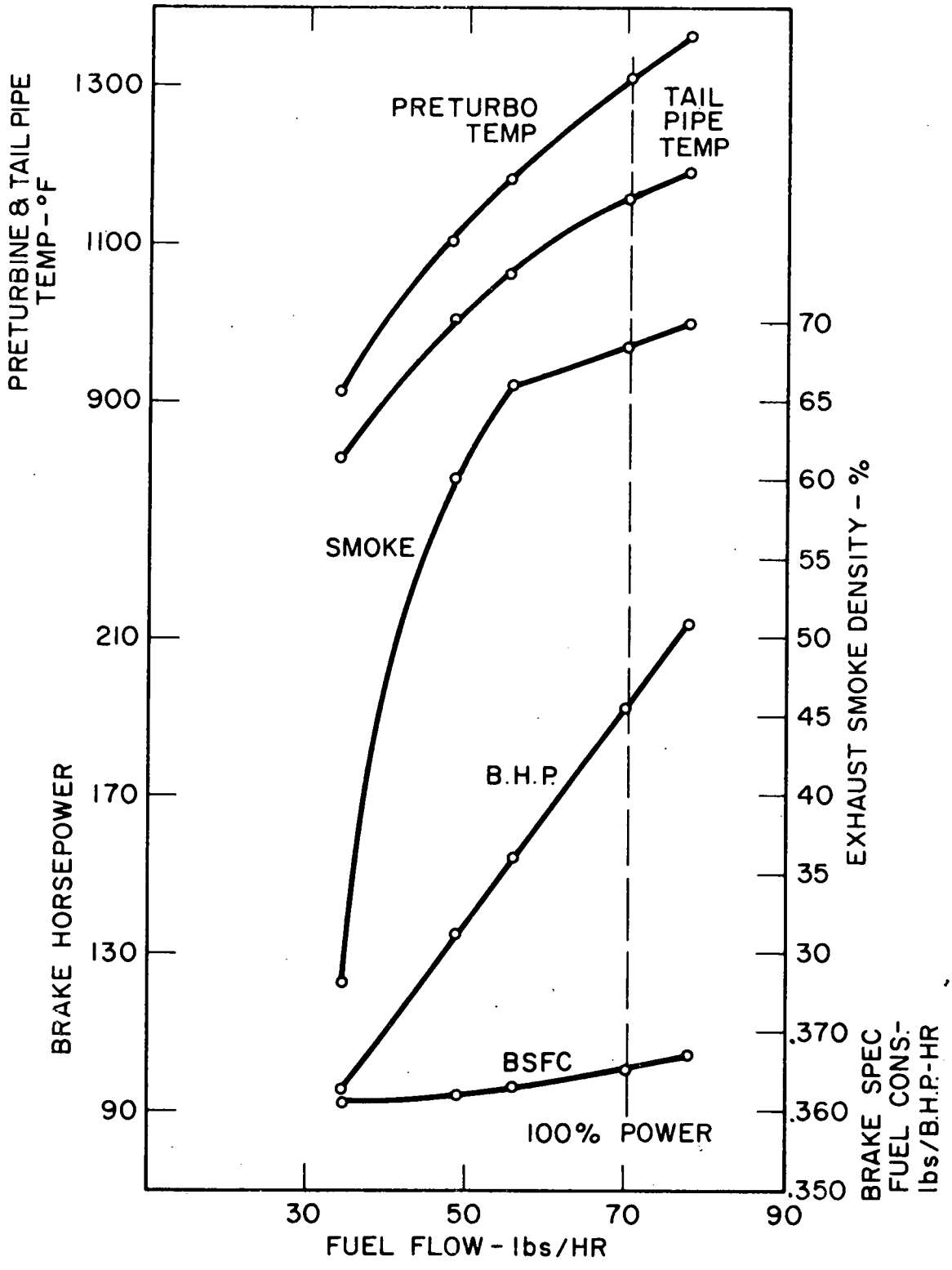

Figure A-14. Performance Data, Mack ENDT676 Engine Partial Throttle, 1000 rpm

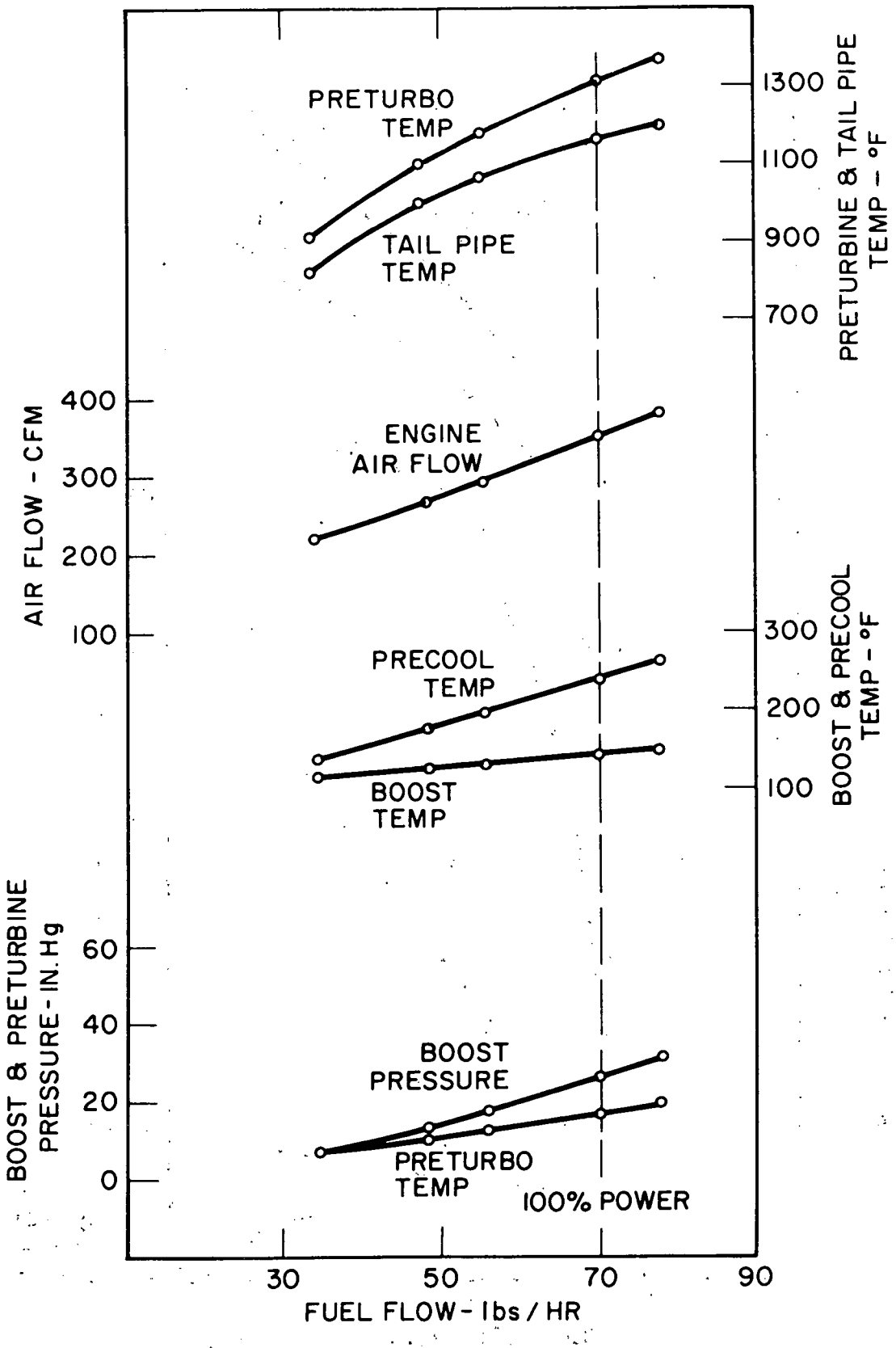

Figure A-15. Performance Data, Mack ENDT676 Engine Partial Throttle, 1000 rpm

APPENDIX B

MAXIMUM POSSIBLE WORK OBTAINABLE FROM THE EXHAUST GAS

The following analysis shows the maximum possible work that can be obtained from the exhaust heat.

Consider the reversible, open-circuit, work-producing device illustrated in Figure B. 1, in which exhaust gases are taken into the device at initial state 1 and delivered from the device at the final state 2. The change from state 1 to state 2 of the gas is accomplished by means of one or more reversible cyclic heat engines operating between the local gas temperature and ambient temperature T_o in such a way that complete reversibility is maintained. This requires that all heat transfer between (1) the exhaust gas and cyclic heat engine, and (2) the cyclic heat engine and environment occur with zero ΔT, as indicated in Figure B. 1. The work obtained in this fashion represents a unique maximum quantity of work produced by an open-circuit device which can exchange heat only with an isothermal energy reservoir, the environment. This maximum obtainable work $(W_{Rev})_{1 \rightarrow 2}$, in the given situation is termed the "available energy" and requires only that all processes which bring about the given change of state are reversible.

The maximum possible work which can be obtained with a given change of state of the gas can be obtained as follows. For each of the differential reversible cyclic heat engines, the efficiency is given by the Carnot efficiency.

$$\eta_i = \frac{dW_i}{dQ_i^h} = \frac{T_i - T_o}{T_i}$$

The differential heat transfer from the gas to the power cycle is:

$$dQ_i^h = - C_p \, dT_i$$

Substitution gives:

$$dW_i - \frac{T_i - T_o}{T_i} C_p \, dT_i = (- C_p) \left\{ \left(1 - \frac{T_o}{T_i} \right) dT_i \right\}$$

Integration results in:

$$\left[W_{Rev} \right]_{1 \to 2} = \int_1^2 dW_i = (- Cp) \left\{ \left(T_2 - T_1 \right) - T_o \ln \frac{T_2}{T_1} \right\}$$

$$= Cp \left\{ \left(T_1 - T_2 \right) - T_o \ln \frac{T_1}{T_2} \right\}$$

This expression can be obtained more directly from the availability function, B, as expressed below:

$$(W_{Rev})_{1 \to 2} = B_1 - B_2 = (h_1 - T_o S_1) - (h_2 - T_o S_2),$$

where S denotes entropy.

Following conventional practice by defining the efficiency of the engine as the ratio of the work out to the maximum possible enthalpy change of the gas heat source,

$$\eta_{Rev} = \frac{(W_{Rev})_{1 \to 2}}{h_1 - h_o} = 1 - \left(\frac{T_o}{T_i} \right) \frac{1}{\left(1 - \frac{T_o}{T_1} \right)} \left\{ \left(\frac{T_2}{T_o} - 1 \right) + \ln \frac{T_1}{T_2} \right\}.$$

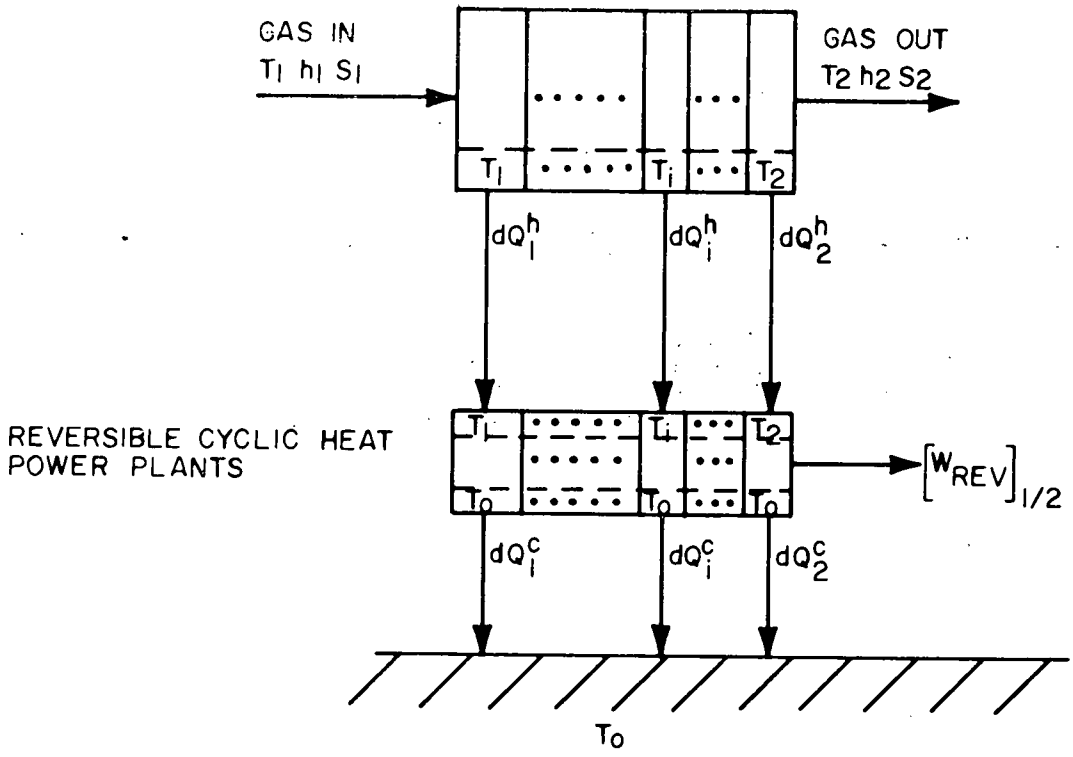

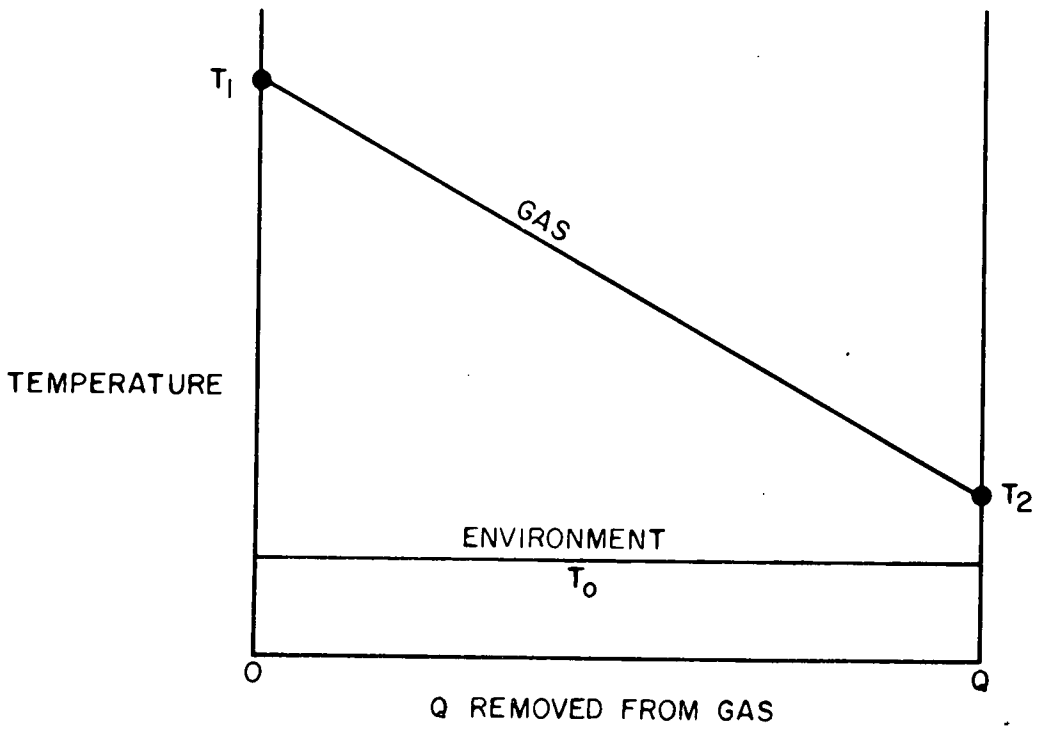

Figure B.1. Schematic of Reversible, Open-Circuit, Work-Producing Device.

The maximum efficiency occurs when ($T_2 = T_o$) or,

$$(\eta_{Rev})_{Max} = 1 - \left(\frac{T_o}{T_i}\right) \frac{1}{\left(1 - \frac{T_o}{T_1}\right)} \ln \frac{T_1}{T_o} .$$

APPENDIX C

ANALYSIS OF TURBINES, GEARBOXES, AND SEALS FOR AN FL-50 TRUCK ENGINE BOTTOMING CYCLE

November 21, 1974

Prepared for: Sudheer Helekar
Thermo Electron Corp.
Waltham, Mass.

Prepared by: Douglas K. Werner
Ralph W. Blakemore

Approved by: Robert E. Barber

1.0 SUMMARY

This report summarizes the analysis of a turbine expander and gearbox for a truck engine bottoming cycle. Working fluid is TFE-50 and the fluid conditions and flow were established by Thermo Electron. Estimated three-stage axial-flow turbine efficiency at 60,000 rpm is 0.71 including gearbox and seal losses, and interstage leakage.

Alternative turbine designs evaluated included multistage axial, both straddle and double cantilever mounted, and a two-stage axial and radial combined turbine. Gearbox and seal losses were found to be primarily caused by the double buffered seals on the high speed shaft.

The recommended turbine design for this application is a three-stage double cantilevered, axial-flow turbine with an overall turbine-gearbox efficiency of 0.73 at 62,000 rpm.

2.0 FLUID CONDITIONS AND DESIGN RESTRICTIONS

Turbine fluid conditions and other requirements were specified in the Work Statement and are summarized below.

Turbine Design Conditions

1. Fluid - Fluorinol 50
2. Inlet Pressure - 800 psia
3. Inlet Temperature - 650°F
4. Exhaust Pressure - 11.0 psia
5. Flow Rate - 1324 lbs/hr
6. Diesel Engine Design Speed - 2100 rpm
7. Normal Operating Speed Range - 1200 to 2100 rpm
8. Idle Speed - 300 rpm
9. Maximum Overspeed - 3000 rpm

Turbine Design Restraints

1. Maximize practical overall efficiency including bearings, seals, and gearbox losses.
2. Critical speeds to be outside the normal operating speed range and/or above the maximum overspeed speed.
3. Maximum shaft seal surface speed of 250 ft/sec at the design speed.
4. Turbine mechanically safe at "runaway" speed.
5. Minimum blade height of approximately 0.1 inch.
6. Low stress wheel for inexpensive manufacturing.
7. Maximum gearbox ratio of 35.

All fluid conditions were evaluated using the gas properties supplied by TECO.

3.0 AERODYNAMIC ANALYSIS PROCEDURE

The first step of the analysis procedure was to arbitrarily select interstage static pressures. The efficiency and geometry of the turbine stage was

then estimated using specific speed correlations. The fluid conditions at the stage exit determined the next stage inlet conditions. Additional stages were evaluated using the same procedure. The power produced by each stage including the effects of carryover and leakage were combined to determined turbine stage performance. The interstage pressures were optimized for maximum turbine performance.

3.1 CARRYOVER

Carryover is associated with the velocity energy in the exhaust of a turbine stage which is available to the next stage. Not all of the velocity energy is recovered for use in the subsequent stage because of losses including a) flow friction, and b) those caused by redistribution of the flow to a larger arc of admission distribution losses.

The arc of admission of each stage was estimated using specific speed correlations and if the arc of admission of a stage was greater than that of the preceeding stage, it was necessary to provide a plenum between the two stages to redistribute the vapor to the nozzles of the following stage. The plenum was assumed to be large and the gas velocity low, so that the distribution losses would be small. However, the large plenum results in a sudden expansion and all the velocity energy is lost resulting in zero carryover.

For consecutive turbine stages with equal admission arcs there is no distribution loss. For this case it was assumed that 72% of a stage's exit velocity energy was available to the next turbine stage which corresponds to a stator velocity coefficient of 0.85 which is attainable for good designs.

3.2 INTERSTAGE LEAKAGE

A multistage axial turbine has leakage across the stators because of the pressure drop across the nozzles. Conventional practice is to reduce the leakage with close clearance, labyrinth type seals. The leakage of a reasonable seal for this hardware was estimated and used in the following calculations when evaluating turbine performance. The seal geometry assumed for this calculation is summarized below.

INTERSTAGE SEAL GEOMETRY

Seal between stages	1 - 2	2 - 3
Radial clearance	0.008	0.008
Throttlings	4	2
Axial length between throttlings	0.13	0.13
Sealing land thickness	0.02	0.02
Shaft diameter	0.60	0.60

All dimensions are in inches.

The seal between the second and third stage can be shorter and have fewer throttlings than the seal between the first and second stage since it seals against lower pressure and density.

4.0 THREE-STAGE STRADDLE-MOUNTED TURBINE, 60,000 RPM DESIGN SPEED

The optimum design will have the highest combined gearbox and turbine efficiency. First the turbine performance was estimated, then the gearbox and seal losses were estimated. These were then combined to obtain an overall efficiency.

4.1 TURBINE

This turbine operated at the fluid conditions specified in section 2.0, and at 60,000 rpm. Turbine efficiency was optimized by using the aerodynamic analysis procedure discussed in section 3.0. It was specified that the turbine was straddle-mounted and the leakage was estimated using the seal design discussed in section 3.2. The turbine configuration is summarized below and shown in the sketch of Figure 1.

Stage	1	2	3
Inlet press. (psia)	800	200	48.7
Inlet temp (^{o}F)	650	527	419
Exit Static press. (psia)	200	48.7	11
Isentropic head (BTU/lb)	41.9	41.9	40.0
Specific speed	13.76	26.9	53.5
Specific dia.	4.3	2.4	1.67
Static effic.	0.675	0.75	0.815
Admission (%)	28	60	100
Pitch dia. (in.)	2.14	2.31	3.15
Blade height (in.)	0.09	0.16	0.196
% Leak	0	8.5	2.6
HP	14.71	14.96	16.68
Reaction (%)	0	0	40
U/C_o	0.387	0.42	0.58

This choice of interstage pressure is felt to be very near optimum for the speed and fluid conditions specified, however, a detailed optimization was not made.

The predicted turbine efficiency including leakage is 0.75 which results in 46.3 turbine shaft horsepower.

4.2 MECHANICAL

The mechanical analysis included the shaft design and analysis of the critical speeds for the straddle-mount three stage turbine shaft assembly.

Maximum practical gearbox efficiencies were also evaluated. The following sections discuss the analysis and offer recommendations for the conceptual design layout.

4.2.1 Critical Speed

The B/N critical speed computer program was utilized to produce the optimum straddle-mount shaft design. This design is shown in Figure 2. Note that this design requires two bearings, one on each end. Also note that the third stage turbine is nearest the gearbox. This is required to result in a first critical speed below the operating speed zone. Exchange of the first and third stages causes the first critical to occur within the operating speed zone. The critical speed map for this design is shown in Figure 3. In no case, for a reasonable design, could both the first and second criticals be made to occur above the operating speed zone. Either rolling element or fluid film type bearings may be used with this design since both types have bearing stiffness which can meet the requirements shown in Figure 3. The design bearing stiffness range shown is easily obtained. In the case of rolling element bearings the stiffness is primarily a function of the bearing geometry and resultant loads. Bearing stiffness for conventional ball bearings under axial preload only are commonly in the range of 2×10^5 to $3 \times (10)^5$ lbs/ in. Fluid film bearing stiffness is also a function of bearing geometry and loading. Common stiffness for fluid film bearings are similar to those for rolling element bearings. Unlike the rolling element bearings, fluid film bearings may have higher stiffness without decreasing bearing life.

Although either bearing type may be used it is recommended that the fluid film bearings be used in this application. Since a bearing life of approximately 10,000 hours is desirable in this system, the most compact, "long lived" bearing will be the fluid film type. Face seal rubbing velocities will be approximately 200 fps for this design. Both seals are cooled and lubricated by the gearbox oil in this configuration.

4.2.2 Gearbox Efficiency

Maximum practical gearbox efficiencies were evaluated from past analytical work and from actual efficiencies established for gearboxes such as might be used in this application. It is assumed that a double reduction helical gearbox, similar in configuration to the one used for the 30 HP TECO turbine would be used. For this type of gearbox, power losses are estimated at .76 HP at 60,000 rpm turbine speed. Two double buffered face seals are required (one at each high speed bearing) and seal losses are estimated at 1.9 HP total for two TECO double face seal assemblies on the turbine shaft and .1 HP for a lip type seal on the output shaft. Seal losses are based on a 60,000 rpm turbine shaft and a 2100 rpm output shaft. The gearbox efficiency is 98% (including the low speed seal loss) for a 46.3 HP turbine. When the high speed seal loss is included, gearbox efficiency is reduced to 94%.

4.3 OVERALL TURBINE GEARBOX EFFICIENCY

The overall efficiency of the three-stage axial-flow turbine and gearbox was determined by decreasing the predicted turbine power by the extimated gearbox loss. The overall turbine and gearbox efficiency is anticipated to be 0.71, which compares well with the 0.727 efficiency predicted by TECO which did not include turbine leakage. The 0.71 efficiency results in 43.8 gearbox output horsepower.

5.0 ALTERNATIVE TURBINE & GEARBOX CONFIGURATIONS

Alternative turbines and gearbox arrangements were evaluated to determine their performance relative to that of the configuration previously discussed. Turbine performance and geometry were estimated using the restrictions and procedures discussed in section 2.0 of this report. Turbine efficiency was estimated neglecting leakage for six configurations and speeds. Gearbox and seal losses and interstage leakage were predicted and the results were combined to estimate the overall turbine gearbox efficiency.

5.1 ALTERNATIVE TURBINE CONFIGURATIONS

The multi-stage turbines were evaluated within the mechanical restrictions of : a) minimum wheel diameter of 2.0 in. (which is consistant with 0.1 in. minimum blade height) and b) a maximum tip speed at "runaway" of 1600 fps (for mechanical safty with low cost wheel materials). The interstage pressure and rotational speed were optimized within these restrictions in order to obtain the maximum efficiency. To obtain the maximum efficiency the turbine must operate at the highest speed which does not result in a turbine diameter less than 2 inches or a tip speed greater than 1600 fps. Consequently for stage numbers up to three the optimum speed was limited by the tip speed of the last stage. For stage numbers above three the optimum speed was limited by the minimum wheel diameter of the first stage. The turbine efficiency and design speed are shown in Figure 4 for one to five stage turbines. It can be seen from this figure that increasing the number of turbine stages increases the achievable turbine efficiency, but with diminishing returns.

An alternative to the multistage axial-flow turbine is a combination axial and radial flow turbine. This configuration has an axial first stage and a radial inflow second stage. The advantages of this configuration are economical manufacturing of the second stage rotor and higher design rotative speeds than the axial turbines. The radial second stage operates at a higher U/C_o (ratio of wheel speed to isentropic spouting velocity) than impulse turbines. The higher design U/C_o of the radial turbine reduces the ratio of "runaway" speed to design speed from that of an impulse turbine which permits greater design speeds than with impulse turbines with the same maximum "runaway" speed. The higher design speed of the radial turbine increases its specific speed and efficiency. The design speed of the axial-radial turbine analyzed here was 73,500 rpm. It can be seen from Figure 4 that the efficiency of the axial-radial turbine (0.774), is greater than that of

the two stage axial machine. However, the higher speed results in increased gearbox losses and decreases overall turbine gearbox efficiency as discussed in sections 5.2 and 5.3 of this report.

All the turbine configurations were evaluated to determine that none of the configurations had rotor inlet relative Mach numbers in the range of 0.95 to 1.05. Operation of turbine rotors in that range generally results in poor turbine efficiency.

5.2 GEARBOX ANALYSIS

Besides the conventional two-stage speed reducer a double cantilever gearbox was investigated for critical speeds and losses. The double cantilever gearbox is a two-stage speed reducer with a double ended high speed shaft. This shaft then cantileter supports one or more stages on each shaft end.

The acceptable cantileter shaft design was evaluated with the B/N critical speed computer program. The basic design is shown in Figure 5. The critical speed map for the design is shown in Figure 6. As can be seen in Figure 6 both the first and second criticals are above the operating speed zone. This was achieved by reducing the overhung shaft lengths. To obtain the required overhang the use of fluid film bearings is necessary because of space limitations. Additionally, this bearing must be supported by the face seal cartridge as shown in Figure 7 in order to fit in the available space. Although this is a unique bearing-seal configuration, state-of-the-art components can be utilized.

Face seal rubbing velocities are approximately 250 fps. Both seals are lubricated and cooled by the gearbox oil in this configuration. An advantage of this configuration as compared to the straddle-mount configuration is that the cantilever design has all bearings, gears, and seals and lubrication in one container, thereby simplifying the lubrication system.

5.3 EFFECT OF SPEED ON GEARBOX AND SEAL LOSS

Gearbox and seal losses as a function of turbine speed were estimated for the configuration discussed in section 4.2.2 and the results are summarized in Figure 8. Again, the disproportionate losses caused by the seals should be noted.

5.4 COMBINED TURBINE AND GEARBOX EFFICIENCY

Predicted overall turbine gearbox efficiencies are summarized in Figure 9 using the turbine efficiency shown in Figure 4 and the gearbox and seal loss shown in Figure 8. A design having zero interstage turbine leakage is shown in the figure for reference. The leakage for the straddle-mounted turbine was calculated for the labyrinth seal discussed in section 3.2.

Comparison of the case for zero leakage with that for the straddle-mounted turbine shows interstage leakage reduces overall efficiency by 2.5 to 4 percentage points, which is significant. A double cantilever configuration reduces interstage leakage by eliminating the leakage in one of the stages. Interstage leakage in the two stage axial-flow turbine can be entirely eliminated by using the double cantilever approach, one stage on each side of the gearbox. This approach requires the same number of high speed seals as the straddle-mount, but has superior performance since interstage leakage is eliminated. If the ducting between the two stages is carefully designed, the pressure drop will be small. For this analysis it was assumed that the pressure drop was equal to the velocity head of the first stage exit gas. The efficiency of a two stage double cantilever turbine equals that for a design having zero leakage as is shown in Figure 9.

The interstage leakage is a three stage turbine is greatest from the first to second stages. By locating the first stage on one side of the gearbox and the second and third stages together on the other side of the gearbox, turbine efficiency is improved as shown in Figure 9. As discussed in section 5.2.1, a double cantilever turbine with the second and third stages on one side of the gearbox can be designed without a critical speed in the operating speed range.

A four-stage double cantilever turbine does not significantly improve efficiency because the greatest leakage (from the first to second stage) is not eliminated. It does not appear that a five-stage double cantilever design is possible from mechanical considerations.

The high speed of the axial-radial turbine results in large seal and gearbox losses and is not recommended for this application.

It should be recalled that the speeds used to estimate the gearbox and seal loss were obtained from analysis of the turbine only. Because higher rotating speeds improve turbine efficiency and also increase gearbox and seal losses, the optimum speeds will be slightly less than those plotted in Figure 4 and used to obtain Figure 9. However, the difference in predicted efficiency (except for the axial-radial machine discussed above) and the optimum efficiency is expected to be small and can be considered as a slight conservative feature of the analysis.

It can be seen from Figure 9 that overall turbine and gearbox efficiency improves with increasing number of stages, but with diminishing returns. We recommend the three stage double cantilever turbine be considered for this application since, in our opinion, it represents the optimum in terms of performance. Table I summarizes the detail design of this configuration and a preliminary layout drawing is presented in B/N drawing TEBC-1.

6.0 CONCLUSIONS AND RECOMMENDATIONS

1. For this application, a multistage turbine is required for high efficiency.

2. A three-stage, axial-flow turbine operating at a design speed of 60,000 rpm would have a predicted efficiency of 0.775 neglecting leakage. The overall efficiency of the turbine gearbox would be approximately 0.71 including leakage and double buffered high speed seal and gearbox losses.

3. A double cantilever turbine design would reduce leakage of the interstage turbine seals, thereby improving turbine efficiency. This configuration also simplifies the lubrication system because the problem of supplying oil to the outboard bearing of a straddle-mounted turbine is eliminated.

4. Most of the gearbox loss is caused by the double buffered face seals. Improved designs should be examined.

5. The recommended turbine for this application is a three-stage, axial-flow, double cantilevered design. The optimum design speed will be approximately 62,000 rpm.

TABLE I

THREE-STAGE TURBINE GEARBOX

Stage	1	2	3
Inlet Temp. (°F)	650	524	415
Inlet Press. (psia)	800	200	48
Exh. Press. (psia)	200	48	11
Adiabatic Head (BTU/lb)	41.9	41.9	39.8
Specific Speed	14.6	28.8	59.0
Specific Diameter	4.1	2.5	1.6
U/Co	0.39	0.048	0.61
Pitch Diameter (inch)	2.0	2.5	3.1
Blade Height (inch)	0.10	0.10	0.28
Blade Width (inch)	0.10	0.10	0.25
Arc of Admission (%)	26	55	100
Nozzle Area Ratio	1.3	1.4	1.0
Number of Nozzles	5	15	12
Nozzle Angle (degrees)	16	16	16
Leakage (%)	0	0	2.2
Stage Effic. (%)	68	76	80

Turbine Effic. (%)	78
Turbine Shaft Power (HP)	48
Speed (RPM)	62,000

FIGURE 1
OPTIMUM THREE-STAGE
60,000 RPM TURBINE

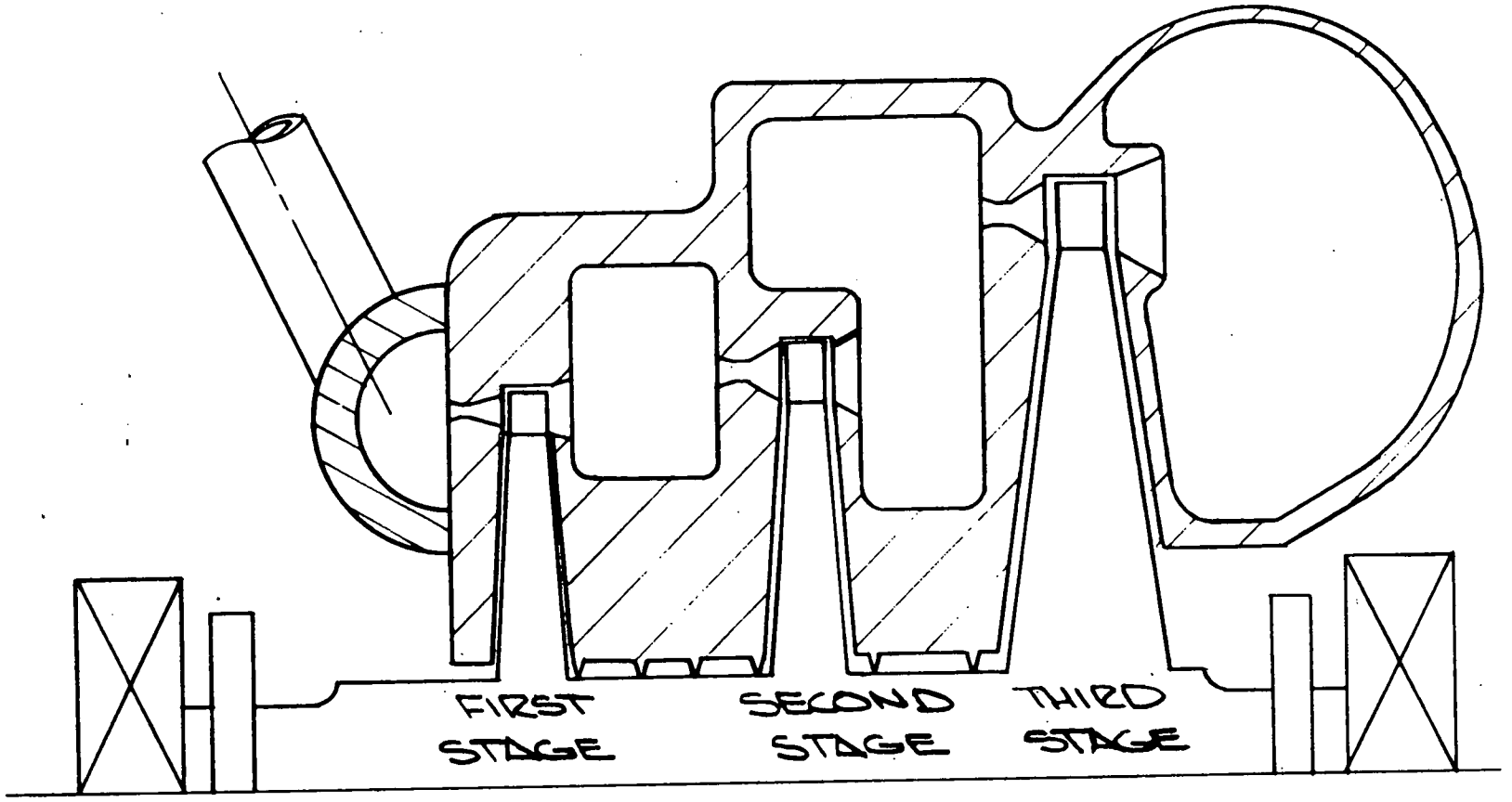

SCALE: 2/1

FIGURE 2
THREE-STAGE STRADDLE MOUNT TURBINE CONFIGURATION

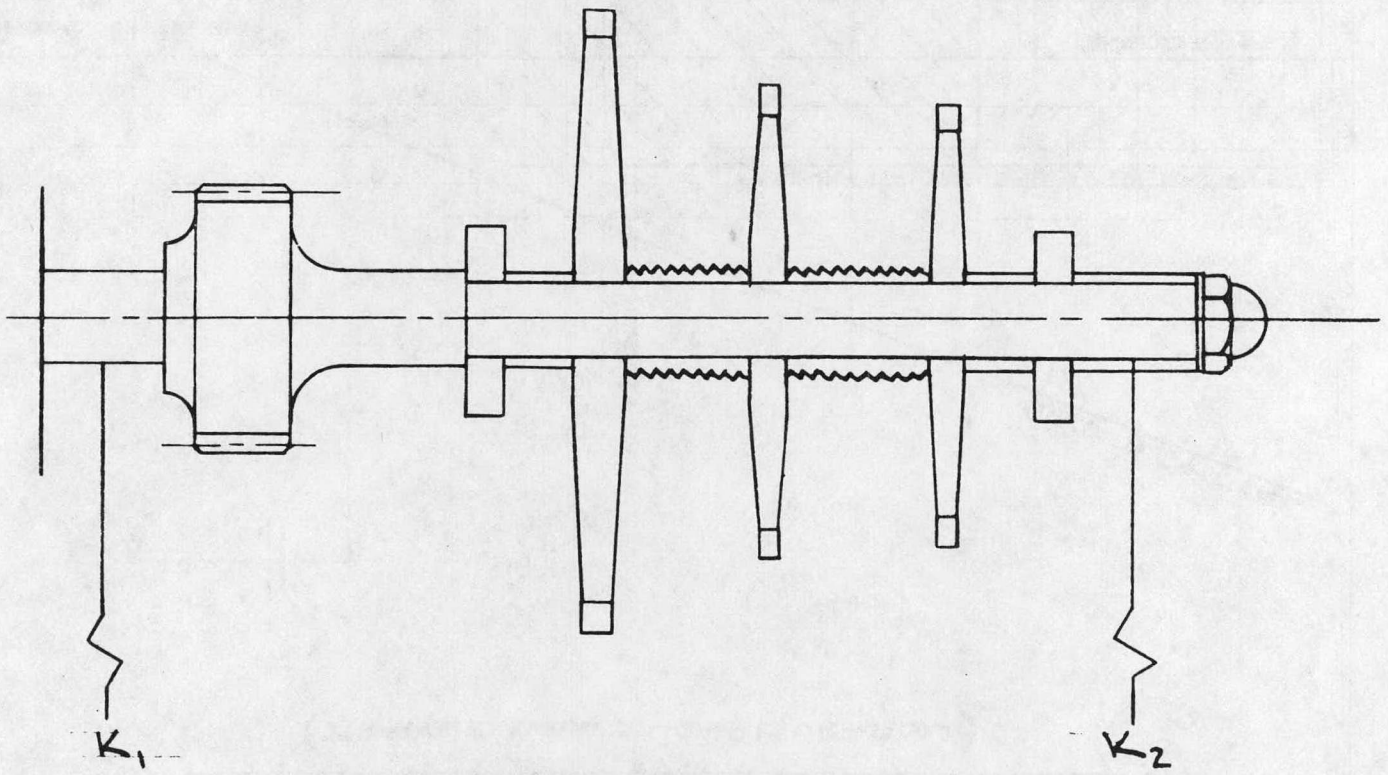

FULL SCALE

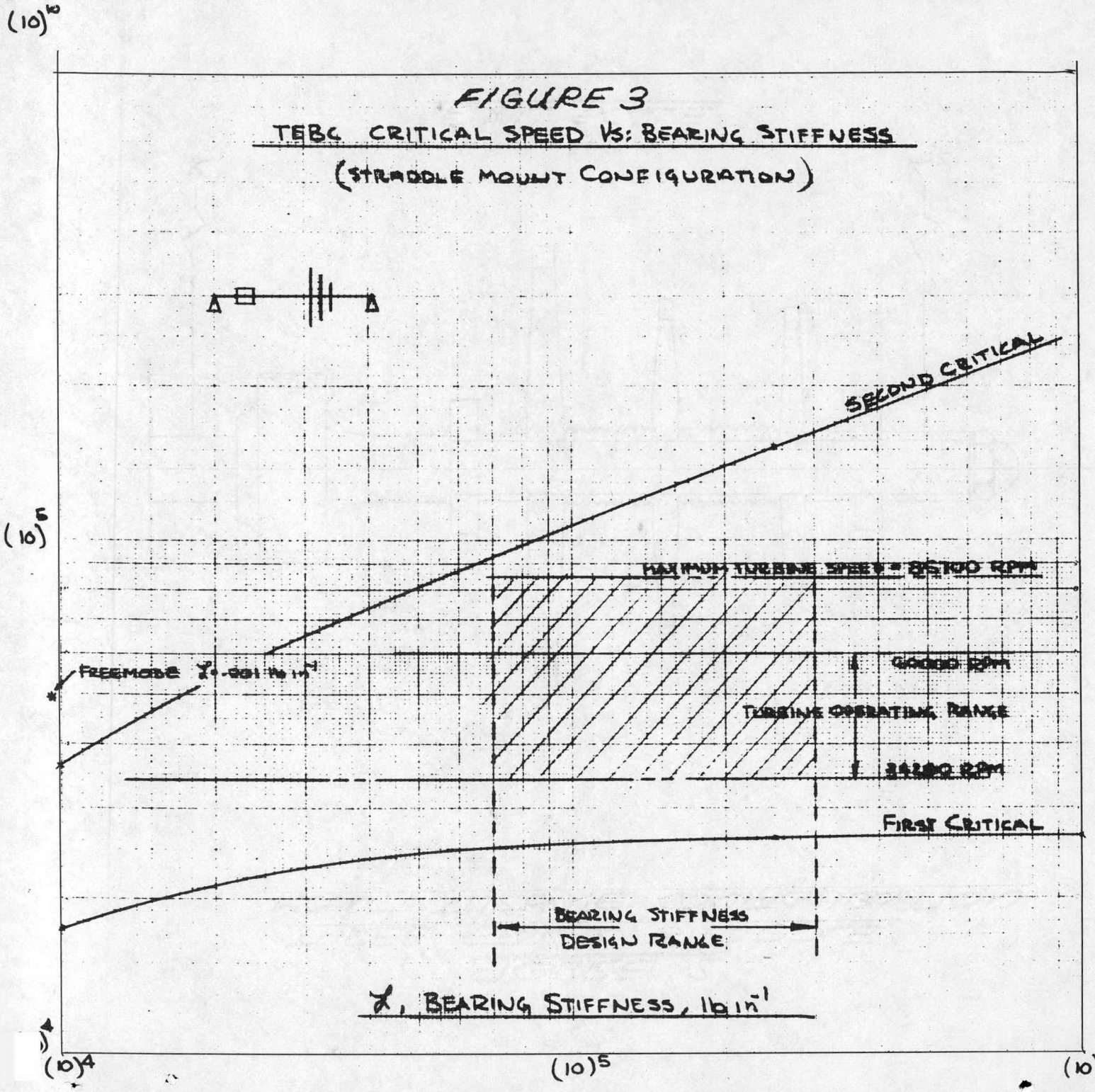

FB
Oct 22, 1974

PROJECT	SUBJECT
TEBC	EFFECT OF STAGE NUMBER ON TURBINE EFFICIENCY
BY: DW / DATE: 11-6-74	

FIGURE 4

MIN. PITCH DIA = 2.0 IN
MAX. ROTARY TIP SPEED = 1600 FT/SEC
AXIAL STAGES UNLESS NOTED
ZERO INTERSTAGE LEAKAGE

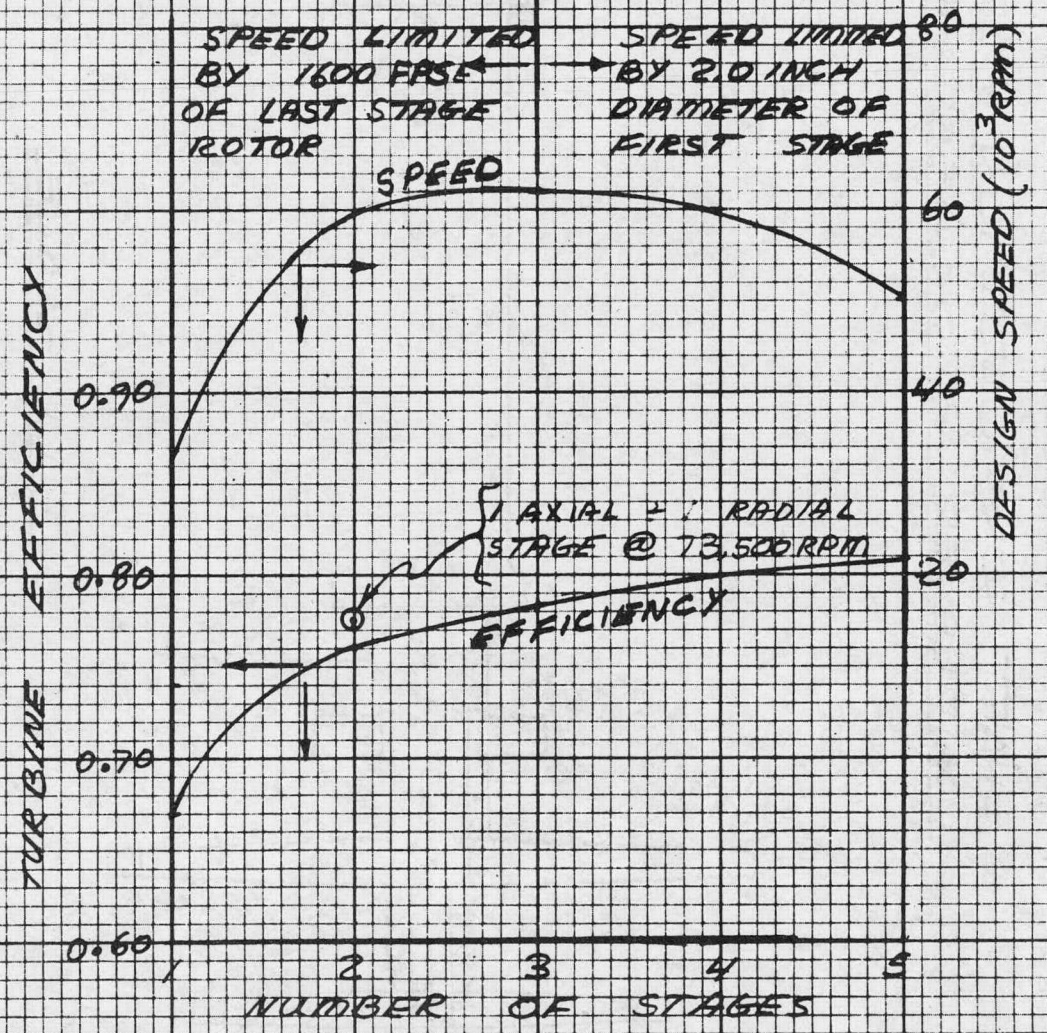

FIGURE 5

SHAFT CONFIGURATION FOR CANTILEVER ROTOR ASSEMBLY

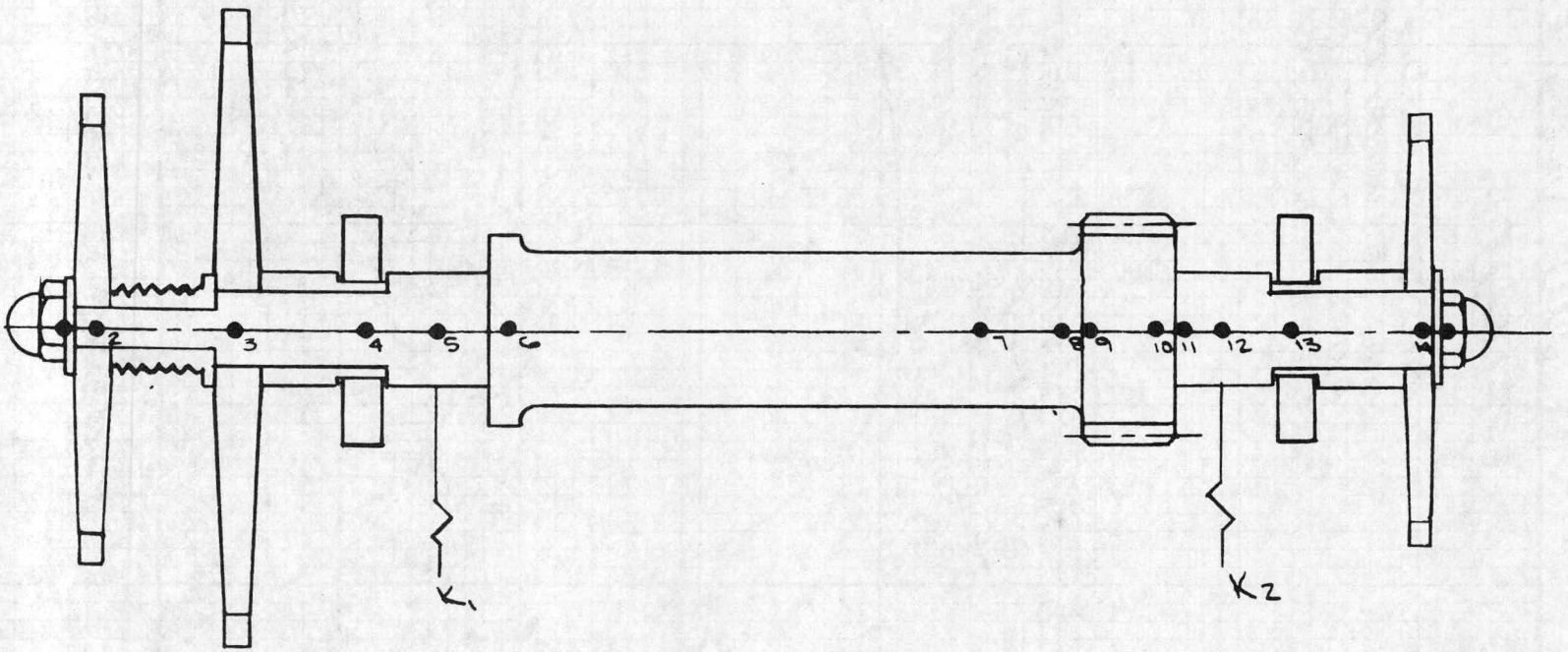

FULL SCALE

FIGURE 6

TEBC CRITICAL SPEED VS: BEARING STIFFNESS

(CANTILEVERED ROTOR CONFIGURATION)

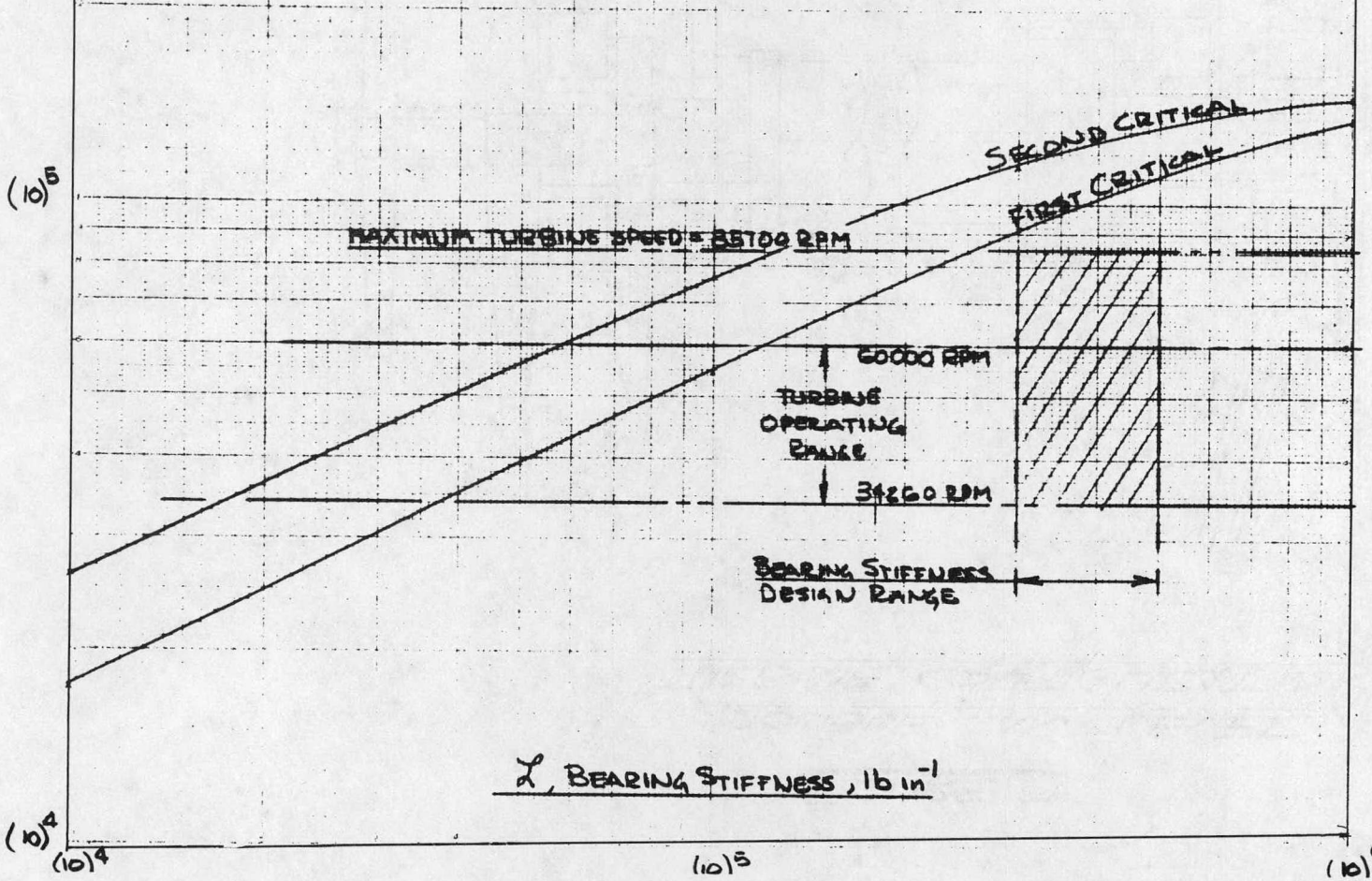

FIGURE 7

DOUBLE CANTILEVER
TURBINE CONFIGURATION

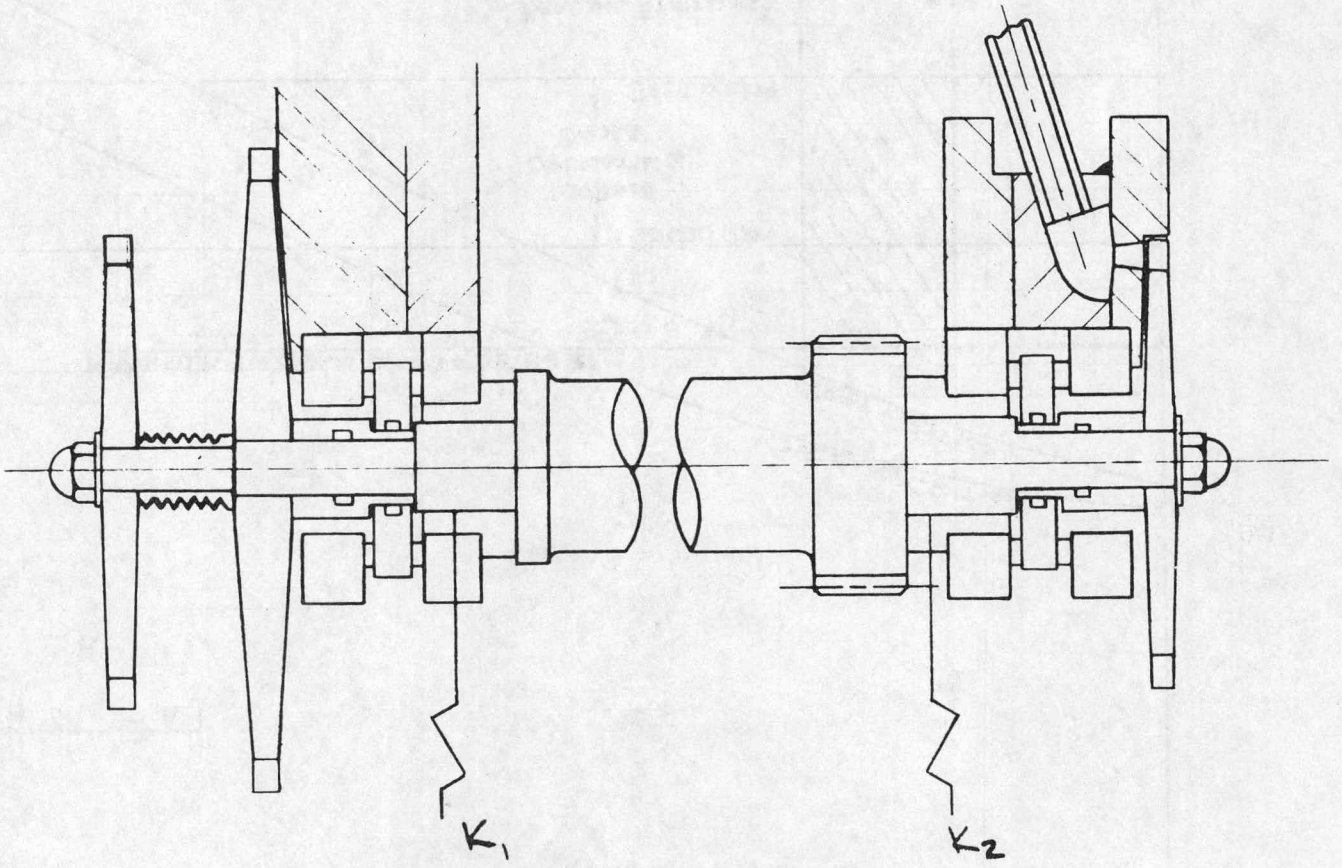

FULL SCALE

PROJECT	SUBJECT
TEBC -T2	ESTIMATED GEAR BOX AND SEAL LOSS
BY: AW	DATE: 10-294

FIGURE 8

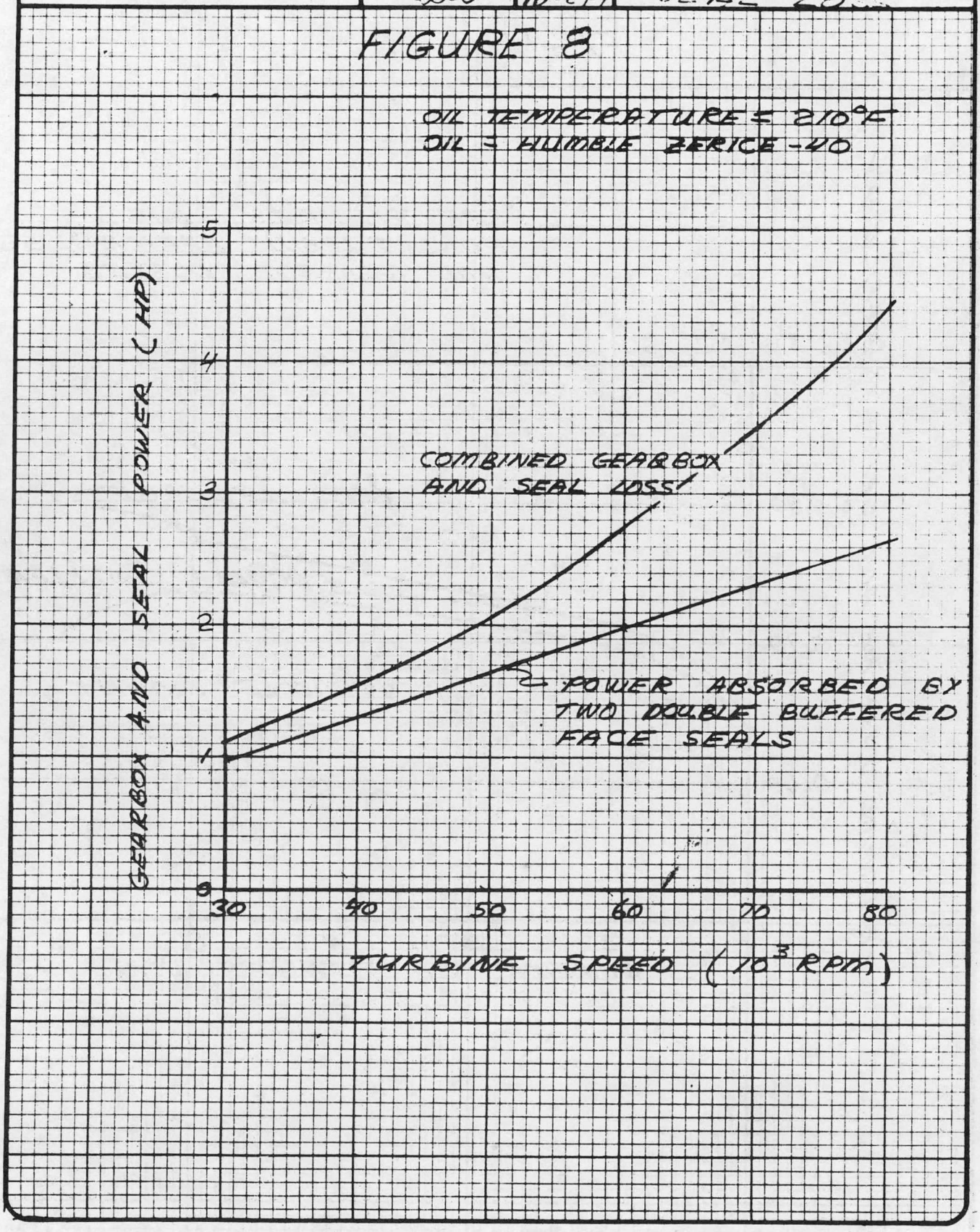

BARBER-NICHOLS ENGINEERING CO.

PROJECT	SUBJECT
TEBC	COMBINED TURBINE AND GEARBOX EFFICIENCY
BY: DW	DATE: 11-6-74

FIGURE 9

SEE FIGURES ___ AND ___ FOR TURBINE EFFICIENCIES AND GEARBOX LOSSES

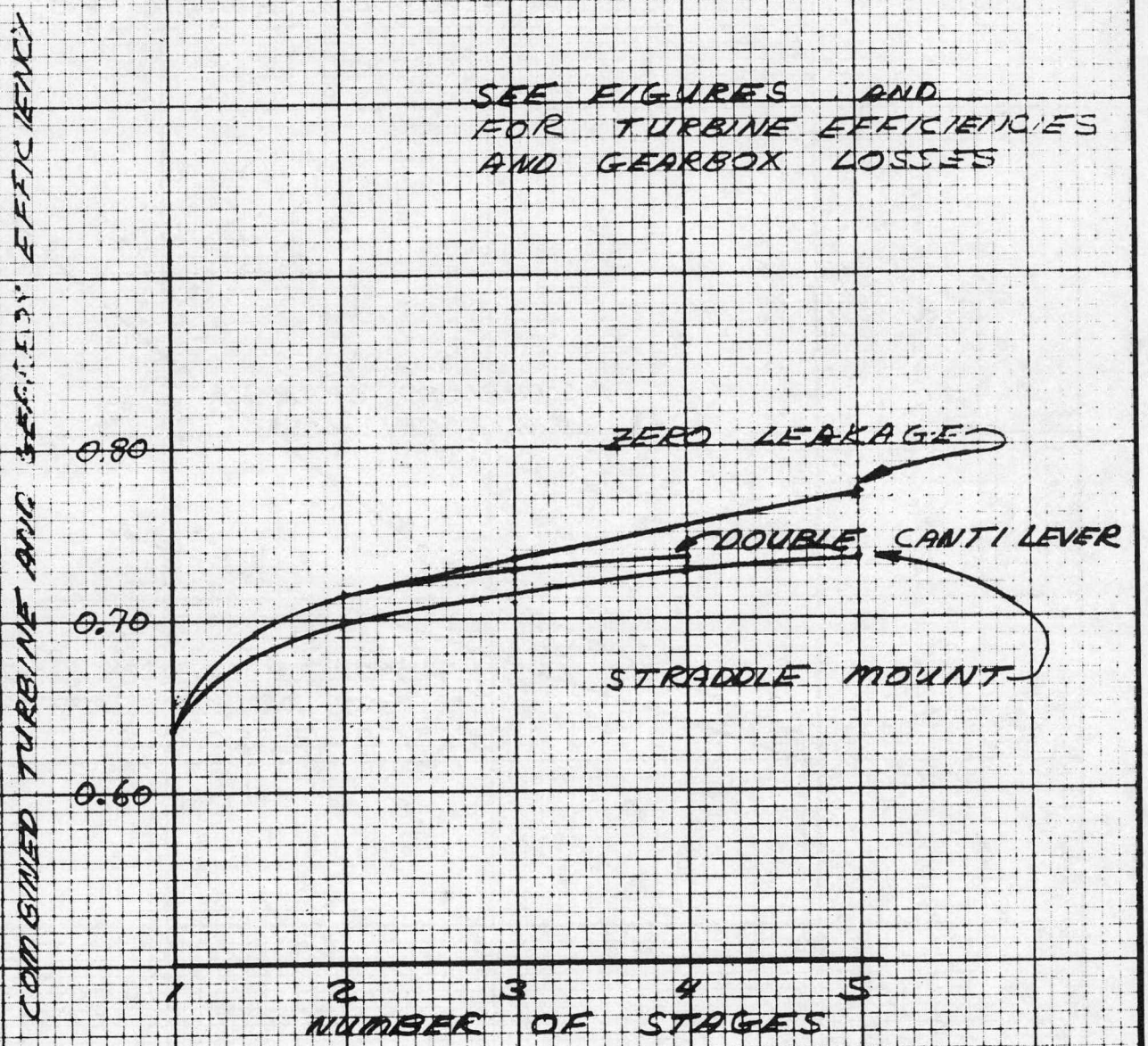

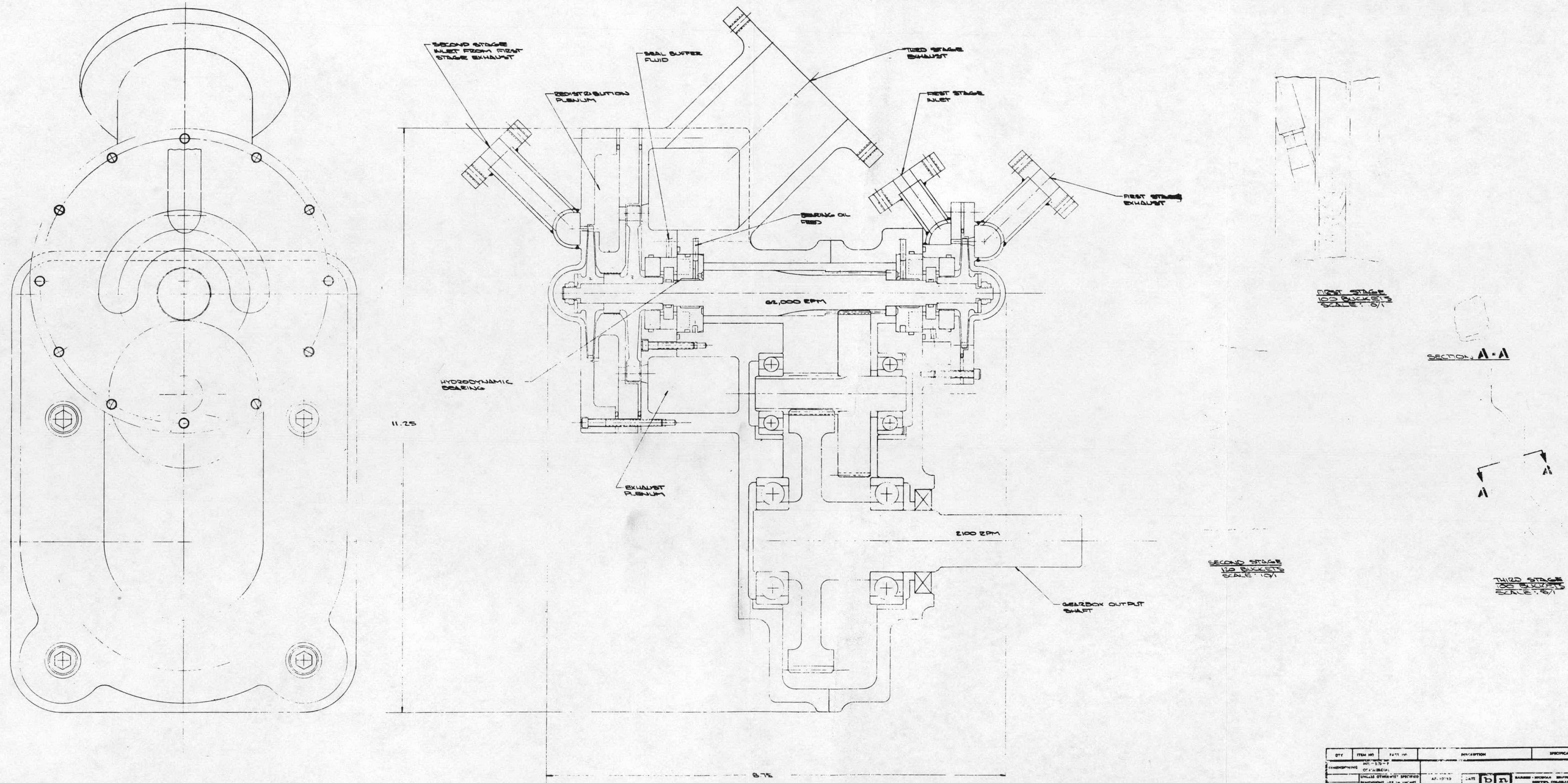

QTY | ITEM NO | PART NO | DESCRIPTION | SPECIFICATION

DIMENSIONING: MIL-STD-? / COMMERCIAL

UNLESS OTHERWISE SPECIFIED DIMENSIONS ARE IN INCHES
TOLERANCES
.XX
.XXX
.XXXX
X°
ALL SURFACES
MATERIAL

APPROVED | DATE
CHIEF
PROJECT
MFG
TEST
CHT. APP
DRAWN

NEXT ASSY | WT

bn BARBER-NICHOLS ENGINEERING CO. DENVER, COLORADO

DOUBLE CANTILEVER TURBINE GEARBOX CONCEPT

SIZE J | CODE IDENT. NO. | DWG NO. TEBC-1 | REV
SCALE 2/1 | SHEET 1 OF 1

APPENDIX D

PART-LOAD PERFORMANCE EVALUATION

In order to evaluate the overall improvement of the Rankine cycle bottoming system to the diesel truck system, the representative part-load condition of the present system design has been analyzed and fully optimized by computer simulation. The other objective of the analysis is to obtain the necessary information for control system. The optimization was carried out by adjusting the organic working fluid flow rate and condenser fan speed with the limitations: (1) that the radiator temperature is not higher than 185°F, and (2) that the organic working fluid temperature is not higher than 650°F. The diesel operating information and its exhaust gas temperature and flow rate are based on the data provided to Thermo Electron by Mack. Because of the limited information of the accessory power requirement, it is assumed to be linear with respect to the diesel speed; it varies from 3.6 hp at a speed of 2100 rpm to 2.05 hp at a speed of 1200 rpm. The range of diesel speed covers the condition of normal operation.

All the components related to the organic Rankine system are included in the analysis: the vapor-generator, the turbine expander and gearbox, the regenerator, the condenser/radiator, the cooling fan, and the feedpump. The modeling of these components is based on the physical dimensions of the actual design and the performance parameters which were obtained from experimental results or provided by the manufacturer. For example, the feedpump and turbine performance is estimated from previous TECO experimental results, and the heat transfer correlation of the vapor-generator tube surface is provided by the manufacturer. The schematic

diagram of the Rankine bottoming system is shown in Figure D. 1. In the present analysis, the turbine expander is connected to the diesel output shaft through the gearbox. Therefore, the ratio between the diesel speed and turbine speed is a fixed number.

The diesel operating conditions, the organic flow rate and the fan speed are the inputs which initiate the calculation. The outlet temperature of the organic fluid from the vapor generator is assumed first. The corresponding pressure is determined by the required choke flow relation of the fluid through the turbine nozzles. With the known outlet conditions of the organic working fluid and diesel system exhaust gas conditions, the inlet condition of the working fluid and the outlet conditions of the gas can be calculated from the physical characteristics of the vapor-generator. It should be noted that the combination of fluid flow rate and its temperature at the outlet of the vapor generator is not a completely free choice. It is limited by the physical ability of the vapor generator (i. e., the amount of heat that can be transferred from the diesel exhaust gas to the organic working fluid). If the assumed values form a bad combination, their values must be adjusted before the calculation can be continued. The logic of adjustment is programmed in the model of the vapor generator. The next component of calculation is the turbine expander. The calculation of performance of the turbine is based on its characteristic and assumed exhaust pressure. The calculation will provide the output power and exhaust temperature.

To evaluate the performance of the regenerator, the inlet conditions of the vapor and liquid must be known. The calculation of the

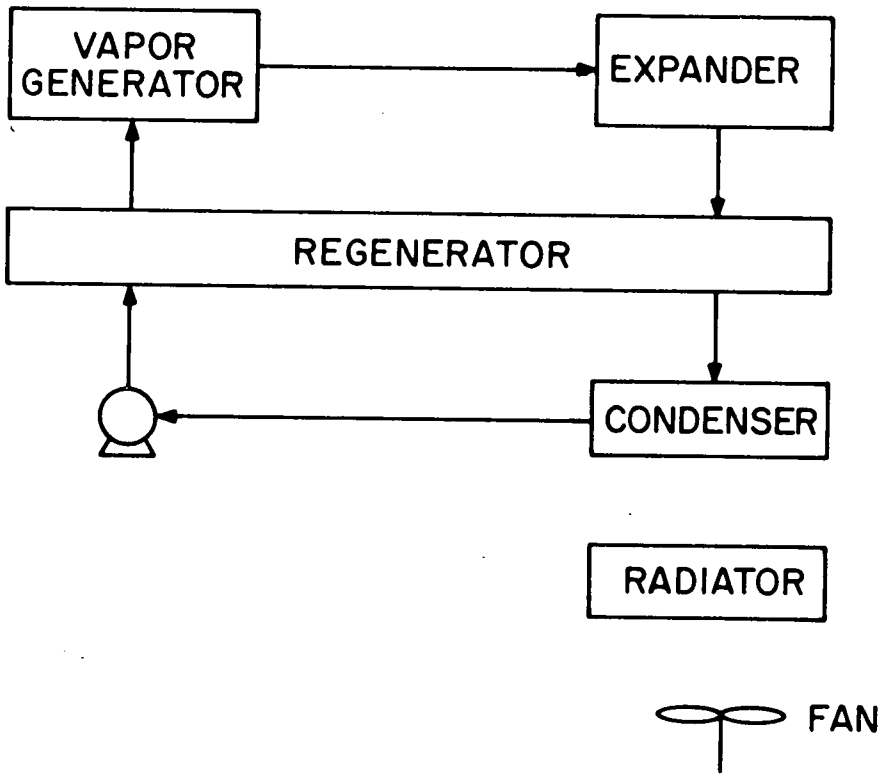

Figure D.1. Schematic of Rankine-Cycle System.

regenerator is skipped for the time being. The outlet condition of the regenerator is estimated by the assumed pressure drop and the regenerator efficiency. The performance of the condenser is determined by the vehicle speed, fan speed working fluid inlet condition, and the required cooling rate for the diesel system. The model of the condenser will determine the condenser temperature which can achieve the dynamic equilibrium among all influential effects. This is achieved by an iteration process. The condenser temperature will be fixed by the corresponding pressure. With the known value of the condenser pressure, we are able to check the correctness of the assumed expander exhaust pressure. If the assumed and calculated values are not within the converge limit, the calculation will go back to the expander and gas through the loop again and again until they are converged. The calculation then proceeds to the feedpump. The only important factor of the feedpump is the head provided by the pump. This value can be easily calculated from the known value of the inlet pressure to the vapor generator and the estimated pressure drop across the regenerator. After the pump, we are in the position to make the detail calculation of the regenerator. The calculation of the regenerator will provide the pressure drop of the liquid side, the efficiency of the regenerator and the liquid outlet temperature. These values must be checked with the assumed values used before. The convergence of each of those variables leads to different iteration loops. The convergence of the liquid side pressure drop requires the adjustment of the feedpump pressure head. The convergence of the regenerator effectiveness leads to the adjustment of the condenser inlet condition. The match between the regenerator

outlet and the vapor generator inlet requires the adjustment of the assumed vapor generator outlet temperature which is the starting point of the calculation. The calculation is completed if all converge requirements are satisfied.

By examining the results of the different organic flow rate and fan speed with the same diesel operating condition, the optimum operating condition of the organic Rankine system is established.

Based on these parametric studies, an optimum organic flow rate schedule, as well as a fan speed schedule corresponding to the maximum net power, is obtained.

FEASIBILITY TEST ON COMPOUNDING THE INTERNAL COMBUSTION ENGINE FOR AUTOMOTIVE VEHICLES, TASK II. Final Report